Variabilitat climàtica ràpida a la conca occidental del Mediterrani: registre sedimentològic

Rapid climate variability in the Western Mediterranean Basin: the sedimentological record

Jaime I. Frigola Ferrer

Variabilitat climàtica ràpida a la conca occidental del Mediterrani: registre sedimentològic

Jaime I. Frigola Ferrer

Memòria de Tesi Doctoral

GRC Geociències Marines

Dpt. d'Estratigrafia, Paleontologia
i Geociències Marines
Universitat de Barcelona

Octubre 2012

Universitat de Barcelona

Departament d'Estratigrafia,
Paleontologia i Geociències Marines
Facultat de Geologia
Universitat de Barcelona

Variabilitat climàtica ràpida a la conca occidental del Mediterrani: registre sedimentològic

Rapid climate variability in the Western Mediterranean Basin: the sedimentological record

Memòria de Tesi Doctoral presentada per

Jaime I. Frigola Ferrer

sota la direcció dels Doctors

Miquel Canals Artigas i Ana Moreno Caballud

al Departament d'Estratigrafia, Paleontologia i Geociències Marines
de la Universitat de Barcelona, dins del programa de doctorat de Ciències del Mar de la
Facultat de Geologia, bienni 2002-2004, per optar al grau de
Doctor per la Universitat de Barcelona.

Barcelona, octubre de 2012

Jaime I. Frigola Ferrer

Miquel Canals Artigas

Ana Moreno Caballud

Aquesta Tesi ha estat possible mercès al suport dels projectes de recerca de la Comissió Europea i del PN I+D+i següents: ADIOS (EVK32000-00035), EURODOM (RTN2-2001-00281), PROMESS 1 (EVR1-CT-2002-40024), EUROSTRATAFORM (EVK3-2002-00079), HERMES (GOCE-CT-2005-511234-1), HERMIONE (226354-HERMIONE), GRACCIE CONSOLIDER (CSD2007-00067) i DOS MARES (CTM2010-21810-C03-01). Hem comptat també amb el suport de la Generalitat de Catalunya a través del programa de Grups d'Excel·lència (refs. 2005SGR 00152 i 2009 SGR 1305).

Als meus pares,
a la memòria de mon pare

RESUM

Aquesta Tesi Doctoral està centrada en la reconstrucció de les condicions climàtiques del passat a la conca occidental del Mediterrani, i més concretament en l'estudi de l'efecte de la variabilitat climàtica d'escala orbital i mil·lenària sobre les condicions oceanogràfiques de la conca. El treball es basa en l'anàlisi i interpretació de dades de indicadors sedimentològics, com ara la mida de gra i la composició elemental dels sediments, d'on s'ha obtingut informació sobre els canvis en les aportacions terrígenes induïts per la variabilitat climàtica i oceanogràfica de la conca, reflectida en canvis del nivell del mar o de la circulació termohalina.

Hom ha pogut investigar els canvis del nivell del mar associats als cicles glacials mitjançant l'estudi de les variacions en la mida de gra de les partícules sedimentàries i en la composició elemental d'un testimoni del marge progradant del Golf de Lleó. Les variacions eustàtiques del nivell del mar han determinat l'apilament d'unitats sedimentaries regressives en el talús superior amb una ciclicitat de 100 ka. Els canvis en el nivell del mar han modulat la sedimentació en el marge, la qual va oscil·lar entre aportacions principalment fluvials durant els períodes glacials coincidint amb nivells del mar baixos, i aportacions degudes a la reactivació de processos erosius a la plataforma continental com les Cascades d'Aigües Denses de Plataforma durant les èpoques amb nivell del mar alt corresponents als períodes interglacials.

L'estudi de l'Estadi Isotòpic Marí 3, entre 65 i 20 ka, caracteritzat per condicions climàtiques fluctuants de escala mil·lenària, ens hauria d'ajudar a entendre com el clima es comporta sota condicions canviants ràpides i per lo tant pot ser clau per entendre millor el ràpid canvi climàtic induït per l'ésser humà. Les variacions de la mida de gra durant aquest període en el marge del Golf de Lleó han revelat per primera vegada l'existència d'oscil·lacions del nivell del mar d'escala mil·lenària associades a la variabilitat climàtica dels cicles de Dansgaard-Oeschger observats a l'Atlàntic Nord. Nivells del mar relativament alts s'associen a les fases càlides dels cicles de Dansgaard-Oeschger. Aquests resultats mostren una ràpida resposta dels casquets polars a la variabilitat climàtica ràpida del darrer període glacial. Resta per identificar, però, amb precisió el inici d'aquestes pujades del nivell del mar i la seva amplitud.

La circulació termohalina del Mediterrani occidental també s'ha vist afectada per les oscil·lacions climàtiques dels cicles de Dansgaard-Oeschger durant l'Estadi Isotòpic Marí 3. Els resultats confirmen que la circulació profunda del Mediterrani occidental funcionà de manera asincrònica respecte a la Circulació de Retorn de l'Atlàntic Nord durant els cicles de Dansgaard-Oeschger. Aquest fet posa de manifest la rapidesa en la transmissió de la variabilitat climàtica entre latituds altes i intermèdies, probablement induïda per un mecanisme de teleconnexió atmosfèrica similar a l'actual Oscil·lació de l'Atlàntic Nord. Tot i així, la circulació profunda del Mediterrani occidental també fou modulada per canvis en la hidrologia de la conca.

A l'Holocè hom ha identificat igualment una sèrie d'esdeveniments de curta durada de intensificació de la circulació termohalina, els quals mostren una ciclicitat d'uns 1000 anys. Hom ha pogut correlacionar aquest esdeveniments amb altres observats a l'Atlàntic Nord i en altres regions del planeta, fet que confirma que les reorganitzacions ràpides del sistema climàtic són també comuns en els períodes interglacials.

ABSTRACT

This PhD Thesis focuses on the reconstruction of past climatic conditions in the Western Mediterranean Basin, and more precisely on the study of the impact of climate variability at orbital and millennial time scales over oceanographic conditions. The work relies on the study of sedimentological proxies like grain-size and elemental geochemical composition of the sediments for unravelling the changes in terrigenous supplies led by oscillations in climate and oceanographic conditions, namely sea level fluctuations and changes in the termohaline circulation of the Western Mediterranean Sea.

Sea level changes associated with glacial cycles have been investigated by analysing the oscillations in grain-size and geochemical composition of the sediment records from the progradational Gulf of Lion margin. Eustatic sea level oscillations have determined stacking of regressive progradational units in the upper slope following a 100 kyr cyclicity. Sea level fluctuations have modulated sediment accumulation over this margin, with a succession of periods dominated by high fluvial supplies, and periods characterized by the reactivation of erosive processes in the continental shelf such as Dense Shelf Water Cascading during glacial lowstands and interglacial highstands, respectively.

The study of climate variability during Marine Isotope Stage 3, between 65 and 20 ka, characterized by rapid climate fluctuations of millennial time scales, may help us to understand how the climate behaves when undergoing rapid changes and therefore might also further increase our understanding of rapid, anthropogenic climate change. The high-resolution study of grain-size oscillations during Marine Isotopic Stage 3 in the Gulf of Lion margin has shown by the first time the occurrence of millennial-scale sea level fluctuations associated with climate variability during the Dansgaard-Oeschger cycles identified in the North Atlantic region. Relative high sea level has been observed to occur during warm interstadials of the Dansgaard-Oeschger cycles. These results point to a rapid response of the ice sheets to climate variability during the last glacial period. However, the precise timing and the amplitude of these millennial-scale sea level rises are still to be determined.

The termohaline circulation of the Western Mediterranean Sea has been affected by Dansgaard-Oeschger climate oscillations during Marine Isotopic Stage 3 too, as determined by the study carried out in the IMAGES core MD99-2343 offshore Minorca island. Our results show that during Dansgaard-Oeschger cycles the circulation of deep-water masses in the Western Mediterranean was not synchronyzed with the Atlantic Meridional Overturning Circulation. This confirms the rapid transmission of climate variability between high and mid-latitudes, likely induced by an atmospheric mechanism similar to the present-day North Atlantic Oscillation. Hydrological oscillations within the basin further modulated the termohaline circulation in the Western Mediterranean Sea.

During the Holocene a series of short-lived events of enhanced deep-water circulation have been identified to occur with a cyclicity close to 1000 yr, which have been correlated to relatively cold periods recently recognized from the North Atlantic region and in other regions of the world. These results confirm that rapid reorganizations of the climate system usually ascribed to glacial stages are also a common feature during interglacial periods.

AGRAÏMENTS

Hi ha molta gent a la que vull agrair el suport que m'han donat durant tots aquest anys de tesi, compartint d'una manera o d'altra l'esforç, el patiment, les il·lusions, les discussions, els viatges, i un munt de coses més que aquesta tesi m'ha permès viure, i que, finalment, arriba al seu desenllaç.

Va ser durant els darrers anys de carrera quan em vaig quedar fascinat per les històries que ens contaven sobre com es podia investigar el clima del passat a través dels sediments del fons marí, i recordo una nit d'aquelles llargues d'estudi parlant amb un company sobre la possibilitat de dedicar-nos a investigar allò, era com viatjar al passat! Qui m'anava a dir a mi que al cap d'uns anys veuria aquell somni realitzat. Poc després d'acabar la carrera, ja per Barcelona, vaig anar a petar a la porta d'en Miquel Canals, qui, després d'una conversa que recordo llarga i plàcida, la qual es podria considerar la meva primera entrevista de treball, em va donar un article que havia estat recentment publicat per una noia del grup i em va dir que tornés després d'haver-lo llegit. [...] Així va començar la meva aventura a la *paleo*. He d'agrair-li en Miquel la confiança que ha dipositat en mi al haver-me acollit al GRCGM i haver-me donat la possibilitat de dur a terme aquesta Tesi, aquest somni. Gràcies!

L'altre pilar en el que m'he pogut sostenir durant el transcurs de la Tesi ha estat l'Ana Moreno, amb qui he pogut gaudir de llargues discussions molt estimulants sobre les dades i els processos que podrien explicar-les, i a qui he d'agrair la seva eficàcia, entusiasme i afabilitat.

Sense ésser part directa de la direcció d'aquest projecte, he d'agrair també el paper que ha jugat la Isabel Cacho en el desenvolupament de la Tesi, amb qui sempre he pogut comptar per tenir una bona dosi de crítica constructiva i amb qui he aprés moltíssim sobre *paleo*.

Vull també agrair als coautors dels treballs la seva aportació en aquesta Tesi, en especial, al Paco Sierro, el Jose Abel Flores i en Joan Grimalt, amb els que ha estat un plaer compartir l'aventura de la ciència durant aquests anys ja sigui en congressos, reunions o campanyes.

No puc passar sense mencionar la inestimable ajuda que he rebut al laboratori de mans de la Montse Guart amb les mostres, discussions sobre com dur a terme les granulometries i de si el Coulter funcionava be o no, quina paciència que has tingut Montse!

Al laboratori, mentre jo feia les granulometries, vaig tenir la sort de compartir una bona temporada amb dos companys de la *paleo*, el Leo i la Gema, amb els que vam passar bones estones i vam tenir bones discussions sobre ciència i sobre el procés de la Tesi, por fin la tengo chicos!!

I com no, sempre que hi penso en els inicis de la Tesi, em venen al cap tots el que han passat per la sala de becaris 337, i les vegades que hem canviat l'orientació de les taules, i també de la gent de la 336, i dels que han passat pel grup en general, amb qui hem compartir tantes i tantes hores, dinars, discussions per l'aire condicionat, festes, boletades sortides i altres esdeveniments que han fet que tots aquests anys hagin sigut molt més alegres i vius: en Galde, l'Anna, en David, en Joan, la Vero, la Diana, la Camino, el Jersi, la Nuna, el Victor, el Pedrito, en Viku, la Sara, la Tina, la Neus, la Gemeta, el SergiO, la Catalina, la Mayte, la Caroline, la Ruth, la miniRuT, la Olaia, la Patri, l'Aitor, en Xavi Rayo, la Pilar, la Marina, l'Oriol, el Xavi, l'Aaron, en Roger, en Ben, l'Angelo, la Renata, la Patricia Ferretti.

També vull agrair a en Toni Calafat el haver estat sempre disponible i amb bon humor per respondre a qualsevol qüestió, així com al Jose Luis per estar a disposició sempre per qualsevol assumpte informàtic, i a les secretaries per ajudar-me en tota la paperassa de tots aquests anys: la Maite, la Teresa, la Eli, la Montse...

També han sigut claus en moltes discussions de ciència i de la vida, alguns companys de Vigo amb qui vaig passar una molt bona època i amb els que segueixo compartint la meva il·lusió: Susi, Pedro, Toni, Micho, Mikelon, Angel, Rox, Jaime M., Gorka, Irene, Íñigo, Raquel, Miguel V., Javi, Juan, Marcos,...

Gràcies al Jordi M., el Jordi F. i la Carmen, per que la vostra amistat i totes les coses que hem viscut junts es una part molt important d'aquesta Tesi. Moltíssimes gràcies per estar sempre.

També vull agrair el suport que he rebut dels companys de Barcelona, el Marino, el Nacho i el Toli, per que fan que esta gran ciutat no sigui tant gran per a un de poble; i als companys del shiatsu, amb els qui he compartit moments molt valuosos: Sergi, Francina, Amaranta, Borja, Thierry, Geni, Nina, Cris P., Dani, Laura, Santi, Cristina H., ...

I com no, gràcies a la meva germana per haver-me ajudat i animat a tirar endavant en tots els estudis, si ara estic aquí, molt és gràcies a tu.

I finalment, als meus pares, per que ells em van ensenyar a ser el que sóc, i em van donar la força i l'empenta per fer tot allò que volia fer. Aquesta Tesi és vostra, és fruit del vostre amor i del vostre esforç per fer que tinguérem una vida millor.

PRESENTACIÓ DE LA TESI

Aquesta Tesi Doctoral s'emmarca en el camp de la Paleoclimatologia i la Paleoceanografia i per tant, s'ocupa de l'estudi de les condicions climàtiques i oceanogràfiques del passat. Per a dur a terme aquest treball hem partit de l'anàlisi de registres sedimentaris marins. Els sediments marins preserven en bona mesura el senyal dels processos de tota mena que condicionaren el transport i arribada de les partícules que els formen, i llur acumulació en el fons marí. Concretament, hem estudiat tres testimonis de sediment recuperats en dos indrets del Mediterrani nordoccidental. Dos dels testimonis corresponen a la seqüència sedimentaria del marge progradant del Golf de Lleó, mentre que el tercer prové del llom contornític de fons de conca situat al nord de la illa de Menorca. Hom ha analitzat la mida de les partícules i ha determinat la composició elemental del sediment. Els testimonis del marge del Golf de Lleó han permès estudiar el registre dels darrers 500.000 anys a dues escales de temps diferents, l'escala orbital, que inclou els cicles glacials/interglacials de 100.000 anys, i l'escala mil·lenària corresponent al darrer període glacial. A més, el testimoni del fons de la conca ha permès dur a terme un estudi de molt alta resolució temporal, de centenars a milers d'anys, del registre dels darrers 50.000 anys, abastant per tant el darrer període glacial i el període interglacial actual, l'Holocè.

Aquesta Tesi es presenta en la modalitat de compendi de publicacions i inclou un total de 3 articles, tots ells publicats en revistes internacionals indexades en els *Journal Citation Reports de l'Institute for Scientific Information* (ISI). La memòria s'inicia amb un capítol introductori (Cap. I) en el que es presenten les temàtiques dels canvis climàtics naturals, els mecanismes generadors dels mateixos i les fluctuacions del nivell del mar associades. En aquest capítol introductori també es fa una descripció de l'àrea d'estudi en el marc regional del Mediterrani, així com dels materials i la metodologia emprats.

El capítol de resultats (Cap. II) recull els tres articles esmentats, que s'ordenen seguint un transsecte nord-sud i de més som a més profund, la qual cosa també s'adiu amb les escales de temps, d'orbital (cicles de 100.000 anys) a mil·lenària (milers d'anys, o kilo-anys, ka).

El treball del Golf de Lleó permet, en primer lloc, avaluar l'evolució seismostratigràfica del marge a escala glacial/interglacial, la qual cosa ha servit per a re-interpretar la història sedimentaria del marge, i en segon lloc, dur a terme un estudi de molt alta resolució temporal dels canvis de nivell del mar durant el període comprès entre 60 i 25 ka, i llur relació amb la variabilitat climàtica descrita a l'Atlàntic Nord.

El treball dut a terme en el testimoni del fons de conca ens ha permès endinsar-nos en la variabilitat de la circulació profunda de la conca occidental del Mediterrani durant els darrers 50 ka, base de dues publicacions. A la primera, que inclou tot el registre dels da-

rrers 50 ka, hom combina els resultats de les anàlisis sedimentològiques, element nuclear d'aquesta Tesi, i les dades obtingudes amb altres metodologies analítiques, com l'anàlisi dels isòtops de l'oxigen ($\delta^{18}O$) i del carboni ($\delta^{13}C$) en foraminífers bentònics. L'avaluació conjunta d'aquests dos tipus de dades permeté millorar el coneixement de la variabilitat en la formació d'aigües fondes a la conca occidental del Mediterrani durant el període glacial. A la segona publicació, hom descriu un seguit de canvis en la circulació profunda del Mediterrani occidental durant la darrera fase de la desglaciació i l'Holocè (darrers 12 ka), així com la seva relació amb la variabilitat climàtica del interglacial actual descrita en altres registres de l'Atlàntic Nord i d'altres indrets.

La integració i interpretació de les dades d'aquests estudis es va dur a terme sota la responsabilitat principal del doctorand, el qual comptà també amb els beneficis del intercanvi de dades i idees amb altres investigadors de diferents països de la Unió Europea, circumstància afavorida per sòlides col·laboracions en el marc de diversos projectes de recerca finançats per la Comissió Europea, el PN d'I+D+i i la Generalitat de Catalunya.

La discussió dels resultats (Cap. III) i les conclusions, amb un breu llistat de possibles vies de treball futures (Cap. IV), completen aquesta Tesi.

INDEX

CAPÍTOL I. INTRODUCCIÓ

1. L'estudi dels climes del passat: la Paleoclimatologia

1.1. Conceptes generals

Segons l'Organització Meteorològica Mundial el clima d'un lloc queda definit per la "descripció estadística en termes de la mitja i la variabilitat de la temperatura, la precipitació i el vent durant un període de temps". Habitualment, per caracteritzar un clima hom considera un període mínim de temps de 30 anys. És obvi, però, que aquesta definició no serveix per a poder caracteritzar el clima del passat, doncs no el podem mesurar. En un sentit més ampli, hom també pot definir el clima com l'estat del sistema climàtic, que inclou els subsistemes de l'atmosfera, la hidrosfera, la criosfera, la litosfera i la biosfera. Aquests subsistemes interaccionen entre ells donant lloc a les condicions climàtiques regionals i globals (Fig. 1.1). El principal motor del sistema climàtic és, però, la radiació solar que arriba a la Terra i el balanç radiatiu del sistema, sotmès a fluctuacions en funció de la fracció de radiació solar d'entrada, la reflectida (l'albedo) i la radiació de sortida de la Terra. El balanç radiatiu del planeta està, per tant, sotmès a canvis causats per forçaments tant externs com interns al sistema climàtic. Entre els primers podem citar processos tectònics, canvis en l'òrbita de la terra i canvis en la pròpia radiació solar, mentre que entre els segons hi hauria els derivats de la interacció entre els propis components del sistema climàtic, els quals poden generar processos de retroalimentació positiva o negativa. A més, el clima local també depèn de la redistribució de la calor per la circulació atmosfèrica i oceànica. Tots aquests factors han estat determinants en els canvis climàtics del passat de la Terra.

Hi ha diferents registres dels que hom pot extraure informació sobre les condicions climàtiques pretèrites del planeta, incloses la caracterització dels subsistemes del sistema climàtic i dels factors que modulen el clima local, regional i global. I d'això s'ocupa precisament la paleoclimatologia, de proporcionar dades sobre el clima i els mecanismes que han provocat canvis en les condicions climàtiques de la Terra en el passat, és a dir, de les èpoques prèvies als registres instrumentals de temperatura, precipitació i altres variables climàtiques. A més del interès que pot tenir per si mateix, el coneixement del comportament del sistema climàtic en front de modificacions en els forçaments durant el passat és rellevant per anticipar la seva resposta a noves modificacions, com ara el increment de la concentració atmosfèrica de CO_2 causat per l'ús extensiu de combustibles fòssils (Jansen et al., 2007).

Així doncs, parlem de canvis climàtics per referir-nos a canvis en l'estat del clima identificables per canvis en la variabilitat de les seves propietats persistents en el temps, sigui per causes naturals o induïdes per l'home (IPCC, 2007). De fet, el clima de la Terra ha canviat a escales de temps ben diferents, des de centenars o milers de milions d'anys (10^8-10^9) fins períodes de durada molt inferior. Degut a la brevetat relativa del registre instrumental, només els darrers 100 anys, és a dir un 10^{-7} de la història del planeta, l'estudi d'indicadors (en anglès *proxies*) de la variabilitat climàtica esdevé essencial per a conèixer el clima del passat (Kutz-

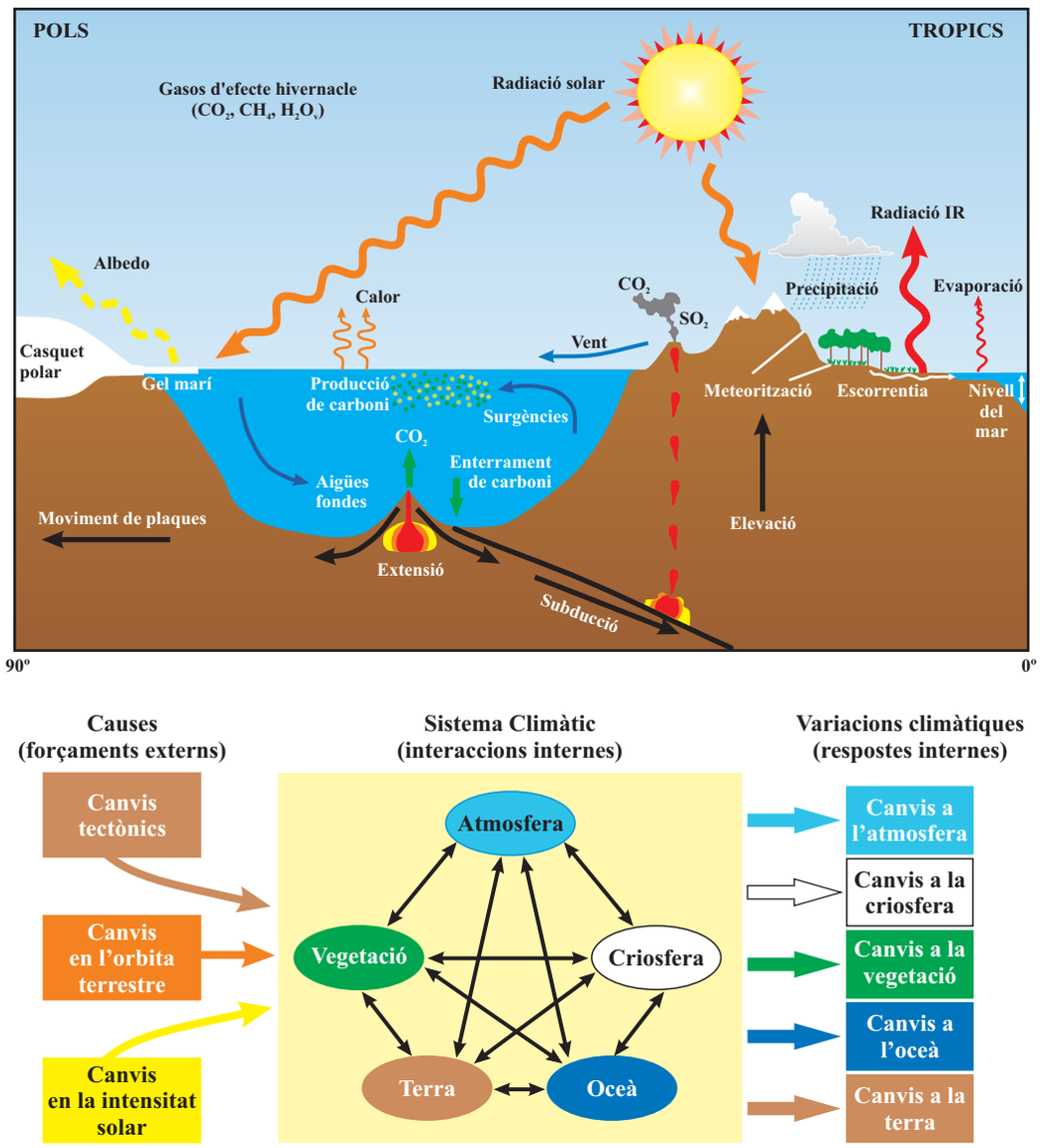

Figura 1.1. Representació esquemàtica del sistema climàtic, els seus components, les interacciones entre ells i els factors que poden generar variacions climàtiques (modificat de Ruddiman, 2001).

bach, 1976). En conseqüència, la paleoclimatologia és necessària per a assolir una visió de llarg recorregut de l'evolució del clima de la Terra, incloent el canvis climàtics més recents i també les projeccions del clima futur.

Davant l'evidència que el canvi climàtic induït per les activitats de l'home és ja inequívoc (IPCC, 2007), aquesta Tesi se centra en l'estudi de les condicions climàtiques i la variabilitat climàtica natural dels darrers 0.5 Ma, dins l'escala de temps que va des de centenars de milers d'anys (10^5) fins a milers i centenars d'anys (10^3-10^2).

1.2. Mecanismes dels canvis climàtics naturals

1.2.1. Escala orbital

Deixant de banda els canvis climàtics naturals induïts per la tectònica global, d'escales de 10^4-10^9 anys (Goodess et al., 1992), i assumint que la configuració de continents i oceans durant el darrer milió d'anys no ha canviat, la major part de la variabilitat climàtica d'alta freqüència del planeta, de 10^4-10^5 anys, està generada per oscil·lacions periòdiques i quasi-periòdiques en els paràmetres orbitals de la Terra que afecten a la quantitat i la distribució de l'energia solar incident en la superfície terrestre (Hays et al., 1976). Va ser l'astrofísic serbi Milutin Milankovitch qui desenvolupà la teoria astronòmica, coneguda com *teoria de Milankovitch*, segons la qual els canvis climàtics a escala glacial-interglacial es podien explicar per variacions en la insolació deguts als moviments cíclics de la Terra en girar al voltant del sol, així com els del seu propi eix, és a dir excentricitat, obliqüitat i precessió. També deia Milankovitch que aquests moviments es podien calcular astronòmicament i que presentaven unes periodicitats principals de 100.000, 41.000 i 23.000 anys, respectivament (Fig. 1.2).

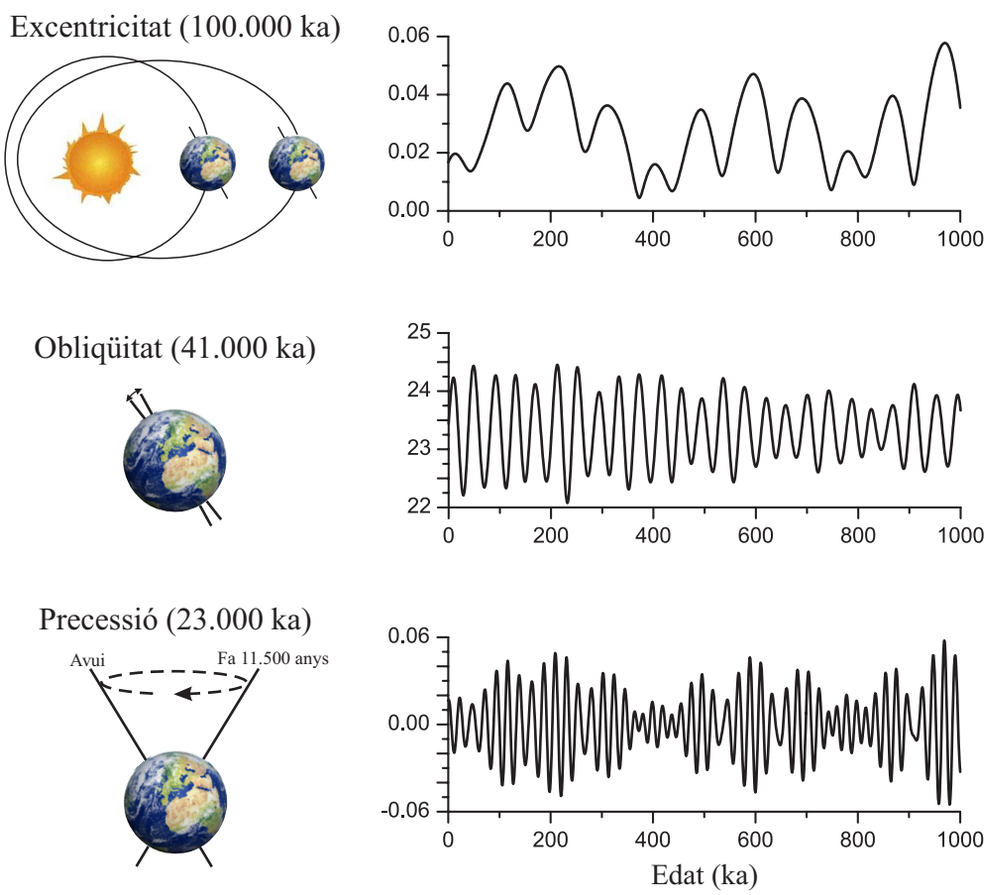

Figura 1.2. Variacions de les tres components de l'orbita terrestre que influeixen en la quantitat de radiació solar que arriba a la Terra calculades pel mètode de Laskar (1990) amb el programa Analyseries 1.1 (Paillard et al., 1996). L'excentricitat defineix la forma de l'el·lipse que la Terra descriu al voltant del sol, l'obliqüitat expressa la inclinació de l'eix de la Terra; i la precessió defineix el moviment a l'espai de l'eix de la Terra i condiciona l'ocurrència temporal de les estacions en relació amb l'orbita terrestre.

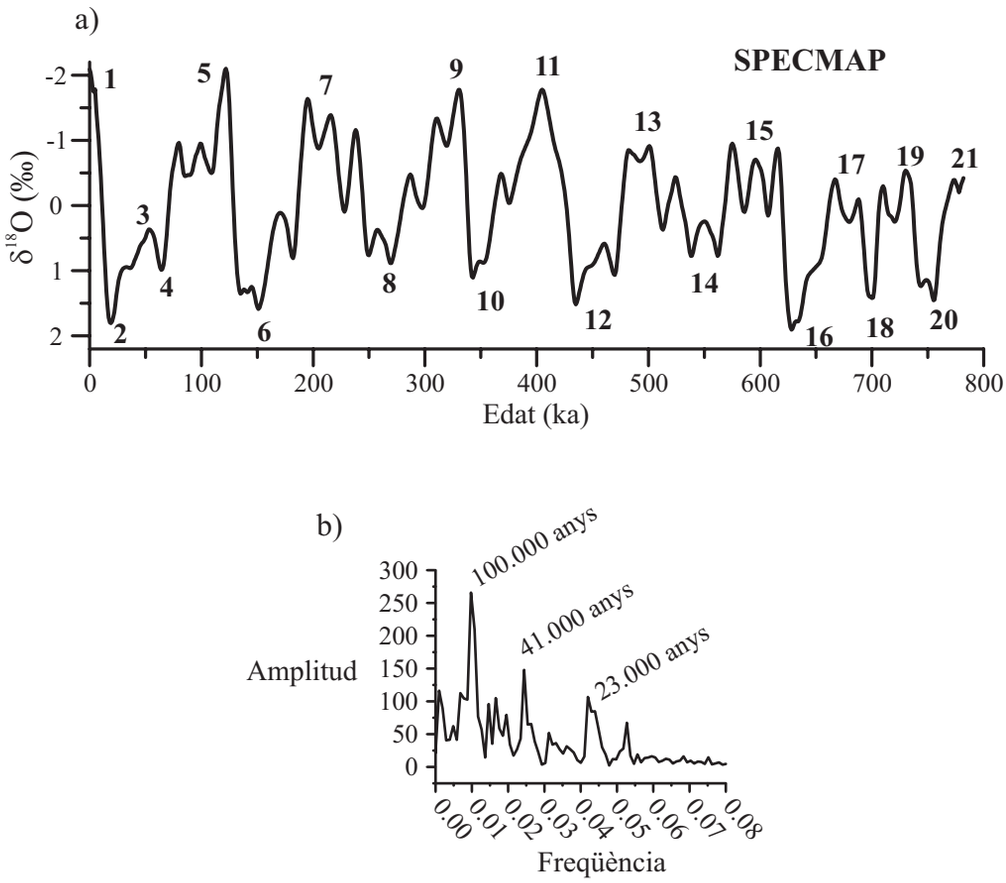

Figura 1.3. a) Corba SPECMAP de isòtops de l'oxigen en foraminífers planctònics que defineix els estadis isotòpics marins i diferencia els períodes glacials, amb números parells, dels interglacials, amb números senars (Imbrie et al., 1984; Martinson et al., 1987). El darrer període glacial és una excepció ja que contempla l'estadi isotòpic 2, el 3 i el 4; **b)** Anàlisi de freqüències de la corba SPECMAP on es poden observar les periodicitats de 100 ka, 41 ka i 23 ka, semblants a les obtingudes en la corba de la insolació.

Més endavant, l'anàlisi d'isòtops de l'oxigen (^{18}O i ^{16}O) en closques de foraminífers recuperats en testimonis de sediments marins mostrà unes oscil·lacions que presentaven ciclicitats similars a les estimades per la teoria de Milankovitch (Fig. 1.3), fet que dugué a afirmar que les variacions en la insolació degudes als moviments orbitals de la Terra exercien un control directe sobre el clima del planeta. Les diferències de pes atòmic fan que els isòtops de l'oxigen experimentin un fraccionament diferenciat dins l'aigua de mar, d'on les oscil·lacions en les seves proporcions relatives es relacionaren amb canvis en el volum de gel global, diferenciant així èpoques glacials i interglacials. La correlació entre diverses corbes de $\delta^{18}O$ d'arreu del mon facilità la generació d'una corba patró, la corba SPECMAP, emprada durant molt anys com a referència clau del passat climàtic del planeta (Imbrie et al., 1984; Martinson et al., 1987) (Fig. 1.3).

D'aleshores ençà, la ciclicitat glacial/interglacial ha estat observada en un gran nombre de registres d'arreu, abastant els darrers 740 ka en testimonis de gel (EPICA community members, 2004) i milions d'anys en sediments marins (Lisiecki i Raymo, 2005). Tot i els grans progressos realitzats les darreres dècades en la recerca del clima del passat a partir de regis-

tres sedimentaris marins, lacustres i terrestres, de gel, i espeleotemes principalment, cal remarcar que encara avui no es coneix amb certesa com ocorre el començament i l'acabament de les èpoques glacials (Ruddiman, 2003). De fet, la teoria de Milankovitch no explica per quina raó les transicions glacial/interglacial són sobtades mentre que les transicions interglacial/glacial són més graduals. Tampoc explica perquè les desglaciacions no sempre coincideixen amb els màxims d'insolació ni el fet que algunes desglaciacions presentin dues fases interrompudes per períodes de refredament marcat, amb tornada a condicions de caràcter glacial, com ara el Younger Dryas (YD) durant la Terminació I (Berger, 1990; Fairbanks, 1990; Sima et al., 2004; Broecker et al., 2010). Per altra banda, la descomposició de la corba de insolació segons les tres freqüències principals mostra que està modulada principalment per les variacions en la insolació produïdes per la precessió i l'obliqüitat (cicles de 23.000 i 41.000 anys), mentre que l'efecte de l'excentricitat és molt baix. En canvi, a l'extreure la influencia del senyal dels paràmetres orbitals del registre isotòpic marí hom observa que la banda dominant en el registre és la de l'excentricitat (cicle de 100.000 anys) (Imbrie et al., 1992; Imbrie et al., 1993) (Fig. 1.4).

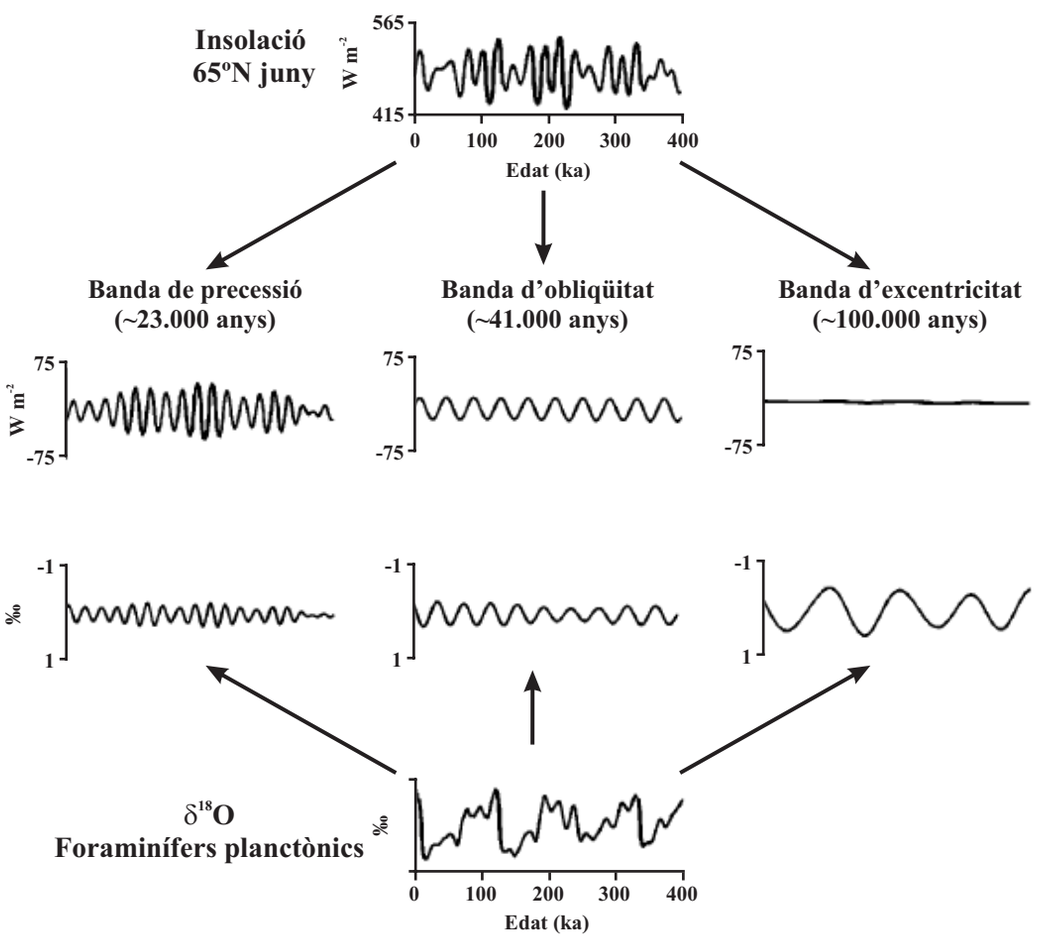

Figura 1.4. Partició de la corba de insolació d'estiu a 65ºN i del registre climàtic SPECMAP amb les seves components periòdiques dominants de precessió, obliqüitat i excentricitat al llarg dels darrers 400 ka (modificat de Imbrie et al., 1993). L'elevada correlació entre els cicles de $\delta^{18}O$ i els de radiació suggereixen una relació directa en les tres bandes. Cal remarcar que l'amplitud de la senyal del cicle de 100 ka és un ordre de magnitud més gran a la corba climàtica de $\delta^{18}O$ que a la de la radiació.

La teoria orbital de Milankovitch no explica, per tant, totes aquests qüestions, circumstància que fa necessari identificar altres mecanismes que intervinguin en la modulació dels canvis climàtics del planeta Terra. Podria tractar-se de mecanismes interns del propi sistema climàtic, els quals podrien generar processos de retroalimentació altament rellevants (Duplessy et al., 2005). Un d'aquests possibles mecanismes de retroalimentació podria ésser generat per les oscil·lacions de la concentració de CO_2 atmosfèric, les quals en el passat seguien els canvis de temperatura a la Antàrtida amb un retard d'uns quants centenars d'anys. De fet, les simulacions de les condicions climàtiques glacials només obtenen resultats realistes si es té en compte el paper del CO_2 atmosfèric (Jansen et al., 2007). També és ben coneguda la influència de la circulació termohalina global en la redistribució global d'energia mitjançant l'anomenada "cinta transportadora de calor" (en anglès *conveyor belt*) (Fig. 1.5) (Broecker i Denton, 1989). Canvis abruptes en la circulació termohalina haurien pogut exercir també un paper fonamental en les transicions climàtiques del cicle de 100 ka (Stocker, 1996). És també probable que processos relacionats amb el recobriment de gel a l'oceà Àrtic i amb els patrons de creixement i decreixement dels mantells de gel polars també hagin pogut generar retroalimentacions accentuadores de les fluctuacions climàtiques en el rang de 10^4-10^5 anys (Duplessy et al., 2005).

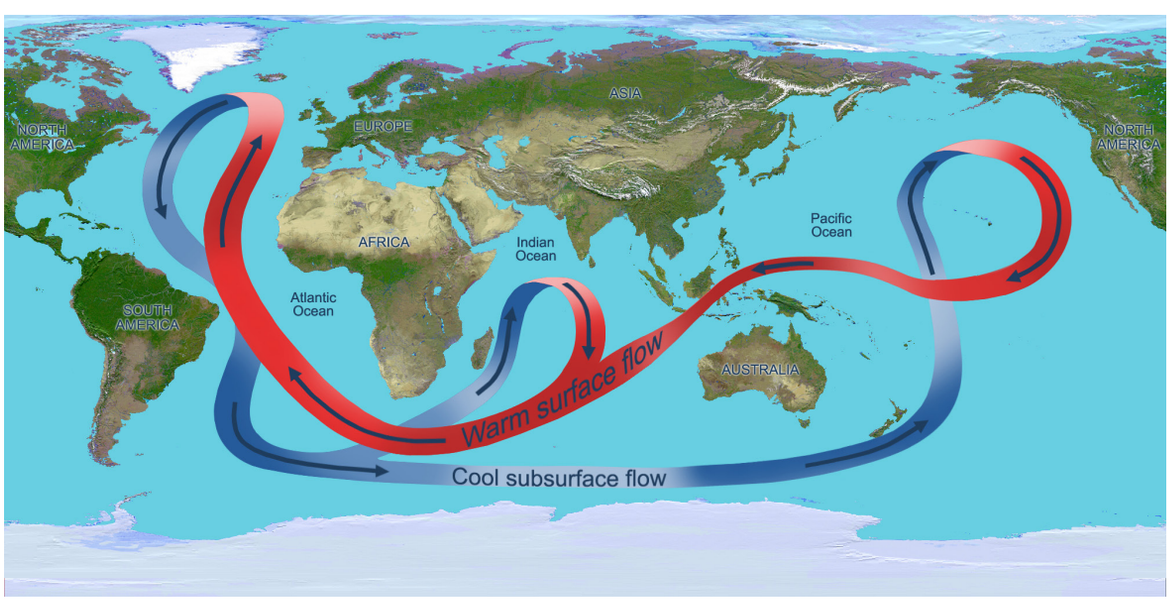

Figura 1.5. Esquema simplificat de la circulació termohalina global en el present. Les aigües calentes i salines superficials (en vermell) es mouen cap a l'Atlàntic Nord, on es produeix una important transferència de calor des de l'oceà cap a l'atmosfera que acaba afavorint la formació i l'enfonsament d'aigua densa que recircula cap als oceans Índic i Pacífic (en blau), on aflora per compensar el dèficit de sals superficial (Broecker i Denton, 1989). Aquesta circulació és un dels mecanismes més importants en la transferència de calor al nostre planeta i per això hom també la coneix amb el nom de cinta transportadora de calor (www.nasa.gov).

1.2.2. Escala mil·lenària

La teoria orbital de Milankovitch tampoc explica les variacions climàtiques d'alta freqüència, de 10^3 i 10^2 anys, com les observades inicialment en els testimonis de gel de Grenlàndia dintre del darrer període glacial (Dansgaard et al., 1993; Grootes et al., 1993), i posteriorment documentades en registres d'arreu del món (Voelker, 2002), fet que demostrà l'abast global dels canvis climàtics d'aquesta freqüència. Semblava obvi que aquests canvis havien d'estar relacionats amb interaccions no lineals dels components del sistema climàtic i amb reorganitzacions internes del mateix sistema climàtic i no pas amb variacions en la insolació.

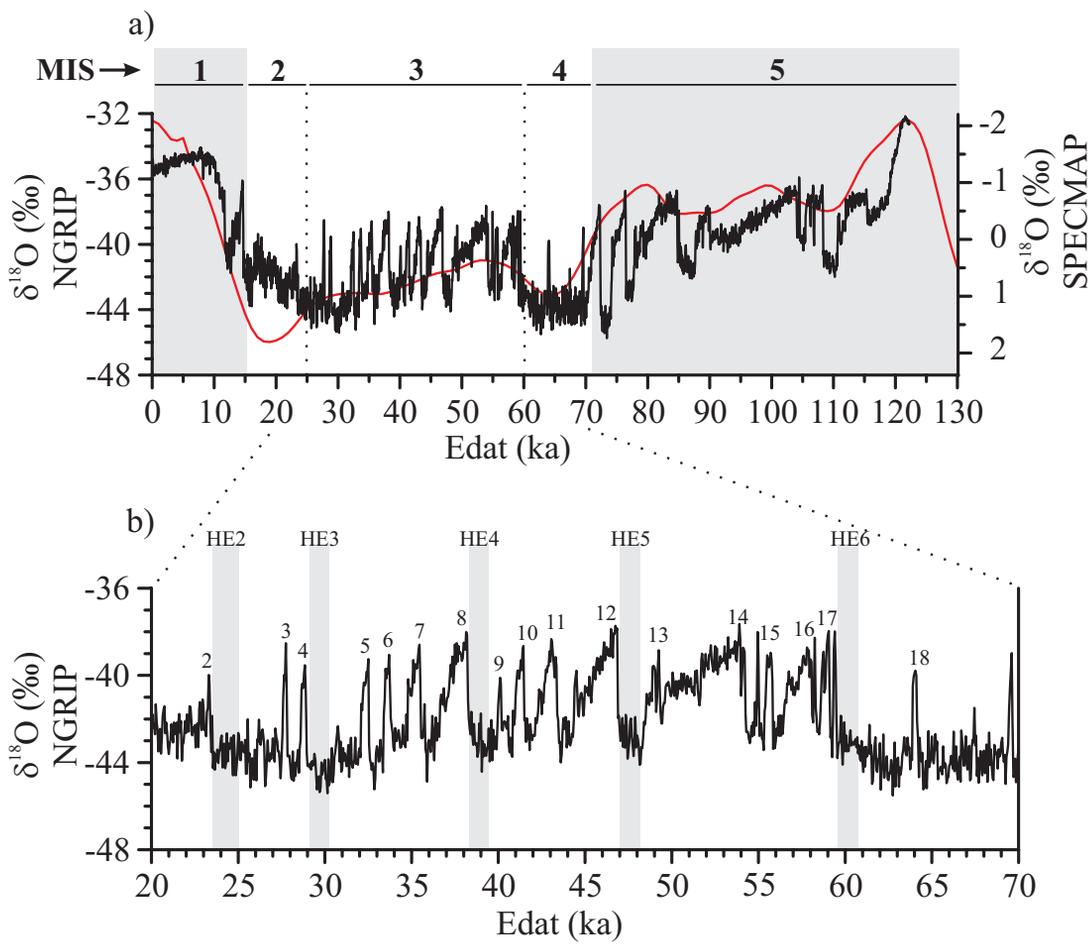

Figura 1.6. a) Registre de la relació dels isòtops de l'oxigen $\delta^{18}O$ mesurada al testimoni de gel NGRIP indicador de les temperatures atmosfèriques damunt Grenlàndia. L'escala de temps emprada és la resultant de la composició entre els models d'edat GICC05 pels darrers 60 ka (Svensson et al., 2008) i el ss09sea fins als 110 ka (Johnsen et al., 2001). En vermell es mostra la corba SPECMAP per referència (Martinson et al., 1987) i els estadis isotòpics marins (MIS) es mostren a la part superior. **b)** Ampliació de la corba $\delta^{18}O$ de NGRIP durant el MIS 3 on es poden observar les oscil·lacions climàtiques d'escala mil·lenària dels cicles de Dansgaard-Oeschger. Els números assenyalen la posició dels períodes càlids "interestadials" que separen períodes freds "estadials". La successió de diversos cicles de DO amb tendència al refredament que acaba en un HE, marcats en bandes grises, es coneix com a cicle de Bond.

Les oscil·lacions climàtiques d'escala mil·lenària observades a l'Atlàntic Nord dins el MIS3 s'anomenen cicles de Dansgaard-Oeschger (DO), els quals són formats per períodes freds, estadials o GS (de l'anglès *stadials* o *Greenland-stadials*), i períodes càlids, interestadials o GIS (de l'anglès *interstadials* o *Greenland-interstadials*). Sèries d'aquests cicles s'agrupen en cicles majors, o cicles de Bond (Bond et al., 1993), que mostren una marcada tendència general al refredament, la qual acaba en episodis extremadament freds anomenats *Heinrich events* (HE) (Heinrich, 1988) (Fig. 1.6). Els HE es caracteritzen per nivells terrígens grollers a les regions centrals de l'Atlàntic Nord entre 40ºN i 50ºN, designats amb les sigles IRD (de l'anglès *ice rafted detritus* o *debris*). Hom creu que els IRDs foren transportats fins aquestes latituds per flotilles d'icebergs alliberats massivament a rel de desestabilitzacions catastròfiques dels mantells polars de l'hemisferi nord (Bond et al., 1992; Broecker et al., 1992; Hemming, 2004). Posteriorment, hom va constatar, però, que durant els GS també hi havia hagut deposició de IRDs (Bond i Lotti, 1995). La injecció d'aigua dolça procedent de la fusió dels icebergs a l'Atlàntic Nord durant els HEs i els GS afectà la hidrologia de la regió (Vidal et al., 1997; Elliot et al., 2002), provocant una disminució en les taxes de formació d'Aigua Fonda de l'Atlàntic Nord (NADW, de l'anglès *North Atlantic Deep Water*), afectant així la circulació termohalina global (Broecker et al., 1985; Cortijo et al., 1995; Zahn et al., 1997). Aquestes observacions han dut a que alguns models climàtics considerin les entrades d'aigua dolça a l'Atlàntic Nord com el principal mecanisme generador de refredament dins de la variabilitat climàtica mil·lenària dels cicles de DO (Stocker et al., 1992).

Més ençà, la sincronització dels registres de metà de l'Antàrtida i Grenlàndia (Blunier et al., 1998; Blunier i Brook, 2001) mostrà que els períodes freds GS de Grenlàndia es corresponien amb escalfaments a l'Antàrtida (EPICA community members, 2006) (Fig. 1.7). Aquesta asincronia entre les dues regions polars fou explicada mitjançant un mecanisme anomenat "balancí bipolar" (de l'anglès *bipolar seesaw*) (Stocker i Johnsen, 2003) associat a la Circulació de Retorn Meridional (MOC, de l'anglès *Meridional Overturning Circulation*) a l'Atlàntic, la qual transporta calor cap a latituds altes, escalfant les regions septentrionals i refredant les meridionals (Crowley, 1992). Si la MOC es deturés, la calor deixaria d'ésser transportada de sud a nord de l'Atlàntic, cosa que causaria un refredament ràpid de Grenlàndia i un escalfament gradual de l'Antàrtida. En conseqüència, hom ha suggerit que el refredament durant els GS causat per l'alliberament d'icebergs també afectaria la temperatura a l'Antàrtida (Hemming, 2004).

L'origen d'aquestes oscil·lacions climàtiques mil·lenàries és, encara avui, controvertit. Hom l'ha relacionat amb forçaments en la insolació (Clemens, 2005), models de sobreacumulació i desestabilització dels grans mantells polars de gel continental (MacAyeal, 1995), canvis en el volum de gel (Siddall et al., 2006b), i la variabilitat solar (Bond et al., 2001), probablement potenciats per processos de ressonància estocàstica del sistema acoblat oceà-atmosfera (Ganopolski i Rahmstorf, 2001).

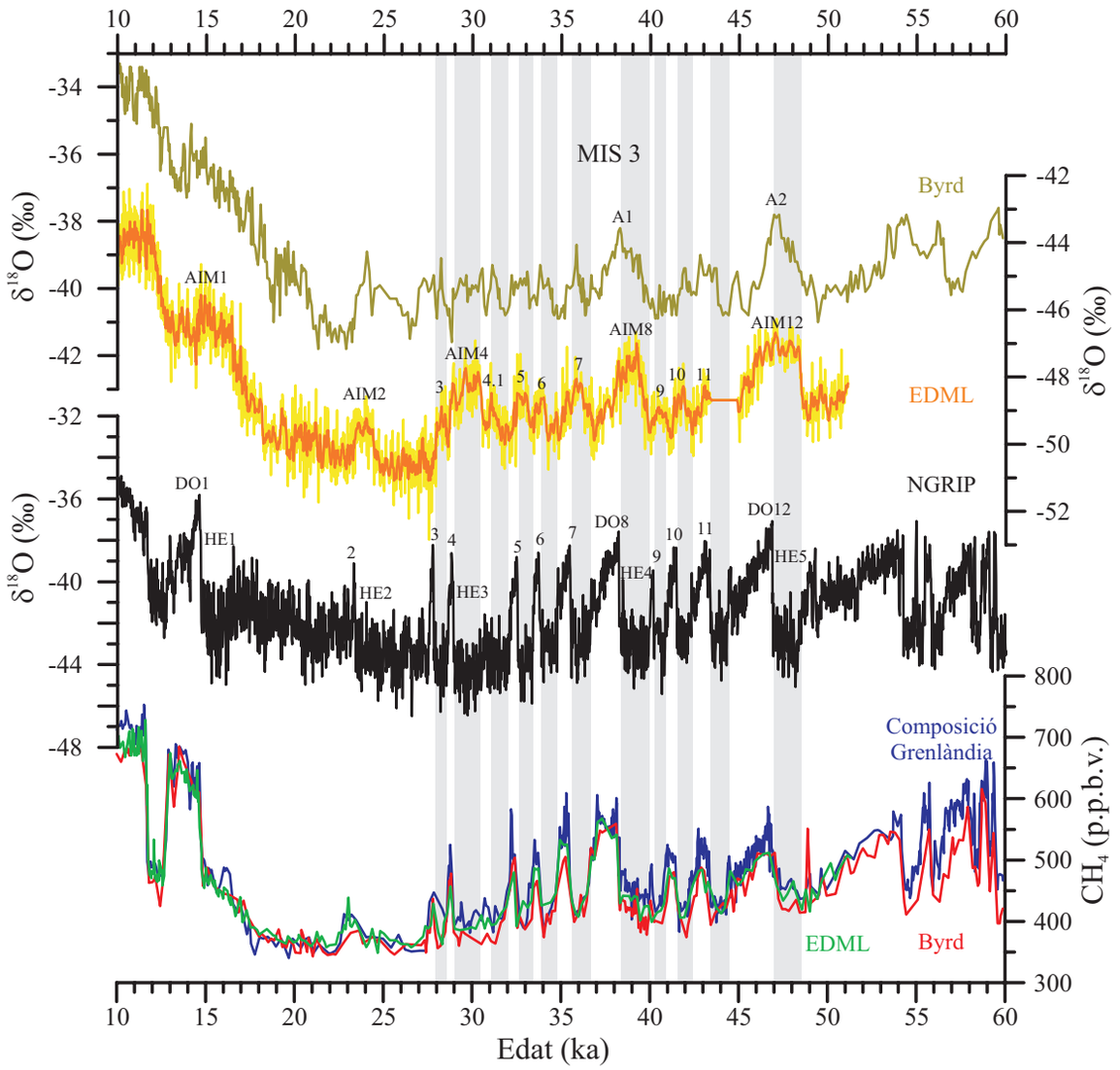

Figura 1.7. Sincronització dels registres de $\delta^{18}O$ de gel de l'Antàrtida, BYRD i EDML, i de Grenlàndia, NGRIP, a través de les corbes de metà (CH_4) i amb el model d'edat GICC05 entre 10 i 60 ka. Evidencia que cada escalfament a l'Antàrtida és sincrònic amb els períodes freds o "estadials" a Grenlàndia, marcats amb les barres grises, la qual cosa demostra l'acoblament en la variabilitat climàtica entre l'hemisferi nord i el sud durant el MIS 3 (modificat d'EPICA community members, 2006).

La identificació a l'Holocé, l'interglacial en que vivim, d'un seguit d'oscil·lacions climàtiques d'abast global, tot i que amb diferències d'uns registres a uns altres, ha canviat la percepció prèvia de la comunitat científica en el sentit que els períodes interglacials eren climàticament estables (Mayewski et al., 2004). Tot i que aquestes oscil·lacions climàtiques són d'amplitud menor que les observades en els períodes glacials, probablement degut a la mida més petita dels mantells polars, sembla que mostrarien una ciclicitat semblant, de 1-2 ka, fet que implicaria que els cicles climàtics d'escala mil·lenària no estarien forçats per inestabilitats dels mantells polars sinó que serien la resposta a la modulació del sistema climàtic per un cicle de 1-2 ka omnipresent (Bond et al., 1999).

Els efectes de la variabilitat climàtica d'escala mil·lenària descrits a l'Atlàntic Nord també afectaren la conca occidental del Mediterrani. Diversos registres han mostrat la influència dels canvis produïts en el clima i en la circulació oceànica i atmosfèrica de l'Atlàntic Nord damunt les condicions climàtiques de la regió mediterrània occidental, on generaren fluctuacions en la circulació termohalina superficial, intermèdia i profunda, en les temperatures de l'aigua superficial, en la productivitat oceànica, en les condicions d'humitat i aridesa a les terres circumdants i en l'aportació de material terrígen per via atmosfèrica i fluvial (Rohling et al., 1995 i 1998b; Allen et al., 1999; Cacho et al., 2000, 2002 i 2006; Watts et al., 2000; Roucoux et al., 2001; Combourieu Nebout et al., 2002; Sánchez Goñi et al., 2002; Perez-Folgado et al., 2003; Martrat et al., 2004; Moreno et al., 2004 i 2005; Sierro et al., 2005 i 2009; Frigola et al., 2007, 2008 i 2012; Fletcher i Sánchez Goñi, 2008; Fletcher et al., 2010; Toucanne et al., 2012). Els treballs citats demostren l'alta sensibilitat de la conca occidental del Mediterrani front els canvis abruptes d'escala mil·lenària en el sistema climàtic global. De fet, hi ha estudis que assenyalen la interacció de l'aigua de sortida del Mediterrani amb la circulació termohalina global a l'Atlàntic Nord com un element determinant en les desestabilitzacions i re-estabilitzacions de la MOC característiques de la variabilitat climàtica d'escala mil·lenària durant l'últim període glacial (Reid, 1979; Bigg i Wadley, 2001; Bigg et al., 2003; Rogerson et al., 2006; Voelker et al., 2006).

1.3. Oscil·lacions del nivell del mar

Les variacions globals del nivell del mar són indicadores de canvis majors en el volum de gel global, és a dir, del creixement i decreixement dels mantells polars en el decurs dels cicles glacials. En conseqüència, l'estudi de la variabilitat del nivell del mar ha estat sempre lligat a l'estudi dels canvis climàtics del passat. Paral·lelament als canvis climàtics d'escala orbital de 100 ka, el nivell del mar durant el Plistocè Superior ha sofert oscil·lacions de l'ordre de 120 m de magnitud (Imbrie et al., 1992; Siddall et al., 2006a). Hom a abordat les reconstruccions dels paleo-nivells del mar generalment des de dos punts de vista. Primer, basant-se en marcadors de la posició del nivell del mar a la costa, com ara plataformes d'abrasió per l'onatge, sistemes dunars, formacions coral·lines, espeleotemes i altres dipòsits que es formen en relació directa amb la posició del nivell del mar (Dabrio et al., 2011). Una de les febleses d'aquesta aproximació és la discontinuïtat dels registres (Siddall et al., 2006a). Segon, basant-se en la interpretació dels registres de $\delta^{18}O$ (cf. Aptat. 2.2). El isòtop més lleuger, ^{16}O, s'evapora preferentment des de les aigües oceàniques i és precipitat en la neu. És per això que el registre de $\delta^{18}O$ en closques de foraminífers és sensible als canvis del nivell del mar, tot i que també és afectat per variacions isotòpiques dintre dels oceans i per la temperatura de l'aigua en que han viscut els foraminífers (Lea et al., 2002; Waelbroeck et al., 2002). Els registres isotòpics són sovint continus i en alguns casos permeten resoldre escales de milers d'anys, per la qual cosa hom els ha emprat com estàndards en cronostratigrafia marina (Emiliani, 1955; Martinson et al., 1987). A la figura 1.8 es mostren alguns dels registres del

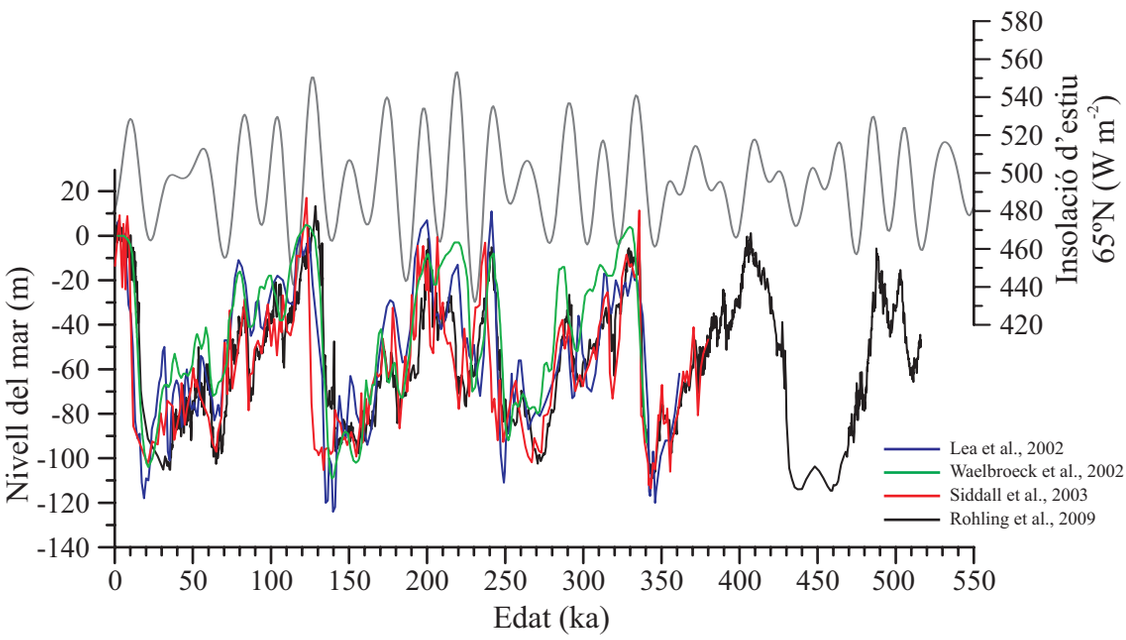

Figura 1.8. Reconstruccions del nivell del mar dels darrers 550 ka basades en els registres isotòpics de $\delta^{18}O$ en foraminífers planctònics i bentònics (Lea et al., 2002; Waelbroeck et al., 2002; Siddall et al., 2003; Rohling et al., 2009b). Cal notar l'elevada correlació amb la corba de insolació d'estiu a 65ºN.

nivell del mar obtinguts els darrers anys a partir de l'estudi dels isòtops de l'oxigen en foraminífers bentònics i planctònics. Tots mostren una clara tendència definida per la ciclicitat orbital de 100 ka, essent les amplituds de canvis del nivell del mar entre condicions glacials i interglacials molt similars. Tot i així, hi ha diferències notables entre els registres pel que fa a l'amplitud dels canvis en certs períodes, com ara el Darrer Màxim Glacial (LGM, de l'anglès *Last Glacial Maximum*) o el MIS 3, i també pel que fa a la cronologia. Aquestes diferencies es deuen principalment a limitacions inherents als mètodes de reconstrucció del nivell del mar, com ara l'efecte de la temperatura en els registres de $\delta^{18}O$, i també a les dificultats per obtenir cronologies més precises.

En relació amb les oscil·lacions del nivell del mar d'escala mil·lenària, hom ha dedicat molta atenció a l'últim període glacial i, més concretament, al ja esmentat MIS 3, període entre 60 i 25 ka, caracteritzat pels canvis climàtics abruptes dels cicles de DO. Com es comentava a l'apartat anterior (cf. Aptat. 1.2.2), l'entrada d'aigua dolça per la fosa massiva d'icebergs a l'Atlàntic Nord podria ser un mecanisme directe per a la desestabilització de la MOC, fet que podria causar el refredament de la regió de Grenlàndia. Així doncs, a l'hora d'establir el paper dels mantells polars en la variabilitat climàtica d'escala mil·lenària és crucial entendre si hi participen de forma activa com a mecanismes desencadenants o amplificadors o si, simplement, responen de manera passiva (Siddall et al., 2008).

Són vàries les reconstruccions del nivell del mar a partir del registre isotòpic de l'oxigen en closques de foraminífers que mostren característiques comuns durant el MIS 3. Per una

banda, s'observa una diferència en el nivell del mar d'uns 20 m entre el inici i el final del MIS 3 i, per una altra banda, totes les reconstruccions mostren quatre oscil·lacions del nivell del mar d'escala mil·lenària (Siddall et al., 2008) (Fig. 1.9). No hi ha, però, consens en la cronologia d'aquestes fluctuacions d'alta freqüència. Mentre uns autors les relacionen amb els canvis de temperatura observats a l'Antàrtida (AIM1-AIM4) (Fig. 1.7) (Shackleton et al., 2000; Siddall et al., 2003; Rohling et al., 2008), altres les vinculen als períodes càlids de major durada observats a l'Atlàntic Nord (GIS16, 14, 12 i 8) (Arz et al., 2007; Sierro et al., 2009).

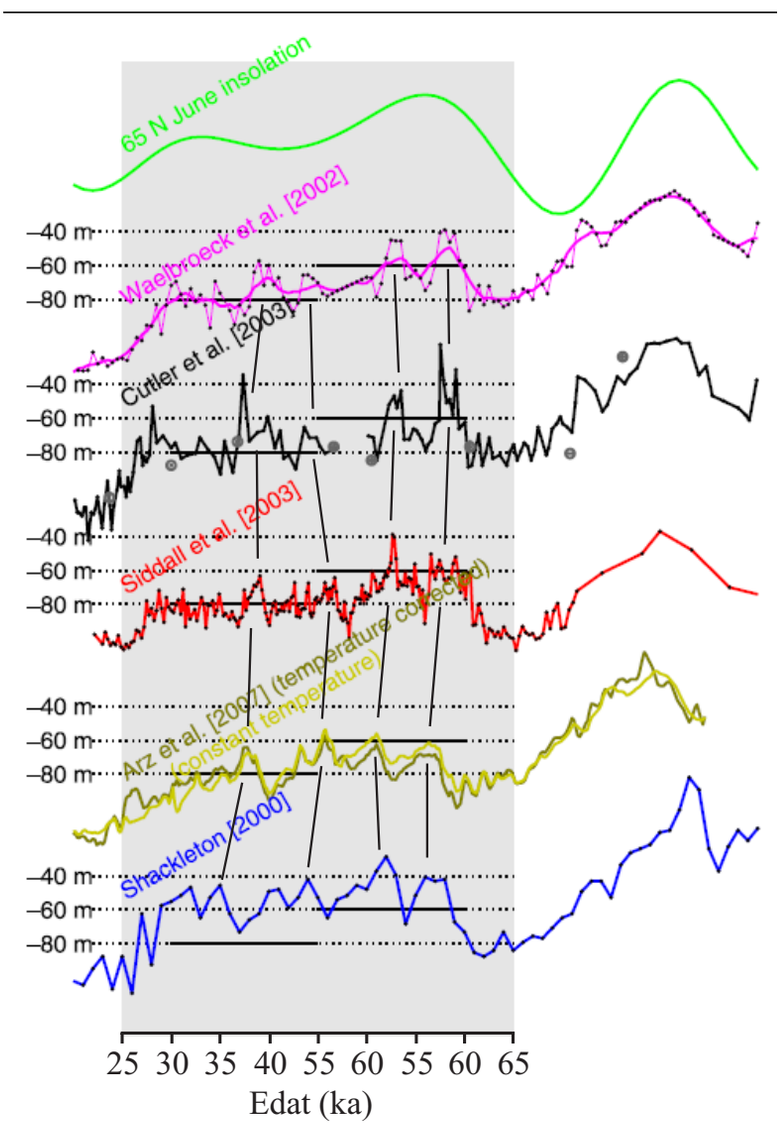

Figura 1.9. Diverses reconstruccions del nivell del mar durant el MIS 3 comparades amb la corba d'insolació d'estiu a 65ºN (Shackleton, 2000; Waelbroeck et al., 2002; Cutler et al., 2003; Siddall et al., 2003; Arz et al., 2007). Totes les reconstruccions mostren que en promig el nivell del mar era 20 m superior al començament del MIS 3, i totes enregistren quatre oscil·lacions principals del nivell del mar d'escala mil·lenària d'uns 20-30 m de magnitud (modificat de Siddall et al., 2008).

Aquestes discrepàncies assenyalen orígens diferents de la font d'aigua que produí els ascensos del nivell del mar, sigui de la fusió del mantell polar antàrtic o de l'Atlàntic Nord (Clark et al., 2007). Algunes simulacions indiquen que ambdues contribucions podrien ésser similars (Rohling et al., 2004). Mentre es treballa per resoldre les incògnites sobre la cronologia de les oscil·lacions mil·lenàries del nivell del mar i la influència d'un o altre mantell polar, hom no ha pogut encara identificar en cap registre oscil·lacions del nivell del mar determinades per la ciclicitat dels DO, tal i com caldria esperar de l'acoblament entre l'Antàrtida i Grenlàndia (EPICA community members, 2006).

1.4. Objectius de la Tesi

La motivació per aquesta Tesi arrenca de la creixent evidència que la conca occidental del Mediterrani havia estat altament sensible als canvis climàtics observats a l'Atlàntic Nord. El primer objectiu general de la Tesi era avaluar la sensibilitat del Mediterrani occidental als canvis climàtics d'escala orbital i mil·lenària a través de l'estudi de les fluctuacions en l'aportació de sediments terrígens. Per a concretar aquest objectiu en uns materials d'estudi específics hom seleccionà dues localitzacions d'especial interès al Mediterrani nordoccidental, el marge progradant del Golf de Lleó i el sistema contornític profund de Menorca, per cadascun dels quals es definiren objectius específics.

Resumidament, els objectius d'estudi en el marge del Golf de Lleó han estat:

1) Avaluació de la variabilitat de les aportacions fluvials al marge continental a escala orbital en relació amb els canvis del nivell del mar associats als cicles glacials/interglacials dels darrers 500 ka.

2) Establiment d'una cronostratigrafia del marge que permetés clarificar la ciclicitat de les unitats seismostratigràfiques descrites prèviament.

3) Comprovació de la influència dels canvis de nivell del mar d'escala orbital damunt la sedimentació en el marge, a fi i efecte d'escatir els mecanismes de sedimentació principals i la seva variació al llarg del temps.

4) Avaluació de les fluctuacions de les aportacions terrígenes al marge a escala mil·lenària durant el darrer període glacial, i especialment el MIS 3, per a identificar possibles oscil·lacions del nivell del mar relacionades amb els canvis climàtics abruptes descrits a l'Atlàntic Nord, i també per avaluar la possible existència d'oscil·lacions del nivell del mar en la banda dels cicles de DO.

També de manera resumida, els objectius d'estudi en el sistema contornític de Menorca han estat:

1) Avaluació de la variabilitat de les aportacions terrígenes al fons de la conca occidental del Mediterrani en els darrers 50 ka a escales orbital i mil·lenària.

2) Determinació de la resposta del sistema de formació d'aigua fonda de la conca occidental del Mediterrani front els canvis climàtics a l'Atlàntic Nord durant el darrer període glacial per la intervenció de mecanismes de teleconnexió entre latituds altes i intermèdies.

3) Avaluació de la sensibilitat del sistema de formació d'aigua fonda del Mediterrani occidental davant oscil·lacions climàtiques al llarg del període interglacial de l'Holocè.

2. Àrea d'estudi. El Mar Mediterrani

2.1. Context geològic i fisiogràfic

El Mediterrani és una regió de convergència i interacció, l'única del món on tres continents conflueixen i on llur interacció ha generat una geologia i una geografia física distintives. El Mediterrani ocupa la part més occidental del cinturó orogènic Alpí-Himalaià que va des de la Península Ibèrica fins a Nova Zelanda. La història tectònica de la regió mediterrània és llarga i complexa. Podem considerar que s'inicià amb la creació del Mar de Tetis i el trencament del supercontinent Pangea fa uns 250 Ma (Fig. 2.1). Un segon esdeveniment fonamental fou la col·lisió de les plaques africana i europea fa uns 40 Ma, la qual comportà l'escanyament del Mar de Tetis (Fig. 2.2) (Stampfli and Borel, 2002; Meulenkamp and Sissingh, 2003).

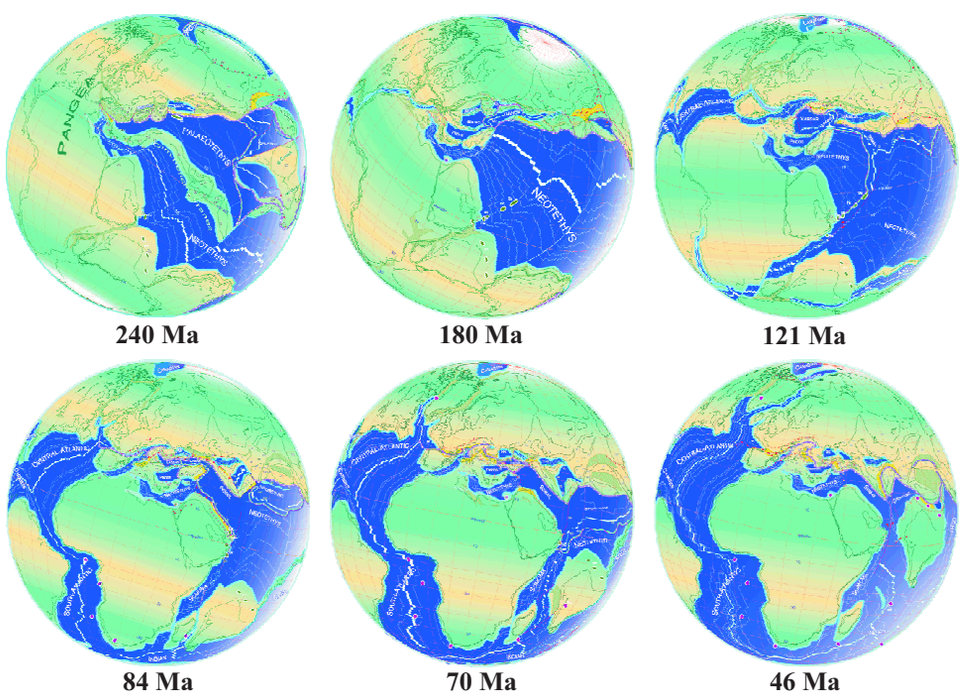

Figura 2.1. Evolució tectònica del supercontinent Pangea i del mar del Tetis entre 240 i 46 Ma (modificat de Stampfli and Borel, 2002).

La connectivitat del Mar de Tetis amb l'oceà global s'anà reduint paulatinament, mantenint-se només per passadissos marins a l'est i a l'oest (Mather, 2009). El primer passadís en tancar-se fou el més oriental, el qual connectava el Mar de Tetis amb l'Oceà Índic, fet que afectà els patrons de circulació oceànica tot i ocasionant, probablement, un refredament global (Miller et al., 1991). D'aleshores ençà l'antic Mar de Tetis passarà a ésser el Mar Mediterrani. Després, es va anar tancant també el passadís occidental degut a la interacció entre processos tectònics i glacio-eustàtics (Garcés et al., 1998; Krijgsman et al., 1999b). El tancament del passadís occidental provocà que el Mar Mediterrani quedés parcialment o totalment aïllat de l'oceà global durant el Messinià (6-5 Ma), situació que originà l'anomenada Crisi de Salinitat del Messinià del Mediterrani. Durant aquest període d'aïllament, el Medi-

terrani es dessecà gairebé del tot per evaporació, amb la conseqüent davallada del nivell del mar i la deposició a les àrees centrals de la conca de capes d'evaporites ben gruixudes (Hsü et al., 1973; Krijgsman et al., 1999a). El passadís occidental, la connexió entre el Mediterrani i l'Atlàntic, es tornà a reobrir al Pliocè, assolin-se així la configuració actual del Mar Mediterrani.

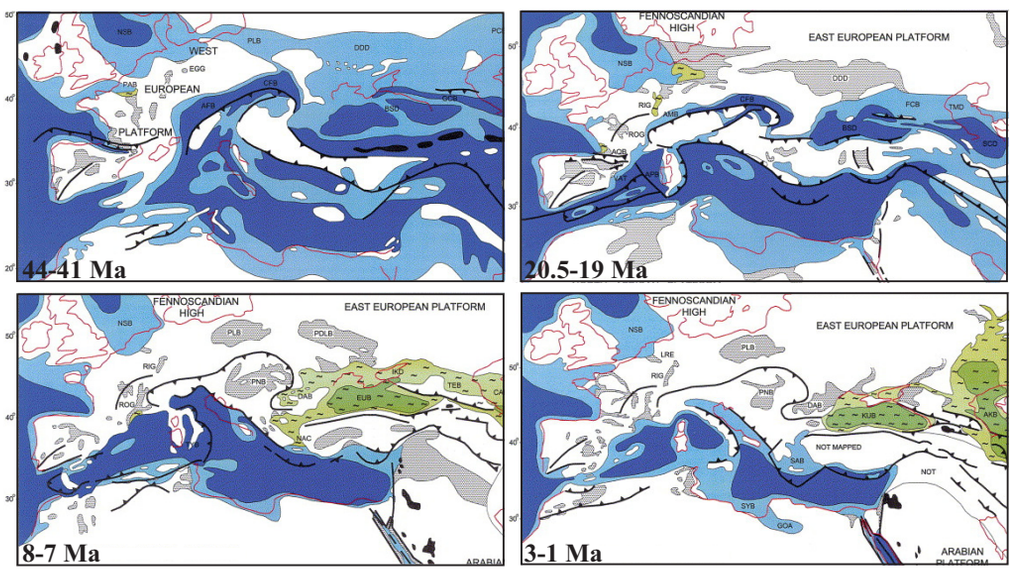

Figura 2.2. Evolució geològica del mar Mediterrani entre 44 i 1 Ma (modificat de Meulenkamp and Sissingh, 2003).

L'evolució geològica de la conca occidental del Mediterrani en els darrers 25 Ma està relacionada amb la disminució de la convergència entre les plaques africana i europea durant l'Oligocè Superior, la qual cosa permeté el inici de processos extensius i de rifting a l'àrea ibèrica i del sud de França. L'obertura d'aquesta àrea, la qual anà acompanyada de la rotació dels blocs del Promontori Balear, Còrsega i Sardenya, generà el canal de València, el Golf de Lleó i el Mar Ligur (Rosenbaum et al., 2002) (Fig. 2.3).

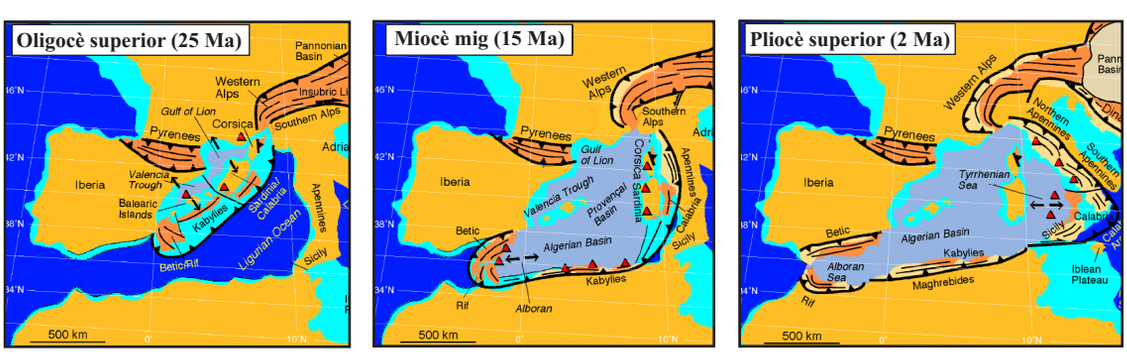

Figura 2.3. Evolució de la conca occidental del Mediterrani entre 25 i 2 Ma (modificat de Rosenbaum et al., 2002).

El resultat de tota aquesta evolució geològica és el Mediterrani actual, una conca semitancada vorejada per sistemes muntanyosos derivats de la col·lisió entre les plaques africana i europea. És precisament aquest context tectònic regional el que fa que la majoria de rius que vessen al Mediterrani siguin conques de drenatge força petites i que el seu recorregut sigui curt, amb l'excepció principal del riu Nil, de caràcter exogen. Les conques de drenatge més extenses són les dels rius Roine (95.590 km^2), Ebre (84.230 km^2) i Po (70.090 km^2). Els intercanvis amb l'Oceà Atlàntic es produeixen només a través de l'estret de Gibraltar, de només 14,4 km d'amplada i 280 m de profunditat a la part central, a l'Alt de Camarinal. El Mar Mediterrani està format per un seguit de subconques amb característiques fisiogràfiques contrastades i, per tant, amb fondàries i règims hidrològics força variables, les quals es poden agrupar en una conca oriental i una conca occidental separades per l'estret de Sicilia, amb una fondària mitjana d'uns 330 m. Les diferents subconques mediterrànies són relativament ben connectades entre elles, excepte la perifèrica del Mar Negre. La profunditat mitjana del Mediterrani és d'uns 1.500 m, mentre que la màxima depassa els 4.200 m a la conca oriental i no arriba als 3.400 m a la conca occidental (Tomczak and Godfrey, 2003).

2.2. Context climàtic

El Mediterrani, situat entre els 30º i 45ºN, ocupa una zona de transició que rep les influències continental d'Euràsia, àrida del nord d'Àfrica i oceànica de l'Atlàntic. Així doncs, des de el punt de vista climàtic, està afectada pel règim climàtic subtropical i monsònic que s'estén al nord d'Àfrica, i pel règim climàtic temperat propi d'Europa central i del nord. Dins el sistema atmosfèric global, està influenciat pels sistemes subtropicals d'alta pressió al sud, i pel cinturó de vents de l'oest (*westerlies*) al nord. Els estius de la regió mediterrània són càlids i secs pel desplaçament cap al nord de les masses d'aire subtropicals, mentre que els hiverns són temperats i més humits (sobretot al litoral septentrional) degut al desplaçament cap al sud del sistema d'altes pressions subtropical, la qual cosa permet una major entrada cap a la regió mediterrània de les masses d'aire humides procedents de l'Atlàntic (Fig. 2.4) (Barry and Chorley, 1998; Harding et al., 2009).

Aquesta ubicació a la franja latitudinal d'acomodació de dos tipus de clima tan diferents fa que la regió mediterrània sigui altament sensible a les variacions que es produeixen en qualsevol d'ells. Un fet no pas poc rellevant és que cadascun d'aquest tipus de règim climàtic afecta paràmetres diferents al Mediterrani. Així, el règim climàtic subtropical afecta principalment el balanç hídric, mentre que el règim climàtic temperat de l'oest determina el refredament de les ribes septentrionals de la conca. Tot plegat fa que el Mediterrani sigui un lloc ideal per a estudiar els impactes i l'acoblament relatiu dels canvis que puguin experimentar ambdós tipus de climes (Rohling et al., 2009a). I això també val per a etapes pretèrites de la història climàtica de l'hemisferi nord. Finalment, les fluctuacions en la influència d'aquests dos tipus de règims climàtics, i l'efecte derivat de la pròpia presència del Mar Mediterrani,

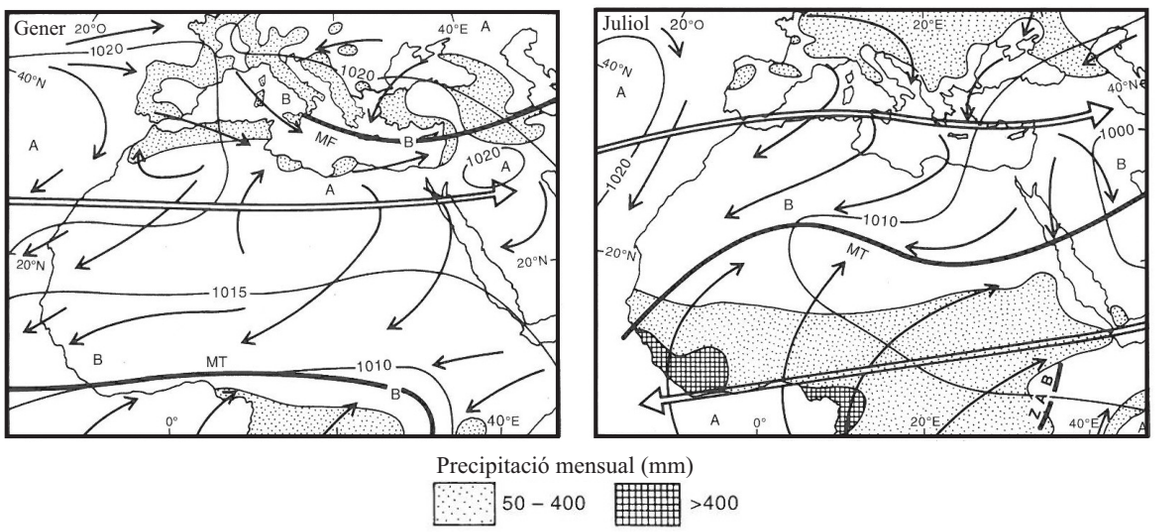

Figura 2.4. Circulació atmosfèrica general a la franja latitudinal que abasta des del sud d'Europa fins l'Àfrica equatorial i que inclou el Mediterrani. Els contorns, les fletxes i les àrees marcades amb relleu mostren la distribució de la pressió superficial, els vents i la precipitació, respectivament, al gener i al juliol. També es mostren les posicions mitjanes dels vents subtropicals de l'oest i del corrent oriental tropical en raig, amb el tàlveg monsònic (MT), el front mediterrani (MF) i el límit aeri del Zaire (ZAB) (modificat de Barry and Chorley, 1998).

fan que la regió sigui vulnerable a canvis climàtics de gran escala (Bolle, 2003; Luterbacher et al., 2006).

El mode principal de variabilitat climàtica al Mediterrani ve expressat per l'anomenada Oscil·lació del Mediterrani (MO, de l'anglès *Mediterranean Oscillation*), que es caracteritza per un patró de teleconnexió amb anomalies de precipitació i de pressió oposades entre les conques occidental i oriental (Conte et al., 1989; Maheras et al., 1999).

De tota manera, la climatologia de la conca occidental del Mediterrani està modulada per la influència de l'Oceà Atlàntic. De fet, hi ha una certa correlació estadísticament significativa entre la MO i l'Oscil·lació de l'Atlàntic Nord (NAO, de l'anglès *North Atlantic Oscillation*) (Fig. 2.5), la qual relaciona valors negatius de l'índex de la NAO amb condicions humides a la conca occidental del Mediterrani. En canvi, la relació de la NAO amb la conca oriental és molt més feble (Maheras et al., 1999; Dünkeloh and Jacobeit, 2003).

Un altre mode de variabilitat d'hivern estadísticament significatiu és el patró de Circulació Meridional del Mediterrani (MMC, de l'anglès *Mediterranean Meridional Circulation*) que descriu els processos de ciclogènesi regional que ocorren a la part nord del Mediterrani degut a l'entrada d'aire del nord fred i relativament sec. Aquesta ciclogènesi té una gran influència en la precipitació de les regions nord-orientals i sud-centrals del Mediterrani (Dünkeloh and Jacobeit, 2003). A la Península Ibèrica la precipitació d'hivern està fortament relacionada amb la variabilitat de la NAO, però més cap a l'est, a sotavent de la influència Atlàntica, aquesta relació és molt feble, apreciant-se en el seu lloc una certa correlació amb l'Oscil·lació

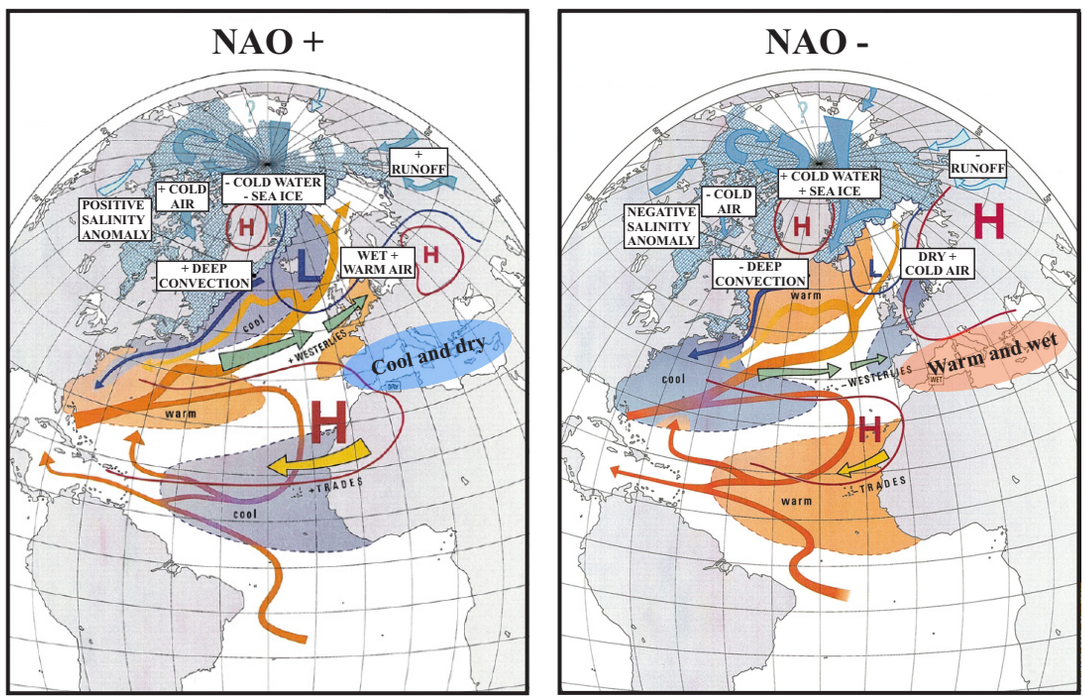

Figura 2.5. Esquema del principal mode de variabilitat climàtica d'hivern a la regió de l'Atlàntic Nord coneguda com Oscil·lació de l'Atlàntic Nord (NAO) (modificat de Wanner et al., 2001). L'índex de la NAO representa la diferència de pressió entre l'anticicló de les Açores i la baixa de Islàndia. Els valors positius de la NAO són deguts a un gradient de pressió latitudinal notable, un anticicló molt potent i una baixa molt profunda, situació que genera vents de l'oest molt forts que provoquen condicions d'hivern temperades i humides al nord d'Europa i condicions fredes i seques al Mediterrani. Els valors negatius de la NAO estan relacionats amb un anticicló i una baixa febles, i per tant amb un gradient de pressió latitudinal escàs, que dona lloc a vents més fluixos que causen condicions d'hivern humides i temperades al Mediterrani i hiverns freds al nord d'Europa.

del Sud "El Niño" (ENSO, de l'anglès *El Niño Southern Oscillation*) (Rodó et al., 1997). De fet, per explicar la precipitació de la conca occidental del Mediterrani, fortament lligada als processos de ciclogènesi deguts a l'entrada d'aire fred del nord, hom ha desenvolupat un nou índex, l'Oscil·lació del Mediterrani Occidental (WeMO, de l'anglès *Western Mediterranean Oscillation*) (Fig. 2.6). La WeMO, expressa l'anomalia de pressió que hi ha entre l'anticicló de les Açores i la baixa del Mar Ligur, prenent com a punts d'observació San Fernando, a Cadis, i Pàdua, al nord de Itàlia (Martín-Vide and Lopez-Bustins, 2006). Així doncs, valors negatius de la WeMO es correlacionen amb períodes de més precipitació a la façana oriental de la Península Ibèrica, relacionats amb una major incidència de les tempestes de llevant durant els mesos d'hivern (Martín-Vide and Lopez-Bustins, 2006; Lopez-Bustins et al., 2008). A més, al Mediterrani no són infreqüents els episodis de pluges fortes i inundacions, ni les tempestes amb ventades fortes, sovint relacionats amb els processos de ciclogènesi en que l'orografia i la massa d'aigua rescalfada del Mar Mediterrani hi juguen un paper primordial (Llasat, 2009). De fet, aquests fenòmens es podrien considerar característics del clima mediterrani. La interacció entre la circulació atmosfèrica i la complexa orografia de la regió mediterrània és l'origen de molts vents locals, com ara al Mediterrani nordoccidental, on vents com la Tramuntana i el Mestral poden bufar durant bona part de l'hivern tot i generant

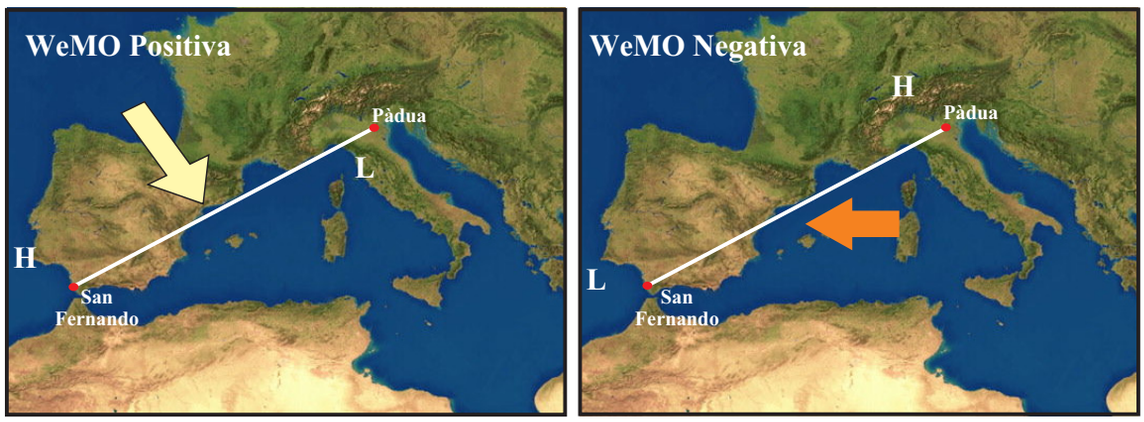

Figura 2.6. Esquema de l'oscil·lació atmosfèrica coneguda com Oscil·lació del Mediterrani Occidental (WeMO), la qual representa les diferències de pressió entre el registre de Pàdua, al nord de Itàlia, i el de San Fernando, a Cadis, al sud de la península Ibèrica. Aquest índex és va crear per a poder explicar la precipitació de la façana est de la Península Ibèrica, escassament relacionada amb la NAO. Els valors negatius de la WeMO es correlacionen amb períodes de més precipitació a la façana oriental de la península Ibèrica degut a processos de ciclogènesis a la conca occidental del Mediterrani i a la formació de tempestes de llevant durant els mesos d'hivern (modificat de Martín-Vide and Lopez-Bustins, 2006) (www.sciencephoto.com).

un temps sec, fred i assolellat que en molts casos està relacionat amb processos residuals de ciclogènesi al golf de Gènova (Harding et al., 2009). Són precisament aquests vents el que donen lloc al refredament i enfonsament de les aigües superficials al Golf de Lleó participant així d'uns dels principals motors de la circulació termohalina del Mediterrani (MEDOC-group, 1970; Lacombe et al., 1985; Millot, 1999) tal i com s'explica en el següent apartat (c.f. Apt. 2.3).

2.3. Masses d'aigua i circulació oceànica

El Mar Mediterrani és una conca de concentració on l'evaporació ultrapassa l'entrada d'aigües dolces d'origen fluvial, subterrani i per precipitació directa (Bethoux, 1980; Tomczak and Godfrey, 2003). Aquest balanç hídric negatiu, resultat de la climatologia mediterrània, genera una circulació antiestuarina amb una entrada superficial d'aigües relativament temperades i poc salines provinents de l'Atlàntic que tendeixen a compensar el dèficit hídric, i una sortida d'aigües més denses en profunditat a través de l'estret de Gibraltar (Tsimplis i Bryden, 2000) (Fig. 2.7). La circulació d'aigües al Mar Mediterrani està doncs totalment condicionada pel balanç hídric negatiu i pel fet que l'única comunicació natural amb l'oceà global sigui a través de l'estret de Gibraltar.

La circulació al Mar Mediterrani té, a grans trets i degut a l'efecte de Coriolis, un caràcter ciclònic, des de la superfície fins al fons (Millot i Taupier-Letage, 2005) (Fig. 2.8). En el procés de transformació de l'aigua Atlàntica en aigua Mediterrània que es duu a terme mitjançant la circulació termohalina del Mediterrani hom diferencia tres tipus principals de masses d'aigua en funció de la profunditat que ocupen, superficial, intermèdia i fonda (Tsim-

plis et al., 2006). El motor d'aquesta circulació termohalina són tres cèl·lules de convecció. La primera correspon a un cinturó zonal que dona lloc a la formació de l'aigua intermèdia, mentre que les altres dues són cèl·lules profundes en cada una de les conques, oriental i occidental, que donen lloc a la formació de l'aigua fonda. Totes elles acaben sortint per l'estret de Gibraltar injectant calor i sal a l'Oceà Atlàntic (Fig. 2.7).

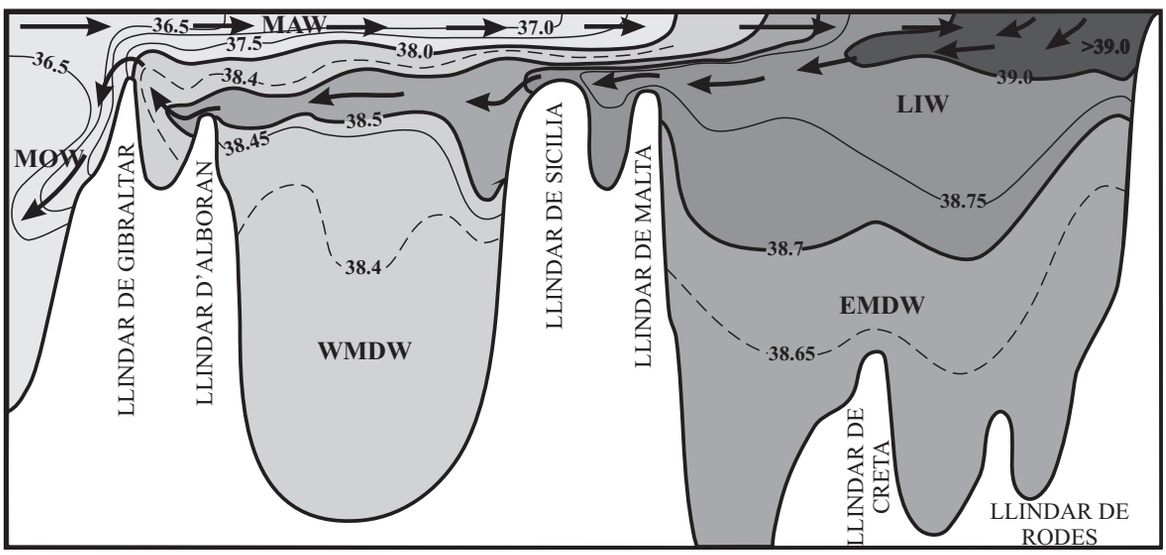

Figura 2.7. Tall hidrogràfic il·lustratiu de la circulació termohalina del Mediterrani on es mostra l'entrada superficial d'aigua Atlàntica per l'estret de Gibraltar, com es transforma successivament en Aigua Atlàntica Modificada (MAW) i va tornant-se més salina i densa al llarg del seu viatge cap a la conca oriental fins que s'enfonsa formant l'Aigua Llevantina Intermèdia (LIW). La figura també mostra les masses d'aigua fondes de les conques oriental i occidental (EMDW i WMDW, respectivament) així com un seguit d'isohalines de referència. Finalment, la LIW i la WMDW surten per l'estret de Gibraltar cap a l'Atlàntic formant l'Aigua de Sortida del Mediterrani (MOW) (modificat de Wüst, 1961).

L'Aigua Atlàntica (AW, de l'anglès *Atlantic waters*, 15ºC, 36,2 psu) que entra en superfície a través de l'estret de Gibraltar, es va barrejant amb l'aigua del Mediterrani a mesura que viatja cap a l'est seguint la costa nord-africana tot i formant l'anomenada Aigua Atlàntica Modificada (MAW, de l'anglés *Modified Atlantic Water*), que ocupa els 100-200 m més superficials (Millot, 1999). La salinitat de la MAW va augmentant en el seu recorregut cap a la conca oriental degut a l'evaporació i a processos de barreja des de 36,2 psu a Gibraltar fins 39,1 psu a l'arribar a l'extrem oriental de la conca de Llevant, prop de l'Illa de Xipre (Wüst, 1960, 1961). En aquesta àrea, les fortes taxes d'evaporació a l'estiu i el precondicionament hidrogràfic degut al gir ciclònic de Rodes (Fig. 2.8) afavoreixen que durant el refredament hivernal de la superfície del mar les aigües superficials s'enfonsin tot i formant l'Aigua Llevantina Intermèdia (LIW, de l'anglès *Levantine Intermediate Water*, 15-16ºC, 38,95-39,05 psu). La LIW s'escampa per tot el Mediterrani on ocupa un nivell intermèdi entre 200 i 600 m de fondària (Lascaratos et al., 1993). La LIW descriu un moviment ciclònic cap a la conca occidental (Millot, 1999; Millot i Taupier-Letage, 2005) fins que acaba sortint per l'estret de Gibraltar cap a l'Atlàntic.

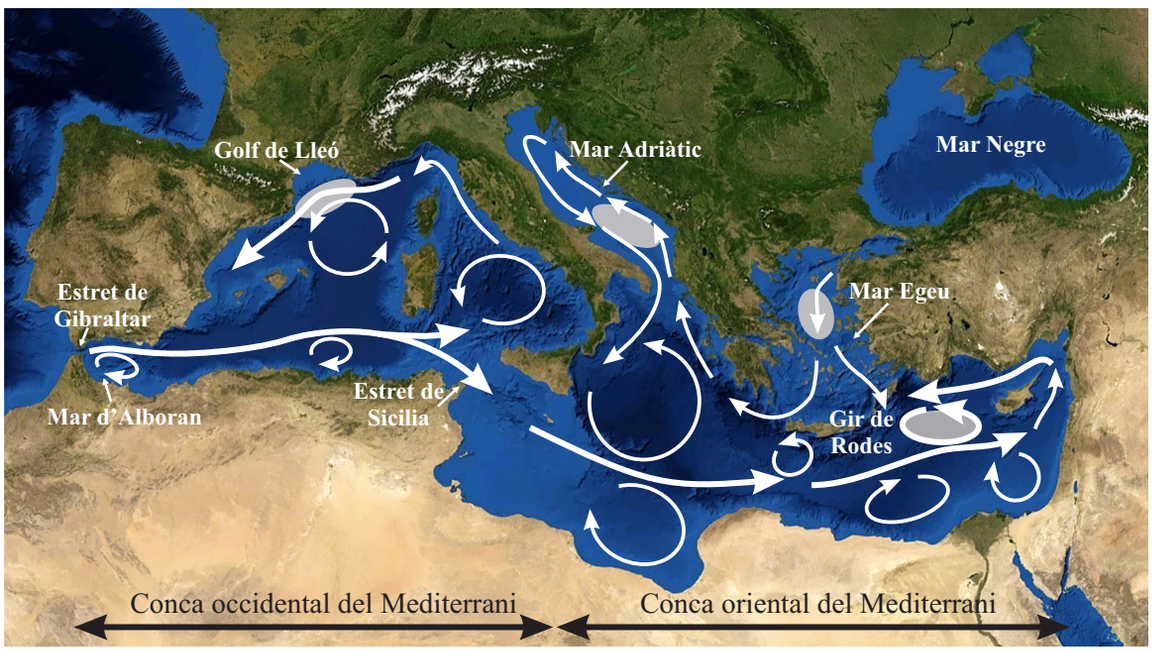

Figura 2.8. Esquema general de la circulació superficial del Mediterrani. Els ovals de color gris mostren les àrees de formació d'aigua intermèdia al voltant del gir de Rodes a la conca oriental i d'aigua fonda a les conques oriental (mars Egeu i Adriàtic), i occidental (Golf de Lleó) (bassat en Millot, 1999; Pinardi i Masetti, 2000; Rohling et al., 2009a).

La LIW és la principal contribució a l'Aigua Sortint del Mediterrani (MOW, de l'anglès *Mediterranean Outflow Water*, 13.5ºC, 38.4 psu) (Lascaratos et al., 1993; Robinson and Golnaraghi, 1994; Tsimplis et al., 2006). Aquesta cèl·lula de transformació d'AW superficial en aigua mediterrània intermèdia és coneguda com el "cinturó zonal de la circulació termohalina del Mediterrani" (Fig. 2.7) (Pinardi and Masetti, 2000).

La circulació termohalina del Mediterrani es completa amb la ventilació de les seves aigües fondes impulsada per la formació d'aigua densa en dues cèl·lules profundes, semblants a la cèl·lula d'enfonsament d'aigües de l'Atlàntic Nord (Pinardi i Masetti, 2000), una a cada conca. A la conca oriental, el Mar Adriàtic havia estat considerat el lloc principal de formació d'aigua densa (Pollak, 1951; Wüst, 1961), però estudis posteriors van determinar que si més no els anys 80 i 90 del segle passat el Mar Egeu va contribuir significativament a la formació de l'Aigua Fonda del Mediterrani Oriental (EMDW, de l'anglès *Eastern Mediterranean Deep Water*) (Robinson et al., 1992; Roether et al., 1996; Lascaratos et al., 1999). I no només això, sinó que a la vegada que es comprovà que el Mar Egeu havia incrementat la seva contribució a la formació de l'EMDW, també es va constatar que havia disminuït la del Mar Adriàtic. Aquest canvi aparent en la font principal d'EMDW des del Mar Adriàtic al Mar Egeu es coneix com a Trànsit del Mediterrani Oriental (EMT, de l'anglès *Eastern Mediterranean Transient*). Hom relacionà l'EMT amb forçaments atmosfèrics produïts per hiverns extremadament freds i el pre-condicionament subseqüent de les aigües superficials al Mar Egeu, ja fos pel transport d'aigües salines a l'àrea de formació d'aigües denses o per

una disminució de l'entrada d'aigua dolça en superfície a la conca oriental degut al pas de la NAO a un estat positiu gairebé permanent a les darreres dècades (Tsimplis i Josey, 2001). Tot i això, no sembla pas que aquest trànsit sigui permanent sinó que l'EMT es podria haver relaxat, tornant així a un escenari en que el Mar Adriàtic seria de nou la font principal de l'EMDW (Klein et al., 2000; Borzelli et al., 2009; Bergamasco i Malanotte-Rizzoli, 2010). Tot plegat suggereix que aquestes oscil·lacions adriàtico-egees estarien relacionades amb l'existència de múltiples estats d'equilibri a la conca oriental del Mediterrani. A la conca occidental la formació d'aigua densa ocorre al Golf de Lleó, on es forma l'Aigua Fonda del Mediterrani Occidental (WMDW, de l'anglès *Western Mediterranean Deep Water*, 12,8 ºC, 34,4-34,48 psu) (MEDOC-group, 1970; Lacombe et al., 1985; Millot, 1999), les característiques de la qual es descriuran amb més detall en l'apartat següent (cf. Aptat. 2.4), dedicat al Mediterrani nordoccidental.

La formació d'aigües denses al Mediterrani està lligada amb la pèrdua de calor de les aigües superficials durant l'hivern degut a forçaments atmosfèrics relacionats amb episodis de vents forts del nord i del nord-oest. Aquests vents són la Tramuntana i el Mestral al Golf de Lleó i sectors propers, a la conca occidental, el Bora al Mar Adriàtic i l'Etesi al Mar Egeu, a la conca oriental (Rohling et al., 2009a). A més, la formació d'aigua densa en aquests indrets està molt influenciada o, fins i tot, controlada per l'aportació de sal a profunditats intermèdies a càrrec de la LIW, la qual pre-condiciona les masses d'aigua susceptibles de ser enfonsades (Pinardi i Masetti, 2000). Així doncs, la circulació termohalina del Mediterrani pot comparar-se amb un motor de dos temps. El primer correspon a la formació de LIW per evaporació i concentració salina, seguida de l'escampada d'aquesta massa d'aigua per tot el Mediterrani, la qual predisposa la formació d'aigües denses en els indrets esmentats. El segon temps comporta el refredament superficial de les aigües per vents forts, freds i persistents del nord a les eventracions més septentrionals del Mar Mediterrani (Rohling et al., 2009a). Pel seu context geològic i climàtic (cf. Aptats. 2.1 i 2.2) la circulació termohalina del Mediterrani és sensible tant a les variacions del monsó africà per la intermediació del riu Nil, que condicionaria part de les aportacions d'aigua dolça a la conca oriental, com per la variabilitat climàtica de les regions situades al nord de la conca mediterrània, com també va succeir en temps passats (cf. Cap. 1). És per això que cal esperar que variacions en la formació de la LIW a la conca oriental puguin afectar la formació de WMDW a la conca occidental a diverses escales de temps (Pinardi i Masetti, 2000; Tsimplis et al., 2006).

La resultant final de la transformació d'aigua atlàntica en aigua mediterrània és el flux de sortida per l'estret de Gibraltar cap a l'Oceà Atlàntic d'una massa d'aigua, la MOW, d'uns 5ºC més calenta que cap de les masses d'aigua de l'Atlàntic Nord a la mateixa latitud i profunditat, i més d'1 psu més salada. Fora ja del Mediterrani, la MOW, s'estabilitza al voltant dels 1.000 m de profunditat tot i formant una llengua d'aigua molt salada recognoscible a tot l'Atlàntic nord-oriental (Artale et al., 2006). Hom creu que la injecció de sal a l'Atlàntic per

mitjà de la MOW pot ajudar a pre-condicionar les aigües de les cèl·lules de convecció on es forma l'Aigua Fonda de l'Atlàntic Nord (NADW, de l'anglès *North Atlantic Deep Water*), contribuint així al reforçament de la Circulació de Retorn de l'Atlàntic Nord (AMOC, de l'anglès *Atlantic Meridional Overturning Circulation*) (Reid, 1994; Lozier et al., 1995; Potter i Lozier, 2004). Tot i així, treballs de modelització indiquen que la influència de la MOW en l'AMOC ha d'ésser limitada i, probablement, està condicionada pel patró d'escampament de la mateixa MOW per l'Atlàntic Nord (Rahmstorf, 1998; Artale et al., 2002; Calmanti et al., 2006). Finalment, hom creu que la interacció de la MOW en l'AMOC pot donar lloc a mecanismes de retroalimentació (en anglès *feedback*) d'escala decadal i mil·lenària amb implicacions climàtiques potencialment rellevants, donat que l'Oceà Atlàntic és responsable d'una part substancial del transport de calor des dels tròpics fins a les regions polars (Artale et al., 2006).

2.4. El Mediterrani nordoccidental: sistemes sedimentaris

Aquesta Tesi se centra en l'estudi de registres marins procedents de dos sistemes sedimentaris particularment interessants situats al Mediterrani nordoccidental: el marge progradant del Golf de Lleó i el sistema contornític de Menorca. El Mediterrani nordoccidental és limitat al nord per les costes del Golf de Lleó, a l'est per la Península Ibèrica, al sud pel promontori Balear i a l'oest per les costes del Mar Ligur. Inclou la part nord de la Conca Algerobalear i la Conca Catalanobalear on hi ha el canal de València (Fig. 2.9). Les fondàries del Mediterrani nordoccidental només ultrapassen els 2.000 m al nord i a l'est de l'illa de Menorca, on el canal de València s'obre a la Conca Algerobalear, en la qual s'atenyen gairebé els 3.400 m. Les plataformes continentals del Mediterrani nordoccidental són força estretes, de menys de 25 km, amb dues excepcions notables: les plataformes de l'Ebre i del Golf de Lleó, amb uns 60 i 70 km d'amplada, respectivament. L'assoliment d'aquestes amplades és atribuïble al caràcter marcadament progradant dels marges respectius a causa de l'aportació continua de sediments des del Pleistocè Superior per part del rius Ebre i Roine (Aloïsi, 1986; Nelson i Maldonado, 1990). Aquest dos rius es compten entre els deu amb més descàrrega anual d'aigua de tot el Mar Mediterrani, i són els dos més cabalosos i amb una major descàrrega sòlida de la conca occcidental (Ludwig et al., 2009). La plataforma continental del Mediterrani nordoccidental també és alimentada per tot un seguit de rius més petits, excepte al promontori Balear, on l'aportació via fluvial de sediments és pràcticament nul·la.

Els marges peninsulars del mar Catalanobalear i del Golf de Lleó són incidits per un alt nombre de canyons submarins que actuen com a via preferent de transport de sediments des de la zona costanera fins el marge profund i la conca. Els canyons dels segments català i de l'Ebre aboquen al canal de València, el qual s'obre a la plana batial algerobalear a través de l'anomenat ventall de València (Maldonado et al., 1985a; Canals et al., 2012), mentre que la xarxa de drenatge submarina del Golf de Lleó, fortament jerarquitzada, sobre a la mateixa

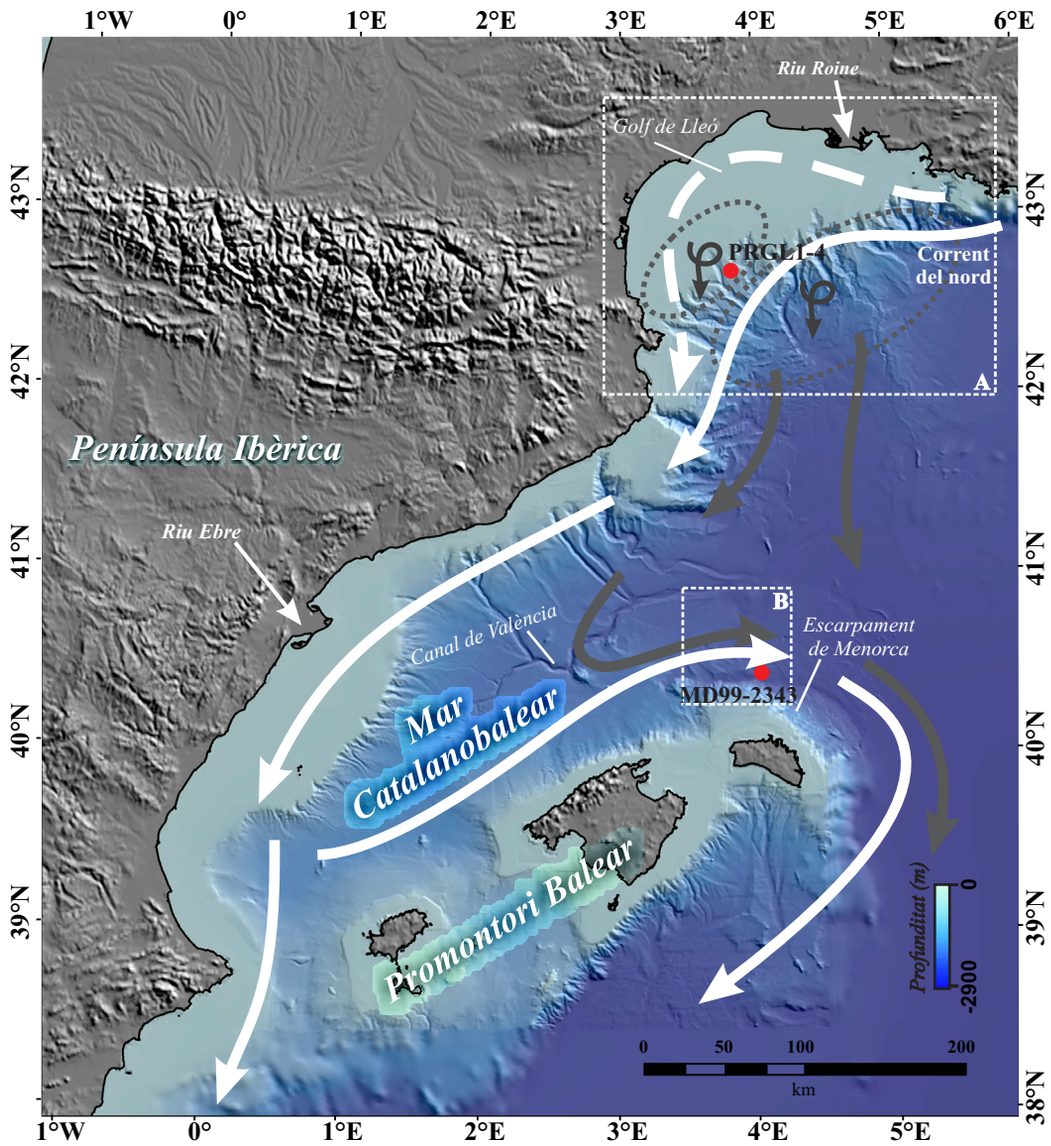

Figura 2.9. Imatge en relleu ombrejat del Mediterrani nordoccidental construïda a partir de dades topogràfiques a terra i de batimetria de multifeix a mar (Amblas, 2012). Les fletxes superposades il·lustren els trets generals de la circulació oceànica superficial (en blanc) i profunda (en gris obscur). Les fletxes cargolades dintre d'un cercle de punts marquen les àrees de formació d'aigua fonda a la plataforma del Golf de Lleó i mar endins. Els testimonis de sediment estudiats en aquesta Tesi estan marcats amb punts rojos. Els requadres de punts A i B marquen les àrees que es mostren en detall a les figures 2.10 i 2.12, respectivament.

plana batial després de creuar un potent cúmul sedimentari de peu de talús el qual han contribuït a formar els mateixos canyons submarins, on hi destaquen el "cos sedimentari profund dels canyons pirinencs" (en anglès *Deep Pyrenean Canyons Sedimentary Body*) (Canals, 1985; Alonso et al., 1991) i el ventall profund del Roine (Bellaiche et al., 1981).

La circulació superficial al Mediterrani nordoccidental està dominada per la circulació ciclònica general de la MAW, la qual a la part septentrional rep el nom de Corrent del Nord (NC, de l'anglès *Northern Current*). A grans trets, el NC circula paral·lel a la costa, damunt el

talús continental i la plataforma externa, en direcció NE-SW (Font et al., 1988; La Violette et al., 1990; Millot, 1999; Millot i Taupier-Letage, 2005). Un punt d'especial interès en aquest sector septentrional és la formació d'Aigua Fonda del Mediterrani Occidental, la WMDW, al Golf de Lleó els mesos d'hivern (cf. Aptat. 2.3). (MEDOC-group, 1970; Millot i Monaco, 1984; Lacombe et al., 1985; Millot, 1999).

La formació d'aigües denses al Mediterrani nordoccidental és afavorida per la presència del gir ciclònic del NC, el qual, juntament amb la força del vent, causa la somerització de la picnoclina i, per tant, l'apropament a la superfície d'aigües més salines procedents de la conca oriental, la LIW. La pèrdua de calor, l'evaporació i la barreja provocades pels forts vents, freds i secs del nord fan que les aigües superficials s'enfonsin i formin la WMDW, que circula a una fondària d'equilibri de densitats i s'escampa per tota la conca occidental (MEDOC-group, 1970; Leaman i Schott, 1991).

Un segon procés en la formació d'aigua fonda al Mediterrani, la rellevància del qual s'ha anat constatant recentment, són les cascades d'aigües denses de plataforma (DSWC, de l'anglès *Dense Shelf Water Cascading*) (Canals et al., 2006). Al Mediterrani, de DSWC se'n produeixen al Golf de Lleó i també al Mar Adriàtic i, molt probablement, a l'Egeu (Canals et al., 2009). L'ocurrència d'aquest procés és coneguda també a molts altres indrets de l'oceà global (Ivanov et al., 2004; Durrieu de Madron et al., 2005; Canals et al., 2006). Les DSWC s'originen per causes molt similars a les que provoquen la formació d'aigües denses enfora de la plataforma, a mar oberta, doncs els responsables principals són, de nou, el refredament i l'evaporació produïts pels vents del nord, ara bufant damunt l'extensa i poc profunda plataforma del Golf de Lleó durant l'hivern. Els hiverns secs, amb poca descàrrega d'aigua dolça, sobretot pel Roine, són particularment favorables a la formació de DSWC, doncs la influència de les aigües continentals, més dolces i lleugeres i, per tant, més difícils de densificar, és menor. Un cop assolida una densitat crítica les aigües superficials de plataforma s'enfonsen fins assolir el seu nivell d'equilibri dintre de la columna d'aigua (Durrieu de Madron et al., 2008). També s'ha observat que poden donar-se amb motiu de tempestes de llevant especialment virulentes (Palanques et al., 2006; Sanchez-Vidal et al., 2012).

Segons Durrieu de Madron et al. (2005), però, el que fa diferent les DSWC de la convecció de mar oberta és que a la plataforma el procés està totalment condicionat per la temperatura, i no per la salinitat. La càrrega sedimentària és una altra diferència rellevant entre els dos mecanismes de formació d'aigua fonda al Golf de Lleó, doncs els vents forts que produeixen la densificació i posterior enfonsament de les aigües de plataforma, siguin del nord o de llevant, també provoquen la resuspensió dels sediments d'origen fluvial acumulats a la plataforma. És per això que la massa d'aigua densa de plataforma que s'enfonsa ho fa carregada de partícules en suspensió (sediments, matèria orgànica i altres substàncies prèviament emmagatzemades a la plataforma) que formen una llengua tèrbola i turbulenta enganxada al

fons, o flux hiperpícnic, de desenes a centenars de metres de gruix i una capa basal sorrenca amb fort potencial abrasiu (Canals et al., 2006; Puig et al., 2008). El flux principal de les aigües denses formades damunt la plataforma del Golf de Lleó segueix la circulació ciclònica general cap al SW fins que topa amb l'obstacle de la península del Cap de Creus, la qual actua de barrera, cosa que juntament amb un marcat estretament de la plataforma, determina el desviament del flux carregat de material en suspensió cap a l'interior del Canyó del Cap de Creus i, d'allí, cap al marge profund i la conca. Tot i tenir un caràcter intermitent depenent de forçaments externs, la formació d'aigua fonda per les cascades d'aigua densa de plataforma constitueix un procés de transferència molt eficaç de partícules, matèria orgànica i altres substancies des de la plataforma interna cap al talús i cap al fons de la conca (Canals et al., 2006; Durrieu de Madron et al., 2008). Finalment, tot i que no tots els hiverns es donen les condicions necessàries per a que les DSWC generin aigua fonda de la conca occidental, és a dir, WMDW, aquest procés té potencial per influir en la formació de WMDW donat que aquesta àrea és l'únic punt de formació d'aigua fonda en tota la conca occidental del Mediterrani (Bethoux et al., 2002; López-Jurado et al., 2005).

2.4.1. El marge passiu progradant del Golf de Lleó

El marge continental del Golf de Lleó és d'on provenen els testimonis MD99-2348 i PRGL1-4 estudiats en aquesta Tesi, sobre els quals hom dona més detalls a l'apartat 3.1 de Materials i mètodes.

El marge passiu del Golf de Lleó s'estén entre el Cap de Creus al SW i el Canyó de Cassidaigne al NE. Té forma de mitja lluna, amb una plataforma d'uns 70 km d'amplada màxima i un talús continental escorxat per nombrosos canyons submarins que connecten la plataforma amb el glacis continental i la conca pregona (Fig. 2.10). La plataforma continental es pot dividir en: 1) plataforma interna, de 0 a 90 m de profunditat, que està caracteritzada per gradients morfològics regulars i graduals, i compren el prisma sedimentari costaner actual; 2) plataforma intermèdia, de 90 fins a 110-120 m de profunditat, que és relativament plana amb una morfologia irregular, majoritariament coberta per una capa de sorres relictes; i 3) plataforma externa, que és una estreta franja que va des dels 110-120 m fins al límit de plataforma, de morfologia generalment suau (Berné et al., 2004a). L'ampla plataforma del Golf de Lleó constitueix un gran espai d'acomodació pels sediments provinents del continent, com ho mostra el notable prisma costaner actual, però també a una extensa làmina d'aigua marina altament sensible als forçaments atmosfèrics (Dufois et al., 2008; Ulses et al., 2008). Tant el prisma deltaic costaner com el volum d'aigua de damunt la plataforma s'han vist afectats per les oscil·lacions del nivell del mar induïdes pels cicles glacials/interglacials del Quaternari, les quals provocaren canvis dràstics en la dinàmica oceanogràfica i sedimentària de la plataforma (Bassetti et al., 2006).

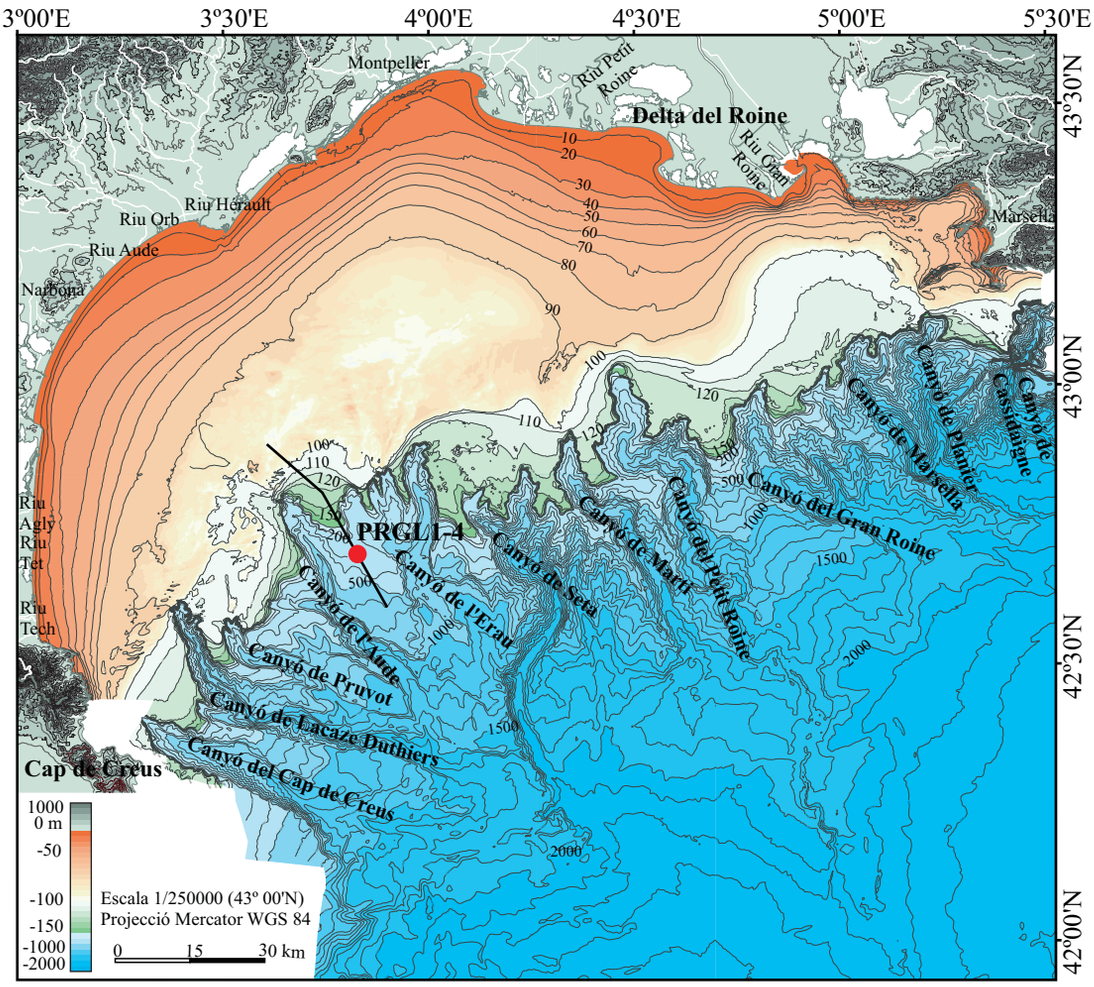

Figura 2.10. Carta morfobatimètrica del Golf de Lleó (modificada de Berné et al., 2004a). L'escala de colors permet identificar els tres dominis de plataforma descrits en el text: 1) el sistema prodeltaic entre 0 i 90 m de profunditat amb colors rogencs i taronja; 2) la plataforma intermèdia entre 90 i 110 m de profunditat amb colors groguencs; i 3) la plataforma externa entre 110 m de profunditat i el vorell amb colors grissos i verdosos. Els colors blavosos representen el talús i el glacis continental. El punt roig marca la localització del testimoni PRGL1-4 i la línea que creua per sobre en direcció NW-SE il·lustra la localització del perfil sísmic que es mostra a la figura 2.12.

El marge continental del Golf de Lleó es va formar al separar-se del sud de França el bloc de Còrsega i Sardenya al final del oligocè, fa uns 23 Ma, la qual cosa generà un micro-oceà (Séranne et al., 1995). Al tractar-se d'un marge molt jove, la taxa de subsidència i l'espai d'acomodació associat són significatius, fets que afavoriren l'acumulació d'un gruix considerable de sediments durant els darrers 20 Ma, de fins a 2 km a la plataforma i fins a 10 km al glacis continental (Berné and Gorini, 2005). L'evolució del marge estigué afectada per la baixada del nivell del mar de fins a 1.500 m durant la Crisis de Salinitat del Messinià, ara fa entre 6 i 5 Ma, la qual provocà una forta erosió en el marge golfllleonès (Hsü et al., 1977; Ryan, 2009), el qual fou reinundat posteriorment durant el Zanclià (5,3 Ma). Des de llavors, durant el Pliocè i el Quaternari (darrers 3,5 Ma), el marge ha anat progradant mercès a les aportacions de sediments provinents dels Alps, el Massís Central i els Pirineus, amb l'efecte

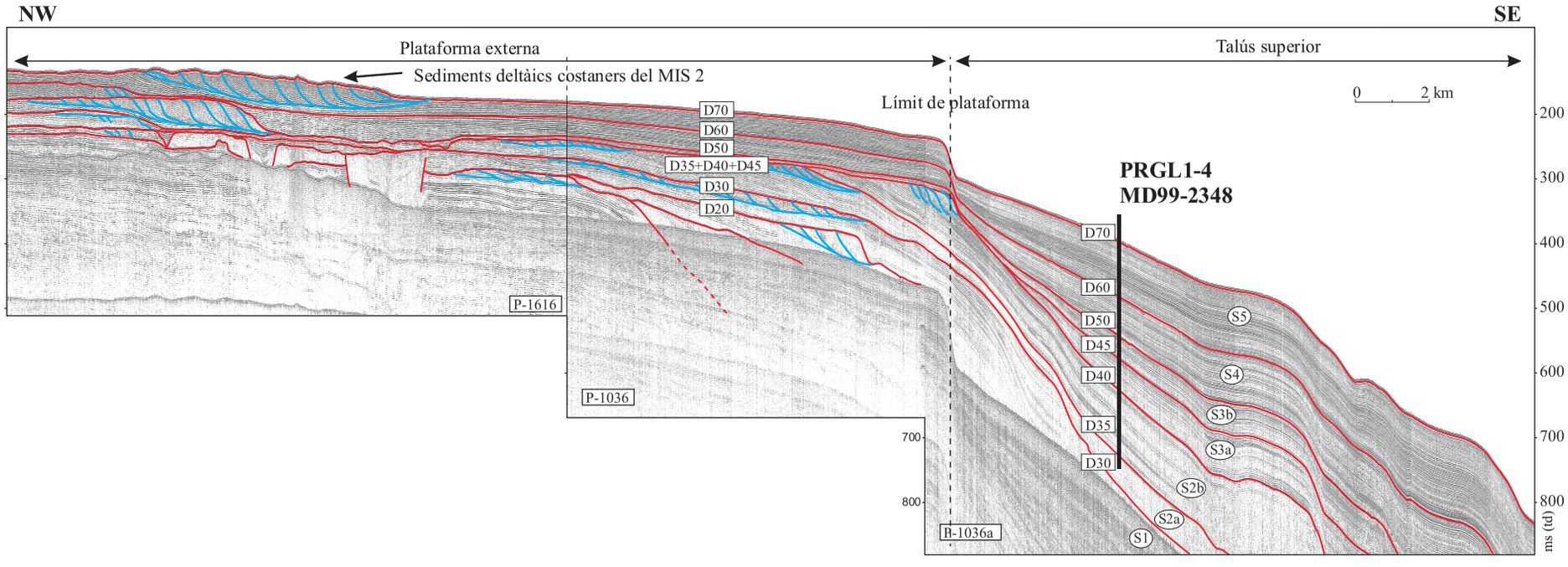

Figura 2.11. Perfil sísmic de molt alta resolució de la plataforma externa i el talús superior del Golf de Lleó a través del interfluvi entre els canyons submarins de l'Aude i l'Erau on es mostra la posició dels testimonis PRGL1-4 i MD99-2348 (modificat de Jouet, 2007). Les seqüències estratigràfiques corresponents a RPUs en el talús superior i els límits de seqüència estan numerats i retolats dins ovals i reqüadres, respectivament. Les línees blaves mostren les restes dels sistemes deltaics progradants dipositats durant períodes glacials pretèrits.

modulador provocat per les pujades i baixades del nivell del mar lligades a la successió de períodes glacials i interglacials durant el Quaternari (Lofi et al., 2003; Berné et al., 2004a; Berné i Gorini, 2005). Aquest context va donar lloc al desenvolupament de seqüències estratigràfiques de caràcter regressiu (tascons regressius) al talús, mentre la plataforma restava exposada temporalment a condicions subaèries durant els períodes de nivell del mar baix centrats en els màxims glacials. Aquesta exposició subaèria i l'efecte erosiu de la pujada del nivell del mar durant les transgressions feren que una gran part de les seqüències glacio-eustàtiques de la plataforma fossin parcialment o totalment erosionades, preservant-se només com a límits de seqüència entre dos cicles, les discontinuïtats associades als períodes transgressius. En canvi, a l'estar sempre per sota del nivell del mar, al talús si que es preservà la successió completa de seqüències glacio-eustàtiques, excepte en els indrets erosionats per canyons submarins (Canals, 1985; Aloïsi, 1986; Rabineau, 2001; Berné et al., 2004a; Jouet, 2007). Aquest model de desenvolupament del marge, profusament estudiat principalment a partir de perfils de sísmica de reflexió i testimonis de sediment, es coneix amb el nom de "sistema regressiu forçat", rebent les unitats cícliques generades el nom d'"Unitats Progradants Regressives" (RPU, de l'anglès *Regressive Progradational Units*) (Posamentier i Vail, 1988; Tesson et al., 1990; Posamentier et al., 1992; Tesson et al., 2000) (Fig. 2.11). Tot i així, els perfils sísmics no permetien demostrar de manera definitiva la ciclicitat de les unitats i durant molts anys hom discutí si aquestes seqüències corresponien a les oscil·lacions del nivell del mar associades a la ciclicitat climàtica de 20 ka o a la de 100 ka, governades per la precessió i l'excentricitat, respectivament (Posamentier i Vail, 1988; Tesson et al., 1990; Posamentier et al., 1992; Rabineau et al., 1998; Lobo et al., 2004; Rabineau et al., 2005). És per això que es feu necessària l'obtenció de testimonis ben llargs per a poder estudiar amb prou detall i ben enrere en el temps el desenvolupament estratigràfic d'aquest tipus de marges i així esbrinar el control exercit pels canvis globals del nivell del mar (Berné i Gorini, 2005). El Golf de Lleó constituïa, en aquest sentit, un indret ideal per a intentar respondre a aquestes qüestions.

Les elevades taxes de subsidència, l'aportació continua de grans volums de sediment, i la gran extensió de la plataforma feien del Golf de Lleó el "laboratori" perfecte per a dur a terme estudis sobre els efectes dels canvis del nivell del mar del Quaternari en la construcció dels marges continentals i, a la inversa, treure l'entrellat dels canvis de nivell del mar a partir de la seva senyal preservada en el registre sedimentari. Amb aquest objectiu, hom seleccionà un indret precís amb taxes de sedimentació altes i continuïtat estratigràfica per a dur-hi a terme una perforació amb obtenció d'un testimoni de 300 m de llarg al talús superior, a 298 m de profunditat d'aigua, al interfluvi entre els canyons de l'Erau (en francès Hérault) i l'Aude (Fig. 2.10).

2.4.2. El sistema contornític profund de Menorca

Una segona zona d'estudi d'aquesta Tesi ha estat el sistema contornític de Menorca, on es recuperà el testimoni de pistó MD99-2343, la descripció del qual també es proporciona més endavant en l'apartat 3.1 de Materials i mètodes.

Els sistemes contornítics (en anglès *contourite systems* o *contouritic systems*) es formen per la interacció d'un seguit de factors: la intensitat dels corrents de fons sotmesos a l'efecte de Coriolis, la morfologia del fons, el volum de sediment aportat, la presència de capes nefeloides, i la profunditat de compensació de la calcita (CCD, de l'anglès *Calcite Compensation Depth*) (Faugères et al., 1993). Es tracta d'ambients deposicionals-erosius on l'acció persistent de corrents de fons és capaç de transportar sediment al·lòcton, de retreballar els dipòsits acumulats prèviament i d'erosionar localment el fons marí (Hein, 1989). Els elements deposicionals solen consistir en un llom o una successió de lloms, mentre que els elements erosius solen estar representats per depressions perifèriques adjacents i/o per superfícies i relleus erosionats. Els lloms contornítics són cossos sedimentaris de gran interès pels estudis paleoceanogràfics i paleoclimàtics, doncs reuneixen un seguit de característiques que els donen un alt potencial com a enregistrament d'esdeveniments del passat. Una de les característiques principals dels lloms, donat que el seu origen i desenvolupament són controlats pels corrents propers al fons, es que poden ajudar a esbrinar els patrons de la circulació termohalina global i també la transferència del senyal climàtic atmosfèric cap al fons de l'oceà (Hein, 1989; Stow et al., 2002). Una altra característica rellevant dels lloms contornítics és que solen comportar taxes de sedimentació elevades o molt elevades en comparació amb els ambients de fons de conca, tret que els hi dona un alt valor per a dur a terme estudis d'alta i molt alta resolució (de centenars a milers d'anys) (Toucanne et al., 2006; Voelker et al., 2006; Toucanne et al., 2012).

El sistema contornític de Menorca és format per un llom contornític i una depressió perifèrica associada, tots dos situats al peu de l'escarpament de Menorca, al nord i est de l'illa, entre 2.000 i 2.700 m de fondària (Figs. 2.9 i 2.12a). Hom atribueix el seu origen a l'acció del flux de la WMDW formada al Golf de Lleó (cf. Aptat. 2.3), la qual en el seu desplaçament per les profunditats de la conca tot i seguint la circulació ciclònica dominant cap al SW i S topa amb el promontori Balear, veient-se així forçada a girar cap al S i SE, fet que provoca excavació al peu de l'escarpament, formant-se així la depressió perifèrica, i acumulació més enllà, paral·lelament a la depressió i enfora de la mateixa, d'on resulta la formació del llom contornític de Menorca (Mauffret et al., 1982; Velasco et al., 1996; Canals et al., 2012). El fort pendent de l'escarpament de Menorca i el gir que aquest obliga a fer al flux de la WMDW per l'efecte d'obstacle provoquen l'acceleració de la circulació, la qual excava el peu de l'escarpament formant-hi la depressió perifèrica i determina l'acumulació en el llom contornític separat de l'escarpament per la pròpia depressió. El llom contornític es forma allà

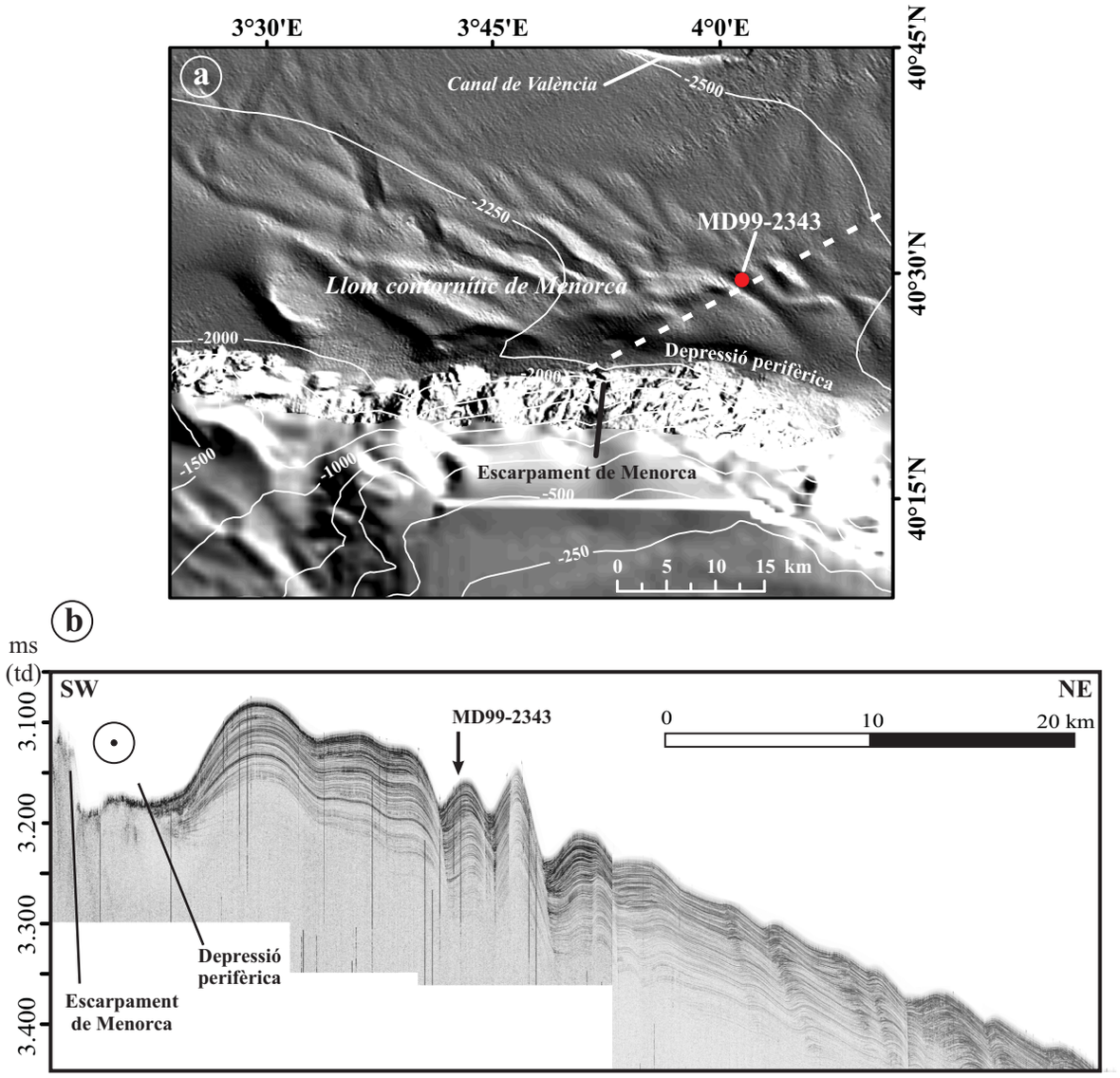

Figura 2.12. a) Imatge en relleu ombrejat del sistema contornític de Menorca i sectors propers construïda amb dades de batimetria de multifeix. El punt roig mostra la posició del testimoni MD99-2343 i la línea discontinua representa el perfil sísmic de sota (D. Amblàs, GRC-GM de la Universitat de Barcelona). **b)** Perfil sísmic de reflexió TOPAS de molt alta resolució a través del llom contornític de Menorca on es mostra la posició aproximada del testimoni MD99-2343. El cercle amb un punt a dins representa el corrent d'aigua fonda que circula per la depressió perifèrica del peu del talús de Menorca, que surt de la imatge. Les dades de batimetria de multifeix i el perfil sísmic s'obtingueren a la campanya HERMESIONE l'any 2009 (Canals, 2009).

on l'acceleració i la turbulència del corrent han minvat prou com per permetre la decantació de les partícules sedimentàries. Com que per les condicions mitges de flux aquesta minva es produeix si fa o no fa a la mateixa distància del peu de l'escarpament al llarg de la depressió, la cresta principal del llom contornític tendirà a situar-se a una distància aproximadament constant del peu del talús o, si es vol, de l'eix de la depressió perifèrica, amb la qual mantindrà, conseqüentment, un paral·lelisme notable, tal i com succeeix. Així ha estat observat també en altres sistemes contornítics, com per exemple al llom extern de Caicos (de l'anglès *Caicos Outer Ridge*) (McCave i Tucholke, 1986; Hein, 1989).

Per tant, el sistema contornític de Menorca voreja el peu de l'escarpament de Menorca en direcció, primer W-E, i després NW-SE. La depressió perifèrica, amb un pendent axial feble i un desnivell mig de 100 m per sota la cresta del llom, és coberta, si més no localment, per sediments grollers provinents de la plataforma i el talús menorquins, els quals han estat interpretats com a dipòsits residuals (en anglès *lag deposits*) després del rentat dels fins pel mateix corrent de fons (Canals, 1980). El relleu de la depressió perifèrica de Menorca es va suavitzant gradualment cap al sud fins a esvair-se a l'alçada de l'acabament de l'escarpament de Menorca cap a l'est (Fig. 2.9). En altres paraules, desaparegut l'obstacle topogràfic format per l'escarpament, desapareix el sistema contornític.

Segons Velasco et al. (1996) el llom contornític arquejat que es desenvolupa enfora de la depressió perifèrica de Menorca per acumulació de fins s'estén al llarg d'uns 150 km i té uns 25 km d'amplada mitja. Dades recents de batimetria de multifeix obtingudes a la campanya HERMESIONE (Canals, 2009) han mostrat, però, que el llom contornític de Menorca té una morfologia prou complexa. Lluny de ser un relleu homogeni, regular i suau, presenta diverses ondulacions de gran escala orientades obliquament a l'eix de la depressió perifèrica, amb crestalls i solcs suaus, que reflecteixen la influència de l'activitat de corrents de fons fluctuants en la seva gènesi i evolució (Figs. 2.12a i 2.13) (Frigola et al., 2010). Aquestes ondulacions podrien ésser interpretades com a onades de fang de gran escala (en anglès *mega-scale mud waves*). Els eixos de les crestes i els solcs presenten una clara direcció NW-SE, la qual cosa indica la procedència de les aportacions des del SW, probablement per causa d'un gir en el flux de la WMDW forçat també topogràficament a la sortida del solc de València. Aquestes ondulacions podrien enllaçar amb un camp d'ones de sediment d'orientació N-S que hi ha a la part més externa i profunda del mateix solc de València (Alonso et al., 1995). Per la seva banda, la configuració interna del llom contornític sembla relativament senzilla, en forma de monticle amb reflectors estratificats paral·lels a sub-paral·lels d'amplitud i freqüència variables i la típica configuració d'encunyament cap a la depressió (Fig. 2.12b). La configuració general dels reflectors li dona una aparença sigmoïdal o ondulada, característica dels lloms contornítics, la qual identifica les zones d'acceleració i disminució de la velocitat dels corrents de fons (McCave i Tucholke, 1986; Hein, 1989).

Més enllà de les aportacions locals, segurament reduïdes, cal preguntar-se quin és l'origen dels sediments que s'acumulen en el llom contornític de Menorca. Al promontori Balear no hi desguassa cap riu permanent i la plataforma Balear té un recobriment sedimentari plio-quaternari de naturalesa carbonatada, molt sovint cimentat i amb gruixos ben migrats (Alonso et al., 1988; Canals i Ballesteros, 1997; Acosta et al., 2004; Fornós i Ahr, 2006). La petita porció de la plataforma balear que s'obre a l'escarpament de Menorca no pot ésser considerada, ni de bon tros, una font de sediment suficient pel llom contornític de Menorca. Cal, doncs, assumir que la major part del volum de sediments acumulats en el llom contornític de Menorca té una altra procedència, amb tota probabilitat septentrional, és a dir, dels

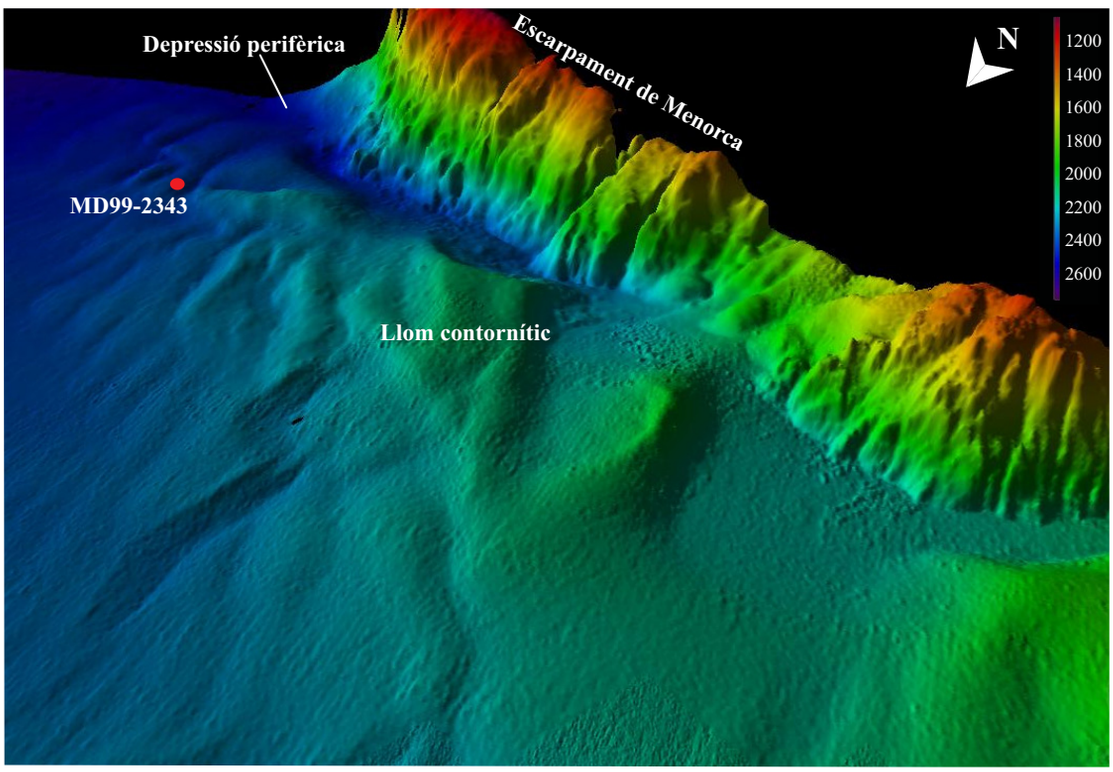

Figura 2.13. Imatge 3D en color de l'àrea del llom contornític de Menorca on es mostra la posició aproximada del testimoni MD99-2343. La visió és des de terra en direcció W-E (D. Amblàs, GRC-GM de la Universitat de Barcelona).

marges català i del Golf de Lleó. En aquests marges hi desemboquen nombrosos rius, alguns amb volums de descàrrega molt notables, com el Roine i l'Ebre (UNEP, 2003). Bona part de la descàrrega fluvial del conjunt de rius i rieres septentrionals s'acumula a les plataformes continentals, escapant-ne només part dels fins que són transportats en suspensió més enllà. L'acumulació a la plataforma té, però, un caràcter temporal, si més no per una proporció significativa dels dipòsits, la qual és remobilitzada i exportada més enllà de la plataforma quan es produeixen esdeveniments meteoceanogràfics d'alt nivell energètic, com ara cascades d'aigües denses i grans tempestes (Canals et al., 2006; Palanques et al., 2006; Sanchez-Vidal et al., 2012). Aital exportació en massa ocorre preferentment seguint els grans canyons submarins encaixats als marges del Golf de Lleó i català, els quals vehiculen les aportacions sedimentàries cap al peu del talús i el fons de la conca (Fig. 2.9) (Amblas et al., 2006). Alguns canyons i valls submarines, com els canyons del Cap de Creus i Seta (en francès *Sète*) i el canal de València, fan en part o en tot el seu recorregut el paper de col·lectors de les aportacions procedents d'altres canyons tributaris, doncs en conjunt el sistema de drenatge dels marges septentrionals forma una xarxa de drenatge submarí marcadament jerarquitzada (Canals et al., 2004; Amblas et al., 2011; Canals et al., 2012).

Donat el context descrit, seria legítim plantejar-se si el llom d'aigües fondes al nord de Menorca és un dipòsit turbidític i no pas contornític. La morfologia del llom, la presència d'una depressió perifèrica associada, la seva posició al peu d'un talús abrupte i la seva configuració

interna, abans descrites, juntament amb el fet de trobar-se en una posició relativa més elevada que els cursos inferiors del sistema de drenatge dels marges septentrionals esmentats i l'absoluta migradesa o manca d'aportacions sedimentàries locals, refermen que es tracta d'un sistema contornític i no pas turbidític. De fet, tots els sistemes contornítics s'alimenten d'aportacions sedimentàries que en l'origen provenen majoritàriament de marges continentals més o menys encaixats per valls submarines de distinta naturalesa.

És, però, probable, que entre el transport i l'acumulació als canyons submarins i l'acumulació estricta en el llom contornític de Menorca hi hagi un pas intermedi, si més no de vegades. Aquest es produiria per la remobilització de sediments acumulats temporalment en altres indrets, també profunds, d'aquest sistema de drenatge, en particular a les parts distals i davant les goles dels canyons i valls principals. En aquest punt, cal tenir present que no tots els esdeveniments que promouen l'exportació de sediment des de la plataforma continental tenen la mateixa intensitat, de manera que alguns són susceptibles de fer sentir els seus efectes fins les profunditats més grans mentre que altres, la majoria, no. La successió d'un seguit d'episodis d'exportació de sediment des de la plataforma de baixa i mitjana intensitat seguida de l'ocurrència d'un episodi d'alta intensitat (vegis la figura suplementària S1 a Canals et al., 2006) il·lustren les condicions més adequades per a que es produeixi el pas intermedi mencionat. De fet, a la llum de les darreres evidències (Canals et al., 2006; Palanques et al., 2006; Sanchez-Vidal et al., 2008; Salvadó et al., 2012; Sanchez-Vidal et al., 2012; Stabholz et al., sotmés; Ramirez-Llodrà et al., sotmés), no hi ha dubte de que, més enllà de processos ocasionals estrictament turbidítics, en el sentit sedimentològic del terme, els esdeveniments de formació i cascading d'aigua densa de plataforma i les grans tempestes costaneres i, en menor mesura, la formació d'aigua fonda mar endins, remobilitzen i carretegen grans volums de materials de tota mena (sediments, matèria orgànica, contaminants i deixalles), provinents segons els casos principalment de la plataforma o també del talús, el peu de talús i més enllà cap a la conca profunda, on està situat el llom contornític de Menorca.

El testimoni sedimentari llarg obtingut al llom contornític ens havia de permetre, doncs, estudiar la variabilitat de la circulació termohalina de la Mediterrània Occidental mitjançant l'anàlisi de les oscil·lacions de la circulació profunda tal i com quedaren enregistrades en el sediment, i establir llur relació amb les variacions climàtiques de l'Atlàntic Nord amb una resolució elevada (centenars a milers d'anys). El testimoni llarg fou complementat posteriorment amb un parell de testimonis curts obtinguts amb un testificador múltiple (en anglès *multicorer*) a fi i efecte d'analitzar la variabilitat dels corrents de fons ens els darrers 2.000 anys (Moreno et al., 2012). El mostratge amb testificador múltiple permet recuperar inalterats els sediments més recents, generalment molt flonjos, els quals sovint es perden en l'operació de mostratge quan hom empra altres sistemes de mostratge o sondeig.

3. Material i mètodes

Aquesta Tesi està centrada en l'estudi de la variabilitat de la mida de gra dels components terrígens i de la composició elemental en testimonis recuperats en dos sistemes sedimentaris propers però de característiques prou contrastades situats al Mediterrani nordoccidental: el marge continental progradant del Golf de Lleó i el llom contornític profund de Menorca (Taula 3.1 i Fig. 2.9). De forma general, els canvis en la mida de gra de les partícules sedimentades aporten informació sobre les condicions energètiques del medi en que s'han dipositat mentre que les fluctuacions en la composició elemental del sediment proporcionen informació sobre modificacions en els processos que controlen l'origen i l'aportació de les partícules. Tant l'un com l'altre són indicadors (de l'anglès *proxy*) àmpliament utilitzats en la caracterització de les condicions ambientals i climàtiques del passat a partir del registre sedimentari. Tot i això, la informació que aporten no es pot quantificar com una variable climàtica, com seria el cas de la temperatura de la superfície del mar (SST, de l'anglès *Sea Surface Temperature*) obtinguda a través de l'anàlisi de biomarcadors moleculars (Cacho et al., 1999). Per aquesta raó cal tenir un coneixement tant precís com sigui possible del context ambiental i dels processos que controlen la sedimentació actual a l'àrea d'estudi.

Testimoni	Vaixell	Campanya (any)	Coordenades	Profunditat (m)	Longitud Testimoni (m)
MD99-2348	*V/O Marion Dufresne*	IMAGES V (1999)	42º41,39'N 03º50,26'N	298	22,77
PRGL1-4	*MV Bavenit*	PROMESS1 (2004)	42º41,39'N 03º50,26'N	298	300
MD99-2343	*V/O Marion Dufresne*	IMAGES V (1999)	40º29,84'N 04º01,69'N	2391	32,44

Taula 3.1. Dades de referència dels testimonis de sediment emprats en aquesta Tesi.

3.1. Testimonis de sediment

Al Golf de Lleó hom ha treballat amb els testimonis MD99-2348 i PRGL1-4, provinents del talús superior (Taula 3.1 i Fig. 2.10), obtinguts amb l'objectiu d'estudiar el control dels canvis glacials i interglacials del nivell del mar en els darrers 500 ka (kilo-anys, 10^3 anys) sobre el desenvolupament estratigràfic del marge. En el llom contornític de Menorca, hom ha analitzat el testimoni MD99-2343 amb la finalitat de conèixer la variabilitat dels corrents de fons i llur relació amb el canvis climàtics a l'Atlàntic Nord en el darrer cicle glacial/interglacial.

La recuperació del testimoni PRGL1-4 al Golf de Lleó tingué lloc en el marc del projecte europeu PROMESS1 (*PROfiles across the MEditerranean Sedimentary Systems*). La fina-

litat principal del projecte era l'obtenció de seqüències sedimentàries llargues en marges continentals dominats per aportacions fluvials a la Mediterrània i, per tant, amb taxes de sedimentació molt elevades. Hom considerava aquesta mena de context com el més adequat per a escatir de quina manera els canvis de nivell del mar són determinants en la construcció dels marges continentals. Amb aquest objectiu, el consorci d'investigadors de PROMESS1 decidí perforar els marges continentals del Mar Adriàtic, i del Golf de Lleó, influenciats pels rius Po i Roine, respectivament, que són els dos rius més cabalosos de la Mediterrània central i occidental (UNEP, 2003).

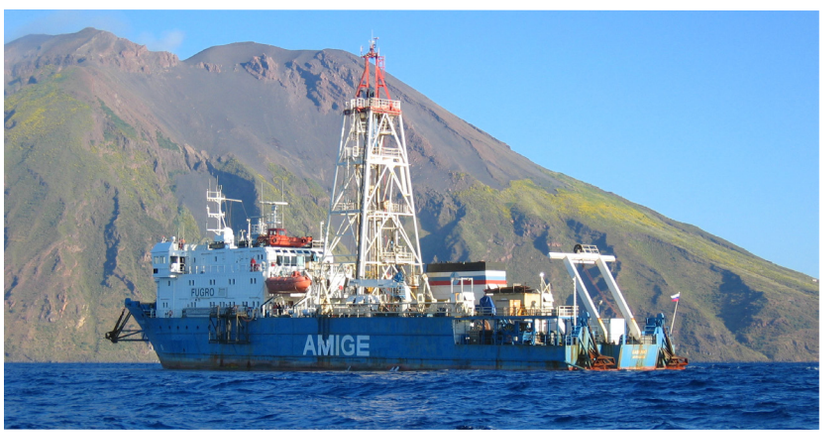

Figura 3.1. Vaixell perforador rus *MV Bavenit* davant l'illa de Stromboli durant la campanya PROMESS1 en que hom va recuperà el sondatge PRGL1-4 al Golf de Lleó.

En el marc d'aquesta Tesi, i com ja s'ha avançat, ens hem centrat únicament en el material del Golf de Lleó. La campanya de perforació s'efectuà l'estiu de l'any 2004 a bord del *MV Bavenit* (Taula 3.1), pertanyent a la corporació pública russa *Arctic Marine Engineering Geological Expeditions* (AMIGE) i operat per la multinacional holandesa d'exploració i enginyeria marines FUGRO Engineers B.V. sota contracte amb la Universitat de Barcelona (Fig. 3.1). Durant la campanya es perforaren dues localitats del marge golfllleonès. La primera localitat a perforar estava situada a la "plataforma intermèdia" de Berné et al. (2004a) (cf. Aptat. 2.4.1), a 103 m de profunditat d'aigua. Tot i així, hom fa referència més sovint a aquest sector com a "plataforma externa". Sigui com sigui, allí s'obtingué el testimoni PRGL2-2, de 100 m de longitud, amb l'objectiu d'estudiar les seqüències sedimentaries progradants regressives de la part de més enfora de la plataforma continental (Bassetti et al., 2008). L'altra localitat, que és la que més ens interessa en el marc d'aquesta Tesi, estava situada al talús superior, a 298 m de profunditat, al interfluvi entre els canyons submarins de l'Aude i l'Erau (Fig. 2.10). Tenint en compte les elevades taxes de subsidència i de sedimentació del marge, a més d'altra informació precisa i abundant de que hom disposava, la previsió era que en aquest interfluvi hi hagués preservada la seqüència estratigràfica contínua dels darrers 500 ka, com a mínim (Rabineau et al., 1998; Rabineau, 2001; Berné i Gorini, 2005). Fou en aquest indret on hom recuperà el testimoni PRGL1-4, de 300 m longitud, el qual s'estimava que incloïa les cinc seqüències estratigràfiques superiors S5, S4, S3, S2 i

S1, associades hipotèticament al darrers cinc cicles glacio-eustàtics segons (Rabineau, 2001; Rabineau et al., 2005) (Fig. 2.11). El material recuperat era format principalment per argiles amb llims de color gris, amb un cert grau de bioturbació i abundants taques negres de matèria orgànica. Intercalats entre aquest material més homogeni s'identificaren cinc capes de pocs centímetres (20-50 cm) amb un contingut de sorres elevat i riques en foraminífers (capes condensades; en anglès *condensed layers*).

L'any 1999, a la mateixa posició en el talús del Golf de Lleó hom va recuperar, durant la campanya IMAGES V del programa internacional "*The International Marine Past Global Change Study*", el testimoni MD99-2348, de 22,77 m de longitud. Aquest testimoni mostrava una capa superficial d'uns 50 cm de gruix amb un contingut elevat de sorres riques en foraminífers, mentre que la resta estava format per argiles llimoses homogènies amb certa bioturbació i taques abundants de matèria orgànica (Jouet et al., 2006; Sierro et al., 2009).

Hom ha pogut establir la cronostratigrafia del talús del Golf del Lleó corresponent als darrers cicles glacials/interglacials a partir de l'anàlisi dels isòtops de l'oxigen en foraminífers planctònics, datacions de ^{14}C, i altres anàlisis que aportaren informacions complementàries, com ara els percentatges de foraminífers temperats i els paràmetres granulomètrics (Jouet, 2007; Sierro et al., 2009; Frigola et al., 2012). Segons les dades obtingudes, el registre del testimoni MD99-2348 cobreix els darrers 25 ka, és a dir, el darrer màxim glacial, la desglaciació i l'Holocé, mentre que el testimoni PRGL1-4 cobreix els darrers 500 ka, és a dir, els darrers cinc cicles glacials/interglacials, amb l'excepció de la darrera desglaciació i l'Holocè degut a la pèrdua de la part superior del testimoni durant la recuperació. Aquest interval, però, sí que està recollit, com ja s'ha dit, en el testimoni MD99-2348.

Els models d'edat de tots dos testimonis mostren la gran influència dels canvis del nivell mar sobre el règim de sedimentació del marge del Golf de Lleó, amb taxes de sedimentació molt elevades en els períodes glacials, de fins a més de 2 m ka^{-1}, i molt baixes en els interglacials, uns pocs centímetres cada 1000 anys. Aquests contrastos en les taxes de sedimentació afecta, lògicament, la resolució temporal dels diferents intervals, que és de 160 i 1550 anys, en promig, pels períodes glacials i interglacials, respectivament.

Cal tenir en compte, però, que l'estratègia de mostreig fou diferent per a cada tipus d'anàlisi. Així doncs, per a les granulometries hom mostrejà cada 20 cm mentre que per a les anàlisis de la composició elemental hom efectuà mesures cada 4 cm. Cal esmentar també que les mostres per anàlisis d'isòtops de l'oxigen s'obtingueren cada 20 cm en promig, tot i que en la majoria de trams la resolució de treball fou de 10 cm (Sierro et al., 2009). Els resultats de les anàlisis rellevants per aquesta Tesi dutes a terme en els testimonis PRGL1-4 i MD99-2348 del Golf de Lleó es presenten en detall al Capítol II de Resultats.

El testimoni MD99-2343 del nord de Menorca (Taula 3.1) fou obtingut amb un testificador de pistó "Calypso" operat des del *V/O Marion Dufresne* durant la mateixa campanya IMAGES V en que fou recuperat el testimoni MD99-2348 del talús golflleonès abans esmentat. El testimoni menorquí feia 32,44 m de longitud, tot i que en aquesta Tesi només hem considerat els 17 m superiors, formats principalment per argiles llimoses, tot i que amb alguna capa de sorra. Mentre que els 5 m superiors eren homogenis, rics en foraminífers i nanofòssils i amb una bioturbació moderada, per sota d'aquesta cota els sediments mostraven moltes més laminacions, mil·limètriques i centimètriques, de tonalitats diverses. Durant l'operació d'extracció del testimoni hom perdé els 20 cm superiors; també es va identificar un buit de 80 cm als voltants dels 4 m de profunditat. Aquest buit fou atribuït a un desenganxament en el sediment durant la recuperació, degut probablement a l'efecte de succió generat pel pistó del testificador, desenganxament que s'hauria vist afavorit per la presència d'un nivell més sorrenc. Per tant, el buit per desenganxament no afectà la continuïtat de la seqüència recuperada, tal i com posteriorment demostraren el registre d'isòtops de l'oxigen i les datacions de ^{14}C a partir de les quals hom confeccionà el model d'edat del testimoni (Sierro et al., 2005; Frigola et al., 2007).

Els 17 m superiors del testimoni MD99-2343 corresponen als darrers 53 ka, i per a les anàlisis dutes a terme en el marc d'aquesta tesi hom seleccionà un interval de mostreig de 4 i 6 cm, d'on en resulten una resolució temporal i una taxa de sedimentació mitjanes de 125 anys i 36 cm ka^{-1}, respectivament.

L'estudi d'aquest testimoni ha permès esbrinar la variabilitat dels corrents de fons a la conca profunda del Mediterrani occidental durant els darrers 53 ka, palesant canvis amb escales temporals des de desenes de milers d'anys fins milers d'anys en el darrer període glacial i també a l'interglacial actual, l'Holocè. Els resultats de les anàlisis rellevants per aquesta Tesi dutes a terme en el testimoni MD99-2343 del nord de Menorca es presenten en detall al Capítol II de Resultats.

3.2. Anàlisi de la mida de gra

Les anàlisis granulomètriques de les mostres de sediment es dugueren a terme al Departament d'Estratigrafia, Paleontologia i Geociències Marines de la Facultat de Geologia de la Universitat de Barcelona amb un analitzador de mida de partícules per difracció de raigs làser Coulter LS100 (Fig. 3.2). Aquesta tècnica es basa en la mesura de la difracció que sofreixen els raigs làser en travessar una mostra en solució aquosa i impactar en les partícules en suspensió que conté. El Coulter LS100 consta d'un mòdul òptic, amb una font de raigs làser, una lent per expandir el feix de raigs, la cel·la per on hi passa la mostra en suspensió, les lents que concentren el feix difractat i l'anella detectora, amb 126 detectors; i un mòdul líquid, per on s'introdueix al mostra en suspensió. La font genera un feix estret de llum mo-

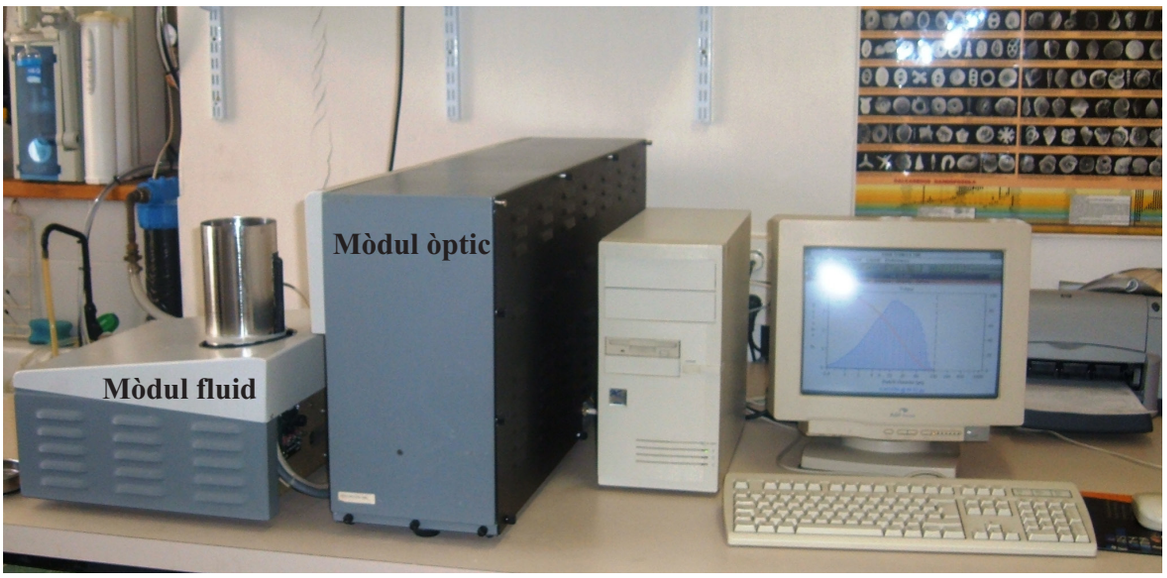

Figura 3.2. Aparell per a l'anàlisi de la mida de gra Coulter LS 100 instal·lat a la Facultat de Geologia de la Universitat de Barcelona, recentment substituit per un Coulter LS 230. Disposa d'un mòdul fluid per on s'introdueix la mostra en fase líquida, un mòdul òptic on es du a terme la mesura i un ordinador des d'on es controlen les mesures i es processen les dades.

nocromàtica amb una longitud d'ona de 0,75 μm la qual es fa passar a través de la mostra en solució en aigua filtrada. Les partícules en suspensió difracten els raigs lumínics, que són concentrats per les lents en el detector. El detector mesura a intervals de temps la distribució angular de la llum difractada i a partir d'ací obté la mida de les partícules aplicant la teoria de la difracció de Fraunhofer, de manera que com més gran és l'angle observat més petit és el diàmetre de les partícules. El Coulter LS100 permet mesurar la mida de partícules entre 0,4 μm i 1 mm. Per sota de 0,4 μm la teoria de Fraunhofer ja no és aplicable, donat que la longitud d'ona del feix de raigs emprat és massa gran pel diàmetre de les partícules (Agrawal et al., 1991). La mida de la partícula es dona com una funció de la seva secció transversal, o diàmetre esfèric equivalent, és a dir el diàmetre equivalent d'una esfera que produís la mateixa difracció que la partícula mesurada.

La qualitat de les mesures amb el Coulter LS100 de la Universitat de Barcelona fou avaluada en el període 2000-02 mitjançant un estudi comparatiu exhaustiu en el que s'analitzaren mostres naturals, de microesferes de vidre i estàndards oficials (Moreno, 2002). Aquest estudi permeté concloure que el Coulter LS100 és un instrument molt precís que proporciona resultats altament comparables amb els obtinguts per altres instruments de difracció de raigs làser. Per a ratificar la precisió i fiabilitat de l'aparell durant la realització de les anàlisis granulomètriques emprades per aquesta Tesi, hom efectuà regularment mesures de verificació amb estàndards de diferents diàmetres.

El fet que els sistemes de mesura de mida de gra per difracció làser, entre ells el Coulter LS100, donin la mida de les partícules com a diàmetre esfèric equivalent ha suscitat la crí-

tica d'algun autor (McCave et al., 2006). Aquesta crítica es fonamenta en que en el cas de partícules planes, com les argiles, aquesta tècnica pot sobreestimar la mida de les partícules, de la qual cosa en resulta una subestimació del percentatge d'argiles. El cert és que un estudi comparatiu entre diverses tècniques i aparells va palesar, primer, que no hi ha cap sistema absolutament perfecte per a mesurar la mida de les partícules donat que cada instrument mesura propietats diferents i, segon, que els instruments basats en la difracció làser són els que donen millors resultats (Goossens, 2008). De tota manera, a fi i efecte de corregir aquesta possible desviació causada per la forma aplanada de les argiles, en aquesta Tesi els càlculs dels percentatges d'aquesta fracció granulomètrica han estat fets tot i ampliant el seu límit fins a les 8 μm, tal i com suggereixen Konert and Vandenberghe (1997). Tot i que els valors absoluts de la fracció argilosa sí que canvien en aplicar aquest nou límit en el càlcul de percentatges, les variacions en profunditat d'aquesta fracció dins el mateix testimoni no es veuen afectades de forma significativa, si més no pel que fa als testimonis estudiats en aquesta Tesi.

Els avantatges principals de la mesura de la mida de gra per difracció làser amb el Coulter LS100 són la rapidesa i la bona reproductibilitat de les anàlisis, la necessitat de fer només una anàlisi a obtenir una forquilla prou ampla de mides de gra (altres sistemes estan limitats per forquilles de mesura força més estretes), la poca quantitat de mostra necessària per a l'anàlisi, la informació detallada de l'espectre granulomètric que proporciona i l'obtenció dels resultats directament en format digital (Moreno, 2002).

En la preparació de les mostres per a l'anàlisi de la fracció terrígena hom seguí el protocol modificat per Moreno (2002) (Fig. 3.3). Primer les mostres són atacades amb aigua oxigenada al 10% per eliminar la matèria orgànica, a fi i efecte d'evitar la formació d'agregats que podrien distorsionar les mesures. Seguidament, hom divideix les mostres en dues parts, una per a obtenir la granulometria de la mostra total i l'altra per a obtenir la de la fracció descarbonatada o terrígena. L'eliminació dels carbonats es fa mitjançant un atac ràpid, de poques hores, amb àcid clorhídric 1M (HCl 1M). Aquest atac ràpid assegura l'eliminació de tots els carbonats i que el clorhídric no afecti a la resta de la mostra, doncs altrament podria provocar canvis en la mineralogia de les argiles (Stuut, 2001). Posteriorment, hom enretira el HCl de la mostra per decantació, diluint amb aigua destil·lada l'àcid que pugui romandre. Finalment, abans de passar pel Coulter LS100 les dues submostres, la total i la descarbonatada, s'hi afegeix polifosfat de sodi per a prevenir la floculació de les argiles, sacsejant-les seguidament durant varies hores en un agitador mecànic. Així, amb molt poca quantitat de sediment hom pogué obtenir la granulometria de la mostra total o carbonatada, la qual pot ésser un indicador de paleoproductivitat, i la de la fracció terrígena o descarbonatada, que es pot assimilar a la població de partícules al·lòctones, essent per tant susceptible de indicar canvis en l'agent de transport, el qual variarà en funció de les característiques locals i/o regionals de cada àrea d'estudi (McCave et al., 1995b).

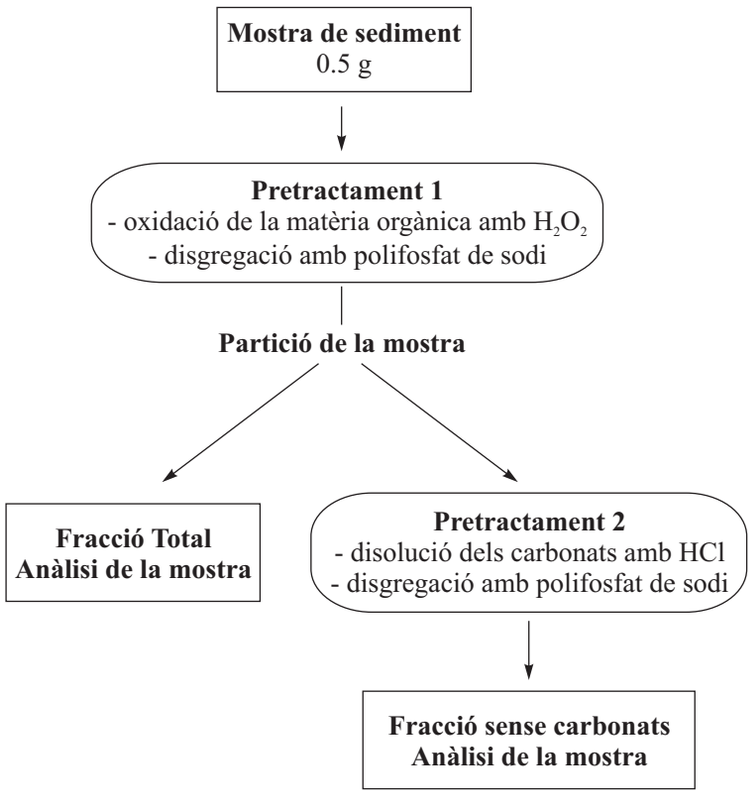

Figura 3.3. Esquema del tractament de les mostres per a l'anàlisi de la mida de gra.

La variabilitat granulomètrica al llarg del temps, és a dir, en profunditat dins un testimoni, pot ésser examinada avaluant un seguit de paràmetres, com ara el contingut en argiles, llims i sorres, la mitja, la mitjana i la moda. Un paràmetre molt emprat en paleoceanografia per a estudiar la intensitat dels corrents de fons és el percentatge de la fracció compresa entre 10 i 63 μm (% SS, de l'anglès Sortable Silt) i la mitjana d'aquesta fracció ($\overline{SS}$) (McCave et al., 1995b; Bianchi et al., 1999; McCave i Hall, 2006). Aquest índex inclou la fracció sedimentària, les partícules de la qual són susceptible d'ésser transportades pels corrents de manera individual, ja que les de mida inferior a 10 μm solen tenir un comportament cohesiu, i per tant, rarament són transportades de forma individual (McCave et al., 1995b). Cal tenir present, però, que el límit de 63 μm neix de les limitacions dels sistemes de mesura a partir dels quals fou definit, basats habitualment en el càlcul de la velocitat de caiguda de les partícules en un medi aquós segons la Llei de Stokes (com ara el Sedigraph), tot i assumint que en sediments hemipelàgics profunds les partícules >63μm corresponen a la fracció biogènica (McCave et al., 1995b). Lògicament, en sediments que puguin tenir una aportació terrígena de mida sorra molt fina o fina, entre 0,063-0,125 i 0,125-0,250 mm, respectivament, és convenient incloure aquestes fraccions més grolleres en l'índex que es defineixi, doncs són partícules que també sofreixen els efectes de la resuspensió i el transport per corrents de fons. De fet, els sediments del testimoni MD99-2343 del llom contornític de Menorca contenen una proporció prou significativa d'arena (5% en promig en la fracció descarbonatada), i més

concretament arena molt fina i fina (2% en promig de cadascuna en la fracció descarbonatada). Fou per la conveniència de tenir en compte aquesta fracció de sediment, les arenes fines i molt fines, en l'estudi dels paleocorrents de fons que definirem i usarem un nou índex, l'UP10, que representa el percentatge de partícules >10 μm i <1 mm, que és límit de mesura del Coulter LS100 en la banda dels grollers (Frigola et al., 2007). A més, també hem emprat la relació entre llims i argiles (en anglès *silt/clay ratio*) com a indicador de l'energia del medi en que es dipositaren les partícules sedimentàries estudiades (Hall i McCave, 2000; Frigola et al., 2008).

3.3. Anàlisi geoquímica amb fluorescència de raigs X

L' anàlisi dels elements majoritaris del sediment s'ha fet per fluorescència de raigs X (FRX), tant amb la tècnica tradicional de preparació de mostres discretes amb perles com mitjançant l'escaneig en continu dels testimonis de sediment amb escàner per fluorescència de raigs X (en anglès *XRF core scanner*). La fluorescència de raigs X és una de les tècniques més emprades en la determinació de la composició química de mostres geològiques, doncs amb poca quantitat hom pot arribar a analitzar fins a 80 elements amb una gran sensibilitat. A més, la preparació de la mostra és força ràpida i hom pot efectuar un alt nombre d'anàlisis amb gran precisió i poc temps (Rollinson, 1993). La limitació d'aquest mètode és que només serveix per mesurar elements per damunt del pes atòmic del Na en el cas de l'anàlisi de mostra discreta, i per damunt del pes atòmic de l'Al en el cas de l'escàner en continu.

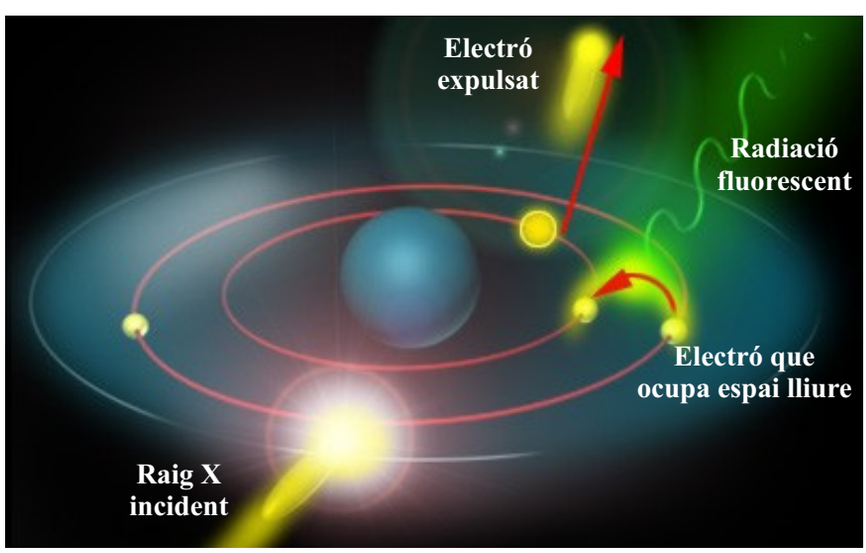

Figura 3.4. Principis de la fluorescència de raigs X. L'aplicació de raigs X sobre els materials provoca l'excitació dels àtoms interns dels elements, els quals deixen espais buits que s'omplen amb àtoms de nivells energètics superiors. La caiguda d'aquests àtoms genera l'emissió de la radiació fluorescent característica de cada àtom.

Figura 3.5. a) Sistema de mesura per fluorescència de raigs X Phillips 2400 instal·lat als Serveis Cientifico-Tècnics de la Universitat de Barcelona (ara Centres Científics i Tecnològics). **b)** Perles preparades per a l'anàlisi dels elements majoritaris per fluorescència de raigs X.

Aquesta tècnica es basa en l'excitació amb raigs X dels electrons dels àtoms dels diferents elements, la qual cosa fa que els electrons de les capes internes saltin a capes superiors tot i deixant espais buits. Això fa que els àtoms es tornin elèctricament inestables, de manera que per a estabilitzar-se cal que electrons de capes superiors ocupin els espais buits alliberant l'excés d'energia en forma de fotons, és a dir de fluorescència de raigs X (Fig. 3.4) (Potts i Webb, 1992). L'energia emesa depèn de la diferència energètica entre les dues capes d'electrons, la qual és característica de cada àtom, cosa que fa que cada àtom emeti una radiació característica. Llavors, en funció de la intensitat de l'energia associada a una longitud d'ona característica hom pot calcular la concentració d'un element per comparació amb estàndards calibrats, aplicant també correccions pels errors instrumentals i de l'efecte matriu (Rollinson, 1993).

Les anàlisis de la composició elemental dels elements majoritaris en el testimoni de Menorca MD99-2343 van ésser fetes amb un espectrofotòmetre seqüencial de raigs X per dispersió de longituds d'ona Philips PW2400 dels Serveis Cientifico-Tècnics de la Universitat de Barcelona, actualment Centres Científics i Tecnològics (CCiTUB), mitjançant la preparació de perles (Fig. 3.5). L'abundància en elements majoritaris s'obté com a percentatge dels seus òxids més freqüents (Al_2O_3, P_2O_5, K_2O, CaO, SiO_2, TiO_2, MnO, Fe_2O_3 i MgO), el quals són quantificats a partir d'una recta de calibratge confeccionada a partir de mostres d'estàndards geològics internacionals. Posteriorment, hom calcula el pes de cada element en el seu òxid i es fa un tancament a 100 per tal d'obtenir els percentatges dels elements majoritaris a cada mostra. Aquest procés simple d'ajust de la suma dels elements majoritaris a 100 pot

	Fe	Mn	Ti	Ca	K	P	Si	Al	Mg
Fe	1								
Mn	0,133	1							
Ti	0,662	0,041	1						
Ca	**-0,701**	0,015	**-0,898**	1					
K	0,709	0,005	0,750	**-0,852**	1				
P	-0,067	0,137	-0,453	0,451	-0,321	1			
Si	0,545	-0,108	0,857	**-0,954**	0,702	-0,540	1		
Al	0,748	0,134	0,796	**-0,822**	0,939	-0,237	0,649	1	
Mg	0,262	-0,012	0,256	-0,343	0,394	-0,187	0,249	0,284	1

Taula 3.2. Matriu de correlació dels elements majoritaris del testimoni del llom contornític de Menorca MD99-2343.

provocar, però, problemes de falta de llibertat estadística, com ara correlacions negatives entre elements (Rollinson, 1993). Per a avaluar aquest efecte hom va calcular la matriu de correlació entre els elements (Taula. 3.2), on es pot veure que el Ca presenta elevades correlacions negatives amb la majoria dels elements, d'on es desprèn que la correlació era forçada. Una de les eines més emprades per a corregir aquest efecte és la normalització amb algun dels elements majoritaris, de manera que hom deixa de parlar de canvis en un element i es passa a parlar de canvis en la relació d'un element respecte a un altre (Rollinson, 1993). Un dels elements més emprats en aquesta mena de normalitzacions és l'Al, considerat com a element conservatiu (Loring i Rantala, 1992; Calvert i Pedersen, 2007). Tot i així, aquesta normalització també pot produir desviacions, de manera que cal fer-la amb cautela, atenent al coneixement de les possibles àrees font i dels processos sedimentaris que puguin afectar al registre (Van der Weijden, 2002; Löwemark et al., 2011).

Comprovàrem així que a l'aplicar la normalització amb l'Al les correlacions negatives amb el Ca desapareixien. Per aquesta raó els registres geoquímics del testimoni de Menorca MD99-2343 són presentats i discutits en la forma normalitzada dins el capítol de resultats (cf. Aptats. 5 i 6). Aquest mètode de normalització és molt útil en paleoceanografia, doncs permet estudiar els canvis en les condicions ambientals que determinen la deposició i el transport de les partícules terrígenes (Calvert i Pedersen, 2007), malgrat no ésser vàlid per a fer anàlisis estadístiques rigoroses pel que fa a les concentracions dels elements.

La composició elemental en elements majoritaris en el testimoni PRGL1-4 del Golf de Lleó fou obtinguda amb un sistema de mesura en continu no destructiu de florescència de raigs X a la Universitat de Bremen (Fig. 3.6). L'aparell emprat fou el primer model de la companyia Avaatech, del *Netherlands Institute for Sea Research* (NIOZ), i els elements amb valors significatius mesurats foren Ca, K, Ti, i Fe. En l'actualitat, Avaatech està entregant la tercera generació dels seus escàners per fluorescència de raigs X, amb unes capacitats molt més

Figura 3.6. Escàner en continu per fluorescència de raigs X de primera generació fabricat per la companyia Avaatech (NIOZ, Holanda) instal·lat a la Universitat de Bremen (http://www.marum.de).

desenvolupades que el primer model, tant en termes de detecció d'elements (des de l'Al fins a l'U) com en termes de resolució màxima mesurable (fins a 100 μm). Aquest escàners han revolucionat el món de la paleoceanografia doncs permeten obtenir una elevada quantitat de dades de manera continua, amb una resolució impensable fins fa ben poc, en un temps molt curt i de forma no destructiva (Jansen et al., 1998; Richter et al., 2006; Rothwell, 2006; St-Onge et al., 2007). Una de les peculiaritats d'aquests instruments és que els valors s'obtenen en comptes per segon (cps, de l'anglès *counts per second*), i que aquests depenen de les condicions d'excitació i mesura, i de les propietats (contingut d'aigua, contingut de matèria orgànica, mida de gra, i altres) de la matriu del sediment analitzat. Per aquest motiu, hom no pot considerar el mètode com quantitatiu sinó com semi-quantitatiu, donat que hom sempre pot calibrar els resultats assolits mitjançant l'anàlisi d'un conjunt de mostres discretes i la construcció d'una recta de calibratge (Rothwell, 2006).

De tota manera, al mantenir-se constants les condicions de mesura d'un testimoni o d'un conjunt de testimonis, tot i que els valors d'un element no corresponguin estrictament a les seves concentracions, sí que es cert que les oscil·lacions observades en el registre corresponen a oscil·lacions en la concentració de l'element de que es tracti. Per tant, l'estudi de les oscil·lacions observades en el registres obtinguts amb aquest mètode permet, sense cap ombra de dubte, interpretar variacions en les condicions ambientals i en l'aportació de sediment, que és el que es pretén en el marc d'aquesta Tesi dins l'àmbit més ampli de la paleoceanografia. Per tot plegat, aquesta tècnica és plenament acceptada i practicada per la comunitat paleoceanogràfica internacional (Calvert i Pedersen, 2007).

Les dades proporcionades pels escàners per fluorescència de raigs X també solen ésser objecte de normalització amb l'Al a fi i efecte d'evitar possibles correlacions falses entre elements. De fet, fins i tot s'ha proposat d'usar els logaritmes dels elements normalitzats (en anglès *log-ratios*) perquè aquests es correlacionen linealment amb els canvis relatius en la

composició química (Aitchison, 1982; Weltje i Tjallingii, 2008). En el cas del testimoni PRGL1-4 no es va poder aplicar la normalització amb l'Al perquè l'aparell utilitzat no permetia encara mesurar aquest element pel fet d'ésser molt lleuger. Els sistemes més moderns si que ho permeten. El que hom va observar és que el registre del Ca mostrava unes tendències en general oposades a la resta d'elements, K, Ti i Fe, els quals mostraven entre ells una correlació molt alta (Taula 3.3).

	Ca	K	Ti	Fe
Ca	1			
K	-0,035	1		
Ti	-0,332	0,841	1	
Fe	-0,400	0,772	0,829	1

Taula 3.3. Matriu de correlació dels elements majoritaris del testimoni del talús continental superior del Golf de Lleó PRGL1-4.

La normalització dels registres amb el Ti, que és un altre element emprat per aquesta finalitat per alguns autors (Calvert i Pedersen, 2007), no comportava cap canvi en les tendències dels registres, els quals seguien mostrant una correlació elevada amb el Ca, amb l'excepció del Fe/Ti. Al tractar-se de dos elements marcadors d'origen terrigen, la seva relació elimina qualsevol tendència i, per tant, no aporta informació. Els resultats, molt similars als que s'obtenien amb l'aplicació dels log-ratios, confirmaren que en aquest testimoni tots els registres dels elements majoritaris mesurats, Ca, K, Fe i Ti, són indicadors d'aportacions terrígenes. El Ca, que és l'element més abundant, fou relacionat amb aportacions carbonatades detrítiques procedents del riu Roine, principal font de sediment del talús continental golflleonès. A més, els registres del percentatge de carbonat càlcic a la mostra, obtingut per calcimetries, i d'argiles de la fracció total (carbonatada) són molt semblants al registre de Ca obtingut per escàners per fluorescència de raigs X, fet que recolza la interpretació donada al registre del Ca i confirma que no està influenciat per la resta d'elements (Fig. 3.7). En conseqüència, en el cas del testimoni PRGL1-4 del Golf de Lleó, a l'apartat de resultats només es farà menció al registre de Ca com a indicador de les aportacions fluvials.

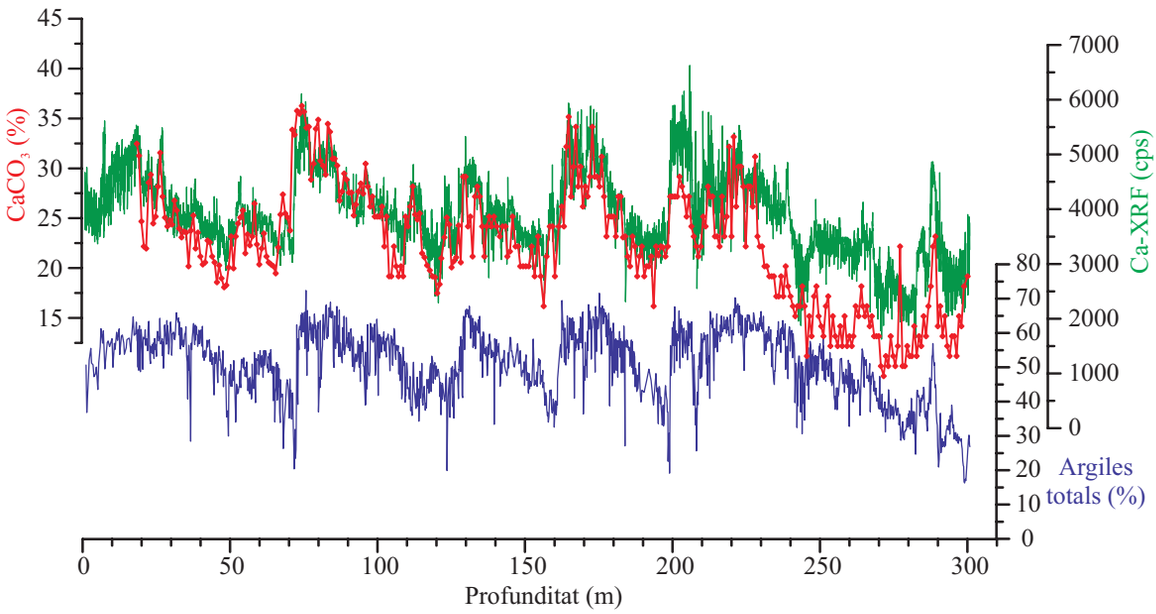

Figura 3.7. Registres del testimoni PRGL1-4 dels continguts en Ca mesurat amb un escàner per fluorencència de raigs X (en verd), en carbonats mesurats mitjançant calcimetries (en roig), i el percentatge d'argiles de la fracció total (carbonatada) mesurat amb el Coulter LS 100 (en lila).

CAPÍTOL II. RESULTATS

4. A 500 kyr record of global sea-level oscillations in the Gulf of Lion, Mediterranean Sea: new insights into MIS 3 sea-level variability

J. Frigola[1], M. Canals[1], I. Cacho[1], A. Moreno[2], F. J. Sierro[3], J. A. Flores[3], S. Berné[4,8], G. Jouet[4], B. Dennielou[4], G. Herrera[1], C. Pasqual[1], J. O. Grimalt[5], M. Galavazi[6], and R. Schneider[7]

[1]CRG Marine Geosciences, Department of Stratigraphy, Paleontology and Marine Geosciences, University of Barcelona, Spain
[2]Pyrenean Institute of Ecology, Spanish Research Council, Zaragoza, Spain
[3]Department of Geology, University of Salamanca, Spain
[4]IFREMER Laboratoire Environnements Sédimentaires, Plouzané, France
[5]Department of Environmental Chemistry, Spanish Research Council, Barcelona, Spain
[6]Fugro Engineers B.V., Leidschendam, The Netherlands
[7]Institut fur Geowissenschaften, Christian-Albrechts-Universität zu Kiel, Germany
[8]Université de Perpignan Via Domitia, Perpignan, France

Abstract

Borehole PRGL1-4 drilled in the upper slope of the Gulf of Lion provides an exceptional record to investigate the impact of late Pleistocene orbitally-driven glacioeustatic sea-level oscillations on the sedimentary outbuilding of a river fed continental margin. High-resolution grain-size and geochemical records supported by oxygen isotope chronostratigraphy allow reinterpreting the last 500 ka upper slope seismostratigraphy of the Gulf of Lion. Five main sequences, stacked during the sea-level lowering phases of the last five glacial-interglacial 100-kyr cycles, form the upper stratigraphic outbuilding of the continental margin. The high sensitivity of the grain-size record down the borehole to sea-level oscillations can be explained by the great width of the Gulf of Lion continental shelf. Sea level driven changes in accommodation space over the shelf cyclically modified the depositional mode of the entire margin. PRGL1-4 data also illustrate the imprint of sea-level oscillations at millennial timescale, as shown for Marine Isotopic Stage 3, and provide unambiguous evidence of relative high sea-levels at the onset of each Dansgaard-Oeschger Greenland warm interstadial. The PRGL1-4 grain-size record represents the first evidence for a one-to-one coupling of millennial time-scale sea-level oscillations associated with each Dansgaard-Oeschger cycle.

Climate of the Past, 8, 1067–1077, 2012
doi:10.5194/cp-8-1067-2012
www.clim-past.net/8/1067/2012/

4.1. Introduction

Sea level oscillations of about 120 m of amplitude paralleled the orbitally-driven 100-kyr climate cycles of the late Pleistocene in response to global ice volume changes (Imbrie et al., 1992; Siddall et al., 2006a). Jointly with sediment input and subsidence, these sea-level oscillations controlled the stratal geometry of passive continental margins where migration of fluvial-influenced deposits generated regressive/transgressive depositional sequences. The seismostratigraphic study of those stacked sequences can help to develop the linkage between sea-level fluctuations and sedimentary unit deposition once the seismic interpretation is placed in a sequence stratigraphy framework (Vail et al., 1977; Posamentier and Vail, 1988). More refined sea-level curves based upon benthic and planktic oxygen isotopes in marine sediment cores, in some cases corrected for temperature variations, and dated uplifted coral terraces have been published during the last decade (Rohling et al., 1998a; Shackleton et al., 2000; Yokoyama et al., 2001; Chappell, 2002; Waelbroeck et al., 2002; Siddall et al., 2003; Miller et al., 2005; Thompson and Goldstein, 2005, 2006; Rohling et al., 2009b). However, intrinsic limitations of sea-level reconstruction methods and limitations of obtaining better and more precise age control of marine records make difficult the task to accurately constrain orbital and millennial time-scale sea-level fluctuations. Thus, continental margin sedimentary records consisting of depositional units characterised with very high sedimentation rates and precise chronology could provide a better time control and resolution high enough to improve the reconstruction of past sea level oscillations.

In the Gulf of Lion (GoL) margin, western Mediterranean Sea, deltaic forced Regressive Progradational Units (RPUs) stacked on the outer-shelf and upper slope during relative sea-level falls (Fig. 4.1), led some authors to describe this margin as a forced regressive system (Tesson et al., 1990; Posamentier et al., 1992; Tesson et al., 2000). The significant subsidence rate of the margin, 250 m Myr^{-1} at the shelf edge (Rabineau, 2001), eased the preservation of RPUs in the upper slope, as it was continuously submerged even during pronounced lowstands. These significant subsidence rate allowed preserving the majority of the regressive/transgressive depositional sequences across the outer shelf (former coastal deposits from old lowstand coast lines) and the upper slope accumulation where dating is easier, thus, resulting in an ideal area for the study of the late Quaternary sedimentary succession. The huge amount of seismic reflection profiles obtained in the GoL margin facilitated the identification of major unconformities defining sequence boundaries in the outer-shelf that become correlative conformities in the upper slope. There five major RPUs were identified and interpreted to correspond to the last five 100-kyr cycle sea level falls (Fig. 4.1b) (Rabineau et al., 1998; Rabineau et al., 2005; Bassetti et al., 2008). However, precise dating of RPUs sequence boundaries was still needed to constrain better the imprint of sea-level oscillations on the GoL margin and to determine the leading cyclicity of the deposition of those units, i.e., if they originated during sea-level lowerings of 20 kyr or 100 kyr cycles (Lobo et al., 2004).

In addition, millennial-scale sea-level oscillations at times of rapid climate change during Marine Isotope Stage (MIS) 3 are of special interest, since determining their amplitude and phasing with ice core records is crucial to understand the behaviour and role of ice sheets on millennial climate variability (Siddall et al., 2008). In fact, MIS 3 relative sea-level rises have been tentatively associated with both contributions from the Antarctic and the Laurentide ice sheets (Siddall et al., 2003 i 2008; Arz et al., 2007; Rohling et al., 2008; Sierro et al., 2009), thus, evidencing the lack of consensus on the sea-level response to rapid climate variability.

Here, we present grain-size and geochemical records from a borehole in the GoL upper slope, together with a robust oxygen isotope chronostratigraphy, which allow identifying and accurately dating the main RPUs of the last 500 ka, and obtaining the timing of millennial-scale sea-level changes in response to abrupt climate variability during MIS 3.

4.2. Setting and present day conditions

The GoL forms a crescent-shaped passive margin that is characterised by a 70 km wide continental shelf covering an area of about 11,000 km^2 (Fig. 4.1a). The GoL continental shelf was mainly built by late Quaternary glacio-eustatic oscillations and post late glacial sedimentation. The shelf can be subdivided in three distinct parts: (i) the inner shelf, extending from 0 to 90 m, is characterised by gradual and regular morphological gradients, as illustrated by parallel and regularly spaced isobaths; the inner shelf corresponds to the modern deltaic prism (Fig. 4.1); (ii) the middle shelf, ranging in depths from 90 to 110–120 m, is mostly flat with an irregular morphology, mainly capped by relict offshore sands shoals; and (iii) the outer shelf, a narrow band with depths ranging from 110–120 m that extends to the shelf break and is characterised by a general smooth morphology (Berné et al., 2004a) (Fig. 4.1a). The shelf break is located at 120–150 m and is indented by numerous submarine canyons and gullies which connect the continental shelf to the deep margin and basin. The overall GoL continental shelf physiography offered a huge accumulation space for water and sediment storage during periods of relative rising and high sea level during late Quaternary deglacial and interglacial intervals, while it remained totally or partly exposed subaerially during late Quaternary sea-level lowerings and lowstand glacial periods.

The Rhone River is the main source of sediment to the GoL shelf while other minor fluvial inputs also occur along the coastline (Pont et al., 2002). Modern fluvial sediments are mainly trapped on the inner shelf, although they can also be remobilised and subsequently transported to the middle and outer shelf and beyond to the upper slope by shelf erosional and re-suspension processes. These processes are mainly driven by dense shelf water formation and cascading events (DSWC) and easterly storms and, to a much lesser extent, by the southwestward general circulation pattern of the Northern Current (NC) (Fig. 4.1a) (Ulses

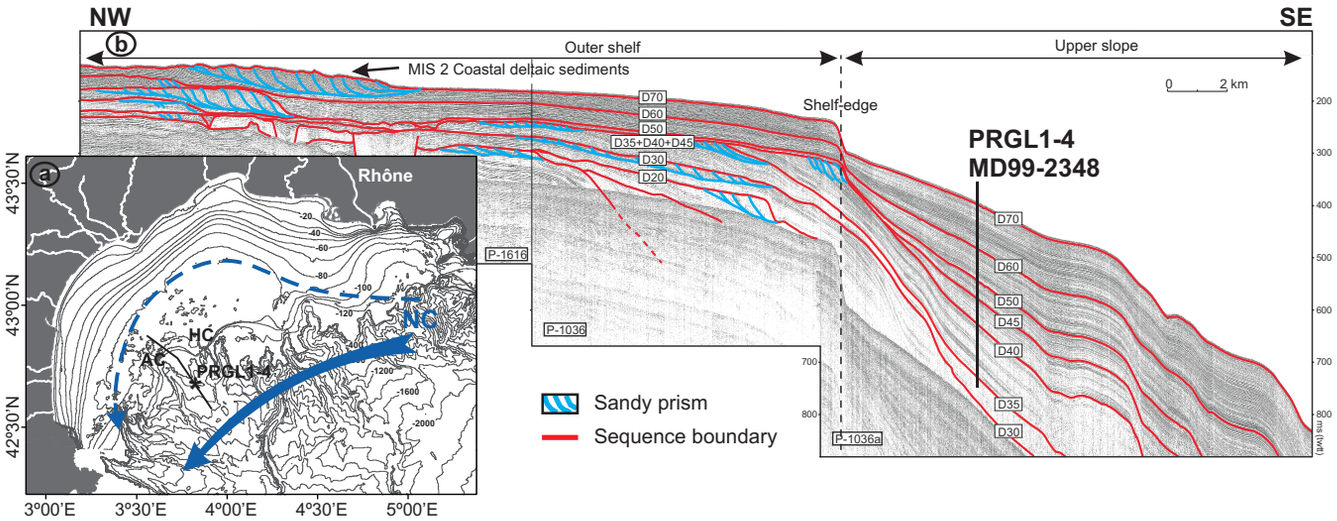

Figure 4.1. a) Bathymetric map of the Gulf of Lion with location of borehole PRGL1-4 in the interfluve separating Aude and Hérault submarine canyons, AC and HC, respectively. The dominant component of the general circulation is shown by the geostrophic Northern Current (NC), which flows southwestward along the slope and occasionally penetrates over the outer shelf, blue arrows. **b)** Part of high-resolution seismic reflection profile P-1036a crossing the borehole location in a NW–SE direction across the outer shelf and upper slope (modified from Jouet, 2007). Stratigraphic sequences S1 to S5 delimited by main reflectors D35 to D70 marked as defined by Jouet (2007). Red reflectors show the main conformities separating RPUs while the blue ones correspond to sandy prisms.

et al., 2005; Bassetti et al., 2006; Canals et al., 2006; Dufois et al., 2008). In addition to northerly wind-induced DSWC, deep-water formation also occurs offshore during windy winters, where it may lead to deep convection (Millot, 1999). However, the sediment load involved in offshore convection is very low when compared to DSWC and major coastal storms, both constituting the most effective processes of sediment export from the shelf to the basin, mainly through submarine canyons (Canals et al., 2006; Palanques et al., 2006; Sanchez-Vidal et al., 2008 i 2012; Pasqual et al., 2010).

4.3. Material and methods

This study is based on detailed analyses of the 300 m-long continuous sediment record recovered in borehole PRGL1-4 (42º 41.39' N and 03º 50.26' E), drilled at 298 m of water depth in the interfluve separating Aude and Hérault submarine canyons during *MV Bavenit* PROMESS1 cruise, and on the overlapping 22.77 m long IMAGES core MD99-2348 retrieved at the same location (Fig. 4.1a).

Grain-size analyses on the bulk and the decarbonated sediment fractions were carried out at 20 cm sampling intervals with a Coulter LS 100 Laser Particle Size Analyser after removing organic matter by treatment with excess H_2O_2 and carbonates by treatment with HCl. Grain-size results are discussed here as the silt/clay ratio of the carbonate-free fraction, an established proxy for energy levels at the time of particle deposition (Frigola et al., 2007).

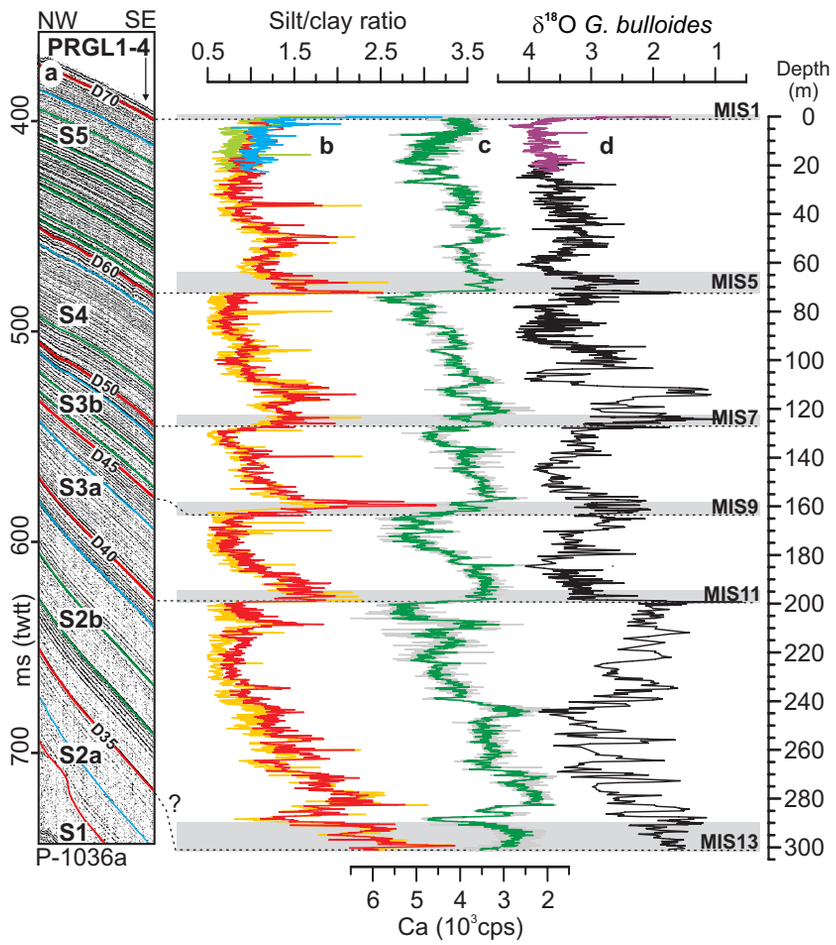

Figure 4.2. a) Close view of high-resolution seismic reflection profile P-1036a at the location of borehole PRGL1-4 (Jouet, 2007), visually correlated with **b)** silt/clay ratio records from total (light orange and green) and Ca-free (red and blue) sediment fractions from PRGL1-4 and MD99-2348 sediment cores, respectively. **c)** 5-point moving average (green) of Ca record (grey) from PRGL1-4. **d)** Oxygen isotopic records from PRGL1-4 (black) and MD99-2348 (purple) obtained from *G. bulloides*. Grey bars correspond to condensed interglacials sequences 1, 5, 7, 9, 11 and 13. Dotted lines correlate the main seismic reflectors (sequence boundaries) and their expression on the different records.

Matching of silt/clay ratio records from both bulk and decarbonated sediments allows discarding the in situ paleoproductivity signal that could affect the grain-size record (Fig. 4.2b).

Semi-quantitative analysis of major elements (Ca, Fe, Ti and K) was carried out at 4 cm resolution using the first generation Avaatech non-destructive X-ray fluorescence (XRF) core scanner of the University of Bremen. The good correlation of the Ca record with sedimentation rates and with the clay content (not shown here), suggest that Ca delivery at the study site is mainly related to detrital carbonate inputs from fluvial sources. Calcite is at present one of the main mineralogical components in suspended matter delivered by the Rhône River (Pont et al., 2002), which is the most relevant sediment source to the GoL, as previously mentioned. These evidences support the use of the Ca record from borehole PRGL1-4 as a trustable proxy of changes in fluvial sediment delivery to the GoL upper slope (Fig. 4.2c).

The age model was obtained by synchronizing the records of planktic *Globigerina bulloides* $\delta^{18}O$ and abundance of temperate to warm planktic foraminifers to the North GRIP ice core isotope record for the last 100 ka (NGRIP, 2004; Andersen et al., 2006; Svensson et al., 2008). From 100 to 530 ka the age model was built by aligning the PRGL1-4 *G. bulloides* $\delta^{18}O$ record to the LR04 benthic isotope stack (Lisiecki and Raymo, 2005) (Fig. 4.3), with the support of the planktic oxygen isotope records from the Portuguese margin (Roucoux et al., 2006) and the North Atlantic region (Stein et al., 2009) for specific time intervals. For more details on the age model, tie points and ^{14}C-AMS dates see Sierro et al. (2009). Work is in progress to further improve time constrains during MIS 12 and 13 (F. J. Sierro, personal communication, 2012). Temporal variability of sedimentation rates (SR) resulted in a mean temporal resolution of 160 and 1550 yr during glacial and interglacial periods, respectively.

4.4. Results and discussion

4.4.1. The orbital 100-kyr sea-level imprint

The silt/clay ratio and Ca records from PRGL1-4 show a seesaw pattern defining five main units characterised by an upwards fining and Ca content increasing trend, which can be correlated with the main seismostratigraphic units in the seismic reflection profiles crossing the borehole location (Jouet, 2007) (Fig. 4.2). The sedimentary units end with an abrupt increase in the silt/clay ratio and a rapid decrease in the Ca content coinciding with the main reflectors corresponding to sequence boundaries in the seismic reflection profile. The excellent correlation of these analytical sequences with the seismostratigraphy, together with chronostratigraphic control from the *G. bulloides* $\delta^{18}O$ record (Sierro et al., 2009), confirm the 100-kyr-cycle origin of these units. The data derived from PRGL1-4 borehole allowed us to reinterpret the seismostratigraphy of the GoL upper slope, where seven units (S1, S2a, S2b, S3a, S3b, S4 and S5) are now documented (Jouet, 2007), instead of the five (S1 to S5) previously identified from seismic reflection profiles alone (Rabineau, 2001). These seven units result from subdividing the former sequences S2 and S3 into S2a and S2b, and S3a and S3b, respectively (Fig. 4.2a). The results obtained suggest that the lowermost seismostratigraphic units S1 and S2a were not penetrated at PRGL1-4, with the base of the drill most likely corresponding to MIS 13 taking into account extinction of coccolith *P. lacunosa* at about 275 m in the borehole (Figs. 4.2 and 4.3). Accordingly, the upper five main depositional sequences stacked on the upper slope of the GoL, corresponding to RPUs driven by global sea-level oscillations of the last five glacial cycles, are identified in the continuous sedimentary record of PRGL1-4 borehole. Consequently, abrupt increases in the silt/clay ratio and decreases in the Ca content respond to rapid sea level rise, continental shelf flooding and subsequent landward migration of deltaic systems during glacial-interglacial transitions, giving birth to sequence boundaries in the upper slope as defined by analytical results (Fig. 4.2).

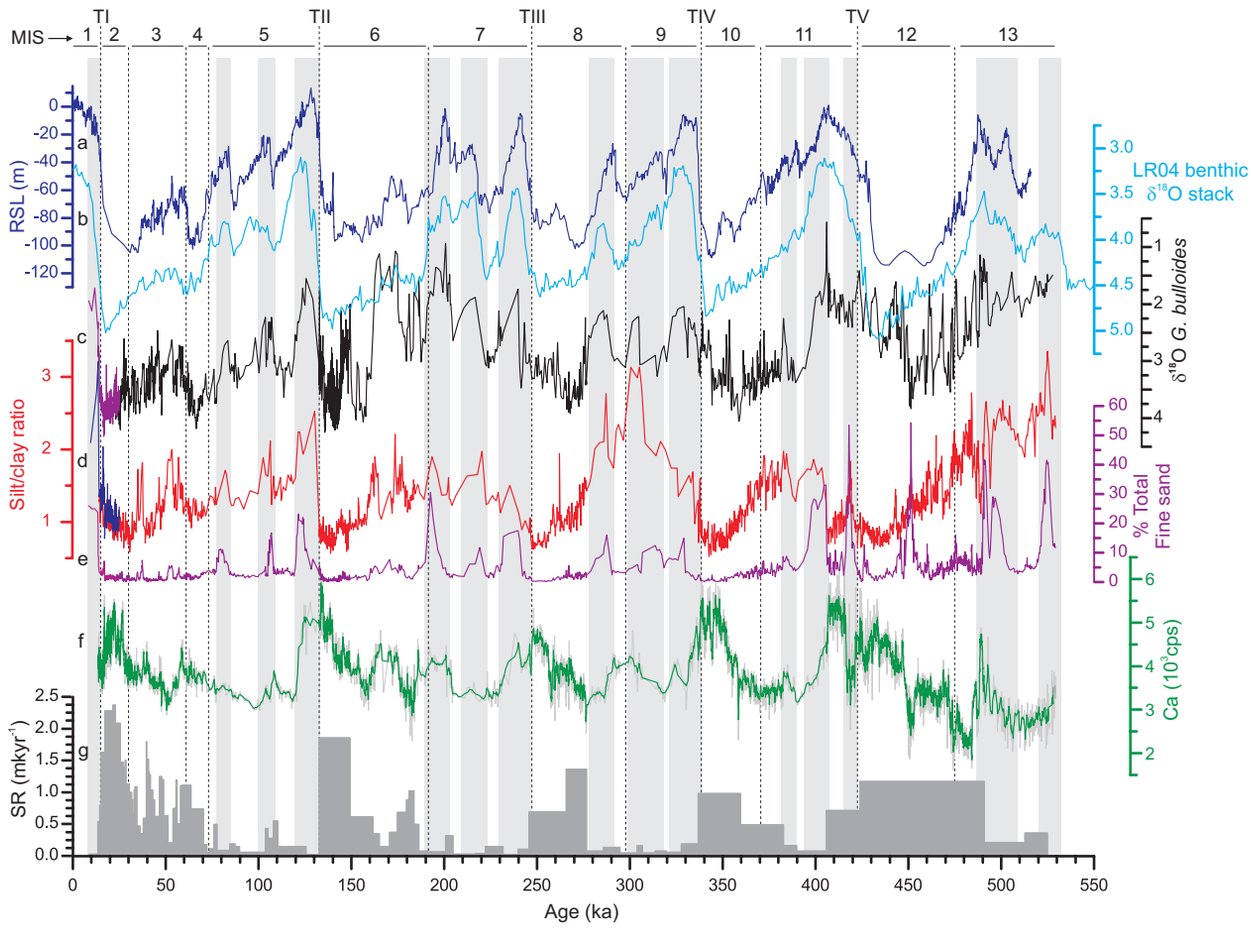

Figure 4.3. Multiproxy continuous records of PRGL1-4 borehole with respect to relative sea-level oscillations for the last 500 ka. **a)** Composite central Red Sea relative sea level reconstruction for the last 500 ka (Rohling et al., 2009). **b)** LR04 benthic isotope stack record used as reference record (Lisiecki and Raymo, 2005). PRGL1-4 records of **c)** *G. bulloides* $\delta^{18}O$, **d)** Ca-free silt/clay ratio, **e)** total fine sand (%) (Sierro et al., 2009), **f)** XRF-Ca, and **g)** linear sedimentation rates. The top 22 ka of the *G. bulloides* $\delta^{18}O$ record (purple), the silt/clay ratio of the carbonate-free fraction (blue) and the total fine sand (pink) are from overlapping core MD99-2348, which include the abrupt change associated with the last deglaciation that is not covered by the XRF-Ca record of PRGL1-4. Vertical grey bars show how the main condensed layers (CLs), defined by abrupt increases in the total fine sand fraction record, fit with interglacial stages.

RPU stacking in the upper slope resulted from seaward migration of deltaic systems and the subsequent enhancement of riverine supply because of the sea level lowering during each 100-kyr cycle. That is why maximum sedimentation rates (1.5–2.5 m kyr^{-1}) in the upper slope were recorded during periods when the distance to river mouths was minimal (i.e., during glacial lowstands) (Figs. 4.3g and 4.4a). The presence of relict offshore sands at 110–115 m depth along the outermost shelf further supports the location of lowstand glacial paleoshorelines in the vicinity of the Aude Canyon head (Aloïsi, 1986; Berné et al., 2004a; Bassetti et al., 2006; Jouet et al., 2006). The increasing trend of SRs linked to sea level lowering across a glacial period is particularly well resolved for the last glacial period (MIS 2, 3 and 4), during which intervals the chronostratigraphic control is particularly robust (Fig. 4.3g). Sedimentation rates also peaked during previous 100-kyr cycles glacial sea level minima, although the weaker chronostratigraphic control with depth does not allow distinguishing SR trends during previous full forced regressions, but only low or high SR during intergla-

cial and glacial stages, respectively. Co-occurrence of lowest silt/clay ratios and highest Ca contents during glacial sea level minima confirms the reinforced influence of nearby glacial river mouths on the sedimentation of fines over upper slope interfluves (Figs. 4.3d and 4.3f). Accordingly, while during glacial lowstands the coarsest fractions were mostly trapped and funnelled by glacial adjacent submarine canyons, as demonstrated by pronounced axial incisions within their upper courses (Baztan et al., 2005), large amounts of fine particles supplied by the nearby river mouths remained in suspension, probably transported by along shore current and un-trapped by the canyons, thus, leading to substantial accumulation in inter-canyon areas.

In contrast, SRs were lowest (0.10–0.25 m kyr^{-1}) during interglacial sea-level highstands associated with the landward migration of deltaic systems far away from the shelfbreak and upper slope (Figs. 4.3g and 4.4b), as illustrated by the modern Holocene epicontinental prism extending down to 90 m water depth over the inner shelf (Aloïsi, 1986; Berné et al., 2004b i 2007). Obviously, these glacial/interglacial contrasting sedimentation rates resulted in expanded glacial intervals (therefore, resulting in higher temporal resolution) and condensed interglacial intervals down the 500 kyr-long record in PRGL1-4 borehole (Fig. 4.3). With each sea level rise, sedimentation rates reduce significantly in the upper slope and PRGL1-4 records experience a reduction of temporal resolution (e.g., just few points represent a full interglacial period). This same limitation in time resolution prevents us to establish the exact timing of SR reductions, which in turn are depending on selection of tie points in the age model. In addition, the very low SRs during the main interglacial highstands led to the formation of condensed layers (CLs), i.e., sandy layers rich in pelagic skeletal material, along the GoL upper slope (Fig. 4.3e), as shown by the total (bulk fraction, non carbonate-free) fine sand record of Sierro et al. (2009) (Fig. 4.3e).

However, the landward excursion of deltaic systems linked to the updip migration of the coastline when sea level rise is rising and the associated reduction in sediment flux to the upper slope during glacial/interglacial transitions, cannot explain the continuous supply of coarse particles to the upper-slope during every interglacial stage, as evidenced by the high values of the carbonate-free silt/clay ratio (Fig. 4.3d), nor the observed increase in non-biogenic sand particles (mainly quartz grains) into the sediment. These results suggest that the interglacial flooding of the 70 km wide GoL shelf (Fig. 4.4b) likely reactivated oceanographic processes able to erode, re-suspend and transport coarse particles, like those contributing to the formation of CLs. While the southwards flowing Northern Current (NC) sweeping the shelf edge and upper slope (Fig. 4.1a) could contribute winnowing the finest particles during long lasting periods of reduced sediment input to the upper slope, it could not explain the arrival of new lithic coarse material found in deposits formed during interglacial periods, including CLs. The inundation of the shelf during interglacial periods generated a relatively thin layer of water that was highly sensitive to atmospheric forcing, which may trigger the

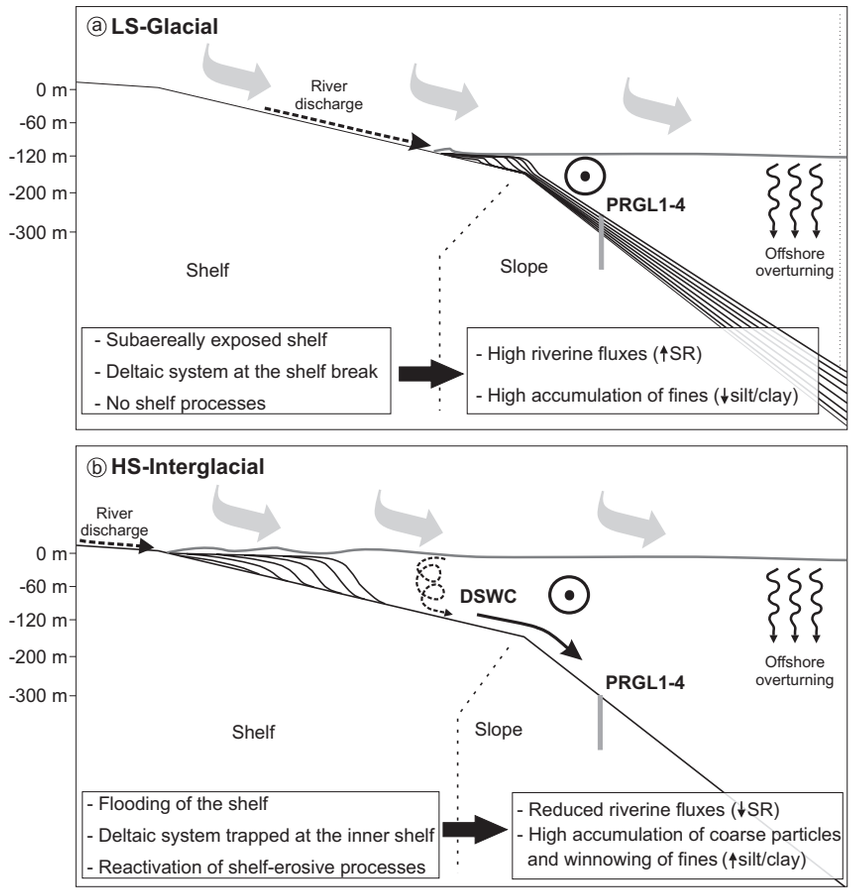

Figure 4.4. Conceptual depositional model of the Gulf of Lion continental margin at orbital scale. **a)** During the lowstand (LS) depositional mode (glacial periods) the continental shelf is subaerially exposed and the basinwards migration of deltaic system results in high amounts of fine particles supplied directly to the upper slope. **b)** Flooding of the shelf during the high-stand (HS) depositional mode (interglacial periods) traps deltaic systems in the inner shelf, thus, disconnecting the upper slope from direct fluvial discharges. Moreover, the creation of a relatively thin layer of water over the continental shelf reactivates shelf erosive processes, such as Dense Shelf Water Cascading (DSWC), that are able to transport coarseparticles down the slope. Both processes contribute to generate thin condensed layers (CLs) in the upper slope. Grey arrows represent the northern winds involved in cooling the superficial shelf water for dense shelf water formation and offshore overturning. Dot in a circle shows the dominant direction of the slope-parallel Northern Current. The discontinuous spiral arrow over the shelf represents shelf-erosive processes, as DSWC.

remobilisation of sedimentary particles temporarily stored on the shelf, as it happens during the present day highstand (Bassetti et al., 2006; Canals et al., 2006; Dufois et al., 2008). Recent studies have demonstrated that nowadays northern cold, strong and persistent winds lead to DSWC down-slope at high speed (up to 1 m s^{-1} or more) during late winter and early spring months in the GoL (Canals et al., 2006). Cascading waters carry large amounts of organic matter and sedimentary particles whose coarser fraction efficiently scours and erodes the shelf edge and canyon heads and upper courses (Gaudin et al., 2006; Lastras et al., 2007; Puig et al., 2008; Sanchez-Vidal et al., 2008; Pasqual et al., 2010). Activation in the past of continental shelf erosive processes like DSWC probably did not lead to significant sediment accumulation in upper slope interfluves, but favoured the winnowing of fines and the supply of coarse lithic particles that, in combination with low sedimentation rates, contributed to

generate CLs. When the "cooling platform" disappeared, i.e., during subaerial exposure of the continental shelf (lowstand conditions, Fig. 4.4a), there was no room left for dense shelf waters to form and, therefore, these type of continental shelf erosive processes ceased. During transitional periods, when the shelf was partly flooded, the volume of water involved in cascading and other continental shelf erosive processes was smaller, subsequently lessening downslope transport by dense shelf waters. Therefore, changes in the silt/clay ratio also respond to the flooded shelf area and, consequently, to sea-level oscillations. This explains the relatively good match between the silt/clay ratio and sea level for the last 500 ka (Figs. 4.3a and 4.3d), which is especially evident for the last glacial cycle when the chronostratigraphic control is more precise. Obviously, the silt/clay ratio did not respond linearly to sea-level oscillations and reactivation of continental shelf erosive processes could be also related to some environmental threshold, e.g., the volume of water stored on the shelf. This, together with significant reductions of SRs during each sea level rise, and subsequent reductions in time resolution, prevent us using the silt/clay ratio as an exact indicator of the beginning of sea level rises. However, the persistent pattern observed in the silt/clay ratio through the last five glacial/interglacial cycles and also at millennial time scales, as described below, confirms this ratio is a good indicator of relative high sea-level conditions (highstands) in the GoL margin.

These results support a combined shelf and upper slope depositional model for inter-canyon RPU stacking over the last 500 ka that considers two main processes: (i) oscillations in sediment supply due to the migration of river mouths and deltaic systems, and (ii) activation-deactivation of continental shelf erosive processes like DSWC, both of them ultimately driven by the 100-kyr glacio-eustatic cyclicity (Fig. 4.4).

4.4.2. The millennial MIS 3 sea level imprint

Since this combined depositional model has been tested at glacial/interglacial scales, it is reasonable to expect that minor scale sea-level oscillations would also result in a similar sedimentary signature in the GoL margin outbuilding. Considering the passive character of the margin, the flatness and width of the GoL shelf, and the robust chronostratigraphic framework for the last glacial cycle (i.e., excellent synchronization between the PRGL1-4 *G. bulloides* $\delta^{18}O$ record and the NGRIP ice core record, Figs. 4.5a and 4.5b) due to elevated SRs (ranging from 0.2 to 2 m kry^{-1}), the PRGL1-4 record could be highly valuable for disentangling the millennial scale sea level variability during MIS 3. Independently of chronologies, the exhaustive compilation of MIS 3 sea-level reconstructions by Siddall et al. (2008) shows two common patterns of variability: (1) the mean sea level during the first half of MIS 3 was approximately 20 m higher than in the second half, and (2) four 20–30 m-amplitude millennial-scale sea-level fluctuations occurred during this period (Fig. 4.5e). These features

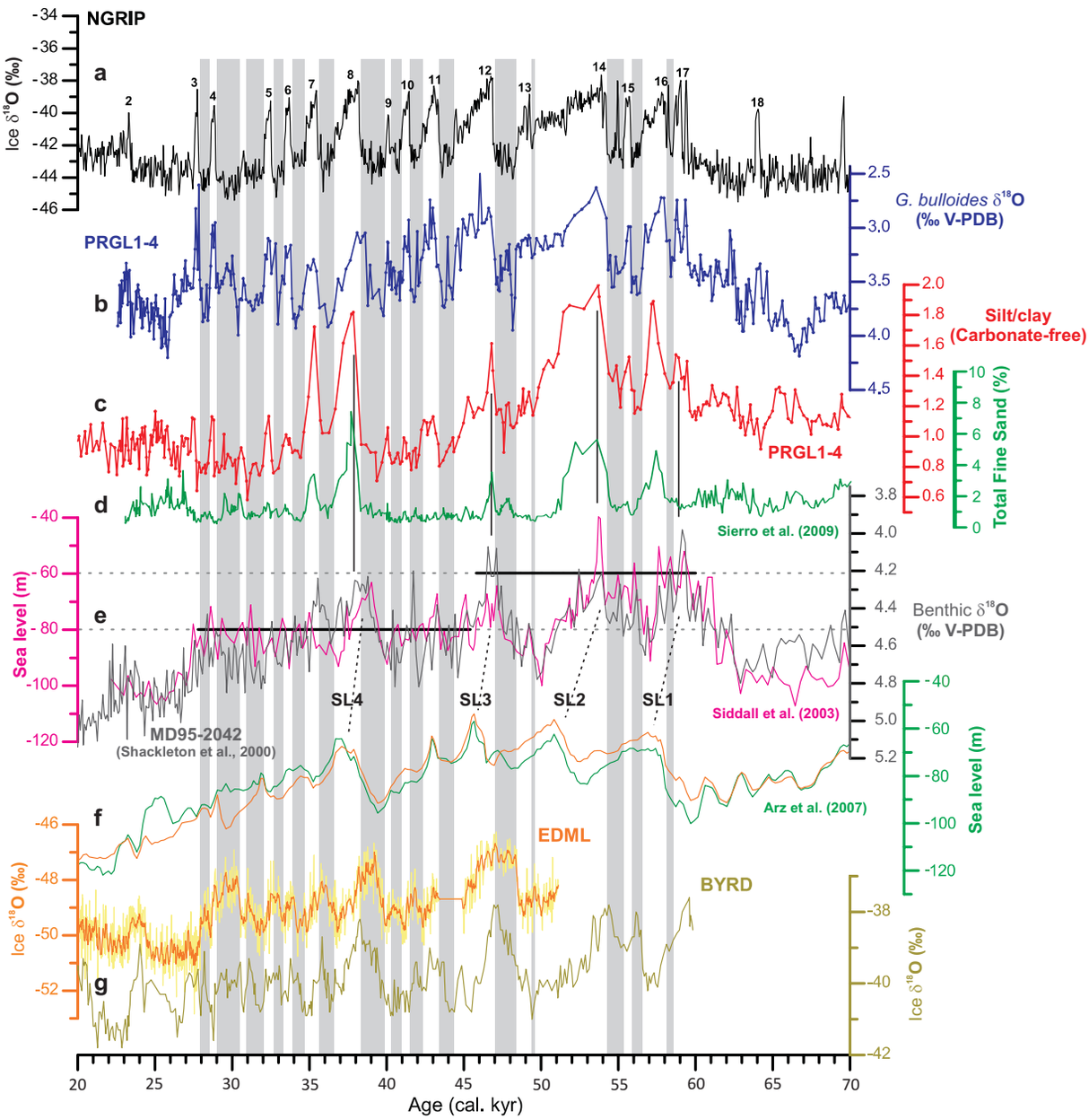

Figure 4.5. Comparison of different records of climate variability and sea-level reconstructions for the MIS 3 period, all of them age-scaled to the Greenland ice core NGRIP (Svensson et al., 2008) **a)**. **b)** *G. bulloides* oxygen isotopic record (blue), **c)** carbonate-free silt/clay ratio (red) and **d)** total fine sand fraction (green) from PRGL1-4 borehole. **e)** Benthic oxygen isotopic record from MD95-2042 (Shackleton et al., 2000) (dark grey) compared to Red Sea sea level reconstruction (Siddall et al., 2003) (pink), with horizontal lines showing that mean sea level was ~20 m higher in early MIS 3 than in late MIS 3. Discontinuous lines point four millennial-scale peaks of relative high sea level (SL1, 2, 3 and 4). **f)** Sea level reconstructions from the northern Red Sea based on two different temperature corrections for the deep basin (Arz et al., 2007). **g)** Oxygen isotopic records from Antarctic ice cores EDML and BYRD (Blunier and Brook, 2001; EPICA community members, 2006) CH_4-synchronized to Greenland ice core NGRIP (Svensson et al., 2008). Numbers above the NGRIP record represent warm GIS, while vertical grey bars correspond to cold GS and HE.

are also observed in the PRGL1-4 silt/clay record (Fig. 4.5c), thereby demonstrating that the GoL system responded to both long and short-term sea-level fluctuations during MIS 3.

The general decreasing trend observed in the PRGL1-4 silt/clay ratio during the progressive sea level lowering of the last glacial cycle (Fig. 4.3), is punctuated by a series of grainsize increases (Fig. 4.5c), which suggest that millennial-scale relative sea level rises occurred during MIS 3. By temporally extending the flooded area of the GoL shelf, MIS 3 relative sea level rises reduced the clay supply to the upper slope and contributed to expose a larger volume of water to atmospheric forcing, eventually leading to DSWC and, hence, indirectly reinforcing the transport of coarse particles to the upper slope. Both mechanisms contributed to increases in the silt/clay ratio (Fig. 4.5c). Those grain-size increases are unrelated to periods of intensification of deep-water formation in the GoL, since most of them occurred during relatively warm Greenland interstadials (GIS) (Figs. 4.5b and 4.5c), in contrast with observations of enhanced Western Mediterranean Deep Water (WMDW) formation during MIS 3 cold Greenland Stadials (GS) (Cacho et al., 2000 i 2006; Sierro et al., 2005; Frigola et al., 2008).

Confirming or discarding the occurrence of sea-level oscillations at Dansgaard-Oeschger (DO) scale has been prevented so far because none of the existing sea-level records was able to resolve variations lower than 12 m in amplitude during time intervals as short as 1 kyr (Siddall et al., 2008). Nevertheless, prominent increases in iceberg calving during cold Greenland stadials (GS) (non Heinrich Events, HE) suggest that sea level should have oscillated within each DO cycle (Bond and Lotti, 1995; van Kreveld et al., 2000; Chappell, 2002; Siddall et al., 2008). Disentangling MIS 3 sea-level variability also faces the difficulty of establishing the absolute timing of the observed oscillations, which is necessary to understand the role of sea level in millennial-scale climate variability during MIS 3 and to determine the relative contribution of "northern" versus "southern" sources (Clark et al., 2007).

Early evidence of millennial-scale sea-level variability was obtained from the benthic $\delta^{18}O$ record of the Portuguese margin core MD95-2042 (Shackleton, 2000) and sea-level reconstruction from the Red Sea (Siddall et al., 2003) (Fig. 4.5e). Although the Portuguese record may be influenced by oscillations in deep ocean temperature and local hydrographic variability, an important part of the record is linked to global sea level change (Skinner et al., 2007). Since both records display a variability pattern that is remarkably similar to the one found in Antarctic ice cores (Figs. 4.5e and 4.5g), it has been suggested that MIS 3 sea-level oscillations followed Antarctic climate variability (Siddall et al., 2003; Rohling et al., 2008). Contrary to these interpretations, recent results from the Red Sea and the GoL have shown millennial-scale sea level rises to occur during major warm Greenland interstadials (GIS) (Figs. 4.5f and 4.5d) (Arz et al., 2007; Sierro et al., 2009; Jouet et al., accepted, 2012), further highlighting the still high uncertainty about the timing of MIS 3 sea-level variability.

The co-occurrence of silt/clay increases and planktic $\delta^{18}O$ depletions in the PRGL1-4 record (Figs. 4.5b and 4.5c) imply, independently of the age model applied, that relative high sea levels occurred during warm GIS events. Concurrently, Shackleton et al. (2000) and Siddall et al. (2003) records also show maximum sea levels to occur during the onset phase of major GIS interstadials (i.e., GIS14, 12 and 8) (Figs. 4.5a and 4.5e). However, discrepancies on the precise timing of the sea level rises exist with our PRGL1-4 record. The excellent time constrains provided by the *G. bulloides* $\delta^{18}O$ record of the PRGL1-4 borehole demonstrate a consistent peak to peak coupling between sea-level variability (as indicated by increases in the silt/clay ratio) and all DO cycles, including the shortest ones. Nevertheless, not every relative high sea level resulted in the formation of CLs, since these were only observed during major GIS (16, 14, 12, 8 and 7) (Sierro et al., 2009), all of which coincide with higher values of the silt/clay ratio (Figs. 4.5c and 4.5d). The differences between the total fine sand record of Sierro et al. (2009) and our silt/clay ratio indicate that sea level increases during minor GIS (15, 13, 11, 10, 9, 6, 5, 4 and 3) were likely not high and/or long enough to generate CLs, therefore, demonstrating once more the strong sensitivity of the silt/clay ratio to sea-level oscillations. The great sensitivity of the silt/clay ratio during MIS 3 could be also related to the fact that sea level was oscillating between −60 m and −80 m, when the continental shelf was not fully exposed and prodeltaic deposits could be close to equilibrium with the accommodation space over the shelf.

A limitation of the PRGL1-4 silt/clay record is that the amplitude of sea level variations cannot be directly derived, as nowhere has it been shown that grain-size oscillations respond linearly to sea-level fluctuations. This very same limitation, and reduction of PRGL1-4 time resolution due to decreasing SRs with sea level increases, also prevents setting up the precise timing of sea level rises, whether they occurred at the beginning of each warm GIS or during the previous cold stadial. This relates to the exact timing of deltaic migration and their relative position following sea-level rise. In addition, the enhanced supply of coarse particles by reactivation of continental shelf erosive processes, such as DSWC, should normally occur some time after the start of each sea-level rise, i.e., when the volume of water over the shelf is again large enough.

Our results imply that sea-level was relatively high during all warm GIS within MIS 3 (Figs. 4.5a and 4.5c), although intrinsic limitations of the methodology applied in this study do not allow establishing the precise time nor the mechanisms involved in such millennial scale sea level rises, which could initiate by instabilities and melting of continental ice-sheets during cold GS, whether or not they correspond to HEs.

4.5. Conclusions

The last 500 ka continuous sediment record of the 300 m long PRGL1-4 borehole drilled in the upper slope of the river fed GoL holds the imprint of sea-level oscillations at orbital and millennial time scales during MIS 3. The sedimentary succession of PRGL1-4 consists of five regressive progradational units (more aggradational on the upper slope) that relate to the glacio-eustatic 100-kyr cyclicity. The consistent chronostratigraphy of the investigated section and the good matching between seismic reflection profiles and the grain-size record provide clues for understanding the nature of seismic reflections in mud-dominated slope sequences like the ones found at the investigated site, and also provides a tool to identify the boundaries of seismostratigraphic units while helping to tie them with global sea-level oscillations. These findings have resulted in the reinterpretation of the stratigraphy of the upper slope in the GoL, following an approach that can be extended to similar continental margin settings.

In addition of pushing the shoreline and associated sedimentary environments landwards, thus, disconnecting the upper slope from direct riverine sediment sources, we propose that sea level rise can reactivate transient energetic hydrosedimentary processes, such as DSWC, which are able of eroding, resuspending and transporting significant volumes of sediment from the continental shelf and upper slope to the deep basin. The sedimentary starvation of the upper slope during highstands, jointly with both episodic and persistent hydrodynamic processes winnowing the fine fraction, determined the formation of CLs that mark the periods of continental shelf flooding during interglacial epochs, as evidenced by our grain-size records.

Finally, the excellent match of the PRGL1-4 silt/clay record with previous records of sea-level variability at millennial-scale during MIS 3, together with the good time constraint provided by the *G. bulloides* $\delta^{18}O$ record, strongly support the occurrence of relatively high sea levels during each single warm GIS, even the smallest ones. Unfortunately, the precise starting time of sea level rises cannot be established solely from the sediment record of the GoL upper slope, which points to the need of further devoted research to resolve the origin and magnitude of MIS 3 sea-level variability.

Acknowledgements

This study has been supported by the EC PROMESS1 (EVR1-CT-200240024) and HERMIONE (226354-HERMIONE) projects, and the Spanish GRACCIE CONSOLIDER (CSD2007-00067) and DOS MARES (CTM2010-21810-C03-01) projects and CGL2005-24147-E complementary action. The IMAGES programme contributed to the research by providing the MD99-2348 sediment core. French partners benefited from additional support

by Agence Nationale de la Recherche (ANR, contract NT05-3-42040). We are also grateful for comments and suggestions of reviewers Jamie Austin and Andre Droxler, which helped to improve the manuscript. We thank Anders Sevensson and Thomas Blunier for providing NGRIP and EDML data, respectively. We are especially grateful to PROMESS1 participating scientists and to the staff of the various laboratories where sediment samples were analysed. We are grateful for the support provided by Fugro Engineers B. V. that made the challenging *MV Bavenit* cruise a success history. *Generalitat de Catalunya* recognises CRG Marine Geosciences within its excellence research groups program (ref. 2009 SGR 1305).

5. Evidence of abrupt changes in Western Mediterranean Deep Water circulation during the last 50 kyr: A high-resolution marine record from the Balearic Sea

J. Frigola[a], A. Moreno[b], I. Cacho[a], M. Canals[a], F.J. Sierro[c], J.A. Flores[c] and J.O. Grimalt[d]

[a]CRG Marine Geosciences, Department of Stratigraphy, Paleontology and Marine Geosciences, Faculty of Geology, University of Barcelona, Campus de Pedralbes, C/Martí i Franquès s/n, 08028 Barcelona, Spain

[b]Pyrenean Institute of Ecology, Consejo Superior de Investigaciones Científicas, Aptdo. 202, 50080 Zaragoza, Spain

[c]Department of Geology, University of Salamanca, Plaza de la Merced s/n, 37008 Salamanca, Spain

[d]Department of Environmental Chemistry, Institute of Chemical and Environmental Research, Consejo Superior de Investigaciones Científicas, C/Jordi Girona 18, 08034 Barcelona, Spain

Abstract

The IMAGES core MD99-2343, recovered from a sediment drift north of the island of Minorca, in the north-western Mediterranean Sea, holds a high-resolution sequence that is perfectly suited to study the oscillations of the overturning system of the Western Mediterranean Deep Water (WMDW). Detailed analysis of grain-size and bulk geochemical composition reveals the sensitivity of this region to climate changes at both orbital and centennial–millennial temporal scales during the last 50 kyr. The dominant orbital pattern in the K/Al record indicates that sediment supply to the basin was controlled by the insolation evolution at 40ºN, which forced changes in the fluvial regime, with more efficient sediment transport during insolation maxima. This orbital control also modulated the long-term pattern of the WMDW intensity as illustrated by the silt/clay ratio.

However, deep convection was particularly sensitive to climatic changes at shorter timescales, i.e. to centennial–millennial glacial and Holocene oscillations that are well documented by all the paleocurrent intensity proxies (Si/Al, Ti/Al and silt/clay ratios). Benthic isotopic records ($\delta^{13}C$ and $\delta^{18}O$) show a Dansgaard–Oeschger (D–O) pattern of variability of WMDW properties, which can be associated with changing intensities of the deep currents system. The most prominent reduction on the WMDW overturning was caused by the postglacial sea level rise.

Three main scenarios of WMDW overturning are revealed: a strong mode during D–O Stadials, a weak mode during D–O Interstadials and an intermediate mode during cooling transitions. In addition, D–O Stadials associated with Heinrich events (HEs) have a very distinct signature as the strong mode of circulation, typical for the other D–O Stadials, was never

reached during HE due to the surface freshening induced by the inflowing polar waters. Consequently, the WMDW overturning system oscillated around the intermediate mode of circulation during HE. Though surface conditions were more stable during the Holocene, the WMDW overturning cell still reacted synchronously to short-lived events, as shown by increments in the planktonic $\delta^{18}O$ record, triggering quick reinforcements of the deep water circulation. Overall, these results highlight the sensitivity of the WMDW to rapid climate change which in the recent past were likely induced by oceanographic and atmospheric reorganizations in the North Atlantic region.

Quaternary International vol. 181, p. 88-104, 2008
doi:10.1016/j.quaint.2007.06.016
www.sciencedirect.com/science/article/pii/S1040618207001760

5.1. Introduction

Abrupt climate changes of different intensity and scales characterize the climate history of the last 50 kyr in the North Atlantic region. During the last glacial period a series of coolings (Stadials) and warmings (Interstadials) known as the Dansgaard–Oeschger (D–O) events punctuated the Marine Isotopic Stage (MIS) 3 (Bond et al., 1993; Dansgaard et al., 1993). Additionally, abrupt coolings (known as Heinrich events, HEs) at the end of sequences of progressively weaker D–O oscillations resulted in massive iceberg discharges accompanied by deposition of ice rafted debris (IRD) (Heinrich, 1988; Bond et al., 1993). Climatic models suggest that reorganizations of the thermohaline circulation (THC) due to changes in the sea surface freshwater balance were the cause for the observed abrupt climate changes (Stocker, 2000). Similarly, the occurrence of abrupt climate changes during the Holocene at similar time-scales than those from the glacial period has been inferred from marine and terrestrial studies worldwide (Mayewski et al., 2004).

The rapid transmission of millennial-scale climate variability from the North Atlantic towards the Mediterranean region is supported by a number of studies (Rohling et al., 1998b; Allen et al., 1999; Cacho et al., 1999, 2000 i 2001; Combourieu Nebout et al., 2002; Moreno et al., 2002 i 2004; Bartov et al., 2003; Martrat et al., 2004; Sierro et al., 2005). Both oceanic and atmospheric processes were proposed as forcing mechanisms for the climatic teleconnections between high and medium latitudes. However, an improved understanding on their effects over terrestrial and marine environments is still required. Recently, it has been demonstrated that the western Mediterranean overturning system was enhanced during collapse or reduction of the formation of North Atlantic Deep Water (NADW), likely favoured by the intensification of north-westerly winds as a consequence of the expansion of ice sheets in the North Atlantic region (Cacho et al., 2000; Moreno et al., 2002; Sierro et al., 2005). However, invasion of low-salinity waters from polar sources, including the melting

of the icebergs released during the collapse of the NADW circulation at HEs, likely resulted in a temporary reduction of the formation of Western Mediterranean Deep Water (WMDW) (Sierro et al., 2005). In addition, changes in the properties and, possibly, in the volume of WMDW formed in the Gulf of Lion likely caused important modifications in the heat and salt volumes injected by the Mediterranean outflow water (MOW) into the North Atlantic, thus preconditioning the North Atlantic THC to switch from one mode to another (Bigg and Wadley, 2001; Voelker et al., 2006). The finding that a strong and dense MOW flowed at deeper levels during the Last Glacial Maximum than today (Rogerson et al., 2006) supports the view that the properties of the WMDW changed along the last deglaciation. Cacho et al. (2006) have reported changes in the deep-water temperature of WMDW related to the D–O cycles in core MD95-2043 from the Alboran Sea. Though on a very different time-scale, monitoring studies have revealed that WMDW density increased after the severe 2004/2005 winter in the north-western Mediterranean region (López-Jurado et al., 2005; Canals et al., 2006). From the above it becomes clear that both the influence of North Atlantic climate variability on WMDW formation and, inversely, the impact of Mediterranean Deep Waters on NADW production must be better understood as they are one of the key components of climate change during the last glacial period and the present interglacial in the concerned regions.

At present, the north/south displacements of the Azores high-Icelandic low-pressure system and their intensity variations control the transmission of heat and moisture between low and high latitudes (Barry and Chorley, 1998; Bolle, 2003). This pattern is known as the North Atlantic Oscillation (NAO), which oscillates at decadal scale modulating much of the present-day climate variability in the entire region (Hurrell, 1995; Rodó et al., 1997). During a positive phase of the NAO, an increased pressure gradient in the North Atlantic region results in more frequent and stronger winter storms following a more northerly track, resulting in warm and wet winters in northern Europe. During a negative phase of the NAO, a reduced pressure gradient results in a southward displacement of the winter storms bringing higher precipitation to the Mediterranean region.

In this work, the analysis and interpretation of combined sedimentological proxies, i.e. grain-size parameters, and bulk geochemical ratios, together with the isotopic signal from planktonic and benthic foraminifera from core MD99-2343, allow the identification of changes in deep water properties and behaviour in the western Mediterranean Basin during the last 50 kyr. The results achieved so far provide new clues for understanding the mechanisms behind and the feedbacks of abrupt climate changes in the western Mediterranean region and their transmission to the deepest part of the western Mediterranean Basin.

5.2. Core location and present conditions

The present work focuses on the study of the 32.44 m long IMAGES-V core MD99-2343 recovered north of the Minorca Island (40º29.84'N, 04º01.69'E) at 2391 m of water depth, onboard *R/V Marion Dufresne* (Fig. 5.1). The core was recovered in a sediment drift formed by deep contour currents belonging to the southward branch of the WMDW flow, which borders the Valencia Trough from north to south following a cyclonic pattern at depths of ~2000m (Millot, 1999) (Fig. 5.1). At this place the abrupt slope of the Balearic Promontory opposes deep circulation that accelerates and turns eastward bordering the base-of-slope of Minorca in its way to the open basin. Although no current meter data have been collected at the core location, intense deep currents have been interpreted from seafloor bedforms (Mauffret et al., 1972; Maldonado et al., 1985a; Palanques et al., 1995). Additionally, the base-of-slope peripheral depression and the associated sediment drift, previously described by Velasco et al. (1996), demonstrate the existence of relatively intense deep currents sweeping the deep slope north of Minorca.

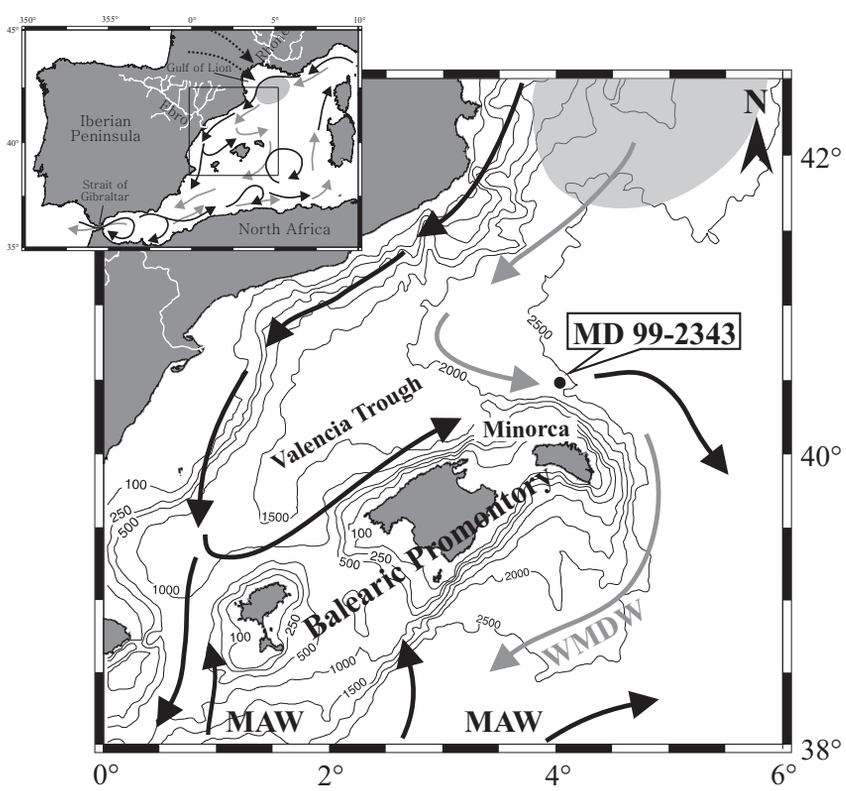

Figure 5.1. Bathymetric map of the study area in the north-western Mediterranean Basin showing the location of core MD99-2343. Surface and deep main circulation patterns are represented by black and gray arrows, respectively. The shaded area shows the region of WMDW formation in the Gulf of Lion under the influence of north-westerly winds, illustrated as dotted arrows (inset). Rhône and Ebro Rivers supplying most freshwater inputs to this basin are also shown.

The formation of a sediment drift is also depending on sediment availability. Most sediment inputs to this region come from the Ebro and Rhône fluvial discharges. However, only 10% of this sediment discharge reaches the deep basin (Martin et al., 1989) and the core location is too far from the coast to directly receive material from riverine origin. In the specific setting of the Balearic margin local mass gravity flows and hemipelagic settling have been identified as significant contributors of sediment to the deep margin and basins surrounding the promontory (Maldonado et al., 1985a i 1985b; Alonso et al., 1995; Palanques et al., 1995; Calafat et al., 1996). Subsequently, deep water currents are assumed to rework, sort and transport these sediments and accumulate specific fractions on the sediment drift where core MD99-2343 was recovered (Fig. 5.1).

This Minorca sediment drift has been built under the action of deep contour currents related to the WMDW, which to a large extent forms in the Gulf of Lion by evaporation and cooling of the sea surface mostly during cold and windy winters, thus increasing the density of offshore surface waters until they sink (MEDOC-group, 1970; Lacombe et al., 1985; Millot, 1999). In addition to offshore convection, episodic dense shelf water cascading in the Gulf of Lion has been recently described to account for large volumes of sinking waters that add to WMDW (Canals et al., 2006). Deep water sources in the Gulf of Lion depend on wind stress variability and fluvial water discharge on the shelf preconditioning buoyancy. The formation of WMDW is also affected by the amount and depth of the warm and salty Levantine Intermediate Water (LIW) available in the basin before each event (Pinardi and Masetti, 2000; Millot and Taupier-Letage, 2005). LIW forms in the eastern Mediterranean basin as a consequence of evaporation and sinking of Modified Atlantic Water (MAW), which entered the Mediterranean Sea across the Strait of Gibraltar due to the negative hydrological balance caused by the excess of evaporation over freshwater inputs (Millot, 1999). At the end of a general cyclonic pattern, the dense LIW and WMDW leave the Mediterranean Basin through the Strait of Gibraltar as the deep MOW (Millot, 1999).

5.3. Material and methods

5.3.1. MD99-2343 core description

This study focuses on the top 17 m of the core that corresponds to the last 50 kyr (see Section 5.3.4 below). The upper 5 m (deglaciation and Holocene) consists of homogeneous gray nannofossil and foraminifer silty clay with moderate bioturbation. Below the top 5 m (last glacial period) the sediments are much more laminated and present mm to cm-thick grayish orange, yellowish brown, light olive brown and brownish black layers within a dominant homogeneous gray silty clay. Rare sandy layers were also described onboard. Moderate bioturbation, pyrite, organic matter, foram-rich and broken-shell layers were also observed

throughout this section. Onboard smear slides showed high contents of detrital minerals with abundant quartz and mica silt grains.

One centimeter thick samples were taken every 4–6 cm for grain-size and major element composition analyses of the bulk sediment. In addition, samples every 2 cm were taken for grain-size analyses along specific intervals.

5.3.2. Geochemical analyses

The content of major elements in sediment samples was determined by means of X-ray fluorescence using a PW 2400 sequential wavelength disperse X-ray spectrometer. Prior to the analysis, samples were ground and homogenized in an agate mortar and glass discs were prepared by fusing about 0.3 g of bulk sediment with lithium tetraborate in an induction oven Perle'X-2. Analytical accuracy was checked by measuring international standards (GSS-1–GSS-7) and was better than 1% of certified values. Precision of individual measurements was better than 0.9% as determined from replicate analyses of sediment samples (repeatability). Precision over the period of measurement was better than 3.4% (reproducibility) for all elements analyzed in this work. In order to avoid spurious correlations between elements due to closure effect to 100%, i.e. dilution effects caused by variations in biogenic carbonate content (Wehausen and Brumsack, 2000), element/Al ratios (Rollinson, 1993) are discussed.

5.3.3. Grain-size analyses

Grain-size analyses were performed on both the total fraction (organic matter removed with 10% H_2O_2) and the non-carbonate fraction (both organic matter and carbonate were removed with H2O2 and HCl, respectively). Grain-size distributions were measured with a Coulter LS 100 laser particle size analyzer (CLS), which determines particle grain-sizes between 0.4 and 900 μm as volume percentages based on diffraction laws (McCave et al., 1986; Agrawal et al., 1991). Diffraction is assumed to be given by spherical particles and the particle size is given as an ''equivalent spherical diameter''. Consequently, laser diffraction methods are claimed to underestimate plate-shaped clay mineral percentages. This underestimation has been corrected following Konert and Vandenberghe (1997). CLS precision and accuracy were tested by several control runs using latex micro-spheres with pre-defined diameters and the LS size control G15, which gave a coefficient of variation of 1.5%. Grain-size results are presented as the median of each sample since it represents the distribution midpoint and it usually constitutes a representative value of grain-size distribution better than the mean. In addition, the UP10 size (i.e. particles coarser than 10 μm) is considered, which adds the fine sand subpopulation to the sortable silt size fraction (10–63 μm) (McCave et al., 1995b) and the silt/clay ratio as both parameters provide information about changes in paleocurrent intensity (Hall and McCave, 2000).

5.3.4. Chronostratigraphy

The age model for the upper 17 m of core MD99-2343 is based on 10 ^{14}C-AMS datings covering the last 17 ka (Sierro et al., 2005; Frigola et al., 2007), the correlation of the *Globigerina bulloides* δ^{18}O signal with the GISP2 oxygen isotopic record (Grootes et al., 1993; Meese et al., 1997) for MIS3 following (Sierro et al., 2005) and four additional tie points with the *G. bulloides* oxygen isotopic record from the Alboran Sea core MD95-2043 for the deglaciation and MIS2 (Cacho et al., 1999; Sierro et al., 2005) (Fig. 5.2 and Table 5.1). The ages were calibrated with the standard marine correction of 408 yr and the regional average marine reservoir correction (ΔR) for the western Mediterranean Sea by means of the Calib 5.0.1 program (Stuiver and Reimer, 1993) and the MARINE04 calibration curve (Hughen et al., 2004). Following this age model, which covers the last 50 kyr, the mean sedimentation rate for the top 17 m of core MD99-2343 is 36 cm kyr^{-1} (Fig. 5.2), therefore allowing a centennial resolution in the study of the sediment record.

Radiocarbon sample or isotope event/foram type	Core depth (cm)	^{14}C age (yr BP)/tie points tuned with	Calendar years
AMS ^{14}C/multispecific	28	790 (±40)	365±55
AMS ^{14}C/*G. inflata*	88	3,110 (±30)	2,816±50
AMS ^{14}C/multispecific	118	3,390 (±50)	3,225±80
AMS ^{14}C/*G. inflata*	208	5,720 (±40)	6,091±70
AMS ^{14}C/multispecific	238	6,210 (±50)	6,601±70
AMS ^{14}C/*G. inflata*	308	7,700 (±40)	8,110±60
TIb–Onset of the Holocene	354	MD95-2043	10,696
AMS ^{14}C/*G. bulloides*	398	10,650 (±50)	11,883±230
AMS ^{14}C/*G. inflata*	418	11,200 (±50)	12,811±30
Base Bolling–Allerod	490	MD95-2043	14,750
AMS ^{14}C/*G. bulloides*	568	13,850 (±40)	15,912±190
AMS ^{14}C/multispecific	604	14,550 (±110)	16,820±240
LGM	630	MD95-2043	18,539
Enrichment after Interstadial 3	904	MD95-2043	25,525
Base Interstadial 3	954	GISP2	27,736
Base Interstadial 4	994	GISP2	29,000
Base warming event	1060	GISP2	30,619
Base Interstadial 5	1110	GISP2	32,300
Base Interstadial 6	1144	GISP2	33,587
Base Interstadial 7	1190	GISP2	35,400
Base Interstadial 8	1260	GISP2	38,432
Base Interstadial 10	1410	GISP2	41,172
Base Interstadial 11	1520	GISP2	42,713
Base Interstadial 12	1584	GISP2	45,360
Base Interstadial 13	1724	GISP2	47,146
Base Interstadial 14			51,933

Table 5.1. Tie points used for the age model of core MD99-2343. Ten ^{14}C-AMS dates were calibrated with the Calib 5.0.1. programme (Stuiver and Reimer, 1993) and the MARINE04 calibration curve (Hughen et al., 2004). Prior to 27 ka the age model is based on the correlation with the GISP2 ice core (Grootes et al., 1993; Meese et al., 1997). Four additional tie points were added through the comparison of the *G. bulloides* δ^{18}O from both cores MD99-2343 and MD95-2043 (Cacho et al., 1999; Sierro et al., 2005). The age model was performed with the AnalySeries Version 1.1 (Paillard et al., 1996).

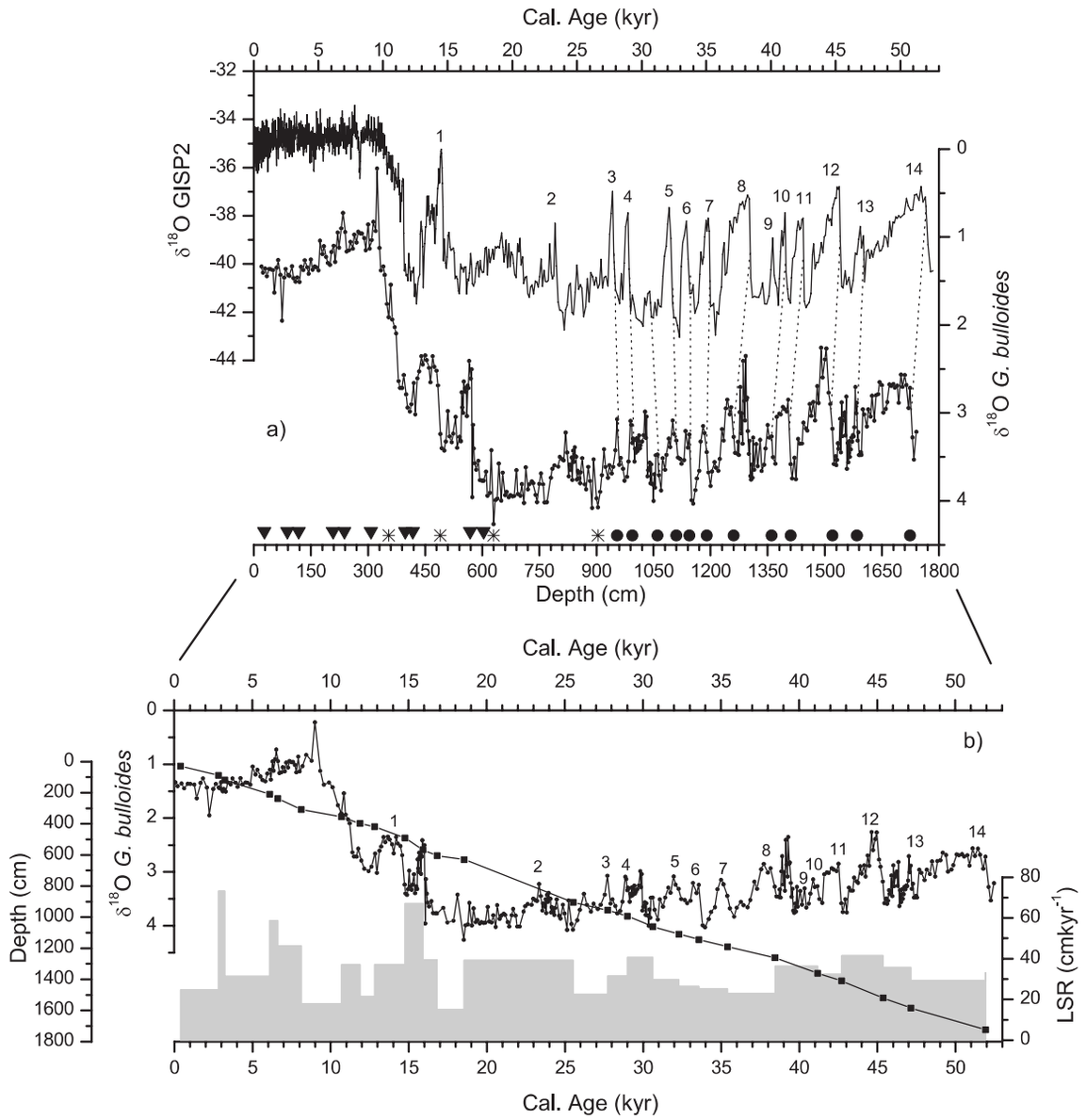

Figure 5.2. a) Age model of core MD99-2343 developed by means of 10 ^{14}C-AMS dates (triangles), the tuning of the *G. bulloides* $\delta^{18}O$ record with the ice $\delta^{18}O$ record from the GISP2 core (circles) and the tuning with the $\delta^{18}O$ record of the core MD95-2043 from the Alboran Sea (asterisks). See Table 5.1 for details. **b)** Linear sedimentation rates (LSR) of core MD99-2343 for the last 50 kyr oscillating between 15 and 73 cm kyr^{-1}.

5.4. Results

5.4.1. Geochemical record

Several authors have used Si/Al, Ti/Al and K/Al ratios as proxies for terrigenous inputs in the Mediterranean region (Wehausen and Brumsack, 1999; Moreno et al., 2002; Weldeab et al., 2003; Frigola et al., 2007). Si mostly comes from alumino-silicates and quartz since biogenic opal is of minor importance in this sea due to its oligotrophic conditions and the dissolution of silica (Weldeab et al., 2003). Ti resides within heavy minerals such as ilmenite and rutile. K is associated with clay minerals, mainly illite (Wehausen and Brumsack, 1998, 2000).

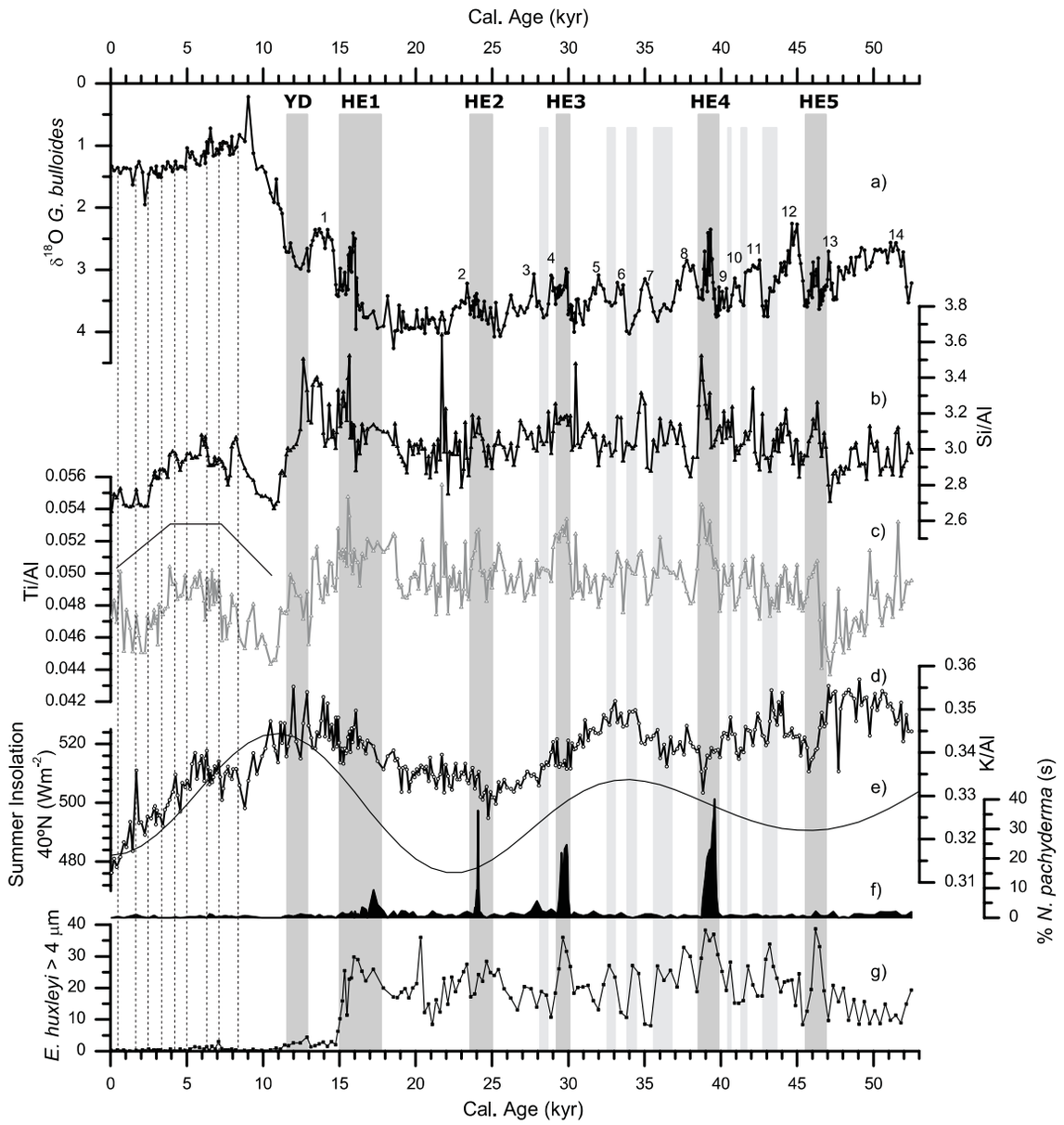

Figure 5.3. a) *G. bulloides* $\delta^{18}O$ record from core MD99-2343 for the last 50 kyr. Numbers above the curve represent warm GIS while gray bars correspond to cold GS, HEs and YD cold events. Vertical dashed lines to the left correspond to the Minorca abrupt events defined by Frigola et al. (2007) during the Holocene. **b, c and d)** Si, Ti and K geochemical records normalized to Al, respectively. A continuous line between the Si/Al and the Ti/Al ratios embracing the 10.5–0 ka period represents three main phases within the general trend (see main text). **e)** Summer insolation curve at 40ºN for the last 50 kyr. **(f)** Percentages of polar water species *Neogloboquadrina pachyderma (s)*. **g)** Percentages of *E. huxleyi* larger than 4 μm.

Si/Al, Ti/Al and K/Al records from core MD99-2343 are shown in Fig. 5.3. The highly similar records of Si/Al and Ti/Al display a minimum from 13 to 10.5 ka that coincides with high summer insolation values (Fig. 5.3e). The decrease in the geochemical signal occurred during a pronounced decreasing trend of the oxygen isotopic signal from *G. bulloides* marking the last deglaciation (Frigola et al., 2007). The observed minima divides the Si/Al and Ti/Al records in to two parts: (i) from 50 to 13 ka, with high though variable values that characterize the glacial period, and (ii) from 10 ka to present time, with lower values and a

smoother pattern. The last 10 kyr record, as described in detail in Frigola et al. (2007), can be divided into three successive phases: (i) an increasing phase in both ratios coincident with the end of the second phase of Termination (TIb) and the early Holocene (10.5–7 ka), (ii) a central plateau with relatively high values during the mid-Holocene (7–4 ka) and (iii) a gradually decreasing phase during the late Holocene (4–0 ka) (Fig. 5.3). The general long-term trend in the Si/Al and Ti/Al ratios is punctuated by eight abrupt relative increasing events coincident with increments in the planktonic $\delta^{18}O$ record. The general pattern of the K/Al record is completely different with its most remarkable feature being its high parallelism with the summer insolation curve at 40ºN, which is particularly apparent for the last 40 kyr (Figs. 5.3d and 5.3e).

In addition to the observed general trends, geochemical ratios from core MD99-2343 exhibit pronounced millennial-scale changes during MIS 3 that roughly correspond to the D–O oscillations described in the planktonic $\delta^{18}O$ record (Sierro et al., 2005), which parallel the Greenland Stadials (GSs) and Interstadials (GISs) from $\delta^{18}O$ ice records (Dansgaard et al., 1993; Grootes et al., 1993). That the geochemical and the isotopic records from core MD99-2343 are not completely in phase can be observed by comparing the plots in Fig. 5.3a–d. Abrupt increases of the geochemical ratios generally occur just after the lightest values of the $\delta^{18}O$ record have been reached coinciding with the GIS/GS transitions. In contrast, the lowest Si/Al and Ti/Al values most often coincide with low values in the $\delta^{18}O$ record corresponding to GIS.

Five abrupt increases in Si/Al and Ti/Al ratios have been identified at 46, 39, 30, 24 and 16 ka that, with one exception, parallel the incursions of the polar water species *Neogloboquadrina pachyderma (s)* (Fig. 5.3f). These increases in the geochemical proxies also fit with peaks of abundance of the coccolithophore *Emiliania huxleyi* (>4 μm) (Fig. 5.3g) (Sierro et al., 2005), which is identified as a cold water species indicator in NE Atlantic and Mediterranean regions (Colmenero-Hidalgo et al., 2002 i 2004). These intervals correlate with HE1–HE5 described in the North Atlantic region (Heinrich, 1988; Bond et al., 1992; Broecker et al., 1992). Opposite to Si/Al and Ti/Al ratios, the K/Al record generally shows abrupt decreases during the HEs, which are especially pronounced during the latest part of HE5, HE4 and HE1 (Fig. 5.3d). The lowest values in the K/Al record are the most recent ones that correspond to the current summer insolation minimum (Figs. 5.3d and 5.3e).

5.4.2. Grain-size record

Median grain-size values (between 4 and 9 μm) of both bulk and non-carbonate sediment fractions show fairly similar features (Fig. 5.4b) thus pointing to the same processes controlling the deposition of the two fractions. However, due to the mixed origin of the carbonate fraction (e.g. sea surface production of carbonate particles and inputs from the carbonate

Balearic shelf), the noncarbonated fraction better represents the intensity of bottom currents (McCave et al., 1995b).

The sortable silt size (10–63 μm) has been used as a proxy to infer the intensity of deep water currents (McCave et al., 1995b). However, since strong contour currents are also able to rework particles coarser than 63 μm, the UP10 fraction has been considered here for the study of paleocurrent intensity (Frigola et al., 2007). The general trend from UP10 and silt/clay ratio profiles through the last 50 kyr shows affinities with the summer insolation record at 40ºN (Fig. 5.4c–e). As for the geochemical proxies, grain-size records present different patterns during the glacial and interglacial periods, with a marked decreasing trend from 15 ka until 10.5 ka, which corresponds to the highest part of the rising limb of the summer insolation curve at 40ºN. This reduction in the grain-size records is two-step and seems to show some relation with the two phases of the deglaciation interval marked by almost synchronous decreases in the *G. bulloides* $\delta^{18}O$ profile (thus embracing the Younger Dryas). After the minimum grain-size values at 10.5 ka, relatively coarse grain-size values quickly resume at the onset of the Holocene. A general decreasing trend characterizes the last 9 kyr of the UP10 and silt/clay records that roughly parallel the *G. bulloides* $\delta^{18}O$ increasing trend (Figs. 5.4a, 5.4c and 5.4d). This overall Holocene tendency towards grain-size reduction coincides with a diminution of the seasonal insolation differences at 40ºN (Fig. 5.4e). Superimposed on the general long-term trend, the grain-size record is punctuated by eight abrupt increases known as Minorca abrupt events (Frigola et al., 2007).

The glacial period is characterized by mean higher and more variable grain-size values than the Holocene. From 50 to 29 ka background levels are punctuated by a series of millennial-scale oscillations at D–O cyclicities (Figs. 5.4c and 5.4d). It is worth to note that these records are not totally synchronous with the *G. bulloides* $\delta^{18}O$: low values of the grain-size proxies are coincident with low values in the $\delta^{18}O$ record (GIS), while abrupt increases in the grain-size proxies occur coincident with the GIS/GS transitions (Figs. 5.4a, 5.4c and 5.4d). In spite of the lack of synchrony among grain-size proxies and the planktonic $\delta^{18}O$ record, the pattern that characterizes a D–O cycle is very systematic. Increases in the silt/clay and in the UP10 fraction are abrupt while decreases are somewhat smoother, e.g. during GIS12 or GIS8, and almost parallel to the increasing trend observed in the $\delta^{18}O$ record from GIS to GS transitions (Figs. 5.4a, 5.4c and 5.4d). In addition, sudden increases in the silt/clay ratio also occur at the end of a series of abrupt progressively shorter oscillations, which are coincident with HE5, HE4 and HE3, identified from the *G. bulloides* $\delta^{18}O$ record (Sierro et al., 2005). The D–O variability in the grain-size proxies is interrupted by an abrupt decrease at 29–28 ka where very low values occur. This reduction in the grain-size proxies was contemporary with an important decrease in the orbitally induced seasonal differences at times when winter insolation values were higher than at present (Fig. 5.4e). After that reduction a general increasing trend in both proxies from 26 to 15 ka is almost coincident with the increase in

the summer insolation at 40ºN or, in other words, with an increase in the orbitally induced seasonal differences (Fig. 5.4e).

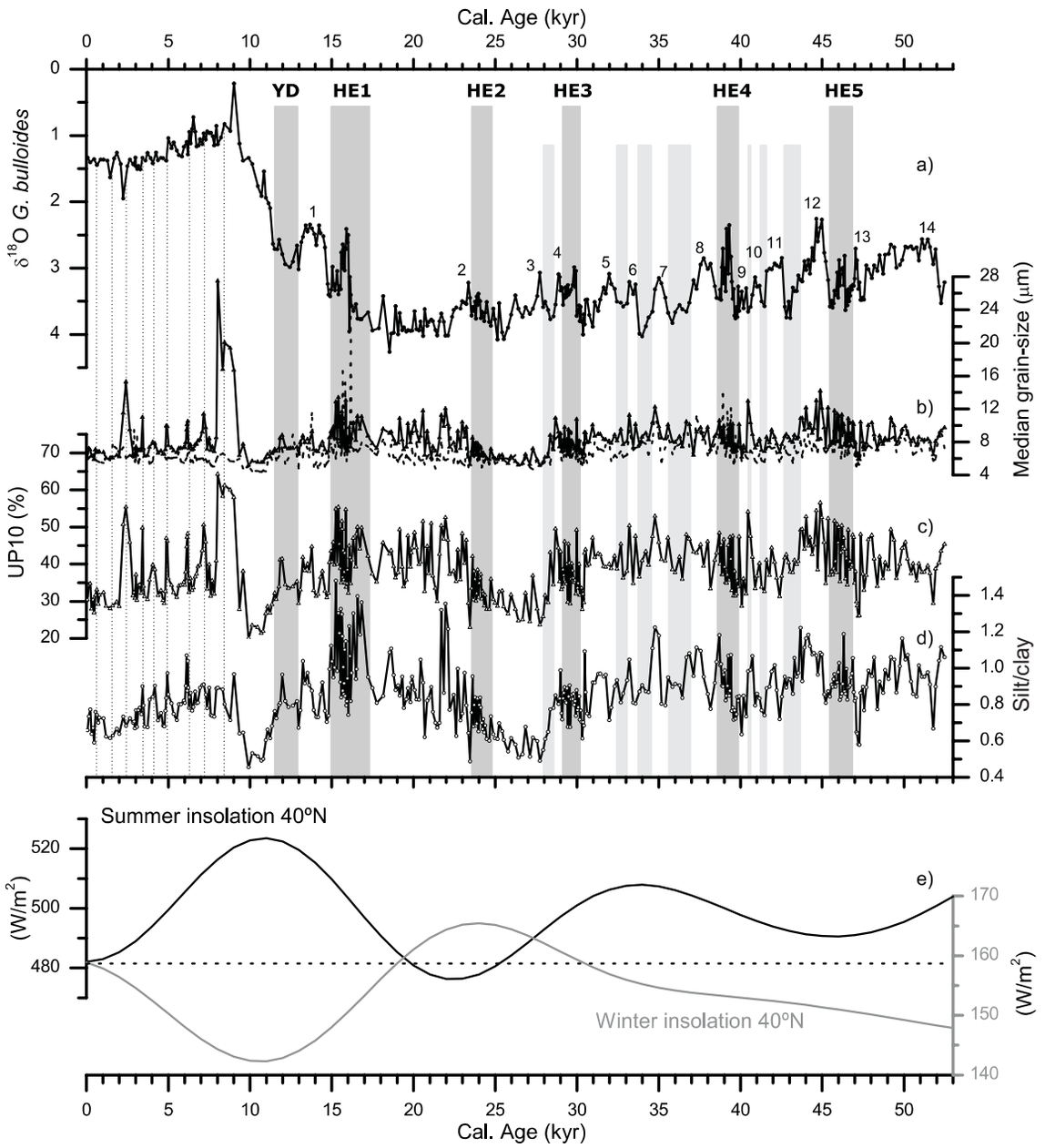

Figure 5.4. a) *G. bulloides* $\delta^{18}O$ record from MD99-2343 for the last 50 kyr. Numbers above the curve represent warm GIS while gray bars correspond to cold GS, HEs and YD cold events. Vertical dashed lines to the left correspond to the Holocene Minorca abrupt events defined by Frigola et al. (2007). **b)** Median grain-size records of the total (dashed line) and non-carbonate sediment fractions (solid line). **c and d)** UP10 fraction (>10 μm) and silt/clay ratio of the non-carbonate fraction, respectively. **e)** Summer and winter insolation curves at 40ºN for the last 50 kyr. Current values of both summer and winter insolation are plotted at the same level so that distances between both records through time can be interpreted as orbitally induced seasonal differences.

5.5. Discussion

5.5.1. Orbitally-driven trends in the terrigenous signal

The K/Al record from core MD99-2343 shows a rather smooth pattern during the last 50 kyr that roughly parallels the summer insolation at 40ºN with minimum values occurring during times of low summer insolation (Fig. 5.3). Superimposed on this long-term trend, millennial-scale oscillations appear as relatively minor features of the record. Sea level changes associated with the last deglaciation did not seem to produce any clear modulation in the K/Al record. These results suggest that K/Al oscillations have been mainly controlled by processes driven by orbitally induced insolation changes. Potassium (K) used to be mainly associated with clays, i.e. illite from continental runoff, and hence the K/Al ratio is interpreted in terms of river discharge (Wehausen and Brumsack, 1998, 2000). In the north-western Mediterranean region the Rhône and the Ebro rivers are the main sources of fluvial sediment inputs, with water supply mostly reflecting precipitation in the Alps and the Pyrenees, respectively. Of these two main rivers, the Ebro clearly has a stronger Mediterranean character (i.e. a more pronounced seasonality). According to the MD99-2343 record, enhanced supply of clays (high K/Al values) occurred during periods of high summer insolation pointing to elevated precipitation or to a more efficient sediment transport regime, such as that produced due to increased torrential rains in general in the watersheds supplying the basin. In addition, enhanced aridification of the watersheds facilitates erosion resulting in higher lithogenic fluxes when seasonal rains occur (Fabres et al., 2002). These results indicate the strong control that orbitally induced insolation changes exerted on the fluvial runoff of detrital material in the western Mediterranean Basin at least during the last 50 kyr. In the Eastern Mediterranean a precession control on Pliocene–Pleistocene sapropel formation and, therefore, on climatic and hydrographic conditions has been proposed by several authors (Hilgen, 1991; Rohling and Hilgen, 1991; Wehausen and Brumsack, 2000). The K/Al record from core MD99-2343 supports the precessional control on the climatic conditions of the western Mediterranean region as well.

Grain-size records, i.e. the silt/clay ratio, display a more complex pattern of variability. Although millennial-scale oscillations are very pronounced, a precessional frequency is also present, especially after 30 ka, when seasonal insolation differences are well marked (Fig. 5.4). Low silt/clay values occur during periods of relatively high winter insolation like the late Holocene and around 28 ka (Fig. 5.4d). Increments in the silt versus the clay fraction are attributed to enhanced deep currents able to transport coarse material to the Minorca sediment drift and winnow the finest sediment fraction. Deep water currents at the drift location belong to the WMDW mass whose overturning occurs in the Gulf of Lion. Formation of WMDW is a wintertime process and is strongly dependent on the intensity of north-westerly winds (MEDOC-group, 1970; Lacombe et al., 1985; Bethoux et al., 1990). The dominance

of weaker deep currents at times of maximum winter insolation, as interpreted from the silt/clay ratio, is consistent with reduced intensities of the north-westerly winds during milder winters due to lower atmospheric pressure gradient and, consequently, with a less intense overturning in the Gulf of Lion.

This precessional-induced long-term pattern in the silt/clay ratio is sharply interrupted at 12-10 ka when winter insolation was at its minimum. Therefore, the silt/clay reduction occurred synchronously with the second phase of the Termination (TIb) suggesting that sea level oscillations also influenced deep water overturning in the basin. The low grain-size values recorded during this specific time interval are consistent with reduced deep water ventilation, which allowed the preservation of an organic rich layer (Cacho et al., 2002) and the dominance of low-oxygen benthic fauna (Caralp, 1988) in the Alboran Sea. Such a reduction in the western Mediterranean overturning further supports the effect of the post-glacial sea level rise on the stratification of Mediterranean waters during TIb, as suggested by former models (Rohling, 1994; Matthiesen and Haines, 2003). In addition, high K/Al values point to increased fluvial discharge because of more humid conditions at that time (Fig. 5.3d), which would also confirm persistent water column stratification. More humid conditions during the 12–10 ka interval have been also inferred from pollen and lacustrine sequences from the borderlands (Harrison and Digerfeldt, 1993; González-Sampériz et al., 2006). Overall, these results demonstrate that the combined effect of the post-glacial sea level rise (and the subsequent global reduction of the salinities of surface waters) and an astronomically induced precipitation increase enhanced water column stratification and, therefore, were responsible for the reduction of the deep water overturning in the western Mediterranean. These mechanisms likely extended to the whole Mediterranean Basin and anticipated the formation of Sapropel 1 in the eastern Mediterranean Basin (Rohling, 1994).

Contrarily to the K/Al ratio, the Si/Al and Ti/Al records do not show consistent patterns of variability related to precessional insolation changes. Both Si/Al and Ti/Al ratios are associated with terrigenous inputs and should reflect changes in the processes controlling the amount and/or distribution of such inputs to the basin (Matthewson et al., 1995; Reichart et al., 1997; Wehausen and Brumsack, 2000; Moreno et al., 2002; Weldeab et al., 2003; Frigola et al., 2007). The observed differences between Si/Al, Ti/Al and K/Al ratios should be related to grain-size geochemical segregation since Si and Ti are related to coarse minerals and K to clay minerals. Consequently, Si/Al and Ti/Al ratios should be linked to processes controlling the grain-size distribution in the Minorca rise at higher frequencies than precessional. This interpretation is supported by the good correlation of these two geochemical ratios and the silt/clay ratio where most variability occurs at millennial time-scales.

5.5.2. Millennial-scale variability during the Holocene

The general pattern of the Si/Al and Ti/Al records during the Holocene, following their marked reduction during the last deglaciation (see Section 6.5.1 and Figs. 5.3b and 5.3c), can be subdivided into three phases. The first phase (10.5–7 ka) shows increasing values in both geochemical ratios but also embraces a sharp increase in the grain-size proxies (Figs. 5.3 and 5.4) indicating the recovery of the WMDW formation at the onset and early Holocene after the highest sea level rise rate was achieved (Fleming et al., 1998).

During the second phase (7–4 ka), which is synchronous with the end of the post-glacial sea level rise (Fleming et al., 1998), a sort of plateau is observed in the Si/Al and Ti/Al ratios (Figs. 5.3b and 5.3c). This mid-Holocene phase illustrates the high control that the sea level rise exerted on the overturning system in the Gulf of Lion. This was a period when the rather small range of variation of the geochemical proxies (Fig. 5.3) suggests no significant changes occurred in the fluvial supply to the basin neither in the overturning cell in the Gulf of Lion. By contrast, during the same interval, strong changes were reported worldwide (Steig, 1999) and, in particular, from the Mediterranean borderlands (COHMAP, 1988; Cheddadi et al., 1997; Prentice et al., 1998; Magny et al., 2002) and the North African region (Vernet and Faure, 2000) as associated with the end of the African Humid Period (deMenocal et al., 2000a). Such a mid-Holocene climate variability is attributed to the reduction of seasonal insolation differences after 5.5 ka (Fig. 5.4e), which lead to an abrupt transition from humid to arid conditions in North Africa and in the western Mediterranean region. However, the Si/Al and Ti/Al records do not seem to respond to those changes and only K/Al shows a clear reduction after that moment. The observed discrepancies between the various geochemical proxies suggest again different forcings: while Si/Al and Ti/Al mainly reflect changes in deep water currents, with a fluvial input modulation, K/Al mainly shows changes of humidity conditions on the borderlands. Therefore, the K/Al descending general trend after 5.5 ka is in phase with the end of the African Humid Period (deMenocal et al., 2000a) and marks the establishment of drier conditions. During the third phase (4–0 ka) the trends of the Si/Al and Ti/Al ratios point to an overall reduction of fluvial inputs likely due to the establishment of drier conditions and reduced precipitation. The overall continued rapid descent of the K/Al recorded also during the late Holocene confirms the reduction of fluvial inputs that parallel diminishing seasonal insolation differences (Figs. 5.3d and 5.4e). In addition, the rather subtle decreasing trend observed in the silt/clay ratio during the late Holocene (Fig. 5.4d) also points to a reduction of the overturning cell in the Gulf of Lion. Less intense deep water currents and reduced fluvial inputs would translate into an overall decreasing trend of the sedimentation rates as observed in Fig. 5.2b. A lower atmospheric pressure gradient due to the diminished seasonal insolation differences likely favoured the establishment of drier conditions during the late Holocene (McDermott et al., 1999; Jalut et al., 2000; Magny et al., 2002). In addition, reduced north-westerly winds from a lowered pressure gradient system

would be responsible for the lessening of deep water overturning and, consequently, for lower values in the silt/clay ratio (Fig. 5.4d).

Superimposed on the general Holocene trends, nine $\delta^{18}O$ incremental events with a periodicity close to 1000 yr relate to short cooling events, known as Minorca abrupt events (Fig. 5.3) (Frigola et al., 2007). Most of these events are characterized by parallel increases in the UP10 and in the Si/Al records (Figs. 5.3b and 5.4c) suggesting an intensification of the deep water currents intensity related to an enhancement in the Gulf of Lion's overturning system likely promoted by strengthened north-westerly winds. The timing of the Minorca abrupt events fits well with temperature oscillations from the Holocene $\delta^{18}O$ record in Greenland (Frigola et al., 2007) and suggests a coupled ocean–atmosphere teleconnection mechanism for climate variability transfer between high latitudes and the Mediterranean region. A similar pattern was proposed by Rohling et al. (2002) for the Aegean Sea in the eastern Mediterranean Sea. The occurrence of rapid climate cooling events during the Holocene has been reported worldwide (Mayewski et al., 2004) although disagreements about their precise timing, character and impact require more devoted research to understand the ultimate causes of these millennial-scale climate variability. Although insolation changes (Bond et al., 2001) and instabilities inherent to the North Atlantic THC (Schulz and Paul, 2002) have been proposed as the main causes of the Holocene climate variability, the climatic oscillations recorded in the terrigenous signal of core MD99-2343 are better linked to the temperature signal from the North Atlantic region as highlighted by the correlation with the GISP2 $\delta^{18}O$ profile (Frigola et al., 2007). These results suggest that the atmospheric teleconnection between high latitudes and the Mediterranean region through the westerly winds system was the main control over the western Mediterranean deep circulation during the Holocene.

5.5.3. DO variability in WMDW formation

Oxygen and carbon isotopic records from benthic foraminifera in cores MD99-2343 (Fig. 5.5) and MD95-2043, the later from the Alboran Sea, follow a pattern that is coherent with the D–O events (Cacho et al., 2000; Sierro et al., 2005). These oscillations have been interpreted in terms of changes in the ventilation rates and properties of the deep water masses indicating the dominance of well-ventilated, colder/saltier, WMDW during the GS in contrast to the GIS (Cacho et al., 2006). The increase of WMDW ventilation was suggested to be associated with the strengthening of the north-westerly winds in the Gulf of Lion during GS (Cacho et al., 2000; Sierro et al., 2005). Prevailing dry and cold conditions on land were observed along the same intervals (Allen et al., 1999; Combourieu Nebout et al., 2002; Sánchez Goñi et al., 2002). Thus, the increased WMDW formation during GS likely favoured stronger deep-water currents, and hence deposition of coarser material in the Minorca sediment drift. However, maximum values in the paleocurrent intensity proxies are not recorded during the intervals of maximum ventilation according to benthic isotopes (maximum $\delta^{13}C$

values). In contrast, grain-size and geochemical increments occur slightly after the warmest phases of GIS (minimum planktonic $\delta^{18}O$ values), that is, during the recovering of deep water ventilation in parallel to the starting of the SST cooling phase (B. Martrat, personal communication) (see dotted lines in Fig. 5.5). This pattern is very consistent for all the GIS/GS cooling transitions and also in all three proxies for paleocurrents intensity (silt/clay, Si/Al and Ti/Al). All three records show synchronous peaks during GIS/GS transitions, which lead by several centuries the maximum ventilation conditions (Figs. 5.5b and 5.5c). These consistent but unexpected results reflect a dichotomy between proxies indicating water chemical properties (benthic and planktonic isotopes) and proxies of water physical properties (grain-size and sediment geochemical proxies).

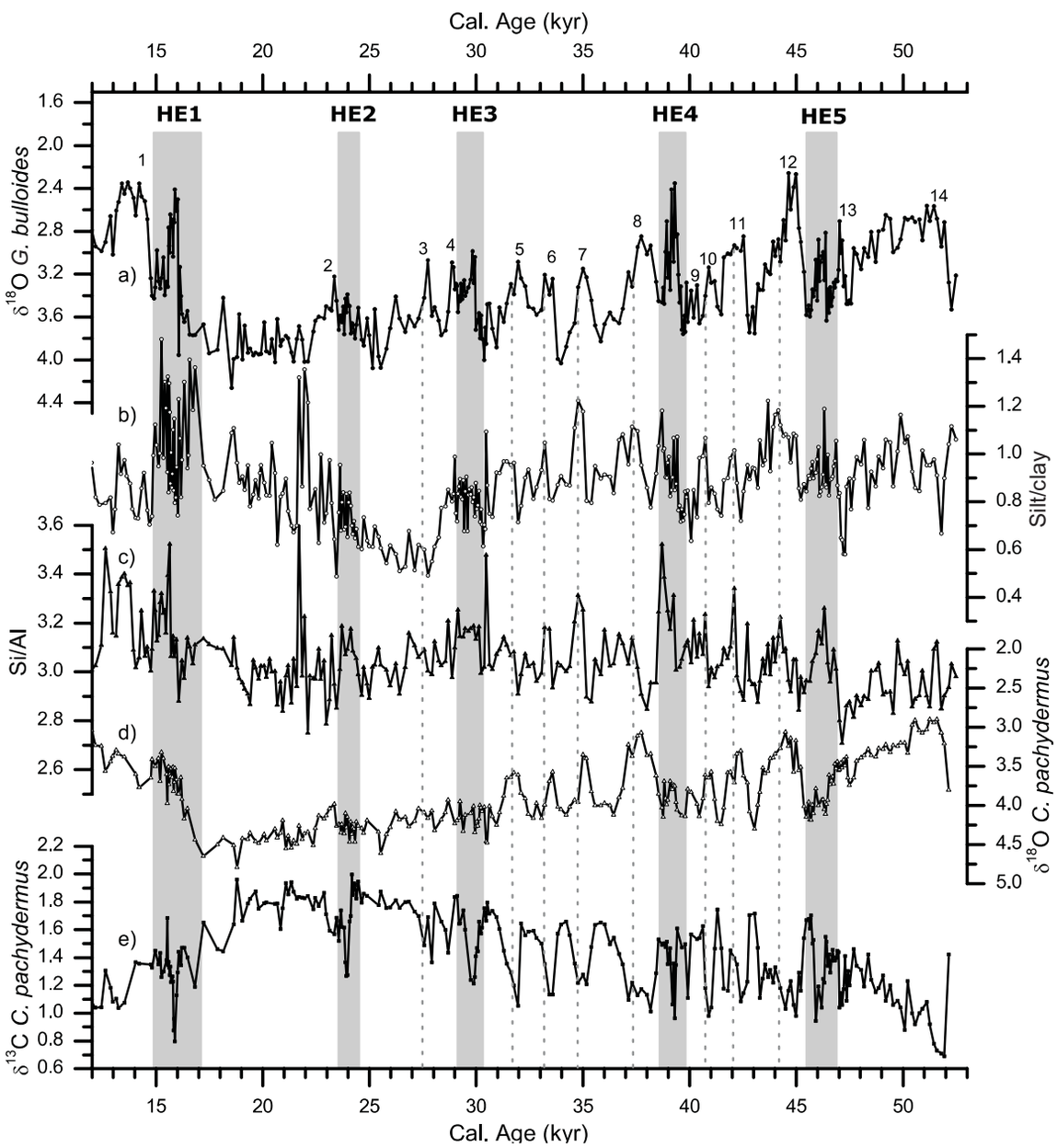

Figure 5.5. Records from core MD99-2343 for the 12–50 ka time interval. **a)** Planktonic $\delta^{18}O$. **b)** Silt/clay ratio. **c)** Si/Al. **d)** Benthic $\delta^{18}O$. **e)** Benthic $\delta^{13}C$. Numbers represent warm GIS while gray bars correspond to HEs. Dashed lines mark maximum values in the silt/clay ratio during MIS3.

Such a pattern as found in the Minorca sediment drift indicates the high sensitivity of deep water conditions to changes in the properties of surface waters associated with GIS/GS transitions. Overall, these results suggest that the deepwater Minorca sediment drift is particularly sensitive to changes in the vertical position of the WMDW core. Considering that the drift extends from 2100 m to more than 2700 m of water depth, the WMDW core may only occasionally flow at the depth of core MD99-2343, that is, 2400 m. Therefore, paleointensity proxies indicate that GIS/GS transitions were the time when the WMDW core reached maximum strength at 2400 m. On the other hand, $\delta^{18}O$ and $\delta^{13}C$ records reflect chemical properties of the whole WMDW mass independently of the intensity and depth location of the flow core.

According to the patterns in the chemical and physical proxies along D–O cycles three main stages related to changes in WMDW properties can be defined (Fig. 5.6a). Stage 1 is a pure GIS stage with the lightest benthic and planktonic $\delta^{18}O$, light benthic $\delta^{13}C$ and low silt/clay values. Stage 2 corresponds to GIS/GS transitions, when SST cooled progressively, and benthic isotopes indicate improving ventilation (increasing $\delta^{13}C$) and incrementing density (increasing $\delta^{18}O$) of the WMDW. It is during Stage 2 when deep current speed proxies (i.e. silt/clay) indicate maximum velocities at the studied site. Stage 3 implies truly GS conditions characterized by maximum $\delta^{18}O$ values in both planktonic and benthic foraminifera, maximum benthic $\delta^{13}C$ and intermediate values of the silt/clay ratio. Stages 1, 2 and 3 can be associated with a weak mode, an intermediate mode and a strong mode of deep-water overturning in the western Mediterranean Sea, respectively. These modes relate to GIS, GIS/GS transitions and GS situations.

Stage 1 corresponds then to intervals of minimum ventilation and lightest WMDW, which is consistent with the relatively warm and humid conditions on land during GISs (Combourieu Nebout et al., 2002; Sánchez Goñi et al., 2002) and minimum deep currents velocities at the MD99-2343 site. Stage 2 started after climate became gradually colder and drier, when the surface water cooling during GIS/GSs transitions likely resulted in an abrupt reduction of the water column density gradient thus favouring reinforcement of deep water convection. Increased convection improved deep ventilation and resulted in maximum deep current velocities at the coring site as suggested by the highest silt/clay ratio (Figs. 5.5 and 5.6). During Stage 3, as surface conditions were becoming colder, the newly formed WMDW became progressively more ventilated and denser (increasing trends in $\delta^{13}C$ and $\delta^{18}O$) leading to a deepening of the bottom current core and, consequently, to a gradual speed reduction at the coring site as decreasing silt/clay ratio values suggest (Figs. 5.5 and 5.6). These results indicate that during times of maximum deep water formation (GS) the influence of the newly formed WMDW over the MD99-2343 site was reduced, likely due to a deeper circulation of those waters. Nevertheless, the silt/clay values recorded during Stage 3 suggest that currents were still active though to a lesser degree than at Stage 2 situations.

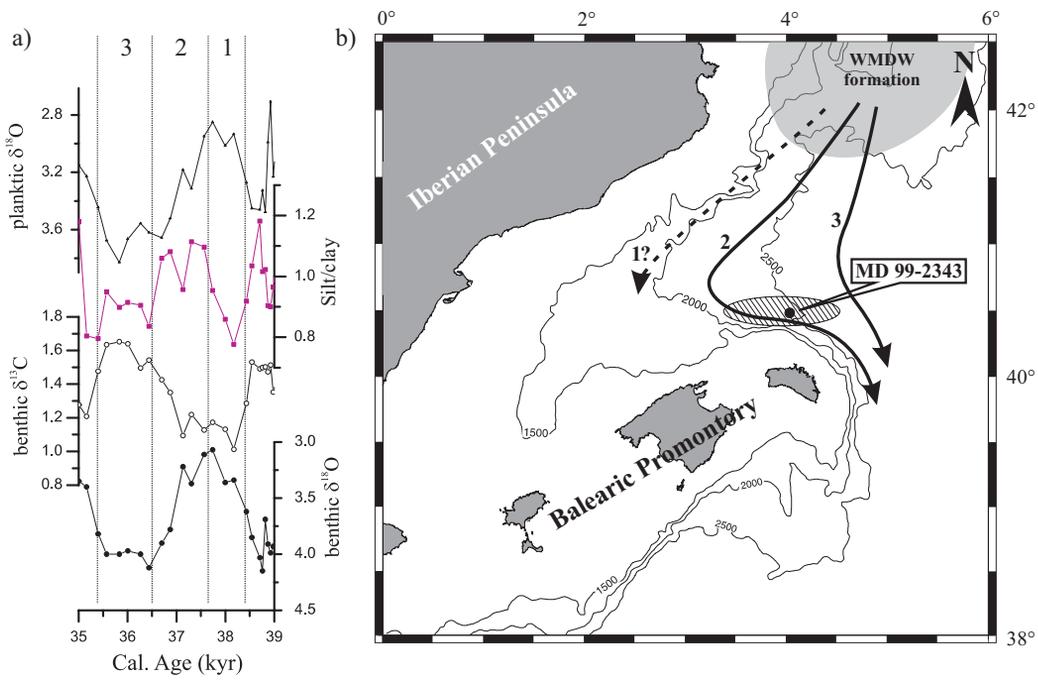

Figure 5.6. a) Detail of the planktonic $\delta^{18}O$, silt/clay, benthic $\delta^{13}C$ and benthic $\delta^{18}O$ records for the 35–39 ka time interval that corresponds to D–O cycle 8 (see Fig. 5.5). Numbers and vertical dotted lines limit the three stages described for each D–O cycle: Stage 1 during GIS, Stage 2 during GIS/GS transition and Stage 3 during GS. **b)** Schematic bathymetric map showing the three modes of circulation within a D–O cycle. (1) weak mode, (2), intermediate mode and (3) strong mode. Depending on the properties of the WMDW formed in the Gulf of Lion (shaded area) the core of the deep currents circulates at different depths, thus having different effects on the Minorca sediment drift (striped area) where core MD99-2343 was recovered.

The comparison among the benthic $\delta^{18}O$ and the grain-size records supports this hypothesis since current intensity systematically decreases when the heaviest $\delta^{18}O$ are reached (Figs. 5.5b and 5.5d). This observation is consistent with a new reconstruction of the properties of WMDW based on Mg/Ca paleothermometry in the Alboran Sea, which documents that the densest WMDW was formed during GS (Cacho et al., 2006). The recurrence of this pattern of variability with D–O cyclicities, with an offset between the physical proxies (e.g. silt/clay ratio) and the planktonic $\delta^{18}O$ record, demonstrates the extremely high sensitivity of the whole water column in the north-western Mediterranean Sea to climate forced changes of surface water properties that modified the entire density gradient. Denser WMDW formed during GS changed the MOW density in a way that, during intervals of denser MOW, the speed of its lower core increases as shown by coarsening mean grain-sizes from core MD99-2339 in the Gulf of Cadiz (Voelker et al., 2006).

The above described three modes of WMDW overturning appear as triggered by a rapid millennial-scale variability teleconnection between high and medium latitudes. Climate on land and intensity of westerly winds are the main forcing factors of present inter-annual variability in the intensity of WMDW formation together with the salt supply at intermediate levels from the eastern basin through the LIW (Lacombe et al., 1985; Schott and Leaman,

1991; Millot and Taupier-Letage, 2005). The westerlies intensity depends on the atmospheric pressure gradient over the North Atlantic region, in which decadal-scale variability presently is controlled by the NAO (Hurrell, 1995; Rodó et al., 1997). Assuming that a similar variability pattern acted during glacial times, it is likely that the observed changes in the WMDW circulation were controlled by NAO shifts. It has been already proposed that NAO oscillations dominated the glacial variability of the vegetation cover in the Iberian Peninsula and dust inputs from the Sahara region to the western Mediterranean Basin (Moreno et al., 2002; Sánchez Goñi et al., 2002). In addition, changes in the precipitation–evaporation budget at basin scale with D–O cyclicity have been inferred from pollen records in Italy, Greece and Iberia (Watts et al., 1996; Tzedakis, 1999; Sánchez Goñi et al., 2002). It is likely that these shifts in the precipitation–evaporation balance affected WMDW formation due to changes in surface salinity and, therefore, water density. These results also suggest that changes in the heat and salt volumes exported through the MOW across the Strait of Gibraltar were associated with WMDW fluctuations and could have played an important feedback role in driving millennial-scale climate changes in the North Atlantic region (Bigg and Wadley, 2001).

5.5.4. Shifts in WMDW formation during HEs

The isotopic record during the GS associated with HEs shows a more complex pattern than the regular GS. Light benthic $\delta^{13}C$ events occur at the middle of these intervals in parallel with planktonic $\delta^{18}O$ depletions (Fig. 5.7). These surface anomalies would correspond to 2–4% salinity lowering caused by the entrance of fresher polar surface waters through the Strait of Gibraltar during each of the HEs (Cacho et al., 1999; Sierro et al., 2005). Such a surface freshening should have reinforced the water column stratification and opposed deep water convection in the Gulf of Lion (Sierro et al., 2005). Weak overturning during HE was not expected since extremely dry and cold conditions on land were reconstructed from pollen sequences (Combourieu Nebout et al., 2002; Sánchez Goñi et al., 2002) and confirmed by the relatively low K/Al values recorded in MD99-2343 (Fig. 5.3d). Nevertheless, the benthic record indicates that, despite the climatic regime, the freshening of surface water was sufficient to reduce deep water formation (Sierro et al., 2005). Consequently, the GS associated with the HEs in the western Mediterranean had a complex deep ventilation evolution with high ventilation during the early and late phases (gray bars in Fig. 5.7) and a weakening in the middle of each HE due to surface water freshening (white bars in Fig. 5.7). All the proxies of deep water current speed (silt/clay, Si/Al and Ti/Al) show high values during the GS associated with the HEs which are consistent with the dominance of stronger deep currents by an active WMDW overturning (Figs. 5.3 and 5.4). These results are in contrast with the relatively low values recorded during the non-Heinrich GS and can only compare to the values recorded during GIS/GS transitions (stage 2 in Fig. 5.6).

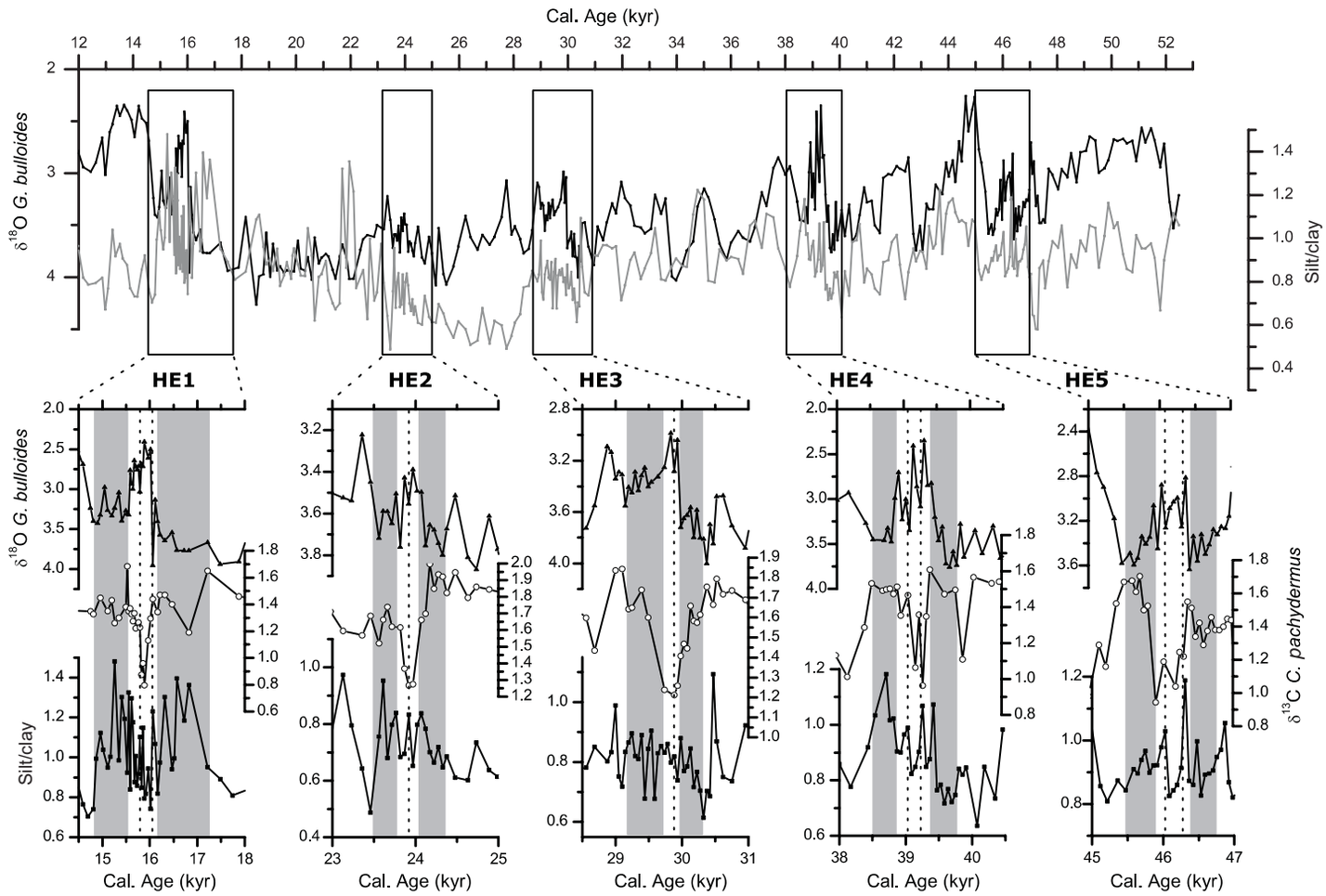

Figure 5.7. Comparison of the planktonic $\delta^{18}O$ and the silt/clay ratio for the 12–50 ka time interval. A centuries long offset is observed among the silt/clay ratio and the planktonic $\delta^{18}O$ record during MIS 3. Below, a close-up of HE1–HE5 through the planktonic $\delta^{18}O$, benthic $\delta^{13}C$ and silt/clay records from core MD99-2343 is shown. Gray bars represent the early and late phases of each HE while the white central bar corresponds to the isotopic anomaly described in the text. The high resolution reached on these records allows identification of several events in the central phase of each HE related to punctual returns to pure HE conditions (vertical dashed lines).

The silt/clay record from the GS associated with the HEs does not show a clear systematic pattern of variability during the three phases described above. During HE1 and, to a lesser extent, during HE2 and HE4 lower silt/clay ratios are observed during the central phase (white bars in Fig. 5.7) compared to the early and late phases (gray bars). This pattern is clearly consistent with a weakening of the deep water current during the entrance of low-salinity polar waters. However, silt/clay values are comparable for all three phases during HE3 and HE5. These discrepancies in the pattern of each HE could be attributed to orbitally induced insolation changes, e.g. HE1 occurs in a period of increasing seasonal differences while HE3 occurs in a period of lessening seasonal differences (Figs. 5.4d and 5.4e).

The very high resolution of the silt/clay and isotopic records allows identifying additional minor structures within HEs (Fig. 5.7). In particular, during the surface freshwater anomaly (white bars in Fig. 5.7) one to two minor *G. bulloides* $\delta^{18}O$ increments are observed (dotted

lines within white bars in Fig. 5.7). Most of them, i.e. those from HE5, HE4 and HE1, coincide with small *C. pachydermus* $\delta^{13}C$ increases. These minor recovering pulses are concurrent with marked increases in the silt/clay ratio, which supports the occurrence of deep currents short-lived strengthening events in the Minorca drift. These results suggest that the invasion of sub-polar less salty water from the North Atlantic was not steady but pulsating within each HE, which in turn triggered a response of the overturning cell in the Gulf of Lion. The combined interpretation of the isotopic and sedimentological records from core MD99-2343 suggests that, during GS associated with HEs, WMDW overturning was always strong enough to release fast currents to the Minorca drift, though not enough to reach the strongest mode 3 (Fig. 5.6) of non-Heinrich related GS. In consequence, sub-polar water pulses entering the western Mediterranean Basin induced changes in the intensity of WMDW ventilation but always allowed an intermediate mode of overturning.

5.6. Conclusions

The high-resolution sedimentological and geochemical analyses of the sediment core MD99-2343, recovered in the deep water Minorca sediment drift, resulted in new contributions to disentangle the variability of WMDW formation during the last 50 kyr. The strong parallelism between the K/Al record and the insolation curve at 40ºN points to orbitally induced insolation changes as the main direct control over fluvial runoff in the western Mediterranean Basin, itself related to changes in the long-term precipitation pattern. This astronomical forcing also had an important effect on deep water formation in the western Mediterranean Basin as reflected by changes in the grainsize records from core MD99-2343, thus highlighting the strong climate sensitivity of the Mediterranean region to orbitally induced changes.

Millennial-scale oscillations from silt/clay, Si/Al and Ti/Al proxies paralleling oscillations in the isotopic records during MIS3 illustrate a pattern of high variability in the deep water formation system in the western Mediterranean Basin that operates at three different intensity modes: strong, intermediate and weak. A centennial offset between the sedimentological and the isotopic proxies suggests that changes of intensity in deep water currents at MD99-2343 site resulted from density and paleodepth variations of the WMDW core flow thus affecting differently the Minorca sediment drift record. Since the formation of deep water during GIS was likely reduced, the cooling conditions prevailing after these warm events promoted the reduction of the column water density gradient thus favouring rapid reinforcement of deep water overturning and formation of denser WMDW that flowed into the deep basin. Accordingly, both silt/clay and Si/Al records from core MD99-2343 suggest maximum deep water currents intensity during the GIS/GS transitions, when WMDW core flowed shallower than the MD99-2343 site water depth. The continuous decreasing trend of silt/clay and Si/Al records until GS suggests a reduction of the effect of deep water currents at the core site location, thus pointing to the deepening of the WMDW core due to its increased density. On

the other hand, silt/clay ratio centennial-scale oscillations recorded during HEs confirm the strong influence that the entrance of sub-polar low-salinity waters had on the overturning system in the Gulf of Lion and suggest the occurrence of fresh water pulses within each HE. The study of additional sequences from shallower and/or deeper water depths from the Minorca sediment drift is the only way to confirm or adjust the hypothesis of WMDW vertical shifts hypothesis during MIS3.

Furthermore, the grain-size and geochemical proxies from core MD99-2343 have shown to be very useful for the study of the deep water conditions in the western Mediterranean Basin providing the first Holocene reconstruction of WMDW variability in the absence of benthic foraminifera. The reduction observed in both grain-size and geochemical records during the 12–10 ka time interval corresponds to the slowing down or collapse of the deep water overturning system due to enlarged freshwater input during the last deglaciation. The general pattern followed by both grain-size and geochemical proxies during the Holocene suggests a transition from relatively high energetic and humid conditions to drier conditions and less intense deep water currents. This transition was modulated by a reduction of the orbitally induced seasonal differences around 4 ka. Superimposed on this general trend, several rapid grain-size and geochemical excursions have been related to abrupt climate events. Thus, parallel increases in both the grain-size and geochemical records suggest a reinforcement of the deep water formation system coinciding with relative increases in the planktonic $\delta^{18}O$. The occurrence of such abrupt events during the Holocene at a periodicity close to 1000 yr and the good agreement with temperature oscillations in Greenland suggest a direct climatic teleconnection between the North Atlantic and the Mediterranean regions. The results from this work highlight the rapid response of the western Mediterranean overturning system to changes in the properties of surface waters, indicating the rapid transmission of climate variability to the deep basin.

Acknowledgments

We are especially grateful to *R/V Marion Dufresne* crew and the IMAGES program that allowed collecting the core MD99-2343. We also thank Montse Guart and Elisenda Seguí for their help in the laboratory. This work has been supported by the European projects PROMESS 1 (EVR1-CT-2001-00041), EURODOM (RTN2-2001-00281), ADIOS (EVK3-2000-00604), EUROSTRATAFORM (EVK3-2001-00200) and HERMES (GOCE-CT-2005-511234-1). The Spanish funded CGL200500642/BTE, SA008C05 and REN2003-08642-C02-02 projects are equally acknowledged. COMER Foundation and I3P postdoctoral program (CSIC) are also acknowledged for their support to I. Cacho and A. Moreno, respectively. CRG Marine Geosciences is recognized within the *Generalitat de Catalunya* excellence research groups program (ref. 2005SGR 00152).

6. Holocene climate variability in the Western Mediterranean region from a deep water sediment record

J. Frigola[1], A. Moreno[2], I. Cacho[1], M. Canals[1], F.J. Sierro[3], J.A. Flores[3], J.O. Grimalt[4], D.A. Hodell[5] and J.H. Curtis[5].

[1]CRG Marine Geosciences, Department of Stratigraphy, Paleontology and Marine Geosciences, Faculty of Geology, University of Barcelona, Campus de Pedralbes, C/Martí i Franquès s/n, 08028 Barcelona, Spain

[2]Pyrenean Institute of Ecology, Spanish Research Scientific Council, Aptdo. 202, 50080 Zaragoza, Spain

[3]Department of Geology, University of Salamanca, Plaza de la Merced s/n, 37008, Salamanca, Spain

[4]Department of Environmental Chemistry (ICER-CSIC), Jordi Girona 18, 08034 Barcelona, Spain

[5]Department of Geological Sciences, University of Florida, Gainesville, FL 32611-2120, USA

Abstract

The detailed analysis of the International Marine Past Global Changes Study core MD99-2343 recovered from a sediment drift at 2391 m water depth north of the island of Minorca illustrates the effects of climate variability on thermohaline circulation in the western Mediterranean during the last 12 kyr. Geochemical ratios associated with terrigenous input resulted in the identification of four phases representing different climatic and deepwater overturning conditions in the Western Mediterranean Basin during the Holocene. Superimposed on the general trend, eight centennial- to millennial-scale abrupt events appear consistently in both grain size and geochemical records, which supports the occurrence of episodes of deepwater overturning reinforcement in the Western Mediterranean Basin. The observed periodicity for these abrupt events is in agreement with the previously defined Holocene cooling events of the North Atlantic region, thus supporting a strong Atlantic-Mediterranean climatic link at high-frequency time intervals during the last 12 kyr. The rapid response of the Mediterranean thermohaline circulation to climate change in the North Atlantic stresses the importance of atmospheric teleconnections in transferring climate variability from high latitudes to midlatitudes.

Paleoceanography, 22, PA2209, 16 pp, 2007
doi:10.1029/2006PA001307
www.agu.org/pubs/crossref/2007.../2006PA001307.shtml

6.1. Introduction

The Holocene (last ~10 kyr) has been classically considered a climatically stable episode, especially when compared with climate changes of the last glacial period. However, there is increasing evidence of significant climate variability at orbital and suborbital scales during the present interglacial (Bianchi and McCave, 1999; Bond et al., 2001; Magny et al., 2002; Kuhlemann et al., 2004; Mayewski et al., 2004; Alley and Agustsdottir, 2005).

Orbitally induced differences in seasonal insolation have determined the long-term climatic evolution of the Holocene with a warm Climate Optimum during the early to-mid Holocene and a transition to colder conditions around 5 ka (COHMAP members, 1988; Cheddadi et al., 1997 and 1998; Prentice et al., 1998; Claussen et al., 1999; Magny et al., 2002; Davis et al., 2003; Sbaffi et al., 2004). Superimposed on this pattern are events of rapid climate change with periods of 2800–2000, 1500 and 900 years (Mayewski et al., 2004). While solar flux variability has been proposed to be the main forcing of these Holocene events (O'Brien et al., 1995; Bond et al., 2001; Rohling et al., 2002; Mayewski et al., 2004), oscillations in the production rates of the North Atlantic Deep Water (NADW) and in the poleward heat transport could also have triggered or amplified such instabilities (Bond et al., 1997; Bianchi and McCave, 1999; Schulz and Paul, 2002; Oppo et al., 2003). In any case, the direct causative mechanism remains unknown.

Paleoclimatic records have demonstrated the high sensitivity of the western Mediterranean region to rapid climate changes during the last glacial interval, including Dansgaard-Oeschger and Heinrich events, thereby supporting the view of a strong link between the Mediterranean and the North Atlantic climate (Rohling et al., 1998b; Cacho et al., 1999, 2000 and 2001; Moreno et al., 2002 and 2004; Rohling et al., 2002; Martrat et al., 2004; Sierro et al., 2005). This rapid connection between both regions has been interpreted to result from the entrance of cold surface waters into the Mediterranean Sea through the Strait of Gibraltar, but also from the intensification of the atmospheric circulation. A strengthened westerly system enhanced the marine overturning cell in the Gulf of Lion leading to a more efficient formation of Western Mediterranean Deep Water (WMDW) and to the enhancement of deep circulation (Cacho et al., 2001; Sierro et al., 2005).

In contrast to the glacial period, information about Holocene rapid variability in the western Mediterranean region and its links to North Atlantic climate is comparatively scarce. One of the most useful proxies for the study of WMDW formation and circulation during glacial periods, carbon and oxygen isotopic records from *Cibicidoides spp* foraminifera, is lacking during the Holocene because of poor ventilation and oxygenation conditions of deep waters that caused the disappearance of this species (Caralp, 1988; Reguera, 2004). Core MD99-2343 was recovered from the deepwater Minorca sediment drift in the path of the southward

branch of the WMDW. In this study, we use grain size distributions and bulk geochemical ratios of terrigenous material down this core to reconstruct Holocene changes in WMDW.

6.2. Study Area

6.2.1. Climate and Physical Oceanography Setting

The climate regime of the Mediterranean region is transitional between the temperate maritime type and the arid subtropical desert climate (Barry and Chorley, 1998). The Icelandic low–Azores high system controls present-day meteorology and climate in western Europe including the western Mediterranean region. Summers in the western Mediterranean are usually hot and dry because of the influence of the expanded Azores anticyclone. The southward displacement of the anticyclone during winter allows Atlantic depressions to enter the western Mediterranean region bringing high atmospheric instability and wetter conditions. At decadal scale, this pattern is known as the North Atlantic Oscillation (NAO), which modulates much of the present-day climate variability in this region (Rodó et al., 1997). The NAO system and the strong influence of the Mediterranean Sea expose the region to large-scale climate changes (Bolle, 2003). The western Mediterranean region is also influenced by Saharan air masses that transport considerable amounts of dust toward the Mediterranean Sea and farther north (Prospero, 1996). This short overview highlights the complexity of the climatic behavior of the western Mediterranean region and evidences its high sensitivity to heat and moisture flux variations.

Because of winter southward displacement of the Azores high, Atlantic depressions follow southern trajectories coming into the Mediterranean region more frequently (Barry and Chorley, 1998). This process leads to the formation of strong and cold northerly and northwesterly winds in the Rhône and Ebro valleys funneling the airflow into the western Mediterranean (i.e., Mistral and Cierzo winds, respectively). These winds cause strong evaporation and cooling offshore in the Gulf of Lion thus increasing surface water density until it sinks to greater depths (MEDOC-group, 1970; Lacombe et al., 1985; Millot, 1999). This process gives birth to the formation of the Western Mediterranean Deep Water (WMDW), which fills the deepest part of the Western Mediterranean Basin (Fig. 6.1). Deep water formation in the Gulf of Lion depends on wind stress variability but is also affected by the amount and depth of the Levantine Intermediate Water (LIW) before WMDW formation events (Pinardi and Masetti, 2000). As consequence of the negative balance of water created by the excess of evaporation over fresh water input in the Mediterranean Sea a compensating surface Atlantic water layer enters through the Strait of Gibraltar as Modified Atlantic Water (MAW) (Fig. 6.1) (Millot, 1999). The dense LIW and WMDW leave the Mediterranean Basin through the Strait of Gibraltar forming the deep Mediterranean Outflow Water (MOW) (Millot, 1999).

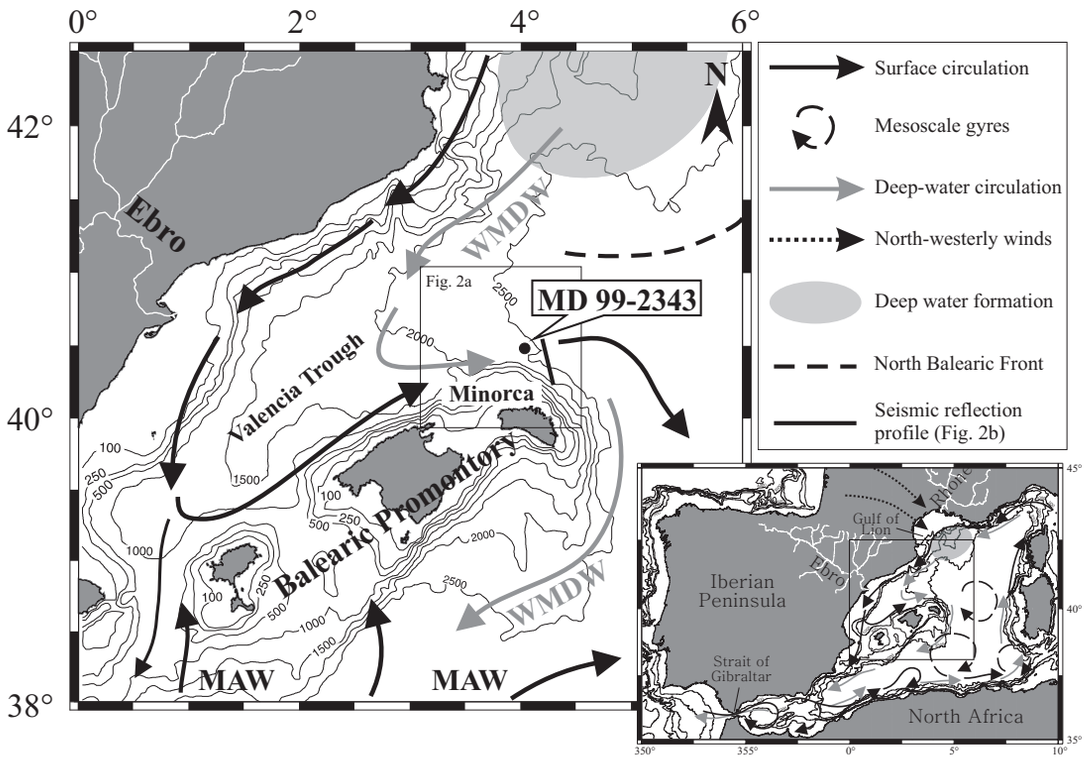

Figure 6.1. Bathymetric map of the study area showing the general surface and deepwater circulation patterns and the position of core MD99-2343. The box in the main map shows the location of Figure 6.2a, while the solid line illustrates the location of the seismic reflection profile in Figure 6.2b. WMDW is Western Mediterranean Deep Water; MAW is Modified Atlantic Water.

In the northwestern Mediterranean Sea the Balearic Promontory influences the circulation acting as a topographic barrier. The dense WMDW that forms and sinks in the Gulf of Lion flows south and southwestward into the Valencia Trough at depths closer to 2000 m (Millot, 1999) (Fig. 6.1). When the deep current encounters the Balearic Promontory it shifts direction eastward and southeastward bordering the Minorca base of slope. The abruptness of the Balearic slope and the topographically induced change in the current direction likely result in an intensification of the current, as this process has been described for the North Atlantic deep sediment drifts (McCave and Tucholke, 1986). Off Minorca this has led to the formation of the Minorca peripheral depression and associated sediment drift (Velasco et al., 1996) (Fig. 6.2a) where our core MD99-2343 was recovered.

6.2.2. Particle Sources and Sedimentary Setting

Sediment is supplied to the northwestern Mediterranean Sea mainly by fluvial discharge from the north, by aeolian inputs form the south, and by primary production from surface waters. The two main rivers are the Rhône and the Ebro (Fig. 6.1) with estimated historical pre-damming sediment fluxes of $30 \cdot 10^6$ t yr^{-1} and $17–25 \cdot 10^6$ t yr^{-1}, respectively (UNEP, 2003). However, only 10% of the fluvial discharge reaches the deep basin while the remaining 90% is deposited in deltaic and inner continental shelf areas (Martin et al., 1989). Sa-

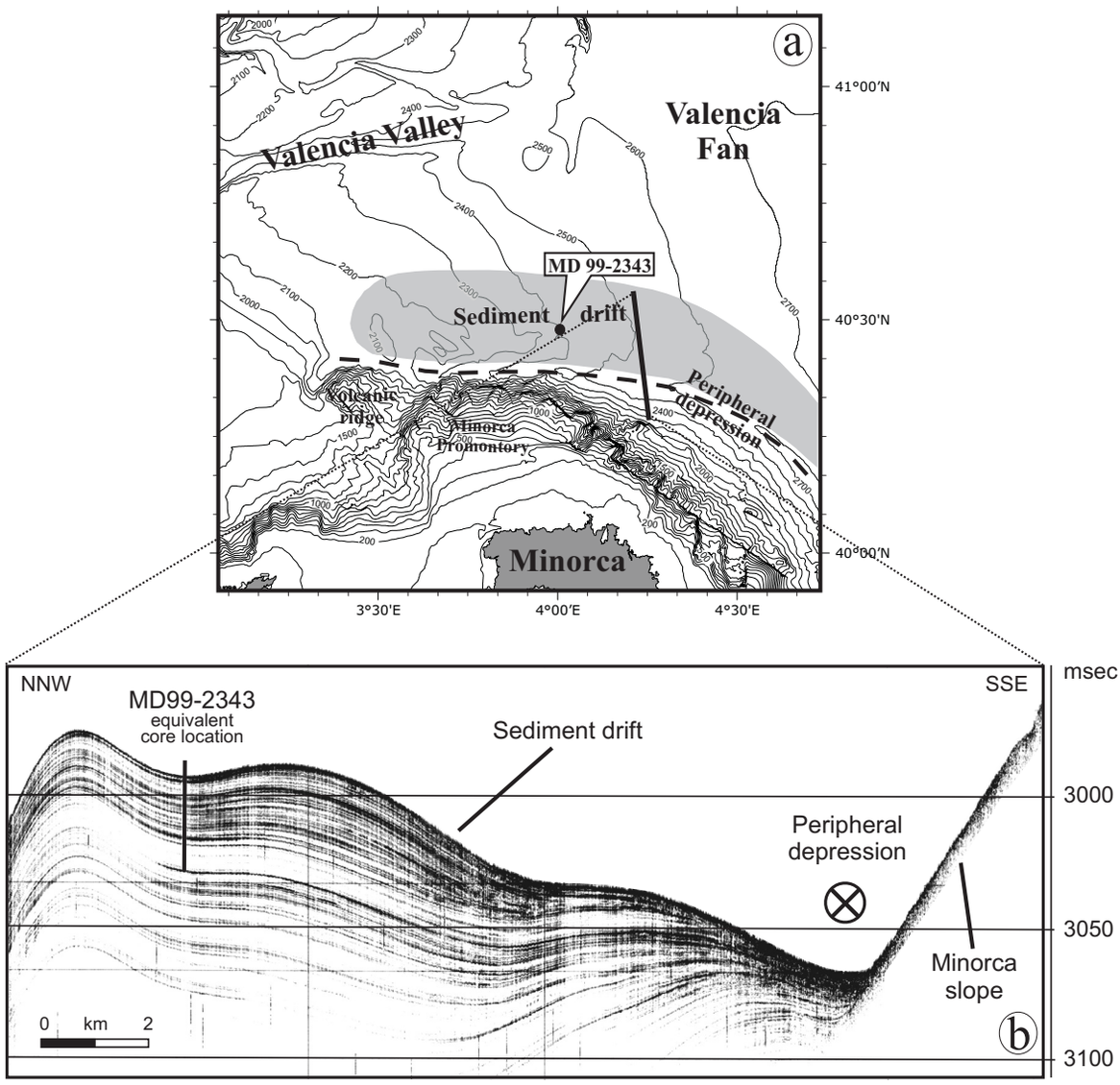

Figure 6.2. a) Detailed bathymetric map showing the main seafloor features nearby core MD99-2343. Shaded area roughly delimits the Minorca sediment drift. The abrupt step on the NE Minorca slope is the result from the merging of the high-resolution swath bathymetry data set with the General Bathymetric Chart of the Oceans (GEBCO) digital database (Intergovernmental Oceanographic Commission et al., 2003). **b)** Very high resolution seismic reflection profile across the Minorca sediment drift and peripheral depression (modified from Velasco et al., 1996). The cross within a circle represents the direction of the contour current that is normal to the image. Equivalent position of core MD99-2343 is also shown.

haran dust fluxes account for 10–20% of presentday deep-sea sedimentation in the western Mediterranean (Loyë-Pilot et al., 1986; Zuo et al., 1991; Guerzoni et al., 1997) although this contribution may have changed substantially through time (Moreno et al., 2002; Weldeab et al., 2003). The contribution of local pelagic, mostly carbonate particles is limited by the oligotrophic character of most of the western Mediterranean Sea (Bethoux et al., 1998). In any case, at the location of the studied sediment core, carbonate may also have been contributed by shelf edge spillover processes from the nearby Balearic Promontory (Maldonado and Stanley, 1979; Maldonado and Canals, 1982).

High-resolution seismic reflection profiles across the Minorca drift show a reflector configuration that is typical of contourite drifts (Fig. 6.2b) (Vanney and Mougenot, 1981; Stow, 1982 and 2002). While the peripheral depression is filled with coarse sediment (Canals, 1980) it is assumed that the fine fraction escaped out of the depression and contributed to the development of the sediment drift in its way toward the basin centre. The MD99-2343 site on the Minorca drift, and the drift itself, occupy a relatively shallower position (Alonso et al., 1995) that is beyond the direct influence of turbidite sedimentation (Fig. 6.2a). However, it is likely that suspended particles escaping from the turbidite systems to the west (Ebro margin) and north (Gulf of Lion margin) may have been caught by the nearbottom circulation and added to the background sedimentation of the Minorca drift (Fig. 6.2a). Large-scale bed forms found in the deep northwestern Mediterranean Basin further indicate that bottom currents likely played a significant role in the shaping of the seafloor, and thus in sediment particle transport, winnowing and sorting in the recent past (Mauffret et al., 1982; Maldonado et al., 1985b; Palanques et al., 1995; Acosta, 2005). Although no current meter data exist for the vicinity of the core site, near-bottom current measurements during a 3-month period at 1800 m water depth in the Gulf of Lion deep margin, where WMDW formation takes place, gave maximum values of 50 cm s^{-1} and mean values of 20 cm s^{-1} (Millot and Monaco, 1984).

6.3. Material and Methods

Sediment core MD99-2343 was recovered with a Calypso piston corer north of Minorca at 40º29.84'N, 04º01.69'E and 2391 m of water depth in the northwestern Mediterranean Sea (Fig. 6.1), during Leg 5 of the *R/V Marion Dufresne* expedition within the International Marine Past Global Changes Study (IMAGES) programme. From the total 32.44 m of core length, only the top 4 m corresponding to the last 12 kyr are discussed in this paper. The top 4 m consists of grey nannofossil and foraminifer silty clay. Layers with high content of pteropod and gastropod shell fragments have been also observed all along the upper core section. As a general rule, one centimeter thick sediment samples were taken every 4 to 6 cm for oxygen and carbon isotope analyses of foraminifer shells, and grain size and major element composition analyses of the bulk sediment. Additional samples for grain size analyses were collected at 2 cm resolution over selected intervals.

Samples for isotope analyses were washed over a 63 μm sieve and the retained fraction was dried and dry-sieved again using a 150-μm sieve. About 10 mg of *Globorotalia inflata* and *Globigerina bulloides* were hand-picked for radiocarbon isotope analyses. The AMS ^{14}C analyses were performed in the U.S. National Ocean Sciences Accelerator Mass Spectrometry Facility (NOSAMS). The ages were calibrated with the standard marine correction of 408 years and the regional average marine reservoir correction (ΔR) for the western Mediterranean Sea by means of the Calib 5.0.1 programme (Stuiver and Reimer, 1993) and the MARINE04 calibration curve (Hughen et al., 2004).

Approximately 5 to 10 specimens of Globigerina bulloides from the 300-350 μm size fraction were picked to measure stable isotope ratios. Foraminifer tests were soaked in 15% H_2O_2 to remove organic matter and sonically cleaned in methanol to remove fine-grained particles. The foraminifer calcite was loaded into individual reaction vessels and each sample was reacted with 3 drops of H_3PO_4 (specific gravity = 1.92) using a Finnigan MAT Kiel III carbonate preparation device. Isotope ratios were measured online using a Finnigan MAT 252 mass spectrometer. Analytical precision was estimated to be ±0.08% for $\delta^{18}O$ and ±0.03% for $\delta^{13}C$ (1σ) by measuring 8 standards (NBS-19) with each carousel containing 38 samples. All isotope results are reported in standard delta notation relative to V-PDB (Coplen, 1996).

Grain size was measured on the total fraction and the noncarbonate fraction after removing organic matter and carbonates by treatment with excess H_2O_2 and HCl, respectively. A Coulter LS 100 Laser Particle Size Analyser (CLS), which determines particle grain sizes between 0.4 and 900 μm, was used to determine grain size distributions as volume percentages. The laser diffraction size analyzer principle is based on the measurement of the diffraction angle produced by the particles when a laser beam goes through the sample in an aqueous solution. The correlation between diffraction angle and particle size is opposite (McCave et al., 1986). Since diffraction is assumed to be given by spherical particles, the resulting particle size is that diameter (known as equivalent spherical diameter). Subsequently, laser diffraction methods are claimed to underestimate plate-shaped clay mineral percentages. To correct such effect we have followed the method proposed by Konert and Vandenberghe (1997). CLS precision and accuracy is tested by systematic control runs using latex microspheres with predefined diameters. The high precision (reproducibility) of the measurements was demonstrated by small variations in the mean diameter (0.97% of variation) and in the standard deviation (1.37% of variation). The accuracy of the measurements, as indicated by the relative departure from the nominal mean diameter is 0.30%, corresponding to absolute deviations between 0.09 and 0.34 μm. Additional test runs were performed using microsphere assemblages with mixed grain sizes to ensure that CLS accurately determined polymodal grain size distributions.

We discuss grain size results as the median of each sample since it represents the distribution midpoint and it usually constitutes a more representative value of the grain size distribution than the mean. In order to extract palaeoclimate information from a mixture of sediments with different sources numerical-statistical modeling of large grain size data sets provides the best results (Weltje and Prins, 2003). However, core MD99-2343 was recovered on a contouritic drift built by the influence of near bottom currents where minor or no changes in sediment sources are expected (see below). Subsequently, instead of statistical modeling of end-members, we have considered the UP10 fraction, which composes the volume percentage of the fraction coarser than 10 μm, a good indicator of deep currents variability at this site. The UP10 integrates the sortable silt fraction (SS, 10–63 μm), defined as the coarser

fraction of the silt with noncohesive behavior during transport and deposition (McCave et al., 1995b), while taking also into account the influence of the fine sand subpopulation (>63 μm) that could be reworked by strong contour currents. Finally, the silt/clay ratio has also proven to be useful for the study of deepwater currents intensity (Hall and McCave, 2000).

The percentages of major elements in sediment samples were determined by means of X-ray fluorescence using a Philips PW 2400 sequential wavelength X-ray spectrometer. Prior to the analyses, samples were dried at 100ºC, and then ground and homogenized in an agate mortar. 0.3 g of homogenized bulk sediment with lithium tetraborate at a 1:20 dilution factor were fused at 1150ºC in an induction oven Perle'X-2 to 30-mm-diameter glass discs. The content of major elements Si, Ti, Al, K, Ca, Fe, Mn, Mg, P and Na was calculated as oxide percentages. Analytical accuracy was checked by measuring international standards (GSS-1 to GSS-7) being better than 1% of certified values. Precision of individual measurements was better than 0.9% as determined from replicate analyses of sediment samples (repeatability). Precision over the period of measurement was better than 3.4% (reproducibility) for all elements analyzed in this work. Spurious correlations between elements due to closure effect to 100% are avoided by discussion of element/Al ratios (Rollinson, 1993).

X-ray diffraction (XRD) analyses were carried out in selected samples using a Siemens D-500 X-ray diffractometer on untreated, glycolated and heated (550ºC) samples. Prior to the analysis, samples were mounted on smear slides after clay separation by decantation.

6.4. Chronostratigraphy

Sierro et al. (2005) provided an age model for core MD99-2343 based on four ^{14}C AMS dates and several tie points with the Greenland ice core GISP2. This age model has been modified to account for six additional monospecific foraminifer ^{14}C AMS dates of which four lie within the 0–12 ka interval (Table 6.1). A mid Termination Ib (TIb) additional tie point has been added by correlating the Minorca G. bulloides oxygen isotopic record to the one from the Alboran Sea core MD95-2043 (Cacho et al., 1999) (Table 7.1). Both oxygen isotopic profiles for the last 12 kyr are plotted in figure 6.3.

Sedimentation rates for the upper 4 m of core MD99-2343 range between 18 and 73 cm kyr^{-1} with an average value of 37 cm kyr^{-1} (Fig. 6.3). These rates are much higher than those determined for nearby sites (e.g., 4 cm kyr^{-1} in core SL87 south of Minorca (Weldeab et al., 2003)), even accounting for potential core stretching (Skinner and McCave, 2003). The high rates likely reflect local enhancement of particle deposition associated with the building of the Minorca sediment drift, as illustrated by seismic reflection profiles (Fig. 6.2b). Because of the variation in sedimentation rates as a consequence of the sedimentary environment and because of the number of available dates, the final age model was constructed by linear

Isotope Event or Radiocarbon Sample/Foram Type	Depth, cm	^{14}C Age, years	Calendar Years
AMS ^{14}C/multispecific	28	790 (±40)	386 ± 55
AMS ^{14}C/*G. inflata*	88	3,110 (±30)	2,816 ± 50
AMS ^{14}C/multispecific	118	3,390 (±50)	3,225 ± 80
AMS ^{14}C/*G. inflata*	208	5,720 (±40)	6,091 ± 70
AMS ^{14}C/multispecific	238	6,210 (±50)	6,601 ± 70
AMS ^{14}C/*G. inflata*	308	7,700 (±40)	8,110 ± 60
TIb–Onset of the Holocene	354		10,696[b]
AMS ^{14}C/*G. bulloides*	398	10,650 (±50)	11,883 ± 230
AMS ^{14}C/*G. inflata*	418	11,200 (±50)	12,811 ± 30
AMS ^{14}C/*G. bulloides*	568	13,850 (±40)	15,912 ± 190
AMS ^{14}C/multispecific	604	14,550 (±110)	16,822 ± 240

Table 6.1. Age model for core MD99-2343. New and previous ^{14}C-AMS dates after (Sierro et al., 2005) calibrated with the Calib 5.0.1 programme (Stuiver and Reimer, 1993). Linear interpolation between dated points was performed with the AnalySeries Version 1.1 (Paillard et al., 1996). **a)** New ^{14}C AMS dates. **b)** Tie point used for the age model of core MD99-2343 by correlation with the oxygen isotopic record from core MD95-2043 in the near Alboran Sea.

interpolation between calibrated ages instead of using other age-depth extrapolation models (Telford et al., 2004). The age model accuracy and the sampling interval result in a mean time resolution of 135 years for the top 4 m section of core MD99-2343.

6.5. Results

6.5.1. Oxygen Isotopic Record

The heaviest values in the *G. bulloides* δ^{18}O record from core MD99-2343 during the last 12 kyr correspond to the late Younger Dryas (12–11.5 ka) (Fig. 6.4). During the deglaciation (11.5–9 ka), the δ^{18}O record shows a continuously decreasing trend that ends at 9 ka when the lightest δ^{18}O values were reached. The Holocene is characterized by a long-term rising trend punctuated by nine centennial to millennial-scale oscillations (Fig. 6.4a). Some of the δ^{18}O increases are significant, e.g., >0.5% from 6.5 to 5.8 ka, or >0.9% from 9 to 7.8 ka. Moreover, as discussed below, these oxygen isotopic anomalies (arrows in Figs. 6.4, 6.5, and 6.6 and Table 6.2) correlated with changes in other proxies (see below). We name these events as ‘‘Minorca abrupt events’’ with M8 being the oldest and M0 the youngest. M0 is not very well expressed in the δ^{18}O record but we have also labeled this event considering the other studied proxies. The duration and intensity of these δ^{18}O shifts are similar to those recorded during some of the glacial period Dansgaard-Oeschger cycles (Sierro et al., 2005) and only M0 may fit within the δ^{18}O analytical error. Following previous results (Cacho et al., 1999; Shackleton et al., 2000; Skinner and Shackleton, 2003; Sierro et al., 2005) these δ^{18}O fluctuations would be driven by SST coolings of about 2º to 3ºC. However, the influence of other properties (i.e., salinity) on the isotopic signal cannot be discarded with the available information.

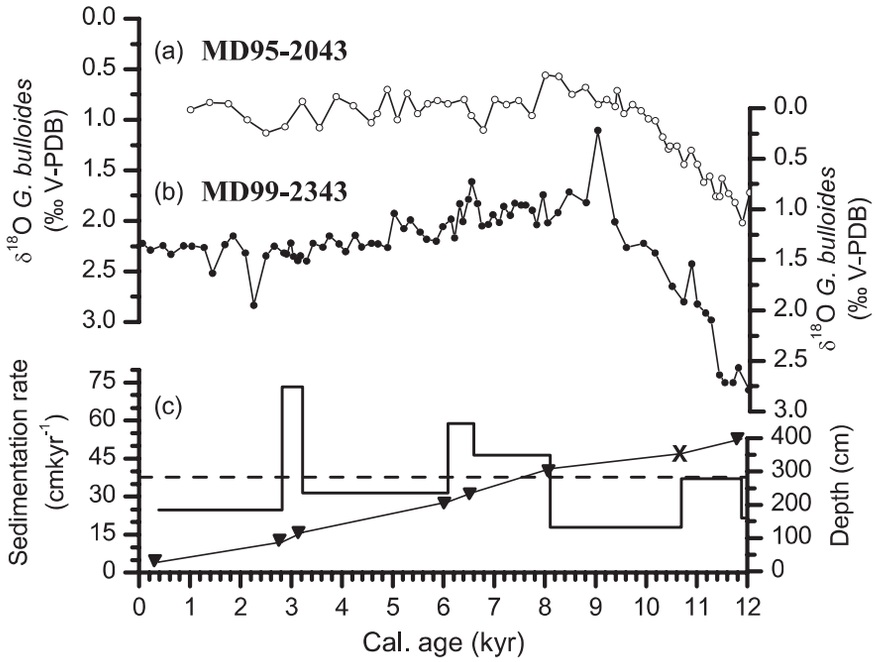

Figure 6.3. Comparison of the *G. bulloides* oxygen isotopic records from **a)** MD95-2043 (Alboran Sea) and **b)** MD99-2343 (this study) cores for the last 12 kyr. **(c)** Sedimentation rates along MD99-2343 sediment core calculated linearly among calendar years from ^{14}C accelerator mass spectrometry (AMS) dates (triangles) and tie points (cross) utilized in the age model (see text for details and Table 6.1). The mean sedimentation rate of 37 cm kyr^{-1} is represented by a dashed line.

6.5.2. Grain Size Distribution

Down-core trends in median grain size are similar for bulk sediment and the noncarbonate fraction (Figs. 6.4b and 6.4c). The median grain size ranges between 5 and 8 μm, thus pointing to the same processes controlling the deposition of the two fractions. Only a small number of samples from the noncarbonate fraction have median grain sizes coarser than 10 μm. Since the carbonate fraction integrates biological production plus detrital carbonate particles, it is considered that the fraction better representing the intensity of bottom currents is the noncarbonate one (McCave et al., 1995b). This noncarbonate fraction displays seven median grain size peaks at 8.4, 7.2, 6.2, 5, 4.1, 3.2 and 2.5 ka, which are coincident with isotopic enrichment events, i.e., M8 to M2 (Figs. 6.4a and 6.4c).

A detailed study of grain size distributions from the noncarbonate fraction reveals that most of the samples within the Holocene are unimodal, with mode values around 8–10 μm (Fig. 6.4d). Few samples show bimodal distributions with a second mode around 150–200 μm (Fig. 6.4d), which is given by the presence of coarser grains, mainly quartz and mica packets, as observed by microscope (see photograph in Fig. 6.4c). Such bimodal samples (marked with an asterisk in Fig. 6.4c) correspond, with rare exceptions, to the samples with

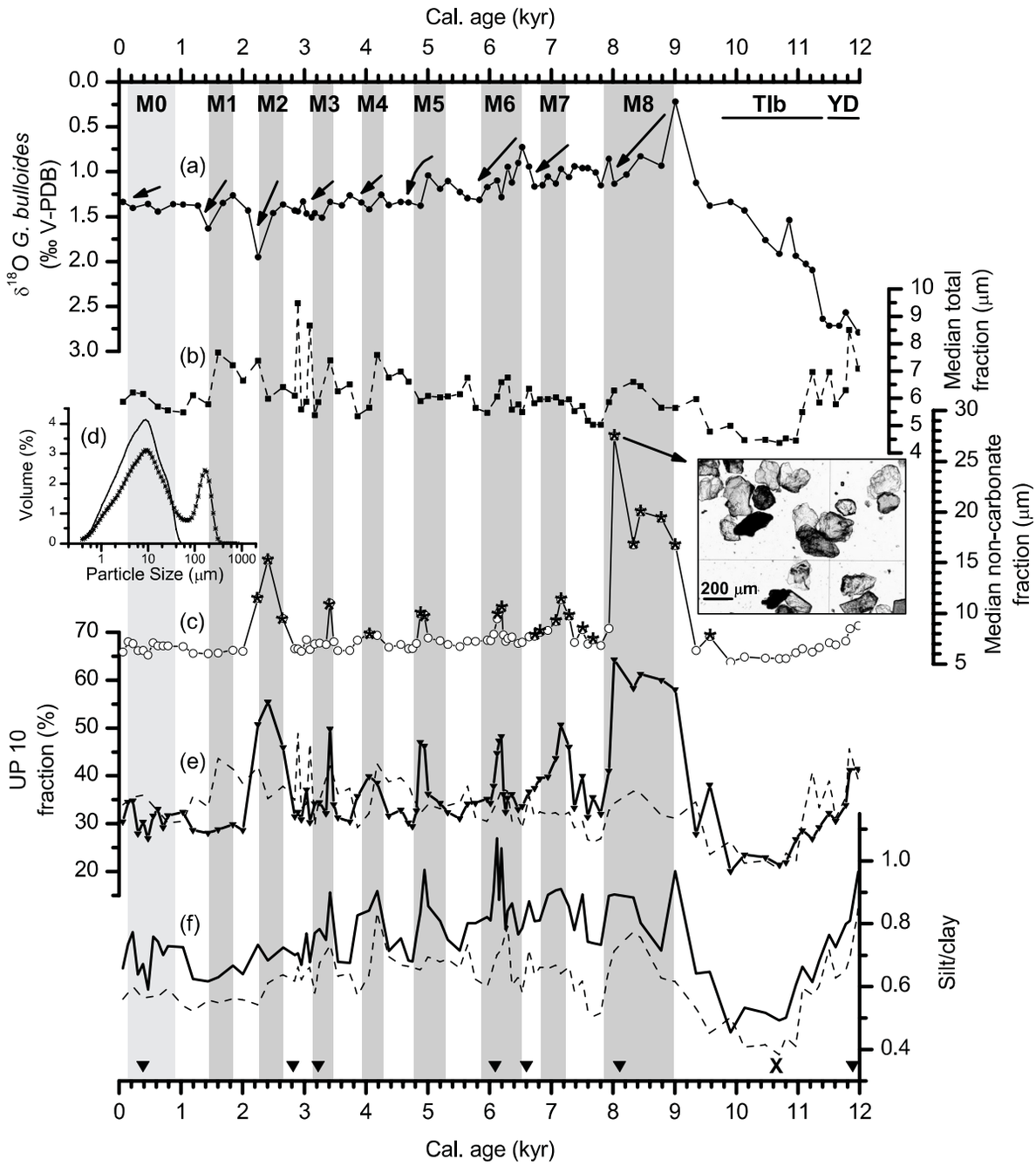

Figure 6.4. a) *G. bulloides* oxygen isotopic record from core MD99-2343 for the last 12 kyr. Grain size records of the **b)** total and **c)** noncarbonate fraction of the sediment, expressed as the median (μm) of each sample. The image is a plane light photograph of the noncarbonate fraction coarser than 63 μm from 304-cm core depth. Asterisks indicate bimodal samples. **d)** Examples of unimodal (solid line, sample between M5 and M6) and bimodal (dotted line, from one M7 sample) grain size distributions. **e)** UP10 fraction (>10 μm) and **f)** silt/clay ratio for the noncarbonate fraction (solid line) and the total fraction (dashed line). Arrows and bars indicate the position of the Minorca abrupt events M8 to M0 as defined in the text. The ^{14}C AMS dates (triangles) and tie point (cross) are also shown.

high median grain size values in the noncarbonate fraction and hence to the Minorca abrupt events M8 to M2.

The UP10 general trend mimics the median grain size records and highlights additional features (Figs. 6.4b, 6.4c, and 6.4e), for example a marked decrease from 11.5 to 10 ka, and a better expression of M4 (Fig. 6.4a). From 9 ka to present, the UP10 fraction oscillates between 30 and 35%, except for M8 to M2 events. In the M8 to M2 peaks the UP10 fraction may represent as much as 50% of the sample (Fig. 6.4e). The UP10 peaks are consistent with the above mentioned median grain size increases (Fig. 6.4c), and correlative with the oxygen isotopic enrichments of the Minorca abrupt events (Fig. 6.4a). A slight increase in the UP10 fraction is recognized in the last millennium.

Silt/clay ratio (Fig. 6.4f) complements the information gathered from grain size parameters. Like UP10, this ratio also illustrates a marked fall of silt accumulation during the deglaciation, displays relatively high values during the early Holocene and shows a decreasing trend during the last 9 kyr ending with relatively low values during the late Holocene (Fig. 6.4f). The overall record is again punctuated by a number of peaks linked to the Minorca abrupt events identified from previous proxies. These long-term trends and short-lived events are visible in both the bulk (dashed lines in Fig. 6.4) and the noncarbonate fraction (solid lines in Fig. 6.4), where they are more obvious.

6.5.3. Geochemical Record

The Si/Al, Ti/Al, K/Al and Ca/Al geochemical profiles of core MD99-2343 are plotted in Figures 5b, 5c, 5e, and 5f. Four main phases or trends are identified through the last 12 kyr: I, a decreasing trend in Si/Al and Ti/Al ratios (Figs. 6.5b and 6.5c) during the deglaciation that leads to a minimum at 10.5 ka that coincides with minimum values in grain size proxies (Fig. 6.4) and maximum values of summer solar insolation at 40ºN (Fig. 6.5d); II, an increasing trend in both Si/Al and Ti/Al ratios coincides with the end of the second phase of Termination (TIb) and the early Holocene (10.5–7 ka); III, high Si/Al and Ti/Al ratios with moderate oscillations during the mid-Holocene (7–4 ka); and IV, a gradual decreasing trend in Si/Al and Ti/Al during the late Holocene (4–0 ka), which parallels the decrease in the insolation curve (Fig. 6.5d). Interestingly, the K/Al record (Fig. 6.5e) presents a distinctive pattern during TIb and the early Holocene (phases I and II), therefore suggesting the operation of differentiated controlling factors on K/Al. The Ca/Al ratio (Fig. 6.5f) shows a rather distinct pattern with an almost continuous increasing trend across the Younger Dryas, TIb and early and mid-Holocene, with maximum values between 4 and 2.4 ka that drop abruptly after 2.4 ka (Fig. 6.5f).

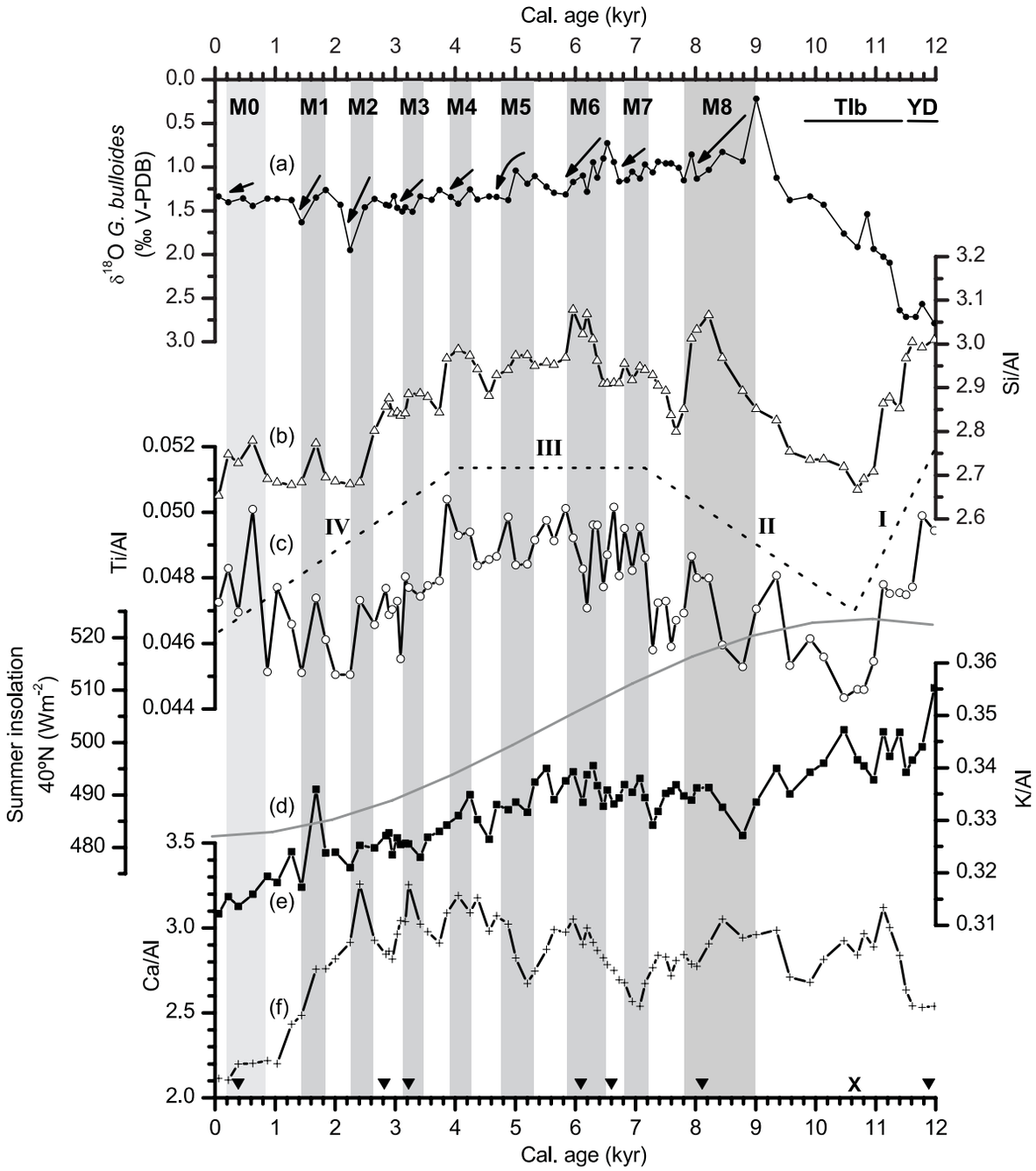

Figure 6.5. a) *G. bulloides* oxygen isotopic record from core MD99-2343 for the last 12 kyr. **b)** Si, **c)** Ti, **e)** K, and **f)** Ca geochemical records from core MD99-2343 normalized to Al. **d)** Summer insolation curve at 40ºN for the last 12 kyr. A dashed line between Si/Al and Ti/Al ratios represents the four distinct phases described in the general trend (see text). Arrows and grey bars indicate the Minorca abrupt events M8 to M0 as defined in the text. The ^{14}C AMS dates (inverted triangles) and tie point (cross) are also shown.

The above described general trends are punctuated by oscillations lasting from centuries to millennia. The Si/Al record shows eight abrupt events during the Holocene that are centered at 8.4, 7.2, 6.2, 5, 4.1, 3.2, 1.6 and 0.5 ka (Fig. 6.5b). Most of these events can be identified in the Ti/Al and Ca/Al records as well (Figs. 6.5c and 6.5f). However, they are not noticeable in the K/Al record (Fig. 6.5e). The abrupt events in the geochemical records coincide with the Minorca abrupt events identified in the *G. bulloides* oxygen isotopic record and the grain size proxies. The only exception to the described overall pattern is M2, which is represented

by one of the largest isotopic excursions (Fig. 6.5a), and a Ca/Al peak but lacks of expression in the Si/Al record (Figs. 6.5f and 6.5b).

The main mineralogical components obtained from the clay size XRD analysis confirm the high percentage of calcite and illite within all the analyzed samples, with chlorite, kaolinite, quartz and very low percentages of feldspars. The lack of major changes in the mineralogical composition of the clay fraction shows that geochemical variability is dominated by the composition of the coarser fraction. This enhances the value of the geochemical records for the interpretation of processes controlling coarse particle release, transport and accumulation.

6.6. Discussion

6.6.1. Particle Sources

Sediment particles resulting from riverine influx, aeolian transport and sea surface biogenic production (see section 7.2.2) form a mixed population that is expected to settle in the water column where it is advected by water mass movements before final deposition on the seabed. The proxies used in our study allow identifying the ultimate factors controlling sediment deposition in the MD99-2343 core site.

The location of the core MD99-2343 on a sediment drift off the carbonate shelf of the Balearic Islands points to a mixed signal in our Ca/Al ratio resulting from carbonate productivity (Rühlemann et al., 1999) and resedimented carbonate particles (Van Os et al., 1994). Surface productivity and subsequent particle settling in such an oligotrophic area (Bethoux et al., 1998) can contribute only partly to the carbonate flux and to the relatively high sedimentation rates of core MD99-2343.

Most of the samples within the Minorca abrupt event layers display a characteristic bimodal distribution (Figs. 6.4c and 6.4d) that could be tentatively attributed to pulses of enhanced aeolian transport. The relatively low rates of Saharan dust deposition and the high sedimentation rates measured in our core lead us to consider the Aeolian contribution as largely diluted within particle populations from other sources. In addition, the coarser grains from these layers yield a 150–200 μm mode that is much coarser than the one found in modern and glacial Saharan dust samples in the western Mediterranean (Guerzoni et al., 1997; Moreno et al., 2002). Furthermore, microscope inspection of the coarse grains observed within the Minorca event layers shows quartz grains with moderate angularity and undisturbed mica packets (sea photograph in Fig. 6.4c), an uncommon feature in aeolian dust particles (Guerzoni et al., 1997). Those observations point to a rather proximal source for these coarse grains whose release and transport did not involve particularly aggressive physical or chemical weathering processes as would be the case for the aeolian transported particles.

Core MD99-2343 was recovered from a contourite drift and the occurrence of this coarse grain population may be related to the formation of the drift itself. The building of the contourite drift demonstrates the efficiency of deepwater circulation in the area to rework, winnow, transport and accumulate originally fluvial terrigenous particles from the Valencia Valley and therefore explains the relatively high sedimentation rates observed in core MD99-2343. We interpret changes in the grain size distribution as mostly governed by the strength of such deep currents as previously observed in other contourite systems (McCave and Tucholke, 1986; Llave et al., 2006; Voelker et al., 2006). Intervals of enhanced currents resulted in a more efficient transport of coarse particles from both far fluvial sources and local sources as pointed out by the presence of coarse quartz and mica grains with minimal alteration. A prominent volcanic ridge (Maillard and Mauffret, 1999) at the very head of the Minorca peripheral depression (Fig. 6.2a), to the west of the Minorca drift, is a firm candidate as source area for such unaltered particles. Therefore the coarse particles deposited during the Minorca abrupt events accumulated during intervals of near-bottom current strengthening able to vigorously erode seafloor relieves and transport to the sediment drift location the coarse particles thus released.

K/Al, Si/Al and Ti/Al ratios are associated with terrigenous inputs (Krom et al., 1999; Wehausen and Brumsack, 1999, 2000; Moreno et al., 2001, 2002, 2005; Martínez-Ruiz et al., 2003; Weldeab et al., 2003), probably from the Ebro and Rhône rivers north of the study site. Si mostly comes from aluminosilicates and quartz as biogenic opal is a minor sediment component in the region (Weldeab et al., 2003), as further confirmed by our microscopic examinations. Ti resides within heavy minerals such as ilmenite and rutile, and Al and K are associated with clay minerals. In particular, the K/Al ratio is considered a good indicator for clay inputs (mainly illite) from river runoff. The presence of noticeable amounts of illite at the study site has been confirmed by peaks in XRD diffractograms. Consequently, the K/Al ratio can be interpreted as an indicator of illite entrance by river discharge and hence may provide a diagnosis of humidity conditions in the northwestern Mediterranean region. The parallelism between the K/Al record and the insolation curve at 40ºN not only for the Holocene (Figs. 6.5d and 6.5e) but also for the last glacial period (Frigola et al., 2008) reinforce the view that precipitation controls long-term K/Al ratio oscillations. The differences observed between Si/Al and Ti/Al, and the K/Al record (Figs. 6.5b, 6.5c, and 6.5e) are attributed to grain size geochemical segregation processes since K is mostly associated with clay particles while Si and Ti relate to coarser grains. Parallel increases of the median grain size and the Si/Al and Ti/Al ratios support the view that grain size distribution controls the variability of these geochemical ratios rather than changes in source area.

6.6.2. Holocene Onset and General Trends

The decrease in the oxygen isotopic record from 12 to 9 ka (Fig. 6.4a) embraces the end of the Younger Dryas, the second phase of Termination (TIb), and the onset of the Holocene. The variations observed in both grain size and geochemical records during this time interval (Figs. 6.4 and 6.5) reflect the strong changes in the sedimentary dynamics driven by the shifting climatic conditions. Diminutions in grain size parameters and Si/Al and Ti/Al ratios (phase I), which reached minimum values between 10 and 11 ka (Figs. 6.4 and 6.5), are consistent with a slowdown of deepwater circulation in the western Mediterranean. Accordingly, the glacial benthic isotopic record from our core ends at 12 ka when C. pachydermus disappears from the benthic assemblage (Reguera, 2004; Sierro et al., 2005), likely replaced by species inhabiting poorly oxygenated environments (Caralp, 1988; Reguera, 2004). Reduced deepwater ventilation conditions for this time interval (12–9 ka) are also suggested by the preservation of an Organic Rich Layer in the Alboran Sea (Cacho et al., 2002). In parallel, TIb sedimentation rates were minimal (Fig. 6.3c) because of the combined effect of the reduction in the input of terrigenous particles forced by the inshore migration of the coastline caused by the postglacial sea level rise, and to a lowered transport of particles into weakened deepwater currents.

The weakening of the deep overturning cell could also result (or be amplified) from more humid conditions in the western Mediterranean region during the time of maximum summer insolation (Fig. 6.5d) as suggested from maximum values of the K/Al record (Fig. 6.5e) and supported by other studies (Harrison and Digerfeldt, 1993; González-Sampériz et al., 2006). A more pronounced stratification in the upper water column favored by an enhanced freshwater input due to increased precipitation during summer insolation maxima, and higher atmospheric stability associated with the retreat of the Northern Hemisphere ice sheet, would have lead to the slowdown of the deepwater overturning cell in the Gulf of Lion and to a reduction of contour current activity in the Minorca sediment drift. After 10.5 ka both grain size and geochemical records show a steady increasing trend (phase II in Figs. 6.5 and 6.6), which points to the recovery of the deepwater overturning cell in the Gulf of Lion coincident with the decreasing trend in the summer insolation at 40ºN (Fig. 6.4d).

The relative stabilization of grain size parameters (Figs. 6.4e and 6.4f) and the Si/Al ratio around 7 ka (phase III in Fig. 6.6e) is synchronous with the end of the postglacial sea level rise (Fleming et al., 1998) and suggests the reestablishment of deepwater circulation and a stable supply of fluvial material. Such a synchronicity illustrates how significant was the sea level rise control on the western Mediterranean thermohaline circulation and, consequently, on the outbuilding of the Minorca sediment drift. The essentially stable conditions found for the mid-Holocene (7–4 ka) in the Minorca deep sea site contrast with marked changes reported in many locations worldwide (Steig, 1999) and, in particular, in the Mediterranean bor-

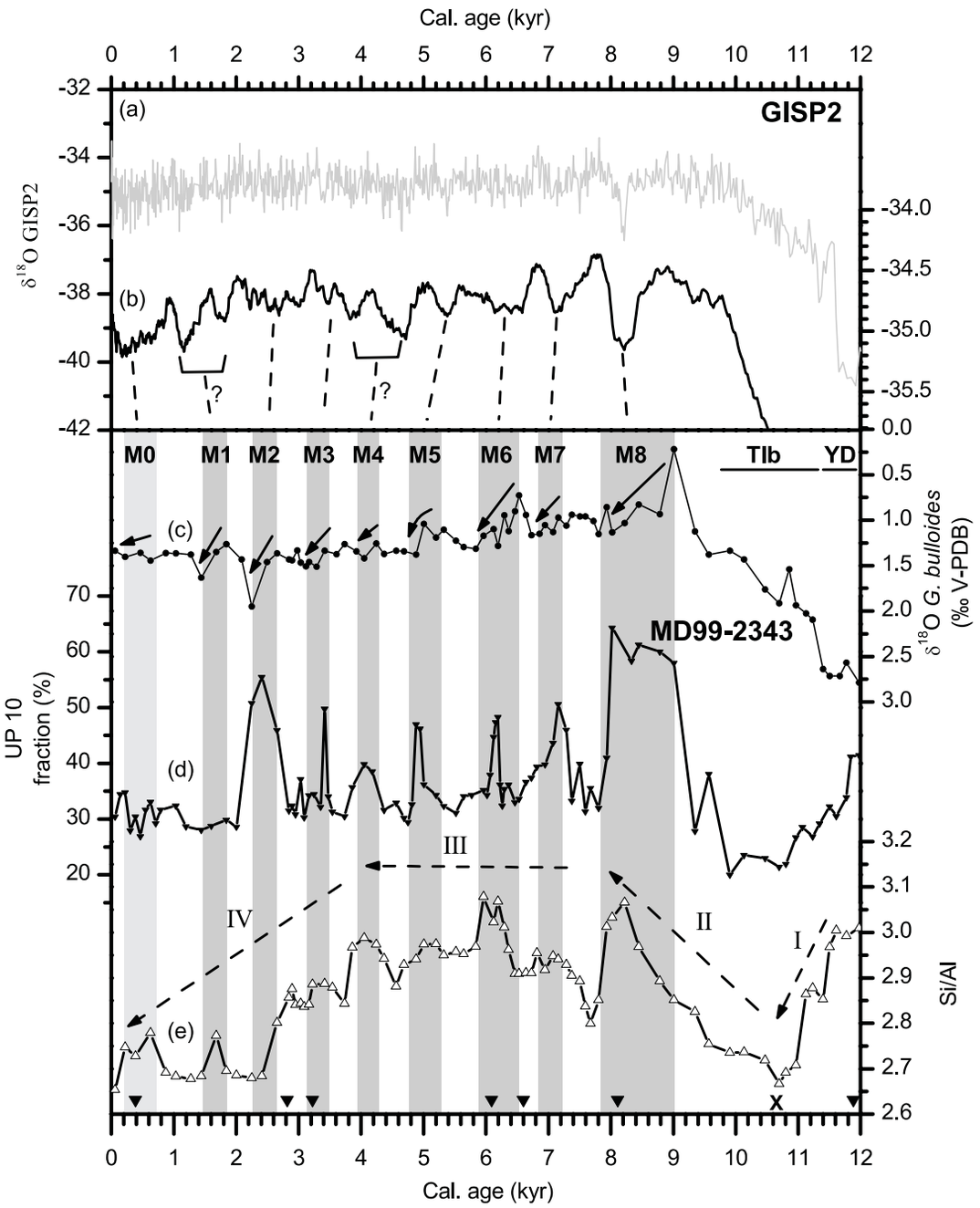

Figure 6.6. a) Continuous and **b)** 300-year running mean records of the oxygen isotopic profile from the GISP2 ice core (Grootes et al., 1993; Meese et al., 1997). **c)** *G. bulloides* oxygen isotopic record from core MD99-2343 for the last 12 kyr. **d)** UP10 fraction (>10 μm) record for the noncarbonate fraction. **e)** Si/Al profile with an indication of the four phases identified (I–IV). The arrows and the grey bars represent the nine Minorca abrupt events M8 to M0. Dashed lines represent an attempt to correlate the Minorca events with the oxygen isotopic record from the GISP2 ice core. The ^{14}C AMS dates (inverted triangles) and tie point (cross) are also shown.

derlands (COHMAP, 1988; Cheddadi et al., 1997; Prentice et al., 1998; Magny et al., 2002) and the North African region (Vernet and Faure, 2000) associated with the end of the African Humid Period (deMenocal et al., 2000a). This mid-Holocene climate variability is attributed to the reduction of seasonal insolation differences after 5.5 ka, which lead to an abrupt transition from humid to arid conditions in North Africa and in the western Mediterranean region.

This well-known mid-Holocene variability does not seem to influence our proxies until 4 ka when an evident decrease in the silt/clay ratio and the Si/Al points to a slowdown of the deepwater overturning cell and to a reduction of fluvial inputs due to drier conditions (Fig. 6.4f and phase IV in Fig. 6.6e). These drier conditions would be also consistent with the $\delta^{18}O$ stabilization at high values during the late Holocene. A southward displacement of the ITCZ and the subsequent decrease in the atmospheric pressure gradient due to reduced seasonal insolation differences likely favored the establishment of drier conditions (McDermott et al., 1999; Jalut et al., 2000). Accordingly, the lessening in the activity of the northwesterlies would account for the reduction of deepwater circulation during the late Holocene. Our results stress the high sensitivity of the western Mediterranean thermohaline circulation to both the atmospheric (i.e., northwesterlies variability that induced changes in the deepwater overturning in the Gulf of Lion) and the hydrologic systems (i.e., orbitally induced precipitation variability and meltwater pulses).

6.6.3. Holocene Abrupt Events

The nine Holocene $\delta^{18}O$ enrichment events had an average duration of 500 years and an observed periodicity close to 1000 years (Table 6.2 and Fig. 6.6). Most of the Holocene increases in the oxygen isotopic record parallel increases in the UP10 fraction and the Si/Al ratio (Fig. 6.6), therefore suggesting that relatively cold surface conditions coexisted with more energetic deepwater conditions. An intensification of the northwesterly winds in the western Mediterranean would account for the conditions described during the Holocene Minorca events, similarly to the mechanism proposed for the glacial Dansgaard-Oeschger variability (Cacho et al., 2000; Sierro et al., 2005). These cold and dry winds enhanced the deepwater overturning in the Gulf of Lion by cooling of the surface waters and, consequently, they steered the activity of bottom currents on the Minorca rise. Such vigorous currents were able to transport coarser particles to the Minorca rise as shown by the accumulation of quartz grains and mica packets coarser than 63 μm. This resulted in the increase of the UP10 fraction (Fig. 6.6d) and the apparition of bimodal samples (Fig. 6.4c). In parallel, higher values in the silt/clay ratio are interpreted as resulting from the winnowing effect of the finest particles (Fig. 6.4f).

While events M8 to M3 are consistently represented in both grain size and geochemical proxies, M0, M1 and M2 are not always well represented. For instance, M2 is not recorded by the Si/Al ratio while it forms one of the larger peaks in the UP10 fraction and, in contrast, M1 and M0 do not show a clear expression in the UP10 ratio but they present significant increases in the Si/Al record (Fig. 6.6). Interestingly, this distinctive sensitivity between the different proxies occurs during the phase IV, late Holocene, related to the establishment of drier conditions due to reduced seasonal insolation differences (section 7.6.2). Overall, re-

Event	Central Age, ka	Time Since Previous Event, ka	Age Interval, ka	Duration, ka	Cold Events in the North Atlantic and Mediterranean Regions				Global Compilation of Events
					SST Alboran	Lakes and Rivers Mediterranean	IRD North Atlantic	Salt and Dust Greenland	
M0	0.5	1.1	0.8–0.2	0.6	-	0.8	-	0.6-0	0.6-0.15
M1	1.6	0.9	1.8–1.4	0.4	1.4	2	1.4	-	1.2-1
M2	2.5	0.7	2.6–2.3	0.3	-	-	-	3.1-2.4	-
M3	3.2	0.9	3.4–3.1	0.3	-	3	2.4		3.5-2.5
M4	4.1	0.9	4.2–4	0.2	-	4	4.2	-	4.2-3.8
M5	5	1.2	6.5–5.8	0.6	5.4	-	-	6.1-5	6-5
M6	6.2	0.9	7.4–6.9	0.7	-	-	5.9	-	-
M7	7.2	1.5	9–7.8	0.5	-	7	-	-	-
M8	8.4	-		1.2	8.24	9	8.1	8.8-7.8	9-8

Table 6.2. Timing of Holocene abrupt climate events. Timings of the Holocene Minorca abrupt events found in core MD99-2343 and tentative correlation with abrupt events recorded from SST in the Alboran Sea (Cacho et al., 2001), in lakes and rivers from the Mediterranean region (Magny et al., 2002), in ice-rafted detritus (IRD) from the North Atlantic region (Bond et al., 1997), in salt and dust from Greenland ice (O'Brien et al., 1995), and the compilation of Holocene rapid climate change events from (Mayewski et al., 2004).

duced deep overturning is interpreted to occur because of the weakening of northwesterlies and more stable conditions. Furthermore, the expression of the Minorca events in the studied proxies seems to become weaker through the Holocene in parallel to the relative stabilization of the oxygen isotopic signal. These different climatic boundary conditions may have determined a lower sensitivity of the system to millennial-centennial-scale climatic variability toward late Holocene and, consequently, provided an ambiguous signature in the studied records.

The fact that Holocene cooling events have been reported elsewhere all around the globe (Mayewski et al., 2004) demonstrates their global extent and the lack of stability of the Holocene climate. There are, however, disagreements about the precise timing, the character and the impact of these Holocene abrupt events. Some of the cooling events recorded in the Atlantic and Mediterranean regions are summarized and tentatively correlated to our Minorca cold events M0 to M8 for the last 9 kyr (Table 6.2). Furthermore, a correlation attempt between the Minorca events and the 300-year running mean of the GISP2 isotopic curve (Fig. 6.6b) results in fairly good agreement, even considering the uncertainties of our age model. This supports the hypothesis of a highly efficient climatic coupling between the North Atlantic and the western Mediterranean region during the last 10 kyr.

The UP10 fraction of our core MD99-2343 displays a periodic oscillation close to 900 years in between 9 and 2 ka (Fig. 6.6e and Table 6.2), which is in agreement with those obtained from the GISP2 ice core oxygen isotopic record (Schulz and Paul, 2002), from a Saharan dust record (Kuhlemann et al., 2004), and from varved sediments in California (Nederbragt and Thurow, 2005). Several hypotheses aim at explaining the periodicity of about 900 years.

Though it may be triggered by insolation changes or result from internal feed back mechanisms (Schulz and Paul, 2002), the recorded climatic oscillations are better linked to the temperature signal from the North Atlantic climate system, in agreement with other records from the Northern Hemisphere (Cacho et al., 2001; Kuhlemann et al., 2004).

The most pronounced Holocene abrupt event, M8, occurred at 9–7.8 ka, therefore embracing the well-known 8.2 ka cold North Atlantic event (Mayewski et al., 2004; Alley and Agustsdottir, 2005; Rohling and Pälike, 2005). The intensification of the atmospheric circulation during M8 led to good ventilation conditions in the Western Mediterranean Basin thus stopping the formation of the ORL in the Alboran Sea (Cacho et al., 2002), synchronously with the middle interruption of sapropel S1 in the Eastern Mediterranean Basin (Rohling et al., 1997; Mercone et al., 2000). We propose that the atmospheric teleconnection between high latitudes and the Mediterranean region through the westerly winds system was the main control over the western Mediterranean thermohaline circulation through the Holocene. This atmospheric forcing of the climate variability for the last 10 kyr is quite similar to the present pattern of the North Atlantic Oscillation (NAO) that exerts a first-order control at decadal scales (Rodó et al., 1997). Positive NAO years are associated with Iberian dryness and cold temperatures in Greenland, and more persistent and stronger winter storms crossing the Atlantic Ocean (Hurrell, 1995). Consequently, the Minorca abrupt events could be associated with periods of persistent positive NAO index, which would strengthen the northwesterlies over the northwestern Mediterranean Basin and hence reinforce deepwater overturning. Although we do not exclude a pervasive solar influence or instabilities inherent to the North Atlantic thermohaline circulation (Bond et al., 2001; Schulz and Paul, 2002) as main precursors of the Holocene climate oscillations recorded in the core MD99-2343, we suggest that the rapid transmission of these changes from high latitudes to the Mediterranean region was mainly driven by the northwesterly wind system variability modulated by a NAO-like mechanism. A similar atmospheric linkage mechanism, though acting at a millennial scale, was proposed to explain the Dansgaard-Oeschger variability in the deepwater ventilation and Saharan dust input during the last glacial period in the Alboran Sea (Cacho et al., 2002; Moreno et al., 2002; Sánchez Goñi et al., 2002).

6.7. Conclusions

The sedimentary record from core MD99-2343 recovered from a deepwater contourite drift reveals the effects of Holocene climate variability over the thermohaline circulation in the Western Mediterranean Basin during the last 12 kyr. Geochemical proxies associated with terrigenous inputs like Si/Al, Ti/Al and K/Al display a decreasing trend through the Holocene that parallels the summer insolation curve at 40ºN showing the marked influence of the precipitation pattern over the region. Four different phases have been identified in the Si/Al and Ti/Al ratios from the last 12 kyr. The first from 12 to 10.5 ka shows a slowdown of dee-

pwater circulation due to the combined effect of the increasing sea level and the relatively humid conditions installed on land which both favored the stratification of water masses. The second phase (10.5–7 ka) is associated with the recovery of deepwater circulation until the end of the postglacial sea level rise at 7 ka. The third phase (7–4 ka) corresponds to a plateau with high values of the terrigenous proxies translating the good functioning of deepwater circulation during a progressive orbitally driven change toward dryer conditions in the western Mediterranean borderlands. Finally, the fourth phase (4–0 ka) indicates a progressive decrease of the terrigenous contributions because of reduced fluvial inputs during drier conditions induced by lower seasonal insolation differences, also modulated by the thermohaline circulation weakening because of more stable atmospheric conditions.

Superimposed on this general Holocene pattern, marked oscillations have been noticed and related to abrupt climate changes. The new grain size parameter presented in this work that represents the fraction coarser than 10 μm (UP10) has been tested as a convenient proxy for paleocurrent intensity in the study area for Holocene sediments. The UP10 record presents a 900-year cycle oscillation, which is consistent with the geochemical record of terrigenous input between 9 and 2 ka and the surface cooling events uncovered by the oxygen isotopic record. Such periodicity fits with temperature oscillations from the Holocene $\delta^{18}O$ record in Greenland and points to the pressure gradient system as a direct teleconnection mechanism for climate variability transfer from the North Atlantic to the Mediterranean region. The centennial to millennial-scale Holocene oscillations observed in our records reveal a coupled atmospheric/oceanographic forcing equivalent to the present-day NAO and sustains the hypothesis of a rapid fitting with Mediterranean climate conditions. Furthermore, our results demonstrate the high sensitivity of deepwater overturning in the Gulf of Lion to the transfer of climate oscillations from high latitudes to midlatitudes.

Acknowledgments

Funding by the European Commission Fifth and Sixth Framework Programmes to projects ADIOS (EVK3-2000-00035), PROMESS 1 (EVR1-CT-2002-40024), EUROSTRATAFORM (EVK3-2002-00079), and HERMES (GOCE-CT-2005-511234-1) supported the research effort behind this paper. The Spanish-funded BTE2002-04670 and REN2003-08642-C02-02 projects are equally acknowledged. We are especially grateful to the *Marion Dufresne* and the IMAGES programme that enabled the collection of cores MD99-2343 and MD95-2043. GRC Geociències Marines is recognized within the *Generalitat de Catalunya* excellence research groups program (reference 2005SGR 00152). We thank M. Guart (Departament d'Estratigrafia, Paleontologia I Geociències Marines, University of Barcelona) and E. Seguí (Serveis Cientifico-Tècnics, University of Barcelona) for their help with the laboratory work and G. Lastras and D. Amblas for their help with the artwork. The Editor G. Dickens, J. B. Stuut, and two anonymous reviewers are greatly acknowledged for their

positive comments on an earlier version of the manuscript. COMER Foundation and I3P postdoctoral programme (CSIC) are also acknowledged for their support to I. Cacho and A. Moreno, respectively. J. Frigola benefited from a fellowship of the University of Barcelona.

CAPÍTOL III. DISCUSSIÓ

Aquesta Tesi està centrada en la reconstrucció del clima del passat a la conca occidental del Mediterrani a través de l'estudi de les variacions en l'aportació de materials terrígens. Aquestes variacions proporcionen informació sobre les condicions d'erosió i transport des dels continents, influïdes pel balanç entre les condicions d'aridesa i humitat, el règim de precipitacions i el règim de vents. També aporten informació sobre els processos d'erosió, transport i acumulació de les partícules sedimentàries un cop incorporades al medi marí, il·lustrant per tant canvis en les condicions de sedimentació per modificacions ambientals locals o regionals (McCave et al., 1995a; Wehausen and Brumsack, 1998; Moreno et al., 2002; Martínez-Ruiz et al., 2003; Weldeab et al., 2003; Weltje and Prins, 2003; Kuhlemann et al., 2004; Jimenez-Espejo et al., 2007 i 2008). El coneixement de les condicions del medi és imprescindible en tota circumstància, i també de les àrees font i dels processos capaços d'afectar a escala local, regional o global la deposició final de les partícules.

En aquesta Tesi ens hem centrat en dos registres prou propers, situats al Mediterrani nordoccidental, amb la finalitat de determinar el impacte dels canvis climàtics dels darrers 500 ka en la sedimentació marina i, a través d'ell, escatir els mecanismes de transferència del senyal climàtic entre latituds altes i mitjanes. Els indicadors emprats, la composició elemental i la granulometria del sediment, han estat els mateixos en tots dos registres, però les marcades diferències pel que fa al context de cadascun d'ells, un provinent del talús continental superior a tan sols 300 m de profunditat i l'altre del fons de conca a 2400 m de profunditat, han determinat que els impactes dels canvis climàtics hi hagin quedat reflectits per processos locals i regionals i escales de temps ben diferents. La discussió dels resultats se centra, doncs, en els dos processos claus que han afectat cadascun dels registres, tot dos relacionats amb les variacions climàtiques del passat: les fluctuacions del nivell del mar i els canvis en la circulació profunda del Mediterrani occidental.

7. Reconstrucció de les oscil·lacions del nivell del mar al marge continental del Golf de Lleó

7.1. Impacte dels canvis del nivell del mar a escala glacial/interglacial

La influència dels mantells de gel polars en el clima es fa notar en molts sub-components del sistema climàtic, com ara en les temperatures de les aigües superficials, la circulació oceànica, el balanç hídric als continents, la vegetació i l'albedo, entre d'altres, els quals, a més, poden generar mecanismes de retroalimentació en el sistema climàtic que poden contribuir a sincronitzar el senyal climàtic global (Clark et al., 1999). Els canvis en el volum de gel acumulat en els mantells polars entre els períodes glacials i els interglacials provocaren canvis globals del nivell del mar d'uns 120 m de magnitud (Imbrie et al., 1992; Miller et al., 2005; Siddall et al., 2006a). El fet que els mantells polars siguin un dels pocs components del sistema climàtic que oscil·la en les periodicitats definides a la teoria orbital (100 ka, 41

ka i 23 ka) dugué a pensar que podien ser els responsables de la transmissió i l'amplificació dels canvis climàtics d'escala orbital des de les latituds altes fins a qualsevol lloc del planeta mitjançant el sistema climàtic (Imbrie et al., 1993).

Les oscil·lacions globals del nivell del mar afectaren decisivament la construcció dels marges continentals, doncs la línea de costa s'anà desplaçant sincrònicament. A l'amplíssima plataforma del Golf de Lleó, aitals oscil·lacions del nivell del mar induïren, molt probablement, canvis prou sobtats de les condicions ambientals (Berné et al., 2004a). L'elevada sensibilitat als canvis abruptes fa que el marge del Golf de Lleó sigui idoni per a intentar reconstruir els canvis passats del nivell del mar tant a l'escala dels cicles glacials com a escala mil·lenària. Actualment, hom pot considerar notablement elevat el grau de coneixement del funcionament del marge del Golf de Lleó des de l'escala de centenars de milers d'anys (10^5) fins l'escala interanual, mercès a un bon nombre de treballs basats en la cartografia d'alta resolució del fons marí, perfils sísmics tant d'alta resolució com d'alta penetració, testimonis del recobriment sedimentari superficial i algun sondeig, i mesura dels fluxos de partícules sedimentàries (Tesson et al., 1990, 1993 i 2000; Berné et al., 2004a; Rabineau et al., 2005; Jouet, 2007; Durrieu de Madron et al., 2008). Tot i que en algun d'aquests treballs hom havia descrit el Golf de Lleó com un marge passiu format per l'acumulació forçada d'unitats regressives progradants (RPU, de l'anglès *Regressive Progradational Units*), la ciclicitat d'aquestes unitats no s'havia pogut establir per la manca de testimonis sedimentaris continus que incloguessin una part prou considerable del registre quaternari. El projecte europeu PROMESS1 fou l'oportunitat esperada per a recuperar un testimoni continu de 300 m de longitud al talús superior, a 298 m de profunditat, el testimoni PRGL1-4, el qual comprèn les quatre RPUs més recents del registre quaternari del Golf de Lleó.

El registre granulomètric de la relació llim/argila (en anglès *silt/clay ratio*) mostra cinc unitats granodecreixents amb increments sobtats de la mida de gra al final de cada unitat. La comparació del registre de la relació llim/argila amb un perfil sísmic d'alta resolució (Fig. 4.2) permet correlacionar aquestes unitats amb altres cinc unitats sismostratigràfiques en que els increments sobtats en la relació llim/argila corresponen a l'expressió física dels principals reflectors associats als límits de seqüència. Aquesta correlació, juntament amb la corba de $\delta^{18}O$ en foraminífers planctònics (Sierro et al., 2009), ens permeteren establir la cronostratigrafia del testimoni PRGL1-4, que abasta els darrers 530 ka. A més, es confirma que els canvis de nivell del mar associats als cicles glacials/interglacials, de 100 ka, són els responsables de la formació d'aquestes unitats sedimentaries, fet que s'havia apuntat en estudis previs (Rabineau, 2001). A partir d'ací poguérem reinterpretar la seqüència sismostratigràfica del talús superior, prèviament feta només a partir de perfils sísmics de reflexió (Rabineau, 2001). Dues de les unitats descrites inicialment, S3 i S2, foren subdividides en S3a i S3b, i S2a i S2b, respectivament. Cadascuna d'aquestes RPUs és el resultat de la baixada del nivell del mar durant un cicle interglacial/glacial complet, on el sobtat increment en la relació llim/

argila al final de la seqüència és conseqüència de la pujada ràpida del nivell mar associada a la desglaciació i al fort impacte que tingué en l'ambient sedimentari, tal i com s'explica més avall.

Les taxes de sedimentació enregistrades en el testimoni PRGL1-4 mostren variacions dràstiques entre els períodes glacials i els interglacials al llarg dels darrers 500 ka (Fig. 4.3g). Aquest fet ha estat atribuït a la migració cap a mar i terra endins dels sistemes deltaics empesos per les oscil·lacions del nivell del mar, potenciada per l'amplada, fins 70 km, i les baixes pendents de la plataforma del Golf de Lleó. Al inici de cada RPU, amb el nivell del mar alt, la plataforma del Golf de Lleó era inundada i els prismes deltaics restaven atrapats a la plataforma, lluny del vorell i del talús superior, com succeeix en l'actual període interglacial (Berné et al., 2004a). Aquesta situació causà que les taxes de sedimentació en el lloc del testimoni PRGL1-4 fossin molt baixes durant els interglacials (10-25 cm ka^{-1}), fet que determinà la formació de capes condensades (CL, de l'anglès condensed layer), riques en arenes de foraminífers. Els increments sobtats de sorra fina total (en anglès total fine sand) retraten la formació d'aquestes CLs (Fig. 4.3e). Seguidament, la baixada progressiva del nivell del mar en el següent període glacial anà exposant la plataforma i apropant la línea de costa i, per tant, les desembocadures fluvials al vorell i al talús superior, la qual cosa provocà un increment progressiu de les taxes de sedimentació al talús superior i, en conseqüència, al lloc del testimoni PRGL1-4 (1.5-2.5 m ka^{-1}) (Fig. 4.3). Unes taxes de sedimentació tant diferenciades entre els períodes glacials i els interglacials afecten directament la resolució temporal del registre PRGL1-4. A cada pujada del nivell del mar i a la corresponent migració dels sistemes deltaics terra endins, li correspon una forta davallada de les taxes de sedimentació al talús superior una amb la minva subseqüent de resolució temporal. En els períodes glacials, quan el nivell del mar era més baix i els sistemes deltaics se situaven en el mateix vorell de la plataforma continental, l'acumulació ràpida de paquets potents proporcionà una gran resolució temporal.

Una interpretació poc curosa del registre de llim/argila del testimoni PRGL1-4 podria semblar contradictòria, doncs seria lògic esperar que la mida de gra fos més gran quan la font dels sediments, en principi fluvial, fos més a prop de la posició del testimoni, és dir, durant els períodes glacials, i viceversa. L'abundància de material més fi en els períodes glacials pot ésser explicada per les voluminoses aportacions d'argiles procedents dels sistemes deltaics, molt propers durant aquests períodes, tal i com ho certifiquen el increment en contingut de Ca (majoritàriament d'origen fluvial) i les elevades taxes de sedimentació mesurades (Fig. 4.3). El registre PRGL1-4 també mostra que els sediments més grollers s'acumularen durant els períodes interglacials, quan la línea de costa i els sistemes deltaics eren molt allunyats del talús superior. Aquest increment de grollers no només es devia a la acumulació de capes riques en foraminífers sinó també a una major aportació de partícules terrígenes, com ara grans de quars. La interpretació d'aquestes observacions requeria identificar el procés o pro-

cessos capaços de transportar partícules grolleres fins al talús superior i que, a més, actués en sintonia amb les oscil·lacions del nivell del mar. Els resultats d'estudis in situ de processos hidrosedimentaris actuals d'alt nivell energètic (cf. Apt. 2.4), suggerien que l'enfonsament d'aigües denses de plataforma (DSWC, de l'anglès *Dense Shelf Water Cascading*) i les llevantades reunien tots els requisits per a ésser els processos que estàvem cercant. Tots dos degueren jugar un paper crucial en els períodes en que la plataforma estava inundada, és a dir, en el períodes interglacials, exactament com succeeix en els nostres dies (Bassetti et al., 2006; Canals et al., 2006; Dufois et al., 2008). La inundació de la plataforma durant la pujada sobtada del nivell del mar donava la possibilitat de la reactivació dels mecanismes erosius i de transport associat a ambdós processos a la vegada que provocava l'allunyament dels sistemes deltaics i reduïa l'aportació de material fi. En canvi, quan la plataforma estava exposada, en els períodes glacials, aquests processos o no podien existir (cas de les DSWC, que necessiten una extensa plataforma inundada damunt la qual es refredin les aigües) o els seus efectes eren menors (cas de les llevantades, al haver-hi una transició ràpida des de la línia de costa a fondàries significatives), i l'aportació de sediment depenia essencialment de la proximitat de les goles fluvials. Per tant, l'explicació del registre sedimentològic del testimoni PRGL1-4 a escala glacial/interglacial requereix que la construcció del marge del Golf de Lleó hagués estat controlada per un model de sedimentació combinat, amb migració dels sistemes fluvials i l'activació i desactivació de processos erosius i de transport relacionats amb la inundació i l'emersió alternants de la plataforma continental, tot plegat controlat per les oscil·lacions globals del nivell del mar.

Entenem que és per aquest motiu que el registre de llim/argila del Golf de Lleó mostra una elevada ressemblança amb registres globals del nivell del mar (Lisiecki and Raymo, 2005; Rohling et al., 2009b) (Fig. 4.3), fet que corrobora el caràcter determinant dels canvis en el volum de gel dels mantells polars a escala orbital sobre la construcció del marge continental del Golf de Lleó. L'estudi de seqüències sedimentaries en marges continentals amb taxes de sedimentació elevades i una bona cronostratigrafia és essencial per a un millor coneixement de les oscil·lacions del nivell del mar i les seves implicacions en el marc del sistema climàtic global.

7.2. Canvis del nivell del mar d'escala mil·lenària durant el MIS 3

Un dels trets més notables del registre del talús superior del Golf de Lleó són les elevades taxes de sedimentació dels períodes glacials. Aquest fet ha permès de dur a terme un estudi de molt alta resolució durant el darrer període glacial, concretament el MIS 3, amb taxes de sedimentació de 0.2-2 m ka^{-1}. La cronologia d'aquest període és molt ben establerta mercès a la sincronització de la corba de $\delta^{18}O$ del testimoni PRGL1-4 amb la del testimoni de gel de Grenlàndia NGRIP08, en el qual s'observen les oscil·lacions climàtiques associades als

cicles de DO (Figs. 4.5a i 4.5b). Aquesta sincronia demostra la teleconnexió climàtica entre latituds altes i el Mediterrani nordoccidental així com la seva rapidesa.

Assumint el model de sedimentació combinada exposat a l'apartat anterior (cf. Aptat. 7.1) i basant-nos també en l'elevada resolució temporal del darrer període glacial, la corba de variació de la mida de gra del testimoni PRGL1-4 pot donar informació clau sobre els canvis de nivell del mar associats a la variabilitat climàtica d'escala mil·lenària durant el MIS 3 (cf. Apt. 1.3). De fet, d'aquest model de sedimentació combinada al Golf de Lleó se'n desprèn que els ascensos del nivell del mar provoquen una major erosió i transport de grollers cap al talús superior, és a dir, un augment en la mida de gra al lloc del testimoni PRGL1-4.

La comparació de la corba de la relació llim/argila i diverses reconstruccions del nivell del mar durant el MIS 3 mostra patrons molts similars (Fig. 4.5). Per una banda, el registre granulomètric és més groller a la primera fase del MIS 3, la qual cosa significa que el nivell del mar era més alt que no pas cap al final del MIS 3. Aquesta circumstància també ha estat descrita en un recull de reconstruccions del nivell del mar, i correspon a una diferència de 20 m entre el inici i el final del MIS 3 (Siddall et al., 2008). Per altra banda, la corba de llim/argila mostra un seguit d'increments d'escala mil·lenària que poden ésser correlacionats amb pujades sobtades del nivell del mar, tal i com ho mostren les reconstruccions (S1-S4, Fig. 4.5) (Shackleton, 2000; Siddall et al., 2003; Arz et al., 2007). Tot i que aquests resultats confirmen la sensibilitat del registre granulomètric als canvis del nivell del mar durant el MIS 3, hi ha certes discrepàncies amb les reconstruccions pel que fa a la cronologia d'aquestes pujades relatives. De fet, tal i com es comentava a l'apartat introductori (cf. Aptat. 1.3), algunes reconstruccions mostren que les pujades del nivell del mar durant el MIS 3 foren sincròniques amb els períodes càlids de l'Antàrtida, al seu torn sincrònics amb els períodes més freds a l'Atlàntic Nord (Shackleton, 2000; Siddall et al., 2003). Altres reconstruccions, però, indicarien que aquestes pujades relatives del nivell del mar ocorregueren durant els períodes més càlids a l'Atlàntic Nord, com ara els GIS16, 14, 12 i 8 (Arz et al., 2007; Sierro et al., 2009).

Potser allò més valuós del registre granulomètric del testimoni PRGL1-4 és que, independentment del model cronològic emprat, mostra increments d'escala mil·lenària que són sincrònics amb valors baixos del registre de $\delta^{18}O$, és a dir, que el nivell del mar era relativament alt durant tots els períodes càlids GIS (Fig. 4.5b i 4.5c). Es tracta de la primera evidència de que durant el MIS 3 el nivell del mar oscil·là acoblat amb els canvis climàtics abruptes d'escala mil·lenària dels cicles de DO. Aquests resultats podrien portar-nos a inferir que les pujades del nivell del mar es produïren durant els períodes càlids GIS del MIS 3, però limitacions diverses en el mètode no ens permeten saber ni el moment exacte en el que es va inicià la pujada del nivell del mar ni tampoc la seva magnitud. El model d'edat emprat pateix l'efecte de la forta baixada de les taxes de sedimentació provocada per les pròpies pujades del nivell

del mar, i tampoc hi ha una relació directa entre els canvis en la granulometria i la magnitud de les oscil·lacions del nivell del mar. Les pujades del nivell del mar del MIS 3 podrien haver estat desencadenades per les desestabilitzacions i la fosa dels icebergs en cadascun dels períodes freds dels GS, tant si eren HE com si no, i es podrien haver iniciat durant les fases d'escalfament a l'Atlàntic Nord o durant les fases d'escalfament a l'Antàrtida. Per aquesta mateixa raó, el fet que el registre granulomètric del testimoni PRGL1-4 sigui sincrònic amb els períodes càlids de l'Atlàntic Nord tampoc és suficient per afirmar quin dels dos mantells polars contribuí en major mesura a les pujades del nivell del mar del MIS 3.

D'acord amb el registre estudiat, l'existència d'oscil·lacions del nivell del mar d'escala mil·lenària acoblats als cicles de DO durant el MIS 3 fa pensar que la influència de la dinàmica dels mantells de gel pot haver estat clau en el desenvolupament dels canvis climàtics abruptes tant en aquest com en altres intervals de temps.

8. Variabilitat de la circulació profunda a la conca occidental del Mediterrani

8.1. Canvis abruptes en la formació d'aigües fondes durant el darrer període glacial

Com s'assenyalava anteriorment (cf. Aptat. 1.2.2), durant el darrer període glacial el Mediterrani occidental ha reaccionat molt ràpidament als canvis climàtics observats a l'Atlàntic Nord, concretament als cicles de DO i als HE. Aquestes oscil·lacions afectaren també la hidrologia de la conca, amb el reforçament de la circulació termohalina en els períodes freds dels GS i els HE (Cacho et al., 2000), relacionat probablement amb una intensificació del sistema de vents del nord i del nord-oest (westerlies) (Moreno et al., 2002) i amb condicions més àrides que afavoriren una menor estratificació de les aigües (Combourieu Nebout et al., 2002; Sánchez Goñi et al., 2002). En contrast, en els períodes càlids dels GIS, amb vents més suaus i condiciones més humides, la circulació termohalina es debilità (Cacho et al., 2000). Segons aquest model, la circulació termohalina del Mediterrani occidental funcionà de manera oposada a la MOC durant el MIS 3. Posteriorment, hom s'adonà que aquest model era un xic simplista, doncs durant els HE l'entrada per l'estret de Gibraltar d'aigües menys salines procedents de la fusió d'icebergs a l'Atlàntic Nord, tingué un fort efecte en la columna d'aigua (Sierro et al., 2005).

El testimoni MD99-2343, recuperat en el llom contornític de Menorca, a escassa distància dels llocs de formació d'Aigua Fonda del Mediterrani Occidental (WMDW), reuneix característiques idònies, en especial taxes de sedimentació elevades i una excel·lent cronologia, per a dur a terme un estudi d'alta resolució dels corrents de fons associats amb la circulació termohalina del Mediterrani occidental en els darrers 50 ka.

A escala orbital, els registres de K/Al i de la relació llim/argila mostren certa modulació orbital deguda als canvis en la insolació estival, la qual cosa apunta a un control climàtic de la precessió que influeix en l'aportació de terrígens al fons de conca, tal i com s'havia observat prèviament a la Conca Oriental del Mediterrani (Wehausen i Brumsack, 2000). La relació K/Al és un bon indicador de la precipitació en el lloc d'estudi, i la seva modulació orbital indica la importància de la precipitació en l'aportació de terrígens (Fig. 5.3). La modulació orbital sobre la relació llim/argila sembla indicar que la circulació profunda del Mediterrani occidental va sofrir reduccions significatives per causa d'oscil·lacions en la insolació, com s'ha constatat, per exemple, als voltants de 28 ka. Tot i aquesta modulació orbital, la davallada en la relació llim/argila durant el moment de màxima insolació estival associada a la desglaciació assenyala una forta reducció de la circulació termohalina al Mediterrani occidental causada, al seu torn, per la corresponent pujada del nivell del mar (Fig. 5.4).

Les característiques de la circulació profunda a escala mil·lenària durant el MIS 3 han estat avaluades a partir de dos grups de dades. Per una banda, els registres de Si/Al, Ti/Al i de llim/argila, relacionats amb canvis en la intensitat dels corrents de fons. I per altra banda, els registres d'isòtops de l'oxigen i del carboni en foraminífers bentònics, indicadors de les propietats de la massa d'aigua fonda i de les condicions de ventilació al fons de la conca, respectivament (Sierro et al., 2005). Tots dos grups de dades mostren una forta variabilitat mil·lenària relacionada amb les oscil·lacions climàtiques de DO. Tot i tractar-se de propietats ben diferents, hom podria esperar que el seu comportament fos sincrònic, en resposta al model bàsic de circulació. Però el més sorprenent és que aquests dos grups d'indicadors mostren un desfasament temporal (Fig. 5.5). Els registres de $\delta^{18}O$ y de $\delta^{13}C$ en foraminífers bentònics del testimoni MD99-2343 presenten un patró similar als del testimoni del Mar d'Alboran MD95-2043, fet que confirma el model de circulació proposat prèviament, amb aigües profundes (WMDW) ben ventilades i més salines i/o fredes durant els GS en comparació amb els GIS (Cacho et al., 2000). Malgrat això, els indicadors de paleocorrents, Si/Al, Ti/Al i la relació llim/argila, mostren els valors més elevats, corresponents als corrents més forts, just després dels períodes càlids dels GIS, és a dir, durant la transició de cada GIS/GS, amb la recuperació de condicions de més ventilació (Fig. 5.5 article) i el inici de la baixada de temperatures superficials.

Aquests resultats il·lustren l'elevada sensibilitat del sistema contornític de Menorca als canvis en la posició vertical del nucli de la WMDW, la qual depèn de la seva densitat. Donada la profunditat a que es troba el llom contornític, entre 2100 i 2700 m, el nucli de la WMDW només devia afectar ocasionalment el indret del testimoni MD99-2343, a 2400 m. L'anàlisi detallada dels resultats durant un cicle de DO sencer permet diferenciar tres modes de variabilitat en la circulació profunda del Mediterrani occidental (Fig. 5.6 article). El primer mode, de circulació dèbil, és el que ocorre durant les condicions càlides dels GIS, períodes en que s'observa una molt baixa ventilació del fons i una massa d'aigua fonda relativament lleuge-

ra, amb la circulació més activa del nucli de la WMDW situada probablement pel damunt del sistema contornític, raó per la qual s'obtindrien els valor més baixos en els indicadors físics (eg. registre llim/argila). El segon mode, de circulació moderada, correspon a les transicions entre GIS i GS, quan el inici del refredament superficial probablement ajudaria a disminuir el gradient de densitat a la columna d'aigua, afavorint així la barreja i l'enfonsament de les aigües superficials. És probable que durant aquests períodes de transició la massa d'aigua fonda generada no tingués prou densitat per assolir el fons de la conca, tal i com indiquen lleugers increments en els valors de $\delta^{13}C$ i $\delta^{18}O$ de foraminífers bentònics. Això implicaria que el nucli de la WMDW circulés a la fondària del sistema contornític, afectant directament el indret del testimoni MD99-2343. Això explica que sigui durant aquests períodes de transició quan el registre llim/argila mostra els valors màxims. El tercer mode, de circulació intensa, correspon als períodes freds dels GS, quan la massa d'aigua fonda estava molt ben ventilada (valors alts de $\delta^{13}C$ de bentònics) i era molt densa (valors alts de $\delta^{18}O$ de bentònics), tal i com també confirma un estudi basat en la reconstrucció de la temperatura de l'aigua de fons al Mar d'Alboran (Cacho et al., 2006). Aquesta combinació provocà la profundització del nucli de la WMDW, de manera que el nivell de circulació més intensa quedava per sota de la profunditat del lloc del testimoni, cosa que resultà en una disminució dels valors del registre de llim/argila (Fig. 5.6). El patró descrit es repeteix a cadascun dels cicles de DO del MIS 3, fet que confirma la gran sensibilitat de la columna d'aigua del Mediterrani occidental als canvis climàtics abruptes de l'Atlàntic Nord.

Un exemple més que demostra la gran sensibilitat del sistema de circulació termohalina mediterrani front els canvis climàtics abruptes es troba en els períodes associats a la descàrrega massiva d'icebergs a l'Atlàntic Nord, és a dir en els HE. Aquests períodes es caracteritzaren per condicions molt fredes i molt àrides al Mediterrani occidental (Cacho et al., 1999; Combourieu Nebout et al., 2002; Sánchez Goñi et al., 2002), condicions favorables per a que la circulació termohalina es veiés reforçada (Cacho et al., 1999). La fosa dels icebergs alliberats massivament a l'Atlàntic Nord durant els HE produí una entrada d'aigua menys salina per l'estret de Gibraltar, documentada per una sèrie d'anomalies en el registre $\delta^{18}O$ en foraminífers planctònics (Cacho et al., 1999; Sierro et al., 2005). L'entrada d'aigua menys salina a la conca occidental del Mediterrani provocà una major estratificació de la columna d'aigua i, en conseqüència, una reducció de la formació d'aigua fonda (Sierro et al., 2005). Això resultà en una reducció de la ventilació i de la intensitat dels corrents de fons coincidint amb les anomalies en superfície dels HE, com ho demostren les caigudes en els registres de $\delta^{13}C$ i de llim/argila (Fig. 5.7). Durant aquests períodes, els valors del registre de llim/argila són més grans que als GS, cosa que fa pensar que la massa d'aigua fonda no assolí valors elevats de densitat donat que estava afectada per les anomalies superficials. Per tant, durant els HE el mode de circulació termohalina devia ésser similar al de les transicions GIS/GS, és a dir el mode moderat o intermedi.

L'elevada sensibilitat i l'alta resolució del registre de Menorca ha permès identificar petits esdeveniments dintre de les anomalies dels HE, les quals mostren una millora temporal de la ventilació i un increment de la intensitat dels corrents de fons associats a moments de menor entrada d'aigua d'origen subpolar. Aquests resultats indiquen que la incursió d'aigua subpolar menys salina procedent de la fosa d'icebergs no fou continua sinó polsant. El sistema de circulació termohalina del Mediterrani occidental es va veure molt afectat per aquests canvis abruptes en les condicions hidrològiques, però sempre va mantenir un mode intermedi de circulació.

Per a poder verificar el model dels tres modes de circulació termohalina a la conca occidental del Mediterrani seria necessari obtenir més registres amb resolució suficient per poder investigar la a/sincronia entre els canvis en la intensitat dels corrents de fons i els canvis en les propietats de la massa d'aigua fonda. Un bon lloc per obtenir-lo seria el mateix sistema contornític però a profunditats diferents, més somes i més pregones que el indret d'on s'extragué el testimoni estudiat.

8.2. Oscil·lacions en la circulació profunda durant l'Holocè

Durant molt de temps hom considerà l'Holocè com un període interglacial amb un clima estable que hauria facilitat el desenvolupament de les comunitats i la civilització humanes fins arribar a la societat actual. El cert, però, és que hi ha diversos registres que demostren que a l'Holocè també hi ha hagut oscil·lacions climàtiques, encara que de menor amplitud que les del darrer període glacial (Mayewski et al., 2004). L'ocurrència d'episodis de refredament dintre del present interglacial, i també en interglacials més antics, ha cridat l'atenció de la comunitat científica, tant per la possible influència d'aitals episodis en el desenvolupament de les societats humanes com pels efectes que situacions semblants podrien tenir damunt la societat actual. A la regió mediterrània hi ha força registres que mostren canvis en les condicions d'aridesa i humitat, en la vegetació, en la temperatura de la superfície del mar, i encara d'altres (Cheddadi et al., 1998; Jalut et al., 2000; Cacho et al., 2001 i 2010; Allen et al., 2002; Davis et al., 2003; Frisia et al., 2006; Incarbona et al., 2008; Morellón et al., 2009; Martín-Puertas et al., 2010; Moreno et al., 2011). Hi havia, però, un gran desconeixement en relació amb la possible afectació d'aquestes oscil·lacions sobre la circulació termohalina del Mediterrani occidental, donat que la baixa ventilació i l'escassa oxigenació de les aigües fondes durant l'Holocè havia provocat la desaparició dels foraminífers bentònics de l'espècie *Cibicidoides*, el més emprat en les reconstruccions de la circulació profunda durant el període glacial (Caralp, 1988; Reguera, 2004; Sierro et al., 2005).

Els registres de la composició elemental i de la mida de gra del testimoni MD99-2343 mostren un seguit d'oscil·lacions al llarg dels darrers 12 ka, tant pel que fa a la tendència general

com a l'escala mil·lenària, les quals es poden correlacionar amb fluctuacions de la circulació termohalina del Mediterrani occidental durant la desglaciació i l'Holocè.

El patró general de la circulació durant aquest període pot ésser subdividit en quatre fases ben diferenciades, totes elles associades a canvis significatius de les condicions climàtiques regionals. A la primera fase, entre 12 i 10.5 ka, s'observa una forta davallada en els registres de Si/Al i Ti/Al (Fig. 6.5), i també en els paràmetres granulomètrics, com ara la relació llim/argila i l'UP10 (Fig. 6.4), la qual cosa indica un afebliment de la circulació profunda. Aquest afebliment de la circulació termohalina del Mediterrani occidental és paral·lel a la pujada del nivell del mar associada a la segona fase de la desglaciació, coincidint amb el màxim de insolació estival. També és en aquesta fase quan es donen els valors més alts de K/Al (Fig. 6.5), indicadors de condicions més humides que haurien afavorit una estratificació més pronunciada de la columna d'aigua, inhibint així la circulació profunda. De fet, el registre de l'indicador de ventilació $\delta^{13}C$ en foraminífers bentònics acaba tot just en aquest interval (Sierro et al., 2005), coincidint amb la formació d'una capa rica en matèria orgànica (ORL, de l'anglès *Organic Rich Layer*) al Mar d'Alboran (Cacho et al., 2002), probablement afavorida pel mateix afebliment de la circulació profunda. Les condicions climàtiques canviants associades a la desglaciació i a la pujada del nivell del mar tingueren, per tant, un paper altament rellevant en l'apaivagament de la circulació termohalina durant la Terminació Ib.

A la segona fase, de 10.5 a 7 ka, els valors de Si/Al, Ti/Al i UP10 mostren increments notables, més accentuats cap als 8.5-8-1 ka, dada que indica una recuperació de la circulació profunda, afavorida probablement per l'estabilització del nivell del mar. Aquesta recuperació sembla estar relacionada amb un esdeveniment climàtic de refredament a l'Atlàntic Nord, conegut com a 8.2 ka (Alley i Agustsdottir, 2005; Rohling i Pälike, 2005), causant també de la fi de l'ORL al Mar d'Alboran (Cacho et al., 2002).

A la tercera fase, entre 7 i 4 ka, les corbes de Si/Al i Ti/Al mostren valors relativament constants, deguts segurament a una circulació profunda estable. En aquest punt sorgeix, però, una contradicció aparent respecte els canvis climàtics abruptes observats a la perifèria del Mediterrani, en especial, al nord d'Àfrica, lligats a la finalització del període humit africà (AHP, de l'anglès *African Humid Period*) (deMenocal et al., 2000b). L'acabament de l'AHP, associat a la reducció de les diferències estacionals al voltants de 5.5 ka, no hauria tingut cap efecte en el registre del llom contornític de Menorca fins més endavant.

La quarta fase, entre 4 i 0 ka, està caracteritzada per una davallada dels valors de Si/Al, segurament indicadora d'un nou afebliment de la circulació profunda a l'Holocè superior, el qual anà acompanyat per una disminució en l'aportació de terrígens coincidint amb condicions més àrides i de menor descàrrega fluvial. Hom a relacionat aquest darrer afebliment de la circulació profunda amb l'establiment de condicions més àrides a la regió, com indica

la davallada progressiva dels valors de K/Al a causa d'una diferència d'insolació estacional mínima (Jalut et al., 2000). El desplaçament cap al sud de la Zona de Convergència Inter-Tropical (ITCZ, de les seves sigles en anglès) i la reducció subseqüent del gradient de pressió a l'Atlàntic haurien afavorit una disminució en la intensitat dels vents que desencadenen la formació d'aigua fonda al Golf de Lleó. Per tant, la circulació termohalina del Mediterrani occidental estigué molt afectada pels canvis hidrològics i atmosfèrics dels darrers 12 ka, mostrant encara millor, si cal, la gran sensibilitat de la regió als forçaments climàtics.

Dintre de la variabilitat de tendència llarga tot just descrita, hom observà també oscil·lacions d'escala mil·lenària tant en el registre de $\delta^{18}O$ com en els de Si/Al i UP10, amb una ciclicitat propera als 1000 anys (Fig. 6.6 i Taula 6.2). Aquests resultats indiquen intervals d'intensificació de la circulació profunda, induïts probablement per vents més forts i aigües més fredes en superfície, un mecanisme semblant al proposat per altres autors per explicar els canvis observats al llarg del període glacial (Cacho et al., 2000; Sierro et al., 2005). Les oscil·lacions climàtiques de l'Holocè observades en el testimoni de Menorca són sincròniques amb anomalies observades arreu del món (Mayewski et al., 2004). Persisteixen, però, certes dificultats de correlació degudes a febleses a l'hora d'establir una cronologia precisa i al caràcter no del tot homogeni del registre de les oscil·lacions climàtiques holocenes. Tot i així, la ciclicitat de les oscil·lacions detectades en el testimoni MD99-2343, propera als 1000 anys com ja s'ha dit, és semblant a l'observada en altres regions. Aquesta ciclicitat seria deguda a canvis en la insolació i/o a mecanismes de retroalimentació interns del sistema (Schulz i Paul, 2002). En qualsevol cas, la variabilitat climàtica holocena detectada al testimoni MD99-2343 estaria relacionada amb les oscil·lacions de l'Atlàntic Nord, i hauria estat transmesa fins a la regió mediterrània mitjançant mecanismes de teleconnexió atmosfèrica anàlegs al patró actual de variabilitat climàtica de la NAO, com també es va proposar per a explicar l'efecte de la variabilitat climàtica de DO en la circulació termohalina durant el MIS 3 (Cacho et al., 2000; Moreno et al., 2002; Sánchez Goñi et al., 2002).

CAPÍTOL IV. CONCLUSIONS

En aquesta Tesi hem demostrat, en primer lloc, que les aportacions de terrígens al Mediterrani occidental han estat modulades per les oscil·lacions climàtiques d'escala orbital i mil·lenària, i hem mostrat que els canvis de la composició elemental i de la mida de gra del sediment al llarg del temps són indicadors molt útils per a conèixer els impactes dels canvis climàtics naturals en la sedimentació a la conca pregona. La interpretació d'aquests indicadors requereix en tots els casos un bon coneixement dels processos i mecanismes sedimentaris d'abast regional i local que han determinat els registres estudiats.

L'estudi dels registres granulomètrics i geoquímics en el testimoni PRGL1-4 del Golf de Lleó ens ha permès avançar en el coneixement de l'efecte de les oscil·lacions del nivell del mar sobre la sedimentació en el talús continental. Per altra banda, l'estudi dels mateixos indicadors en el testimoni MD99-2343 del sistema contornític profund del nord de Menorca ens ha servit per a conèixer el impacte dels canvis climàtics globals en la circulació termohalina del Mediterrani occidental.

Els resultats del testimoni PRGL1-4 han confirmat que les oscil·lacions del nivell del mar associades als cicles climàtics d'escala orbital de 100 ka exerciren un control determinant en la construcció del marge. El testimoni PRGL1-4 inclou cinc unitats corresponents al cinc darrers cicles glacials, que abasten els darrers 530 ka. La baixada del nivell del mar associada a cada cicle interglacial/glacial conduí a la formació d'una unitat regressiva progradant en el talús continental del Golf de Lleó, la qual cosa permeté re-interpretar la seismoestratigrafia del marge.

Les oscil·lacions del nivell del mar d'escala orbital (100 ka) afectaren molt significativament la sedimentació en el marge. En aquesta Tesi hem mostrat que la construcció del marge a escala glacial/interglacial estigué dominada per un model combinat de sedimentació. En els períodes de nivell del mar baix (*lowstands*, associats als glacials) la sedimentació era controlada totalment per les aportacions fluvials, ja que els sistemes deltaics eren a tocar del talús continental i la plataforma estava emergida. Per contra, en els períodes de nivell del mar alt (*highstands*, associats als interglacials), la inundació de la plataforma incrementà l'espai d'acomodació i determinà l'atrapament dels sistemes prodeltaics lluny de la vora de plataforma, tot i afavorint a l'ensems la reactivació de processos erosius i de transport com ara les cascades d'aigua densa de plataforma. En els períodes de transició pel que fa al nivell del mar, la sedimentació de fins d'origen fluvial es combinà amb l'aportació de grollers per processos altament energètics com les cascades esmentades. Per tot plegat el registre granulomètric del testimoni PRGL1-4 és un bon indicador dels canvis globals del nivell del mar.

Les oscil·lacions del nivell del mar d'escala glacial/interglacial condicionaren també la circulació termohalina del Mediterrani occidental, com ho demostra el marcat afebliment que

experimentà durant la pujada del nivell del mar associat a la darrera desglaciació, d'acord amb el registre granulomètric del testimoni MD99-2343.

Els canvis climàtics d'escala mil·lenària associats als cicles de DO també tingueren un fort impacte en la circulació termohalina del Mediterrani occidental. Els registres sedimentològics del testimoni MD99-2343 confirmen el model prèviament establert, amb un reforçament de la circulació profunda durant els períodes freds dels GS i un afebliment durant els períodes càlids dels GIS. Hom ha relacionat amb un mecanisme de transferència atmosfèrica entre latituds altes i mitjanes aquesta reacció ràpida del sistema de circulació termohalina del Mediterrani occidental front els canvis abruptes observats a l'Atlàntic nord.

Els registres sedimentològics d'aquest mateix testimoni MD99-2343 mostren que la recuperació de la circulació profunda durant les transicions GIS/GS generà un mode de circulació més activa pel damunt de les profunditats màximes de la conca (circulació intermèdia) al inici del refredament superficial, doncs la massa d'aigua fonda més dinàmica era menys densa que l'aigua que hi havia directament sobre el fons a les fondalades més profundes de la conca. És probable que aquest mode de circulació intermèdia també es donés durant els HE, doncs tot i estar associats a condicions molt fredes amb vents molt forts, l'entrada per l'estret de Gibraltar d'aigua superficial menys salina produïda per la fosa d'icebergs induí una major estratificació de les aigües de la conca i, per tant, dificultà l'enfonsament de les aigües superficials.

El registre granulomètric del talús superior del Golf de Lleó ha permès constatar per primera vegada que les oscil·lacions climàtiques d'escala mil·lenària associades als cicles de DO anaren acompanyades de canvis significatius del nivell de mar. La sincronia entre el registre granulomètric i el de $\delta^{18}O$ en foraminífers planctònics mostra que els nivells del mar alt van ocórrer coincidint amb els períodes càlids de l'Atlàntic Nord, els GIS. La no linealitat dels indicadors granulomètrics en relació amb els canvis del nivell del mar i les pronunciades reduccions en les taxes de sedimentació associades a cada ascens fan que no es pugui determinar ni l'amplitud exacta ni el moment precís en que s'inicià l'ascens del nivell del mar. Caldrà, per tant, treballar més en el futur per a escatir quina fou la font principal d'aquestes pujades del nivell del mar, sigui septentrional (Grenlàndia) o meridional (Antàrtida).

El suposadament estable Holocè anà acompanyat de fluctuacions apreciables en la circulació termohalina del Mediterrani occidental, associades a canvis significatius en les condicions climàtiques regionals a llarg termini. La pujada del nivell del mar durant la fase final de la desglaciació, i l'estabilització de les condicions climàtiques amb un increment de la humitat, afebliren notablement la circulació profunda, situació que afavorí probablement la formació d'una ORL al Mar d'Alboran. L'estabilització del nivell del mar durant l'òptim de l'Holocè permeté el restabliment de la circulació profunda, reforçada també per condicions més fredes

durant el refredament 8.2 ka. A l'Holocè mig la circulació profunda es mantingué estable tot i haver-hi un canvi en la tendència del clima cap a condicions més àrides, associades probablement a la migració cap al sud de la ITCZ. Fou a partir de 4 ka quan la circulació profunda del Mediterrani occidental tornà a afeblir-se, degut probablement a un retard en el impacte de l'aridesa regional, la qual també afectà l'aportació de terrígens cap al fons de conca.

Dins l'Holocè hem identificat diversos episodis curts caracteritzats per condicions relativament més fredes, durant els quals es reforçà la circulació termohalina al Mediterrani occidental. Aquests episodis o esdeveniments presenten una ciclicitat propera als 1000 anys i els hem pogut correlacionar amb registres de l'Atlàntic Nord i d'altres regions del planeta.

Entenem que els resultats d'aquesta Tesi confirmen que el mecanisme principal de transferència de variabilitat climàtica ràpida entre latituds altes i baixes està relacionat amb una teleconnexió atmosfèrica, però també palesen la influència que els canvis hidrològics regionals han tingut sota determinades circumstàncies en la modulació de la circulació termohalina del Mediterrani occidental.

Línies de treball futures

Creiem que mitjançant aquesta Tesi hem pogut donar resposta a bona part de les qüestions plantejades en els objectius, però també som conscients que alguns aspectes han quedat sense resposta i que, fins i tot, han sorgit noves preguntes com a conseqüència dels resultats assolits. Tot plegat, res de sorprenent, sobretot si es té en compte que el coneix científic avança per increments successius.

Arribats a aquest punt volem plantejar, a títol de suggeriments per a nosaltres mateixos i també per altres, una sèrie de línies d'investigació futures pensades per a respondre, o respondre millor, a allò que hagi pogut quedar pendent:

1) Creiem convenient dedicar més esforç a l'estudi de seqüències sedimentàries en sistemes progradants amb taxes de sedimentació elevades, donat que permeten analitzar amb molt alta resolució els efectes dels canvis climàtics abruptes, així com les relacions de causa i efecte involucrades en la variabilitat climàtica ràpida.
2) Entenem que caldria aprofundir en el coneixement dels processos erosius que afectaren la plataforma continental en el passat, com ara les DSWC, a fi i efecte de calibrar la capacitat de transport de sediment cap al talús i el fons de conca en relació amb els canvis del nivell del mar, de manera que hom pugui determinar l'amplitud mínima dels canvis necessària per a produir una variació significativa en la mida de les partícules transportades i dipositades.

3) Considerem prioritari efectuar més estudis en localitats seleccionades per a aportar evidències addicionals dels canvis de nivell del mar associats a les oscil·lacions climàtiques de DO i de la seva l'amplitud. Cal també una cronologia precisa que permeti esbrinar els moments exactes en que es produïren aquests canvis. L'assoliment d'aquestes fites també és necessari per aclarir fins quin punt cadascun dels mantells polars contribuí a aquests canvis del nivell del mar, ajudant així a diferenciar el seu paper respectiu en la variabilitat climàtica d'escala mil·lenària, merament passiu o plenament actiu.

4) Convindria verificar i refinar el model de variabilitat de la circulació termohalina passada al Mediterrani occidental insistint en l'estudi de més seqüències sedimentàries sensibles a les variacions en les masses d'aigua fonda de la conca.

5) També pensem que seria bo invertir en la millora del coneixement de la variabilitat de la circulació intermèdia del Mediterrani, així com de les connexions pretèrites entre les conques oriental i occidental amb la finalitat d'avaluar el seu impacte sobre la circulació profunda del Mediterrani i el seu possible acoblament amb la variabilitat de l'Atlàntic Nord.

6) Estem convençuts que cal estudiar amb més detall la relació entre la variabilitat en la circulació termohalina del Mediterrani occidental i la variabilitat climàtica a l'Atlàntic Nord, a fi i efecte de poder avaluar més acuradament de quina manera les modificacions de la WMDW podrien haver estat precursors de variacions en l'AMOC i, per tant, en la variabilitat climàtica ràpida.

7) Sens dubte seria una bona inversió millorar la comprensió de les excursions climàtiques holocenes atenent al seu potencial per a enfortir les capacitats predictives del sistema climàtic en el context actual de canvi accelerat pels forçaments antropogènics.

CAPÍTOL V. BIBLIOGRAFIA

Acosta, J., Canals, M., Carbó, A., Muñoz, A., Urgeles, R. i Uchupi, E., 2004. Sea floor morphology and Plio-Quaternary sedimentary cover of the Mallorca Channel, Balearic Islands, Western Mediterranean; Marine Geology, 206: 165-179.

Acosta, J., 2005. El Promontorio Balear: morfología submarina y recubrimiento sedimentario; Tesi Doctoral, Universitat de Barcelona, 154 p.

Agrawal, Y.C., McCave, I.N. i Riley, J.B., 1991. Laser diffraction size analysis, In: Syvitski, J.P.M. (Ed.), Principles, methods, and application of particle size analysis; Cambridge University Press, Cambridge, p. 119-129.

Aitchison, J., 1982. The statistical analysis of compositional data. Journal of the Royal Statistical Society, Series B (Methodological), 44: 139-177.

Aloïsi, J.C., 1986. Sur un modèle de sédimentation deltaïque: contribution à la connaissance des marges passives; Tesi Doctoral, Université de Perpignan, 162 p.

Alonso, B., Guillen, J., Canals, M., Serra, J., Acosta, J., Herranz, P., Sanz, J.L., Calafat, A. i Catafau, E., 1988. Los sedimentos de la plataforma continental balear; Acta Geologica Hispanica, 23 (3): 185-196.

Alonso, B., Canals, M., Got, H. i Maldonado, A., 1991. Seavalleys and related depositional systems in the Catalan Sea (northwestern Mediterranean Sea); American Association of Petroleum Geologists Bulletin, 75 (7): 1195-1214.

Alonso, B., Canals, M., Palanques, A. i Rehault, J.P., 1995. A deep-sea channel in the Northwestern Mediterranean Sea: Morphology and seismic structure of the Valencia channel and its surroundings; Marine Geophysical Researches, 17: 469-484.

Allen, J.R.M., Brandt, U., Brauer, A., Hubberten, H.W., Huntley, B., Keller, J., Michael, K., Mackensen, A., Mingram, J., Negendank, J.F.W., Nowaczyk, N.R., Oberhänsli, H., Watts, W.A., Wulf, S. i Zolitschka, B., 1999. Rapid environmental changes in southern Europe during the last glacial period; Nature, 400: 740-743.

Allen, J.R.M., Watts, W.A., McGee, E. i Huntley, B., 2002. Holocene environmental variability-the record from Lago Grande di Monticchio, Italy; Quaternary International, 88: 69-80.

Alley, R.B. i Agustsdottir, A.M., 2005. The 8k event: cause and consequences of a major Holocene abrupt climate change; Quaternary Science Reviews, 24: 1123-1149.

Amblas, D., Canals, M., Urgeles, R., Lastras, G., Liquete, C., Hughes-Clarke, J.E., Casamor, J.L. i Calafat, A., 2006. Morphogenetic mesoscale analysis of the northeastern Iberian margin, NW Mediterranean Basin; Marine Geology, 234: 3-20.

Amblas, D., Gerber, T.P., Canals, M., Pratson, L.F., Urgeles, R., Lastras, G. i Calafat A., 2011. Transient erosion in the Valencia Trough turbidite systems, NW Mediterranean Basin; Geomorphology, 130: 173-184.

Amblas, D., 2012. Morfodinàmica sedimenària de marges continentals passius silicoclàstics, Tesi Doctoral, Dept. d'Estratigrafia, Paleontologia i Geociències Marines, Universitat de Barcelona, 181 p.

Andersen, K.K., Svensson, A., Johnsen, S.J., Rasmussen, S.O., Bigler, M., Rothlisberger, R., Ruth, U., Siggaard-Andersen, M.-L., Peder Steffensen, J., Dahl-Jensen, D., Vinther, B.M. i Clausen, H.B., 2006. The Greenland Ice Core Chronology 2005, 15-42 ka. Part 1: constructing the time scale; Quaternary Science Reviews, 25: 3246-3257.

Artale, V., Calmanti, S. i Sutera, A., 2002. Thermohaline circulation sensitivity to intermediate-level anomalies; Tellus A, 54: 159-174.

Artale, V., Calmanti, S., Malanotte-Rizzoli, P., Pisacane, G., Rupolo, V. i Tsimplis, M., 2006. The Atlantic and Mediterranean Sea as connected systems, In: Lionello, P., Malanotte-Rizzoli, P., Boscolo, R. (Eds.), Mediterranean Climate Variability, Vol. 4 (Developments in Earth and Environmental Sciences); Elsevier, Amsterdam, p. 283-323.

Arz, H.W., Lamy, F., Ganopolski, A., Nowaczyk, N. i Patzold, J., 2007. Dominant Northern Hemisphere climate control over millennial-scale glacial sea-level variability; Quaternary Science Reviews, 26: 312-321.

Barry, R.G. i Chorley, R.J., 1998. Atmosphere, weather and climate; Routledge, Londres, 536 p.

Bartov, Y., Goldstein, S.L., Stein, M. i Enzel, Y., 2003. Catastrophic arid episodes in the Eastern Mediterranean linked with the North Atlantic Heinrich events; Geology, 31: 439-442.

Bassetti, M.A., Jouet, G., Dufois, F., Berne, S., Rabineau, M. i Taviani, M., 2006. Sand bodies at the shelf edge in the Gulf of Lions (Western Mediterranean): Deglacial history and modern processes; Marine Geology, 234: 93-109.

Bassetti, M.A., Berné, S., Jouet, G., Taviani, M., Dennielou, B., Flores, J.A., Gaillot, A., Gelfort, R., Lafuerza, S., Sultan i N., 2008. The 100-ka and rapid sea level changes recorded by prograding shelf sand bodies in the Gulf of Lions (western Mediterranean Sea), Geochemistry Geophysics Geosystems, 9, Q11R05, doi:10.1029/2007GC001854.

Baztan, J., Berne, S., Olivet, J.L., Rabineau, M., Aslanian, D., Gaudin, M., Rehault, J.P. i Canals, M., 2005. Axial incision: The key to understand submarine canyon evolution (in the western Gulf of Lion); Marine and Petroleum Geology, 22: 805-826.

Bellaiche, G., Droz, L., Aloisi, J.-C., Bouye, C., Got, H., Monaco, A., Maldonado, A., Serra-Raventos, J. i Mirabile, L., 1981. The Ebro and the Rhone deep-sea fans: First comparative study; Marine Geology, 43: M75-M85.

Bergamasco, A. i Malanotte-Rizzoli, P., 2010. The circulation of the Mediterranean Sea: a historical review of experimental investigations; Advances in Oceanography and Limnology, 1 (1): 11-28.

Berger, W.H., 1990. The younger dryas cold spell—a quest for causes; Palaeogeography, Palaeoclimatology, Palaeoecology, 89: 219-237.

Berné, S., Carré, B., Loubrieu, B., Mazé, J.P., Morvan, L. i Normand, A., 2004a. Notice de la carte morpho-bathymétrique du Golfe du Lion. IFREMER, Brest.

Berné, S., Rabineau, M., Flores, J.A. i Sierro F.J., 2004b. The impact of Quaternary Global Changes on strata formation. Exploration of the shelf edge in the Northwest Mediterranean Sea; Oceanography, 17: 92-103.

Berné, S. i Gorini, C., 2005. The Gulf of Lions: An overview of recent studies within the French 'Margins' programme; Marine and Petroleum Geology, 22: 691-693.

Berné, S., Jouet, G., Bassetti, M.A., Dennielou, B. i Taviani, M., 2007. Late Glacial to Preboreal sea-level rise recorded by the Rhone deltaic system (NW Mediterranean); Marine Geology, 245: 65-88.

Bethoux, J.-P., 1980. Mean water fluxes across sections in the Mediterranean Sea, evaluated on the basis of water and salt budgets and of observed salinities; Oceanologica Acta, 3: 79-88.

Bethoux, J.P., Gentili, B., Raunet, J. i Tailliez, D., 1990. Warming trend in the western Mediterranean deep water; Nature, 347: 660-662.

Bethoux, J.P., Morin, P., Chaumery, C., Connan, O., Gentili, B. i Ruiz-Pino, D., 1998. Nutrients in the Mediterranean Sea, mass balance and statistical analysis of concentrations with respect to environmental change; Marine Chemistry, 63: 155-169.

Bethoux, J.P., Durieu de Madron, X., Nyffeler, F. i Tailliez, D., 2002. Deep water in the western Mediterranean: peculiar 1999 and 2000 characteristics, shelf formation hypotesis, variability since 1970 and geochemical inferences; Journal of Marine Systems, 33-34: 117-131.

Bianchi, G.G., Hall, A., McCave, I.N. i Joseph, L., 1999. Measurement of the sortable silt current speed proxy using the Sedigraph 5100 and Coulter Multisizer IIe: precesion and accuracy; Sedimentology, 46: 1001-1014.

Bianchi, G.G. i McCave, I.N., 1999. Holocene periodicity in North Atlantic climate and deep-ocean flow south of Iceland; Nature, 397: 515-517.

Bigg, G. i Wadley, M.R., 2001. Millennial-scale variability in the oceans: an ocean modelling view; Journal of Quaternary Science, 16: 309-319.

Bigg, G.R., Jickells, T.D., Liss, P.S. i Osborn, T.J., 2003. The role of the oceans in climate; International Journal of Climatology, 23: 1127-1159.

Blunier, T., Chappellaz, J., Schwander, J., Dallenbach, A., Stauffer, B., Stocker, T.F., Raynaud, D., Jouzel, J., Clausen, H.B., Hammer, C.U. i Johnsen, S.J., 1998. Asynchrony of Antarctic and Greenland climate change during the last glacial period; Nature, 394: 739-743.

Blunier, T. i Brook, E.J., 2001. Timing of millennial-scale climate change in Antarctica and Greenland during the Last Glacial period; Science, 291: 109-112.

Bolle, H.-J., 2003. Mediterranean Climate: variability and trends. Springer-Verlag, Berlin-Heidelberg-Nova York, 372 p.

Bond, G., Heinrich, H., Broecker, W.S., Labeyrie, L., McManus, J., Andrews, J.T., Huon, S., Jantschik, R., Clasen, S., Simet, C., Tedesco, K., Klas, M., Bonani, G. i Ivy, S., 1992. Evidence for masive discharges of icebergs into the North Atlantic ocean during the last glacial period; Nature, 360: 245-249.

Bond, G., Broecker, W.S., Johnsen, S.J., McManus, J., Labeyrie, L., Jouzel, J. i Bonani, G., 1993. Correlations between climate records from North Atlantic sediments and Greenland ice; Nature, 365: 143-147.

Bond, G. i Lotti, R., 1995. Iceberg discharges into the North Atlantic on millennial time scales during the last deglaciation; Science, 267: 1005-1010.

Bond, G., Showers, W., Cheseby, M., Lotti, R., Almasi, P., de Menocal, P., Priore, P., Cullen, H., Hajdas, I. i Bonani, G., 1997. A pervasive millenial-scale cycle in North Atlantic Holocene and glacial climates; Science, 278: 1257-1266.

Bond, G., Showers, W., Elliot, M., Evans, M., Lotti, R., Hajdas, I., Bonani, G. i Johnson, S., 1999. The North Atlantic's 1-2 kyr climate rhythm: relation to Heinrich Events, Dansgaard/Oeschger cycles and the Little Ice Age, In: Alley, R.B., Clark, P.U., Keigwin, L.,

Webb, R. (Eds.), Mechanisms of Global Climate Change at Millennial Time Scales; American Geophysical Union, p. 35-58.

Bond, G., Kromer, B., Beer, J., Muscheler, R., Evans, M., Showers, W., Hoffmann, S., Lotti-Bond, R., Hajdas, I. i Bonani, G., 2001. Persistent solar influence on North Atlantic climate during the Holocene; Science, 294: 2130-2136.

Borzelli, G.L.E., Ga, Miroslav, Cardin, V. i Civitarese, G., 2009. Eastern Mediterranean Transient and reversal of the Ionian Sea circulation; Geophysical Research Letters, 36, L15108.

Broecker, W.S., Dorothy, M.P. i Rind, D., 1985. Does the ocean-atmosphere system have more than one stable mode of operation?; Nature, 315: 21-26.

Broecker, W.S. i Denton, G.H., 1989. The role of ocean-atmosphere reorganizations in glacial cycles; Geochimica et Cosmochimica Acta, 53: 2465-2501.

Broecker, W.S., Bond, G., Klas, M., Clark, E. i McManus, J., 1992. Origin of the North Atlantic's Heinrich Events; Climate Dynamics, 6: 265-273.

Broecker, W.S., Denton, G.H., Edwards, R.L., Cheng, H., Alley, R.B. i Putnam, A.E., 2010. Putting the Younger Dryas cold event into context; Quaternary Science Reviews, 29: 1078-1081.

Cacho, I., Grimalt, J.O., Pelejero, C., Canals, M., Sierro, F.J., Flores, J.A. i Shackleton, N.J., 1999. Dansgaard-Oeschger and Heinrich event imprints in Alboran Sea temperatures; Paleoceanography, 14: 698-705.

Cacho, I., Grimalt, J.O., Sierro, F.J., Shackleton, N.J. i Canals, M., 2000. Evidence for enhanced Mediterranean thermohaline circulation during rapid climatic coolings; Earth and Planetary Science Letters, 183: 417-429.

Cacho, I., Grimalt, J.O., Canals, M., Sbaffi, L., Shackleton, N., Schönfeld, J. i Zahn, R., 2001. Variability of the western Mediterranean Sea surface temperature during the last 25,000 years and its connection with the northern hemisphere climatic changes; Paleoceanography, 16: 40-52.

Cacho, I., Grimalt, J.O. i Canals, M., 2002. Response of the Western Mediterranean Sea to rapid climate variability during the last 50,000 years: a molecular biomarker approach; Journal of Marine Systems, 33-34: 253-272.

Cacho, I., Shackleton, N., Elderfield, H., Sierro, F.J. i Grimalt, J.O., 2006. Glacial rapid variability in deep-water temperature and d18O from the Western Mediterranean Sea; Quaternary Science Reviews, 25: 3294-3311.

Cacho, I., Valero-Garcés, B.L. i González-Sampériz, P., 2010. Review of paleoclimate reconstructions in the Iberian Peninsula since the last glacial period, In: Pérez, F.F., Boscolo, R. (Eds.), Climate in Spain: past, present and future. Regional climate change assessment report, CLIVAR Spain, p. 9-24.

Calafat, A.M., Casamor, J.L., Canals, M. i Nyffeler, F., 1996. Distribución y composición elemental de la materia particulada en suspensión en el Mar Catalano-Balear; Geogaceta, 20: 370-373.

Calmanti, S., Artale, V. i Sutera, A., 2006. North Atlantic MOC variability and the Mediterranean Outflow: a box-model study; Tellus A, 58: 416-423.

Calvert, S.E. i Pedersen, T.F., 2007. Elemental proxies for palaeoclimatic and palaeoceanographic variability in marine sediments: interpretation and application, In: Claude, H.M., Anne De, V. (Eds.), Developments in Marine Geology; Elsevier, p. 567-644.

Canals, M., 1980. Sedimentos y procesos en el margen continental sur-Balear: control climático y oceanográfico sobre su distribución y evolución durante el Cuaternario superior; Tesi de Llicenciatura, Institut "Jaume Almera" (CSIC) i Universitat de Barcelona, 210 p.

Canals, M., 1985. Estructura sedimentaria y evolución morfológica del talud y el glacis continentales del Golfo de León: Fenómenos de desestabilización de la cobertura pliocuaternaria; Tesi Doctoral, Universitat de Barcelona, 618 p.

Canals, M. i Ballesteros, E., 1997. Production of carbonate particles by phytobenthic communities on the Mallorca-Menorca shelf, northwestern Mediterranean Sea; Deep Sea Research II, 44 (3-4): 611-629.

Canals, M., Casamor, J.L., Lastras, G., Monaco, A., Acosta, J., Berné, S., Loubrieu, B., Weaver, P.P.E., Grehan, A. i Dennielou, B., 2004. The role of canyons in strata formation; Oceanography, 17 (4): 80-91.

Canals, M., Puig, P., de Madron, X.D., Heussner, S., Palanques, A. i Fabres, J., 2006. Flushing submarine canyons; Nature, 444: 354-357.

Canals, M., Danovaro, R., Heussner, S., Lykousis, V., Puig, P., Trincardi, F., Calafat, A., Durrieu de Madron, X., Palanques, A. i Sanchez-Vidal, A., 2009. Cascades in Mediterranean submarine grand canyons; Oceanography, 22: 26-43.

Canals, M., 2009. HERMESIONE cruise report, Strait of Gibraltar-Western Mediterranean (Cartagena-Cartagena), 15th September-9th October 2009. Universitat de Barcelona, Barcelona, 65 p. + 4 anexos (no publicat).

Canals, M., Amblàs, D., Lastras, G., Sànchez-Vidal, A., Calafat, A., Rayo, X. i Casamor, J.L., 2012. Els canyons submarins; Suplement de la Història Natural dels Països Catalans, La terra a l'univers: astronomia, Addenda geològica, Enciclopèdia Catalana, Barcelona, p. 251-272.

Caralp, M.H., 1988. Late Glacial to recent deep-sea benthic foraminifera from the Northeastern Atlantic (Cadiz Gulf) and Western Mediterranean (Alboran Sea): Paleoceanographic results; Marine Micropaleontology, 13: 265-289.

Clark, P.U., Alley, R.B. i Pollard, D., 1999. Northern hemisphere ice-sheet influences on global climate change; Science, 286: 1104-1111.

Clark, P.U., Hostetler, S.W., Pisias, N.G., Schmittner, A. i Meissner, K., 2007. Mechanisms for an ~7-kyr climate and sea-level oscillation during Marine Isotopic Stage 3, In: Schmittner, A., Chiang, J.C.H., Hemming, S.R. (Eds.), Ocean circulation: Mechanisms and impacts; AGU Geophysical Monograph Series, Washington, D. C., p. 209-246.

Claussen, M., Kubatzki, C., Browkin, V. i Ganopolski, A., 1999. Simulation of an abrupt change in Saharan vegetation in the mid-Holocene; Geophysical Research Letters, 26: 2037-2040.

Clemens, C., 2005. Millennial-band climate spectrum resolved and linked to centennial-scale solar cycles; Quaternary Science Reviews, 24: 521-531.

COHMAP members, 1988. Climatic changes of the last 18,000 years: observations and model simulations; Science, 241: 1043-1052.

Colmenero-Hidalgo, E., Flores, J.-A. i Sierro, F.J., 2002. Biometry of Emiliania huxleyi and its biostratigraphic significance in the Eastern North Atlantic Ocean and Western Mediterranean Sea in the last 20000 years; Marine Micropaleontology, 46: 247-263.

Colmenero-Hidalgo, E., Flores, J.-A., Sierro, F.J., Bárcena, M.A., Löwemark, L., Schönfeld, J. i Grimalt, J.O., 2004. Ocean surface water response to short-term climate changes revealed by coccolithophores from the Gulf of Cadiz (NE Atlantic) and Alboran Sea (W Mediterranean); Palaeogeography, Palaeoclimatology, Palaeoecology, 205: 317-336.

Combourieu Nebout, N., Turon, J.L., Zahn, R., Capotondi, L., Londeix, L. i Pahnke, K., 2002. Enhanced aridity and atmospheric high-pressure stability over the western Mediterranean during the North Atlantic cold events of the past 50 k.y.; Geology, 30: 863-866.

Conte, M., Giuffrida, S. i Tedesco, S., 1989. The Mediterranean oscillation: impact on precipitation and hydrology in Italy; Proceedings of the Conference on Climate and Wate, Publications of Academy of Finland, Helsinki, p. 121-137.

Coplen, T.B., 1996. New guidelines for the reporting of stable hydrogen, carbon, and oxygen isotope ratio data; Geochimca and Cosmochimica Acta, 60: 3359-3360.

Cortijo, E., Yiou, P., Labeyrie, L. i Cremer, M., 1995. Sedimentary record of rapid climatic variability in the North Atlantic ocean during the last glacial cycle; Paleoceanography, 10: 911-926.

Crowley, T.J., 1992. North Atlantic deep water cools the southern hemisphere; Paleoceanography, 7: 489-497.

Cutler, K.B., Edwards, R.L., Taylor, F.W., Cheng, H., Adkins, J., Gallup, C.D., Cutler, P.M., Burr, G.S. i Bloom, A.L., 2003. Rapid sea-level fall and deep-ocean temperature change since the last interglacial period; Earth and Planetary Science Letters, 206: 253.

Chappell, J., 2002. Sea level changes forced ice breakouts in the Last Glacial cycle: new results from coral terraces; Quaternary Science Reviews, 21: 1229-1240.

Cheddadi, R., Yu, G., Guiot, J., Harrison, S.P. i Prentice, I.C., 1997. The climate of Europe 6000 years ago; Climate Dynamics, 13: 1-9.

Cheddadi, R., Lamb, H.F., Guiot, J. i van der Kaars, S., 1998. Holocene climatic change in Morocco: a quantitative reconstruction from pollen data;. Climate Dynamics, 14: 883-890.

Dansgaard, W., Johnsen, S.J., Clausen, H.B., Dahl-Jensen, D., Gundestrup, N.S., Hammer, C.U., Hvidberg, C.S., Steffensen, J.P., Sveinbjörnsdóttir, A.E., Jouzel, J. i Bond, G., 1993. Evidence for general instability of past climate from a 250-kyr ice-core record; Nature, 364: 218-220.

Davis, B.A.S., Brewer, S., Stevenson, A.C. i Guiot, J., 2003. The temperature of Europe during the Holocene reconstructed from pollen data; Quaternary Science Reviews, 22: 1701-1716.

deMenocal, P., Ortiz, J., Guilderson, T., Adkins, J., Sarnthein, M., Baker, L. i Yarusinsky M., 2000a. Abrupt onset and termination of the African Humid Period: rapid climate responses to gradual insolation forcing; Quaternary Science Reviews, 19: 347-361.

deMenocal, P., Ortiz, J., Guilderson, T.P. i Sarnthein, M., 2000b. Coherent high- and low-latitude climate variability during the Holocene warm period; Science, 288: 2198-2202.

Dufois, F., Garreau, P., Le Hir, P. i Forget, P., 2008. Wave- and current-induced bottom shear stress distribution in the Gulf of Lions; Continental Shelf Research, 28: 1920-1934.

Dünkeloh, A. i Jacobeit, J., 2003. Circulation dynamics of Mediterranean precipitation variability 1948–98; International Journal of Climatology, 23: 1843-1866.

Duplessy, J.-C., Cortijo, E., Masson-Delmotte, V. i Paillard, D., 2005. Reconstructing the variability of the climate system: Facts and theories; Comptes Rendus Geoscience, 337: 888-896.

Durrieu de Madron, X., Zervakis, V., Theocharis, A. i Georgopoulos, D., 2005. Comments on "Cascades of dense water around the world ocean"; Progress In Oceanography, 64: 83-90.

Durrieu de Madron, X., Wiberg, P.L. i Puig, P., 2008. Sediment dynamics in the Gulf of Lions: the impact of extreme events; Continental Shelf Research, 28: 1867-1876.

Elliot, M., Labeyrie, L. i Duplessy, J.-C., 2002. Changes in North Atlantic deep-water formation associated with the Dansgaard–Oeschger temperature oscillations (60–10 ka); Quaternary Science Reviews, 21: 1153-1165.

Emiliani, C., 1955. Pleistocene temperatures; Journal of Geology, 63: 538-578.

EPICA community members, 2004. Eight glacial cycles from an Antarctic ice core; Nature, 429: 623-628.

EPICA community members, 2006. One-to-one coupling of glacial climate variability in Greenland and Antarctica; Nature, 444: 195-198.

Fabres, J., Calafat, A., Sanchez-Vidal, A., Canals, M. i Heussner, S., 2002. Composition and spatio-temporal variability of particle fluxes in the Western Alboran Gyre, Mediterranean Sea; Journal of Marine Systems, 33-34: 431-456.

Fairbanks, R.G., 1990. The age and origin of the "Younger Dryas climate event" in Greenland ice cores; Paleoceanography, 5: 937-948.

Faugères, J.-C., Mézerais, M.L. i Stow, D.A.V., 1993. Contourite drift types and their distribution in the North and South Atlantic Ocean basins; Sedimentary Geology, 82: 189-203.

Fleming, K., Johnston, P., Zwartz, D., Yokoyama, Y., Lambeck, K. i Chappell, J., 1998. Refining the eustatic sea-level curve since the Last Glacial Maximum using far- and intermediate-field sites; Earth and Planetary Science Letters, 163: 327-342.

Fletcher, W.J. i Sánchez Goñi, M.F., 2008. Orbital- and sub-orbital-scale climate impacts on vegetation of the western Mediterranean basin over the last 48,000 yr; Quaternary Research, 70: 451-464.

Fletcher, W.J., Sánchez Goñi, M.F., Peyron, O. i Dormoy, I., 2010. Abrupt climate changes of the last deglaciation detected in a Western Mediterranean forest record; Climate of the Past, 6: 245-264.

Font, J., Salat, J. i Tintoré, J., 1988. Permanent features of the circulation in the Catalan Sea; Oceanologica Acta, S-9: 51-57.

Fornós, J.J. i Ahr, W.M., 2006. Present-day temperate carbonate sedimentation on the Balearic Platform, western Mediterranean: compositional and textural variation along a

low-energy isolated ramp; Geological Society, Londres, Special Publications 255: 71-84.

Frigola, J., Moreno, A., Cacho, I., Canals, M., Sierro, F.J., Flores, J.A., Grimalt, J.O., Hodell, D.A. i Curtis, J.H., 2007. Holocene climate variability in the western Mediterranean region from a deepwater sediment record; Paleoceanography, 22, PA2209, doi:10.1029/2006PA001307.

Frigola, J., Moreno, A., Cacho, I., Canals, M., Sierro, F.J., Flores, J.A. i Grimalt, J.O., 2008. Evidence of abrupt changes in Western Mediterranean Deep Water circulation during the last 50 kyr: A high-resolution marine record from the Balearic Sea; Quaternary International, 181: 88-104, doi:10.1016/j.quaint.2007.06.016.

Frigola, J., Cacho, I., Herrera, G., Canals, M., Moreno, A., Amblas, D., Grimalt, J.O., Masqué, P. i Esparza, M., 2010. Holocene changes in deep-water circulation of the Western Mediterranean Basin, links to North Atlantic climate variability; Geo-Temas, 7: 31-32.

Frigola, J., Canals, M., Cacho, I., Moreno, A., Sierro, F.J., Flores, J.A., Berné, S., Jouet, G., Dennielou, B., Herrera, G., Pasqual, C., Grimalt, J.O., Galavazi, M. i Schneider, R., 2012. A 500 kyr record of global sea level oscillations in the Gulf of Lion, Mediterranean Sea: new insights into MIS 3 sea level variability; Climate of the Past, 8: 1067-1077.

Frisia, S., Borsato, A., Mangini, A., Spotl, C., Madonia, G. i Sauro, U., 2006. Holocene climate variability in Sicily from a discontinuous stalagmite record and the Mesolithic to Neolithic transition; Quaternary Research, 66: 388-400.

Ganopolski, A. i Rahmstorf, S., 2001. Rapid changes of glacial climate simulated in a coupled climate model; Nature, 409: 153-158.

Garcés, M., Krijgsman, W. i Agustí, J., 1998. Chronology of the late Turolian deposits of the Fortuna basin (SE Spain): implications for the Messinian evolution of the eastern Betics; Earth and Planetary Science Letters, 163: 69-81.

Gaudin, M., Berne, S., Jouanneau, J.M., Palanques, A., Puig, P., Mulder, T., Cirac, P., Rabineau, M. i Imbert, P., 2006. Massive sand beds attributed to deposition by dense water cascades in the Bourcart canyon head, Gulf of Lions (northwestern Mediterranean Sea); Marine Geology, 234: 111-128.

González-Sampériz, P., Valero-Garcés, B.L., Moreno, A., Jalut, G., García-Ruíz, J.M., Martí-Bono, C., Delgado-Huertas, A., Navas, A., Otto, T. i Dedoubat, J.J., 2006. Climate variability in the Spanish Pyrenees during the last 30,000 yr revealed by the El Portalet sequence; Quaternary Research, 66: 38-52.

Goodess, C.M., Palutikof, J.P. i Davis, T.D., 1992. The nature and causes of climate change: assessing the long-term future; Belhaven Press, Londres, 248 p.

Goossens, D., 2008. Techniques to measure grain-size distributions of loamy sediments: a comparative study of ten instruments for wet analysis; Sedimentology, 55: 65-96.

Grootes, P., Stuiver, M., White, J.W.C., Johnsen, S.J. i Jouzel, J., 1993. Comparison of oxygen isotope records from the GISP2 and GRIP Greenland ice cores; Nature, 366: 552-554.

Guerzoni, S., Molinaroli, E. i Chester, R., 1997. Saharan dust inputs to the western Mediterranean Sea: depositional patterns, geochemistry and sedimentological implications; Deep Sea Research Part II: Topical Studies in Oceanography, 44: 631-654.

Hall, I.R. i McCave, I.N., 2000. Palaeocurrent reconstruction, sediment and thorium focussing on the Iberian margin over the last 140 ka; Earth and Planetary Science Letters, 178: 151-164.

Harding, A., Palutifof, J. i Holt, T., 2009. The climate system, In: Woodward, J. (Ed.), The physical geography of the Mediterranean; Oxford University Press, Oxford, p. 69-88.

Harrison, S.P. i Digerfeldt, G., 1993. European lakes as palaeohydrological and palaeoclimatic indicators; Quaternary Science Reviews, 12: 233-248.

Hays, J.D., Imbrie, J. i Shackleton, N., 1976. Variations in the earth's orbit: pacemaker of the ice ages; Science, 194: 1121-1132.

Hein, F.J., 1989. Contourite drifts, In: Pickering, K.T., Hiscott, R.N., Hein, F.J. (Eds.), Deep marine environments: clastic sedimentation and tectonics; Unwin Hyman Inc., Londres, p. 219-245.

Heinrich, H., 1988. Origin and consequences of cyclic ice rafting in the Northeast Atlantic Ocean during the past 130.000 years; Quaternary Research, 29: 142-152.

Hemming, S., 2004. Heinrich events: massive late pleistocene detritus layers of the North Atlantic and their global climate imprint; Review of Geophysics, 42, doi:10.1029/2003RG000128.

Hilgen, F.J., 1991. Astronomical calibration of Gauss to Matuyama sapropels in the Mediterranean and implication for the Geomagnetic Polarity Time Scale; Earth and Planetary Science Letters, 104: 226-244.

Hsü, K.J., Ryan, W.B.F. i Cita, M.B., 1973. Late Miocene desiccation of the Mediterranean; Nature, 242: 240-244.

Hsü, K.J., Montadert, L., Bernoulli, D., Erickson, A., Garrison, R.E., Kidd, R.B., Mèlierés, F., Müller, C. i Wright, R., 1977. History of the Mediterranean salinity crisis; Nature, 267: 399-403.

Hughen, K., Baillie, M., Bard, E., Bayliss, A., Beck, J., Bertrand, C., Blackwell, P., Buck, C., Burr, G., Cutler, K., Damon, P., Edwards, R., Fairbanks, R., Friedrich, M., Guilderson, T., Kromer, B., McCormac, F., Manning, S., Bronk Ramsey, C., Reimer, P., Reimer, R., Remmele, S., Southon, J., Stuiver, M., Talamo, S., Taylor, F., van der Plicht, J. i Weyhenmeyer, C., 2004. Marine04 Marine radiocarbon age calibration, 26 - 0 ka BP; Radiocarbon, 46: 1059-1086.

Hurrell, J.W., 1995. Decadal trends in the North Atlantic Oscillation: regional temperatures and precipitation; Science, 269: 676-679.

Imbrie, J., Hays, J.D., Martinson, D.G., McIntyre, A., Mix, A.C., Morley, J.J., Pisias, N.G., Prell, W. i Shackleton, N., 1984. The orbital theory of Pleistocene climate: support from a revised chronology of the marine d18O record, In: Berger, A. (Ed.), Milankovitch and climate, Proceedings of the NATO Advanced Research Workshop on Milankovitch and Climate; D. Reidel Publishing Company, Palisades, Nova York, p. 269-305.

Imbrie, J., Boyle, E., Clemens, C., Duffy, A., Howard, W., Kukla, G., Kutzbach, J.E., Martinson, D.G., McIntyre, A., Mix, A.C., Molfino, B., Morley, J.J., Peterson, L.C., Pisias, N.G., Prell, W., Raymo, M.E., Shackleton, N.J. i Toggweiler, J.R., 1992. On the structure and origin of major glaciation cycles. 1. Linear responses to Milankovitch forcing; Paleoceanography, 7: 701-738.

Imbrie, J., Berger, A., Boyle, E.A., Clemens, S.C., Duffy, A., Howard, W.R., Kukla, G., Kutzbach, J., Martinson, D.G., McIntyre, A., Mix, A.C., Molfino, B., Morley, J.J., Peterson, L.C., Pisias, N.G., Prell, W.L., Raymo, M.E., Shackleton, N. i Toggweiler, J.R., 1993. On the structure and origin of major glaciation cycles 2. The 100,000-year cycle; Paleoceanography, 8: 699-735.

Incarbona, A., Di Stefano, E., Patti, B., Pelosi, N., Bonomo, S., Mazzola, S., Sprovieri, R., Tranchida, G., Zgozi, S. i Bonanno, A., 2008. Holocene millennial-scale productivity variations in the Sicily Channel (Mediterranean Sea); Paleoceanography, 23, PA3204, doi:3210.1029/2007PA001581.

Intergovernmental Oceanographic Commission, International Hydrographic Organization, and British Oceanographic Data Centre, 2003. Centenary Edition of the GEBCO Digital Atlas (CD-ROM,) British Oceanographic Data Centre, Liverpool, Regne Unit.

IPCC, 2007. Climate change 2007: The physical science basis. Contribution of working group I to the fourth assessment report of the Intergovernmental Panel on Climate Change; Cambridge University Press, Cambridgel, Regne Unit i Nova York, EE.UU, 996 p.

Ivanov, V.V., Shapiro, G.I., Huthnance, J.M., Aleynik, D.L. i Golovin, P.N., 2004. Cascades of dense water around the world ocean; Progress In Oceanography, 60: 47-98.

Jalut, G., Esteban Amat, A., Bonnet, L., Gauquelin, T. i Fontugne, M., 2000. Holocene climatic changes in the Western Mediterranean, from south-east France to south-east Spain; Palaeogeography, Palaeoclimatology, Palaeoecology, 160: 255-290.

Jansen, E., Overpeck, J.T., Briffa, K.R., Duplessy, J.C., Joos, F., Masson-Delmotte, V., Olago, D., Otto-Bliesner, B., Peltier, W.R., Rahmstorf, S., Ramesh, R., Raynaud, D., Rind, D., Solomina, O., Villalba, R. i Zhang, D., 2007. Paleoclimate, In: Solomon, S., Qin, D., Manning, M., Chen, Z., Marquis, M., Averyt, K.B., Tignor, M., Miller, H.L. (Eds.), Climate change 2007: The physical science basis. Contribution of working group I to the fourth assessment report of the Intergovernmental Panel on Climate Change; Cambridge University Press, Cambridge, Regne Unit i Nova York, EE.UU, p. 433-497.

Jansen, J.H.F., Van der Gaast, S.J., Koster, B. i Vaars, A.J., 1998. CORTEX, a shipboard XRF-scanner for element analyses in split sediment cores; Marine Geology, 151: 143-153.

Jimenez-Espejo, F.J., Martinez-Ruiz, F., Sakamoto, T., Iijima, K., Gallego-Torres i D., Harada, N., 2007. Paleoenvironmental changes in the western Mediterranean since the last glacial maximum: High resolution multiproxy record from the Algero-Balearic basin; Palaeogeography, Palaeoclimatology, Palaeoecology, 246: 292-306.

Jimenez Espejo, F.J., Martinez-Ruiz, F., Rogerson, M., Gonzalez-Donoso, J.M., Romero, O., Linares, D., Sakamoto, T., Gallego-Torres, D., Rueda Ruiz, J.L., Ortega-Huertas i M., Perez-Claros, J.A., 2008. Detrital input, productivity fluctuations, and water mass circulation in the westernmost Mediterranean Sea since the Last Glacial Maximum; Geochemistry Geophysics Geosystems 9 (11), Q11U02, doi:10.1029/2008GC002096.

Johnsen, S.J., Dahl-Jensen, D., Gundestrup, N., Steffensen, J.P., Clausen, H.B., Miller, H., Masson-Delmotte, V., Sveinbjörnsdottir, A.E. i White, J., 2001. Oxygen isotope and palaeotemperature records from six Greenland ice-core stations: Camp Century, Dye-3, GRIP, GISP2, Renland and NorthGRIP; Journal of Quaternary Science, 16: 299-307.

Jouet, G., Berne, S., Rabineau, M., Bassetti, M.A., Bernier, P., Dennielou, B., Sierro, F.J., Flores, J.A. i Taviani, M., 2006. Shoreface migrations at the shelf edge and sea-level changes around the Last Glacial Maximum (Gulf of Lions, NW Mediterranean); Marine Geology, 234: 21-42.

Jouet, G., 2007. Enregistrements stratigraphiques des cycles climatiques et glacio-eustatiques du Quaternaire terminal-Modélisations de la marge continentale du Golfe du Lion, Tesi Doctoral, Laboratoire Environnements Sédimentaires, Géosciences Marines. Ifremer, Brest, 443 p.

Jouet, G., Berné, S., Sierro, F.J., Bassetti, M.A., Canals, M., Dennielou, B., Flores, J.A., Frigola, J. i Haq, B.U., 2012. Geological imprints of millennial-scale sea-level changes; Terra Nova, sotmés.

Klein, B., Roether, W., Civitarese, G., Gacic, M., Manca, B.B. i Alcala, M.R., 2000. Is the Adriatic returning to dominate the production of Eastern Mediterranean Deep Water?; Geophysical Research Letters, 27: 3377-3380.

Konert, M. i Vandenberghe, J., 1997. Comparison of laser grain size analysis with pipette and sieve analysis: a solution for the underestimation of the clay fraction; Sedimentology, 44: 523-535.

Krijgsman, W., Hilgen, F.J., Raffi, I., Sierro, F.J. i Wilson, D.S., 1999a. Chronology, causes and progression of the Messinian salinity crisis; Nature, 400: 652-655.

Krijgsman, W., Langereis, C.G., Zachariasse, W.J., Boccaletti, M., Moratti, G., Gelati, R., Iaccarino, S., Papani, G. i Villa, G., 1999b. Late Neogene evolution of the Taza–Guercif Basin (Rifian Corridor, Morocco) and implications for the Messinian salinity crisis; Marine Geology, 153: 147-160.

Krom, M.D., Michard, A., Cliff, R.A. i Strohle, K., 1999. Sources of sediment to the Ionian Sea and western Levantine Basin of the Eastern Mediterranean during S-1 sapropel times; Marine Geology, 160: 45-61.

Kuhlemann, J., Freudenthal, T., Helmke, P. i Meggers, H., 2004. Reconstruction of paleoceanography off NW Africa during the last 40,000 years: influence of local and regional factors on sediment accumulation; Marine Geology, 207: 209-224.

Kutzbach, J.E., 1976. The nature of climate and climatic variations; Quaternary Research, 6: 471-480.

La Violette, P.E., Tintoré, J. i Font, J., 1990. The surface circulation of the Balearic Sea; Journal of Geophysical Research, 95: 1559-1568.

Lacombe, H., Tchernia, P. i Gamberoni, L., 1985. Variable bottom water in the Western Mediterranean Basin; Progress in Oceanography, 14: 319-338.

Lascaratos, A., Williams, R.G. i Tragou, E., 1993. A mixed-layer study of the formation of Levantine Intermediate Water; Journal of Geophysical Research, 98: 14739-14749.

Lascaratos, A., Roether, W., Nittis, K. i Klein, B., 1999. Recent changes in deep water formation and spreading in the eastern Mediterranean Sea: a review; Progress in Oceanography, 44: 5-36.

Laskar, J., 1990. The chaotic motion of the solar system: a numerical estimate of the size of the chaotic zones; Icarus, 88: 266-291.

Lastras, G., Canals, M., Amblas, D., Frigola, J., Urgeles, R., Calafat, A.M. i Acosta, J., 2007. Slope instability along the northeastern Iberian and Balearic continental margins; Geologica Acta, 5, doi: 10.1344/105.000000308, 35-47.

Lea, D.W., Martin, P.A., Pak, D.K. i Spero, H.J., 2002. Reconstructing a 350 ky history of sea level using planktonic Mg/Ca and oxygen isotope records from a Cocos Ridge core; Quaternary Science Reviews, 21: 283-293.

Leaman, K.D. i Schott, F., 1991. Hydrographic structure of the convection regime in the Gulf of Lions: winter 1987; Journal of Geophysical Research, 21: 575-597.

Lisiecki, L.E. i Raymo, M.E., 2005. A Pliocene-Pleistocene stack of 57 globally distributed benthic d18O records; Paleoceanography, 20, PA1003, doi: 10.1029/2004PA001071.

Lobo, F.J., Tesson, M. i Gensous, B., 2004. Stratral architectures of late Quaternary regressive-transgressive cycles in the Roussillon Shelf (SW Gulf of Lions, France); Marine and Petroleum Geology, 21: 1181-1203.

Lofi, J., Rabineau, M., Gorini, C., Berne, S., Clauzon, G., De Clarens, P., Tadeu Dos Reis, A., Mountain, G.S., Ryan, W.B.F., Steckler, M.S. i Fouchet, C., 2003. Plio-Quaternary prograding clinoform wedges of the western Gulf of Lion continental margin (NW Mediterranean) after the Messinian Salinity Crisis; Marine Geology, 198: 289-317.

Lopez-Bustins, J.-A., Martin-Vide, J. i Sanchez-Lorenzo, A., 2008. Iberia winter rainfall trends based upon changes in teleconnection and circulation patterns; Global and Planetary Change, 63: 171-176.

López-Jurado, J.L., González-Pola, C. i Vélez-Belchí, P., 2005. Observation of an abrupt disruption of the long-term warming trend at the Balearic Sea, western Mediterranean Sea, in summer 2005; Geophysical Research Letters, 32, doi:10.1029/2005GL024430.

Loring, D.H. i Rantala, R.T.T., 1992. Manual for the geochemical analyses of marine sediments and suspended particulate matter; Earth-Science Reviews, 32: 235-283.

Löwemark, L., Chen, H.F., Yang, T.N., Kylander, M., Yu, E.F., Hsu, Y.W., Lee, T.Q., Song, S.R. i Jarvis, S., 2011. Normalizing XRF-scanner data: A cautionary note on the interpretation of high-resolution records from organic-rich lakes; Journal of Asian Earth Sciences, 40: 1250-1256.

Loyë-Pilot, M.D., Martin, J.D. i Moreli, J., 1986. Influence of Saharan dust on the rain acidity and atmospheric input to the Mediterranean; Nature, 321: 427-428.

Lozier, M.S., Owens, W.B. i Curry, R.G., 1995. The climatology of the North Atlantic; Progress In Oceanography, 36: 1-44.

Ludwig, W., Dumont, E., Meybeck, M. i Heussner, S., 2009. River discharges of water and nutrients to the Mediterranean and Black Sea: Major drivers for ecosystem changes during past and future decades?; Progress In Oceanography, 80: 199-217.

Luterbacher, J., Xoplaki, E., Casty, C., Wanner, H., Pauling, A., Küttel, M., Rutishauser, T., Brönnimann, S., Fischer, E., Fleitmann, D., González-Rouco, F., García-Herrera, R., Barriendos, M., Rodrigo, F.S., González-Hidalgo, J.C., Saz, M.A., Gimeno, L., Ribera, P., Brunet, M., Paeth, H., Rimbu, N., Felis, T., Jacobeit, J., Dünkeloh, A., Zorita, E., Guiot, J., Türkes, M., Alcoforado, M.J., Trigo, R., Wheeler, D., Tett, S., Mann, M.E., Touchan, R., Shindell, D.T., Silenzi, S., Montagna, P., Camuffo, D., Mariotti, A., Nanni, T., Brunetti, M., Maugeri, M., Zerefos, C., De Zolt, S., Lionello, P., Nunes, M.F., Rath, V., Beltrami, H., Garnier, E. i Le Roy Ladurie, E., 2006. Mediterranean climate

variability over the last centuries: a review, In: Lionello, P., Malanotte-Rizzoli, P., Boscolo, R. (Eds.), Mediterranean climate variability; Elsevier, Amsterdam, p. 27-148.

Llasat, M.C., 2009. Storms and floods, In: Woodward, J. (Ed.), The physical geography of the Mediterranean; Oxford University Press, Oxford, Regne Unit, p. 513-540.

Llave, E., Schonfeld, J., Hernandez-Molina, F.J., Mulder, T., Somoza, L., Diaz del Rio, V. i Sanchez-Almazo, I., 2006. High-resolution stratigraphy of the Mediterranean outflow contourite system in the Gulf of Cadiz during the late Pleistocene: The impact of Heinrich events; Marine Geology, 227: 241-262.

MacAyeal, D.R., 1995. Challenging an ice-core paleothermometer; Science, 270: 444-445.

Magny, M., Miramont, C. i Sivan, O., 2002. Assessment of the impact of climate and anthropoenic factors on Holocene Mediterranean vegetation in Europe on the basis of palaeohydrological records; Palaeogeography, Palaeoclimatology, Palaeoecology, 186: 47-59.

Maheras, P., Xoplaki, E., Davies, T., Martin-Vide, J., Bariendos, M. i Alcoforado, M.J., 1999. Warm and cold monthly anomalies across the Mediterranean basin and their relationship with circulation; 1860–1990; International Journal of Climatology, 19: 1697-1715.

Maillard, A. i Mauffret, A., 1999. Crustal structure and riftogenesis of the Valencia Trough (north-western Mediterranean Sea); Basin Research, 11: 357-379.

Maldonado, A. i Stanley, D.J., 1979. Depositional patterns and Late Quaternary evolution of two Mediterranean submarine fans: a comparison; Marine Geology, 31: 215-250.

Maldonado, A. i Canals, M., 1982. El margen continental sur-balear: un modelo deposicional reciente sobre un margen de tipo pasivo; Acta Geologica Hispanica, 17: 241-254.

Maldonado, A., Got, H., Monaco, A., O'Connell, S. i Mirabile, L., 1985a. Valencia Fan (Northwestern Mediterranean): distal deposition fan variant; Marine Geology, 62: 295-319.

Maldonado, A., Palanques, A., Alonso, B., Kastens, K.A., Nelson, C.H., O'Connell, S. i Ryan, W.B.F., 1985b. Physiography and deposition on a distal deep-sea system: the Valencia Fan (Northwestern Mediterranean); Geo-Marine Letters, 5: 157-164.

Martín-Puertas, C., Jiménez-Espejo, F., Martínez-Ruiz, F., Nieto-Moreno, V., Rodrigo, M., Mata, M.P. i Valero-Garcés, B.L., 2010. Late Holocene climate variability in the southwestern Mediterranean region: an integrated marine and terrestrial geochemical approach; Climate of the Past, 6: 807-816.

Martín-Vide, J. i Lopez-Bustins, J.-A., 2006. The Western Mediterranean Oscillation and rainfall in the Iberian peninsula; International Journal of Climatology, 26: 1455-1475.

Martin, J.-M., Elbaz-Poulichet, F., Guieu, C., Loyë-Pilot, M.-D. i Han, G., 1989. River versus atmospheric input of material to the Mediterranean Sea: an overview; Marine Chemistry 28: 159-182.

Martínez-Ruiz, F., Paytan, A., Kastner, M., Gonzalez-Donoso, J.M., Linares, D., Bernasconi, S.M. i Jimenez-Espejo, F.J., 2003. A comparative study of the geochemical and mineralogical characteristics of the S1 sapropel in the western and eastern Mediterranean; Palaeogeography, Palaeoclimatology, Palaeoecology, 190: 23-37.

Martinson, D.G., Pisias, N.G., Hays, J.D., Imbrie, J., Moore, T.C. i Shackleton, N., 1987. Age dating and the orbital theory of the ice ages: development of a high-resolution 0 to 300,000-years chronostratigraphy; Quaternary Research, 27: 1-29.

Martrat, B., Grimalt, J.O., Lopez-Martinez, C., Cacho, I., Sierro, F.J., Flores, J.A., Zahn, R., Canals, M., Curtis, J.H. i Hodell, D.A., 2004. Abrupt temperature changes in the Western Mediterranean over the past 250,000 years; Science, 306: 1762-1765.

Mather, A.E., 2009. Tectonic setting and landscape development, In: Woodward, J.C. (Ed.), The physical geography of the Mediterranean; Oxford University Press, Oxford, Regne Unit, p. 5-32.

Matthewson, A.P., Shimmield, G.B., Kroon, D. i Fallick, A.E., 1995. A 300 kyr high-resolution aridity record of the North African continent; Paleoceanography, 10: 677-692.

Matthiesen, S. i Haines, K., 2003. A hydraulic box model study of the Mediterranean response to postglacial sea-level rise; Paleoceanography, 18, (4), 1084, doi:1010.1029/2003PA000880.

Mauffret, A., Auzende, J., Olivet, J.L. i Pautot, G., 1972. Le bloc continental Baleare (Espagne)--Extension et evolution; Marine Geology, 12: 289-300.

Mauffret, A., Labarbarie, M. i Montadert, L., 1982. Les affleurements de series sedimentaires pre-pliocenes dans le bassin Mediterraneen nord-occidental; Marine Geology, 45: 159-175.

Mayewski, P.A., Rohling, E.E., Stager, J.C., Karlen, W., Maasch, K.A., Meeker, L.D., Meyerson, E.A., Gasse, F., van Kreveld, S. i Holmgren, K., 2004. Holocene climate variability; Quaternary Research, 62, 243-255.

McCave, I.N., Bryant, R.J., Cook, H.F. i Coughanowr, C.A., 1986. Evaluation of a laser-diffraction-size analyzer for use with natural sediments; Journal of Sedimentary Research, 56: 561-564.

McCave, I.N. i Tucholke, B.E., 1986. Deep current-controlled sedimentation in the western North Atlantic, In: Vogt, P.R., Tucholke, B.E. (Eds.), The Geology of North America, Vol. M, The Western North Atlantic Region: The Geological Society of America, p. 451-468.

McCave, I.N., Manighetti, B. i Beveridge, N.A.S., 1995a. Circulation in the glacial North Atlantic inferred from grain-size measurements; Nature, 374: 149-151.

McCave, I.N., Manighetti, B. i Robinson, S.G., 1995b. Sortable silt and fine sediment size/composition slicing: parameters for palaeocurrent speed and palaeoceanography; Paleoceanography, 10: 593-610.

McCave, I.N. i Hall, A., 2006. Size sorting in marine muds: Processes, pitfalls, and prospects for paleoflow-speed proxies; Geochemistry Geophysics Geosystems, 7, Q10N05, doi:10.1029/2006GC001284.

McCave, I.N., Hall, I.R. i Bianchi, G.G., 2006. Laser vs. settling velocity differences in silt grainsize measurements: estimation of palaeocurrent vigour; Sedimentology, 53: 919-928.

McDermott, F., Frisia, S., Huang, Y., Longinelli, A., Spiro, B., Heaton, T.H.E., Hawkesworth, C.J., Borsato, A., Keppens, E. i Fairchild, I.J., 1999. Holocene climate variability in Europe: Evidence from d18O, textural and extension-rate variations in three speleothems; Quaternary Science Reviews, 18: 1021-1038.

MEDOC-group, 1970. Observation of formation of Deep Water in the Mediterranean Sea, 1969; Nature, 227: 1037-1040.

Meese, D.A., Gow, A.J., Alley, R.B., Zielinski, P.M., Grootes, G.A., Ram, M., Taylor, K.C., Mayewski, P.A. i Bolzan, J.F., 1997. The Greenland Ice Sheet Project 2 depth-age scale: Methods and results; Journal of Geophysical Research, 102: 26411-26423.

Mercone, D., Thomson, J. i Croudace, I.W., 2000. Duration of S1, the most recent sapropel in the eastern Mediterranean Sea, as indicated by accelerator mass spectrometry radiocarbon and geochemical evidence; Paleoceanography, 15: 336-347.

Meulenkamp, J.E. i Sissingh, W., 2003. Tertiary palaeogeography and tectonostratigraphic evolution of the Northern and Southern Peri-Tethys platforms and the intermediate domains of the African–Eurasian convergent plate boundary zone; Palaeogeography, Palaeoclimatology, Palaeoecology, 196: 209-228.

Miller, K.G., Wright, J.D. i Fairbanks, R.G., 1991. Unlocking the ice house: Oligocene-Miocene oxygen isotopes, eustasy and margin erosion; Journal of Geophysical Research, 96: 6829-6948.

Miller, K.G., Kominz, M.A., Browning, J.V., Wright, J.D., Mountain, G.S., Katz, M.E., Sugarman, P.J., Cramer, B.S., Christie-Blick, N. i Pekar, S.F., 2005. The Phanerozoic record of global sea-level change; Science, 310: 1293-1298.

Millot, C. i Monaco, A., 1984. Deep strong currents and sediment transport in the northwestern Mediterranean Sea; Geo-Marine Letters, 4: 13-17.

Millot, C., 1999. Circulation in the Western Mediterranean Sea; Journal of Marine Systems, 20: 423-442.

Millot, C. i Taupier-Letage, I., 2005. Circulation in the Mediterranean Sea, In: The Handbook of Environmental Chemestry; Springer-Verlag, Berlin-Heidelberg, Alemania, p. 29-66.

Morellón, M., Valero-Garcés, B., Vegas-Vilarrúbia, T., González-Sampériz, P., Romero, Ó., Delgado-Huertas, A., Mata, P., Moreno, A., Rico, M. i Corella, J.P., 2009. Lateglacial and Holocene palaeohydrology in the western Mediterranean region: The Lake Estanya record (NE Spain); Quaternary Science Reviews, 28: 2582-2599.

Moreno, A., Targarona, J., Henderiks, J., Canals, M., Freudenthal, T. i Meggers, H., 2001. Orbital forcing of dust supply to the North Canary Basin over the last 250 kyrs; Quaternary Science Reviews, 20: 1327-1339.

Moreno, A., 2002. Registro del aporte de polvo de origen sahariano y de la productividad oceánica en la Cuenca del Norte de Canrias y en el Mar de Alborán. Respuesta a los últimos 250.000 años de cambio climático.Tesi Doctoral, Universitat de Barcelona, 230 p.

Moreno, A., Cacho, I., Canals, M., Prins, M.A., Sanchez-Goni, M.-F., Grimalt, J.O. i Weltje, G.J., 2002. Saharan dust transport and high-latitude glacial climatic variability: the Alboran Sea record; Quaternary Research, 58: 318-328.

Moreno, A., Cacho, I., Canals, M., Grimalt, J.O. i Sanchez-Vidal, A., 2004. Millennial-scale variability in the productivity signal from the Alboran Sea record, Western Mediterranean Sea; Palaeogeography, Palaeoclimatology, Palaeoecology, 211: 205-219.

Moreno, A., Cacho, I., Canals, M., Grimalt, J.O., Sanchez-Goni, M.F., Shackleton N. i Sierro, F.J., 2005. Links between marine and atmospheric processes oscillating on a

millennial time-scale. A multi-proxy study of the last 50,000 yr from the Alboran Sea (Western Mediterranean Sea); Quaternary Science Reviews, 24: 1623-1636.

Moreno, A., López-Merino, L., Leira, M., Marco-Barba, J., González-Sampériz, P., Valero-Garcés, B., López-Sáez, J., Santos, L., Mata, P. i Ito, E., 2011. Revealing the last 13,500 years of environmental history from the multiproxy record of a mountain lake (Lago Enol, northern Iberian Peninsula); Journal of Paleolimnology, 46: 327-349.

Moreno, A., Pérez, A., Frigola, J., Nieto-Moreno, V., Rodrigo-Gámiz, M., Martrat, B., González-Sampériz, P., Morellón, M., Martín-Puertas, C., Corella, J.P., Belmonte, Á., Sancho, C., Cacho, I., Herrera, G., Canals, M., Grimalt, J.O., Jiménez-Espejo, F., Martínez-Ruiz, F., Vegas-Vilarrúbia, T. i Valero-Garcés, B.L., 2012. The Medieval Climate Anomaly in the Iberian Peninsula reconstructed from marine and lake records; Quaternary Science Reviews, 43: 16-32.

Nederbragt, A.J. i Thurow, J., 2005. Geographic coherence of millennial-scale climate cycles during the Holocene; Palaeogeography, Palaeoclimatology, Palaeoecology, 221: 313-324.

Nelson, C.H. i Maldonado, A., 1990. Factors controlling late Cenozoic continental margin growth from the Ebro Delta to the western Mediterranean deep sea; Marine Geology, 95: 419-440.

North Greenland Ice Core Project (NGRIP) members, 2004. High-resolution record of Northern Hemisphere climate extending into the last interglacial period; Nature, 431: 147-151.

O'Brien, S.R., Mayewski, P.A., Meeker, L.D., Meese, D.A., Twickler, M.S. i Whitlow S.I., 1995. Complexity of Holocene climate as reconstructed from a Greenland Ice core; Science, 270: 1962-1964.

Oppo, D.W., McManus, J.F. i Cullen, J.L., 2003. Deepwater variability in the Holocene epoch; Nature, 422: 277-278.

Paillard, D., Labeyrie, L. i Yiou, P., 1996. Macintosh program performs time-series analysis; Eos Trans., AGU, 77, 379.

Palanques, A., Kenyon, N.H., Alonso, B. i Limonov, A., 1995. Erosional and depositional patterns in the Valencia channel mouth: an example of a modern channel-lobe transition zone; Marine Geophysical Researches, 17: 503-517.

Palanques, A., Durrieu de Madron, X., Puig, P., Fabres, J., Guillen, J., Calafat, A., Canals, M., Heussner, S. i Bonnin, J., 2006. Suspended sediment fluxes and transport processes in the Gulf of Lions submarine canyons. The role of storms and dense water cascading; Marine Geology, 234 (1-4): 43-61.

Pasqual, C., Sanchez-Vidal, A., Zúñiga, D., Calafat, A., Canals, M., Durrieu de Madron, X., Puig, P., Heussner, S., Palanques, A. i Delsaut, N., 2010. Flux and composition of settling particles across the continental margin of the Gulf of Lion: the role of dense shelf water cascading; Biogeosciences, 7: 217-231.

Perez-Folgado, M., Sierro, F.J., Flores, J.A., Cacho, I., Grimalt, J.O., Zahn, R. i Shackleton, N., 2003. Western Mediterranean planktonic foraminifera events and millennial climatic variability during the last 70 kyr; Marine Micropaleontology, 48: 49-70.

Pinardi, N. i Masetti, E., 2000. Variability of the large scale general circulation of the Mediterranean Sea from observations and modelling: a review; Palaeogeography, Palaeoclimatology, Palaeoecology, 158: 153-173.

Pollak, M.I., 1951. The sources of deep water in the Eastern Mediterranean Sea; Journal of Marine Research, 10: 128-152.

Pont, D., Simonnet, J.P. i Walter, A.V., 2002. Medium-term changes in suspended sediment delivery to the ocean: Consequences of catchment heterogeneity and river management (Rhône River, France); Estuarine, Coastal and Shelf Science, 54: 1-18.

Posamentier, H.W. i Vail, P.R., 1988. Eustatic controls on clastic deposition II - sequence and systems tract models, In: Wilgus, C.K., Hastings, B.S., Kendall, C.G.S.C., Posamentier, H., Ross, C.A., Van Wagoner, J.C. (Eds.), Sea-level changes: an integrated approach; Society of Economic Paleontologists and Mineralogists, Tulsa, Oklahoma, EE.UU, p. 125-154.

Posamentier, H.W., Allen, G.P., James, D.P. i Tesson, M., 1992. Forced regressions in a sequence stratigraphic framework: concepts, examples, and exploration significance; American Association of Petroleum Geologists Bulletin, 76: 1687-1709.

Potter, R.A. i Lozier, M.S., 2004. On the warming and salinification of the Mediterranean outflow waters in the North Atlantic; Geophysical Research Letters, 31, L01202, doi:01210.01029/02003GL018161.

Potts, P.J. i Webb, P.C., 1992. X-ray fluorescence spectrometry; Journal of Geochemical Exploration, 44: 251-296.

Prentice, I.C., Harrison, S.P., Jolly, D. i Guiot, J., 1998. The climate and biomes of Europe at 6000 yr BP: comparison of model simulations and pollen-based reconstructions; Quaternary Science Reviews, 17: 659-668.

Prospero, J.M., 1996. Saharan dust transport over the North Atlantic ocean and Mediterranean: an overview, In: Guerzoni, S., Chester, R. (Eds.), The impact of desert dust across the Mediterranean; Kluwer Academic Publishers, Holanda, p. 133-151.

Puig, P., Palanques, A., Orange, D.L., Lastras, G. i Canals, M., 2008. Dense shelf water cascades and sedimentary furrow formation in the Cap de Creus Canyon, northwestern Mediterranean Sea; Continental Shelf Research, 28: 2017-2030.

Rabineau, M., Berné, S., Ledrezen, E., Lericolais, G., Marsset, T. i Rotunno, M., 1998. 3D architecture of lowstand and transgressive Quaternary sand bodies on the outer shelf of the Gulf of Lion, France; Marine and Petroleum Geology, 15: 439-452.

Rabineau, M., 2001. Un modèle géométrique et stratigraphique des séquences de dépôts quaternaires de la plate-forme du Golfe du Lion: enregistrement des cycles glacioeustatiques de 100000 ans; Tesi Doctoral. Université de Rennes 1 and IFREMER, Rennes, 2 volums, 392 p. i 70 p., http://www.ifremer.fr/docelec/.

Rabineau, M., Berne, S., Aslanian, D., Olivet, J.-L., Joseph, P., Guillocheau, F., Bourillet, J.-F., Ledrezen, E. i Granjeon, D., 2005. Sedimentary sequences in the Gulf of Lion: A record of 100,000 years climatic cycles; Marine and Petroleum Geology, 22: 775-804.

Rahmstorf, S., 1998. Influence of Mediterranean Outflow on climate; Eos Trans., AGU, 79: 281-282.

Ramirez-Llodrà, E., De Mol, B., Company, J.B., Coll, M. i Sardà, F., 2012. Effects of natural and anthropogenic processes in the distribution of marine litter in the deep Mediterranean Sea; Progress in Oceanography, sotmés.

Reguera, I., 2004. Respuesta del Mediterráneo Occidental a los cambios climáticos bruscos ocurridos durante el último ciclo glacial: estudio de las asociaciones de foraminíferos, Tesi Doctoral, Dept. de Geología. Universidad de Salamanca, 231 p.

Reichart, G.J., den Dulk, M., Visser, H.J., van der Weijden, C.H. i Zachariasse, W.J., 1997. A 225 kyr record of dust supply, paleoproductivity and the oxygen minimum zone from the Murray Ridge (northern Arabian Sea); Palaeogeography, Palaeoclimatology, Palaeoecology, 134: 149-169.

Reid, J.L., 1979. On the contribution of the Mediterranean Sea outflow to the Norwegian-Greenland Sea; Deep Sea Research, 26A: 1199-1223.

Reid, J.L., 1994. On the total geostrophic circulation of the North Atlantic Ocean: Flow patterns, tracers, and transports; Progress in Oceanography, 33: 1-92.

Richter, T.O., Van der Gaast, S.J., Koster, B., Vaars, A., Gieles, R., De Stigter, H.C., de Haas, H. i Van Weering, T.C.E., 2006. The Avaatech XRF core scanner: technical description and applications to NE Atlantic sediments, In: Society, L.G. (Ed.), New techniques in sediment core analysis; Geological Society, London, Special Publications, 267, p. 39-50.

Robinson, A.R., Malanotte-Rizzoli, P., Hecht, A., Michelato, A., Roether, W., Theocharis, A., Ünlüata, Ü., Pinardi, N., Artegiani, A., Bergamasco, A., Bishop, J., Brenner, S., Christianidis, S., Gacic, M., Georgopoulos, D., Golnaraghi, M., Hausmann, M., Junghaus, H.G., Lascaratos, A., Latif, M.A., Leslie, W.G., Lozano, C.J., Og˛uz, T., Özsoy, E., Papageorgiou, E., Paschini, E., Rozentroub, Z., Sansone, E., Scarazzato, P., Schlitzer, R., Spezie, G.C., Tziperman, E., Zodiatis, G., Athanassiadou, L., Gerges, M. i Osman, M., 1992. General circulation of the Eastern Mediterranean; Earth-Science Reviews, 32: p. 285-309.

Robinson, A.R. i Golnaraghi, M., 1994. The physical and dynamical oceanography of the Mediterranean Sea, In: Malanotte-Rizzoli, P., Robinson, A.R. (Eds.), Ocean Processes in Climate Dynamics: Global and Mediterranean Examples; Kluwer Academic Publishers, Holanda, 419, p. 255-306.

Rodó, X., Baert, E. i Comin, F.A., 1997. Variations in seasonal rainfall in Southern Europe during the present century: relationships with the North Atlantic Oscillation and the El Niño-Southern Oscillation; Climate Dynamics, 13: 275-284.

Roether, W., Manca, B.B., Klein, B., Bregant, D., Georgopoulos, D., Beitzel, V., Kovačević, V. i Luchetta, A., 1996. Recent Changes in Eastern Mediterranean deep waters; Science, 271: 333-335.

Rogerson, M., Rohling, E.J. i Weaver, P.P.E., 2006. Promotion of meridional overturning by Mediterranean-derived salt during the last deglaciation; Paleoceanography, 21, PA4101, doi:4110.1029/2006PA001306.

Rohling, E.J. i Hilgen, F.J., 1991. The eastern Mediterranean climate at times of sapropel formation: a review; Geologie en Mijnbouw, 70: 253-264.

Rohling, E.J., 1994. Review and new aspects concerning the formation of eastern Mediterranean sapropels; Marine Geology, 122: 1-28.

Rohling, E.J., den Dulk, M., Pujol, C. i Vergnaud-Grazzini, C., 1995. Abrupt hydrographic change in the Alboran Sea (western Mediterranean) around 8000 yrs BP; Deep Sea Research, 42: 1609-1619.

Rohling, E.J., Jorissen, F.J. i de Stigter, H.C., 1997. 200 Year interruption of Holocene sapropel formation in the Adriatic Sea; Journal of Micropaleontology, 16: 97-108.

Rohling, E.J., Fenton, M., Jorissen, F.J., Bertrand, P., Ganssen, G. i Caulet, J.P., 1998a. Magnitudes of sea-level lowstands of the past 500,000 years; Nature, 394: 162-165.

Rohling, E.J., Hayes, A., Rijk, D., Kroon, D., Zachariasse, W.J. i Eisma, D., 1998b. Abrupt cold spells in the northwest Mediterranean; Paleoceanography, 13: 316-322.

Rohling, E.J., Mayewski, P.A., Abu-Zied, R.H., Casford, J.S.L. i Hayes, A., 2002. Holocene atmosphere-ocean interactions: records from Greenland and the Aegean Sea; Climate Dynamics; 18: 587-593.

Rohling, E.J., Marsh, R., Wells, N.C., Siddall, M. i Edwards, N.R., 2004. Similar meltwater contributions to glacial sea level changes from Antarctic and northern ice sheets; Nature, 430: 1016-1021.

Rohling, E.J. i Pälike, H., 2005. Centennial-scale climate cooling with a sudden cold event around 8,200 years ago; Nature, 434: 975-979.

Rohling, E.J., Grant, K., Hemleben, C., Kucera, M., Roberts, A.P., Schmeltzer, I., Schulz, H., Siccha, M., Siddall, M. i Trommer, G., 2008. New constrains on the timing of sea level fluctuations during early to middle isotope stage 3; Paleoceanography, 23, PA3219, doi:10.1029/2008PA001617.

Rohling, E.J., Abu-Zied, R.H., Casford, J.S.L., Hayes, A. i Hoogakker, B.A.A., 2009a. The marine environment: present and past, In: Woodward, J. (Ed.), The physical geography of the Mediterranean; Oxford University Press, Oxford, Regne Unit, p. 33-67.

Rohling, E.J., Grant, K., Bolshaw, M., Roberts, A.P., Siddall, M., Hemleben, C. i Kucera, M., 2009b. Antarctic temperature and global sea level closely coupled over the past five glacial cycles; Nature Geoscience, 2: 500-504.

Rollinson, H., 1993. Using geochemical data. Evaluation, presentation, interpretation. Ed. Longman Scientific and Technical, Nova York, EE.UU, 352 p.

Rosenbaum, G., Lister, G.S. i Duboz, C., 2002. Reconstruction of the tectonic evolution of the western Mediterranean since the Oligocene, In: Rosenbaum, G., Lister, G.S. (Eds.), Reconstruccion of the evolution of the Alpine-Himalayan Orogen; Journal of the Virtual Explorer, 8: p. 107-130.

Rothwell, R.G., 2006. New techniques in sediment core analysis: an introduction, In: Society, L.G. (Ed.), New techniques in sediment core analysis; Geological Society of London, Special Publications, 267: p. 1-29.

Roucoux, K.H., Shackleton, N., De Abreu, L., Schönfeld, J. i Tzedakis, P.C., 2001. Combined marine proxy and pollen analyses reveal rapid Iberian vegetation response to North Atlantic millennial-scale climate oscillations; Quaternary Research, 56: 128-132.

Roucoux, K.H., Tzedakis, P.C., de Abreu, L. i Shackleton, N.J., 2006. Climate and vegetation changes 180,000 to 345,000 years ago recorded in a deep-sea core off Portugal; Earth and Planetary Science Letters, 249: 307-325.

Ruddiman, W., 2001. Earth's climate: past and future; W.H. Freeman and Company, Nova York, 465 p.

Ruddiman, W.F., 2003. Orbital insolation, ice volume, and greenhouse gases; Quaternary Science Reviews, 22: 1597-1629.

Rühlemann, C., Müller, P.J. i Schneider, R., 1999. Organic carbon and carbonate as paleoproductivity proxies: examples from high and low productivity areas of the tropical Atlantic, In: Fischer, G., Wefer, G. (Eds.), Use of Proxies in Paleoceanography: Examples from the South Atlantic; Springer-Verlag, Berlin-Heidelberg-Nova York, p. 1-31.

Ryan, W.B.F., 2009. Decoding the Mediterranean salinity crisis; Sedimentology, 56: 95-136.

Salvadó, J.A., Grimalt, J.O., López, J.F., Palanques, A., Heussner, S., Pasqual, C., Sanchez-Vidal, A. i Canals, M., 2012. The role of dense shelf water cascading in the transfer of organochlorine compounds to open marine waters; Environmental Science & Technology, 46: 2614-2632.

Sanchez-Vidal, A., Pasqual, C., Kerhervé, P., Calafat, A., Heussner, S., Palanques, A., Durrieu de Madron, X., Canals, M. i Puig, P., 2008. Impact of dense shelf water cascading on the transfer of organic matter to the deep western Mediterranean basin; Geophysical Research Letters, 35, doi:10.1029/2007GL032825, 5.

Sanchez-Vidal, A., Canals, M., Calafat, A., Lastras, G., Pedrosa-Pàmies, R., Menéndez, M., Medina, R., Company, J.B., Hereu, B., Romero, J. i Alcoverro, T., 2012. Impacts on the deep-sea ecosystem by a severe coastal storm; PLoS ONE, 7 (1): e30395, doi:10.1371/journal.pone.0030395.

Sánchez Goñi, M.F., Cacho, I., Turon, J.-L., Guiot, J., Sierro, F.J., Peypouquet, J.-P., Grimalt, J.O. i Shackleton, N.J., 2002. Synchroneity between marine and terrestrial responses to millenial scale climatic variability during the last glacial period in the Mediterranean region; Climate Dynamics, 19: 95-105.

Sbaffi, L., Wezel, F.C., Curzi, G. i Zoppi, U., 2004. Millennial- to centennial-scale palaeoclimate variations during Termination I and the Holocene in the central Mediterranean Sea; Global and Planetary Change, 40: 201-217.

Schott, F. i Leaman, K.D., 1991. Observations with moored acoustic doppler current profiles in the convection regime in the Gulfe de Lion; Journal of Physical Oceanography, 13: 316-322.

Schulz, M. i Paul, A., 2002. Holocene climate variability on centennial-to-millennial time scales: 1. Climate records from the North-Atlantic realm, In: Wefer, G., Berger, W., Behre, K.-E., Jansen, E. (Eds.), Climate development and history of the North Atlantic realm; Springer-Verlag, Berlin-Heidelberg-Nova York, p. 41-54.

Séranne, M., Benedicto, A., Labaum, P., Truffert, C. i Pascal, G., 1995. Structural style and evolution of the Gulf of Lion Oligo-Miocene rifting: role of the Pyrenean orogeny; Marine and Petroleum Geology, 12: 809-820.

Shackleton, N.J., 2000. The 100,000-Year ice-age cycle identified and found to lag lemperature, carbon dioxide, and orbital eccentricity; Science, 289: 1897-1902.

Shackleton, N.J., Hall, M.A. i Vincent, E., 2000. Phase relationships between millennial-scale events 64,000-24,000 years ago; Paleoceanography, 15: 565-569.

Siddall, M., Rohling, E.J., Almogi-Labin, A., Hemleben, C., Meischner, D., Schmelzer I. i Smeed, D.A., 2003. Sea-level fluctuations during the last glacial cycle; Nature, 423: 853-858.

Siddall, M., Chappell, J. i Potter, E.-K., 2006a. Eustatic sea level during past interglacials., In: Sirocko, F., Litt, T., Claussen, M., Sanchez Goñi, M.-F. (Eds.), The climate of past interglacials; Elsevier, Amsterdam, Holanda, p.75-92.

Siddall, M., Stocker, T.F., Spahni, R., Blunier, T., McManus, J. i Bard, E., 2006b. Using a maximum simplicity paleoclimate model to simulate millennial variability during the last four glacial cycles; Quaternary Science Reviews, 25, 3185-3197, doi:3110.1016/j.quascirev.2005.3112.3014.

Siddall, M., Rohling, E.J., Thompson, W.G. i Waelbroeck, C., 2008. MIS 3 sea level fluctuations: data synthesis and new outlook; Review of Geophysics, 46, RG4003, doi:10.1029/2007RG000226.

Sierro, F.J., Hodell, D.A., Curtis, J.H., Flores, J.A., Reguera, I., Colmenero-Hidalgo, E., Bárcena, M.A., Grimalt, J.O., Cacho, I., Frigola, J. i Canals, M., 2005. Impact of iceberg melting on Mediterranean thermohaline circulation during Heinrich events; Paleoceanography, 20, PA2019, doi:2010.1029/2004PA001051.

Sierro, F.J., Andersen, N., Bassetti, M.A., Berné, S., Canals, M., Curtis, J.H., Dennielou, B., Flores, J.A., Frigola, J., Gonzalez-Mora, B., Grimalt, J.O., Hodell, D.A., Jouet, G., Pérez-Folgado, M. i Schneider, R., 2009. Phase relationship between sea level and abrupt climate change; Quaternary Science Reviews, 28: 2867-2881.

Sima, A., Paul, A. i Schulz, M., 2004. The Younger Dryas--an intrinsic feature of late Pleistocene climate change at millennial timescales; Earth and Planetary Science Letters, 222: 741-750.

Skinner, L.C. i McCave, I.N., 2003. Analysis and modelling of gravity- and piston coring based on soil mechanics; Marine Geology, 199: 181-204.

Skinner, L.C. i Shackleton, N., 2003. Millennial-scale variability of deep-water temperature and d18Odw indicating deep-water source variations in the Northeast Atlantic, 0-34 cal. ka BP; Geochemistry Geophysics Geosystems, 4, 1098, doi:1010.1029/2003GC000585.

Skinner, L.C., Elderfield, H. i Hall, M., 2007. Phasing of millennial climate events and Northeast Atlantic deep-water temperature change since 50 ka BP, In: Schmittner, A., Chiang, J.C.H., Hemming, S.R. (Eds.), Ocean Circulation: Mechanisms and Impacts; AGU Geophysical Monograph Series, p. 197-208.

St-Onge, G., Mulder, T., Francus, P. i Long, B., 2007. Continuous Physical Properties of Cored Marine Sediments, In: Claude, H.M., Anne De, V. (Eds.), Developments in Marine Geology; Elsevier, p. 63-98.

Stabholz, M., Durrieu de Madron, X., Canals, M., Khripounoff, A., Taupier-Letage, I., Testor, P., Heussner, S., Kerhervé, P., Delsaut, N., Houpert, L., Lastras, G. i Dennielou, B., 2012. Impact of open-ocean convection on particle fluxes and sediment dynamics in the deep margin of the Gulf of Lion; Biogeosciences, sotmés.

Stampfli, G.M. i Borel, G.D., 2002. A plate tectonic model for the Paleozoic and Mesozoic constrained by dynamic plate boundaries and restored synthetic oceanic isochrons; Earth and Planetary Science Letters, 196: 17-33.

Steig, E.J., 1999. Mid-Holocene Climate Change; Science, 286: 1485-1487.

Stein, R., Hefter, J., Grützner, J., Voelker, A. i Naafs, B.D.A., 2009. Variability of surface water characteristics and Heinrich-like events in the Pleistocene midlatitude North

Atlantic Ocean: biomarker and XRD records from IODP Site U1313 (MIS 16-9); Paleoceanography, 24, PA2203, doi:10.1029/2008PA001639.

Stocker, T.F., Wright, D.G. i Broecker, W.S., 1992. The influence of high-latitude surface forcing on the global thermohaline circulation; Paleoceanography, 7: 529-541.

Stocker, T.F., 1996. The ocean in the climate system: observing and modeling its variability, In: Boutron, C.F. (Ed.), Topics in Atmospheric and Interstellar Physics and Chemistry, European Research Course on Atmospheres; Les Editions de Physique, Les Ulis, France, p. 39-90.

Stocker, T.F., 2000. Past and future reorganizations in the climate system; Quaternary Science Reviews, 19: 301-319.

Stocker, T.F. i Johnsen, S., 2003. A minimum thermodynamic model for the pibolar seesaw; Paleoceanography, 18, 1087, doi: 1010.1029/2003PA000920.

Stow, D.A.V., 1982. Bottom currents and contourites in the North Atlantic; Bulletin de l'Institut de Geóligie du Bassin d'Aquitaine, 31: 151-166.

Stow, D.A.V., Faugères, J.C., Howe, J.A., Pudsey, C.J. i Viana, A.R., 2002. Bottom currents, contourites and deep-sea sediment drifts: current state-of-the-art, In: Stow, D.A.V., Pudsey, C.J., Howe, J.A., Faugères, J.C., Viana, A.R. (Eds.), Deep-water contourite systems: modern drifts and ancient series, seismic and sedimentary characteristics; Geological Society Memoir, Londres, p. 7-20.

Stuiver, M. i Reimer, P.J., 1993. Extended 14C database and revised CALIB radiocarbon calibration program; Radiocarbon, 35: 215-230.

Stuut, J.-B., 2001. Late Quaternary Southwestern African terrestrial-climate signals in the marine record of Walvis Ridge, SE Atlantic Ocean. Tesi Doctoral, Utrecht University, Utrecht, 129 p.

Svensson, A., Andersen, K.K., Bigler, M., Clausen, H.B., Dahl-Jensen, D., Davies, S.M., Johnsen, S.J., Muscheler, R., Parrenin, F., Rasmussen, S.O., Röthlisberger, R., Seierstad, I., Steffensen, J.P. i Vinther, B.M., 2008. A 60000 year Greenland stratigraphic ice core chronology; Climate of the Past, 4: 47-57.

Telford, R.J., Heegaard, E. i Birks, H.J.B., 2004. All age-depth models are wrong: but how badly?; Quaternary Science Reviews, 23: 1-5.

Tesson, M., Gensous, B., Allen, G.P. i Ravenne, C., 1990. Late Quaternary deltaic lowstand wedges on the Rhône continental shelf, France; Marine Geology, 91: 325-332.

Tesson, M., Allen, G.P. i Ravenne, C., 1993. Late Pleistocene shelf-perched lowstand wedges on the Rhone continental shelf, In: Posamentier, H., Summerhayes, C., Haq, B.U., Allen, G.P. (Eds.), Sequence stratigraphy and facies associations, IAS Special Publications, 18; Blackwell Science Publishers, Oxford, Regne Unit, p. 183-196.

Tesson, M., Posamentier, H.W. i Gensous, B., 2000. Stratigraphic organization of late pleistocene deposits of the western part of the Golfe du Lion shelf (Languedoc shelf), Western Mediterranean Sea, using high-resolution seismic and core data; American Association of Petroleum Geologists Bulletin, 84: 119-150.

Thompson, W.G. i Goldstein, S.L., 2005. Open-System Coral Ages Reveal Persistent Suborbital Sea-Level Cycles; Science, 308: 401-404.

Thompson, W.G. i Goldstein, S.L., 2006. A radiometric calibration of the SPECMAP timescale; Quaternary Science Reviews, 25: 3207-3215.

Tomczak, M. i Godfrey, J.S., 2003. Regional oceanography: an introduction; Daya Publishing House, Delhi, 390 p.

Toucanne, S., Mulder, T., Schonfeld, J., Hanquiez, V., Gonthier, E., Duprat, J., Cremer, M. i Zaragosi, S., 2006. Contourites of the Gulf of Cadiz: A high-resolution record of the paleocirculation of the Mediterranean outflow water during the last 50,000 years; Palaeogeography, Palaeoclimatology, Palaeoecology, 246: 354-366.

Toucanne, S., Jouet, G., Ducassou, E., Bassetti, M.-A., Dennielou, B., Angue Minto'o, C.M., Lahmi, M., Touyet, N., Charlier, K., Lericolais, G. i Mulder, T., 2012. A 130,000-year record of Levantine Intermediate Water flow variability in the Corsica Trough, western Mediterranean Sea; Quaternary Science Reviews, 33: 55-73.

Tsimplis, M.N. i Bryden, H.L., 2000. Estimation of the transports through the Strait of Gibraltar; Deep Sea Research Part I: Oceanographic Research Papers, 47: 2219-2242.

Tsimplis, M.N. i Josey, S.A., 2001. Forcing of the Mediterranean Sea by atmospheric oscillations over the North Atlantic; Geophysical Research Letters, 28: 803-806.

Tsimplis, M., Zervakis, V., Josey, S.A., Peneva, E.L., Struglia, M.V., Stanev, E., Theocharis, A., Lionello, P., Malanotte-Rizzoli, P., Artale, V., Tragou, E. i Oguz, T., 2006. Changes in the oceanography of the Mediterranean Sea and their link to climate variability, In: Lionello, P., Malanotte-Rizzoli, P., Boscolo, R. (Eds.), Mediterranean climate variability; Elsevier, Amsterdam, Holanda, p. 227-282.

Tzedakis, P.C., 1999. The last climatic cycle at Kopais, central Greece; Journal of the Geological Society of London, 156: 425-434.

Ulses, C., Grenz, C., Marsaleix, P., Schaaff, E., Estournel, C., Meulé, S. i Pinazo, C., 2005. Circulation in a semi-enclosed bay under influence of strong freshwater input; Journal of Marine Systems, 56: 113-132.

Ulses, C., Estournel, C., Durrieu de Madron, X. i Palanques, A., 2008. Suspended sediment transport in the Gulf of Lions (NW Mediterranean): Impact of extreme storms and floods; Continental Shelf Research, 28: 2048-2070.

UNEP (United Nations Environment Programme), 2003. Riverine transport of water, sediments and pollutans to the Mediterranean Sea. MAP Technical Reports Series 141, Atenes, 111 p.

Vail, P.R., Mitchum, R.M., Jr., Todd, R.G., Widmier, J.M., Thompson, S., III, Sangree, J.B., Bubb, J.N. i Hatleid, W.G., 1977. Seismic stratigraphy and global changes of sea level, In: Payton, C.E. (Ed.), Seismic stratigraphy - applications to hydrocarbon exploration; The American Association of Petroleum Geologists, Tulsa, EE.UU, p. 49-212.

Van der Weijden, C.H., 2002. Pitfalls of normalization of marine geochemical data using a common divisor; Marine Geology, 184: 167-187.

van Kreveld, S.A., Sarnthein, M., Erlenkeuser, H., Grootes, P., Jung, S.J.A., Nadeau, M.-J., Pflaumann, U. i Voelker, A., 2000. Potential links between surging ice sheets, circulation changes, and the Dansgaard-Oeschger cycles in the Irminger Sea, 60-18 kyr; Paleoceanography, 15: 425-442.

Van Os, B.J.H., Lourens, L.J., Hilgen, F.J., de Lange, G.J. i Beaufort, L., 1994. The formation of Pliocene and carbonate cycles in the Mediterranean: Diagenesis, dilution and productivity; Paleoceanography, 9: 601-617.

Vanney, R. i Mougenot, D., 1981. La plate-forme continentale du Portugal et des provinces adjancetes: analyse géomorphologique; Direcção-Geral de Geologia e Minas (Ed.), Memorias dos Serviços Geologicos de Potugal, 28, 86 p.

Velasco, J.P.B., Baraza, J. i Canals, M., 1996. La depresión periférica y el lomo contourítico de Menorca: evidencias de la actividad de corrientes de fondo al N del talud balear; Geogaceta, 20: 359-362.

Vernet, R. i Faure, H., 2000. Isotopic chronology of the Sahara and the Sahel during the late Pleistocene and the early and Mid-Holocene (15,000-6,000 BP); Quaternary International, 68-71: 385-387.

Vidal, L., Labeyrie, L., Cortijo, E., Arnold, M., Duplessy, J.C., Michel, E., Becque, S. i van Weering, T.C.E., 1997. Evidence for changes in the North Atlantic Deep Water linked to meltwater surges during the Heinrich events; Earth and Planetary Science Letters, 146: 13-27.

Voelker, A., 2002. Global distribution of centennial-scale records for marine isotope stage (MIS) 3: a database; Quaternary Science Reviews, 21: 1185-1212.

Voelker, A.H.L., Lebreiro, S.M., Schonfeld, J., Cacho, I., Erlenkeuser, H. i Abrantes, F., 2006. Mediterranean outflow strengthening during northern hemisphere coolings: A salt source for the glacial Atlantic?; Earth and Planetary Science Letters, 245: 39-55.

Waelbroeck, C., Labeyrie, L., Michel, E., Duplessy, J.C., McManus, J.F., Lambeck, K., Balbon, E. i Labracherie, M., 2002. Sea-level and deep water temperature changes derived from benthic foraminifera isotopic records; Quaternary Science Reviews, 21: 295-305.

Watts, W.A., Allen, J.R.M. i Huntley, B., 1996. Vegetation history and palaeoclimate of the last glacial period of Lago Grande di Monticchio, southern Italy; Quaternary Science Reviews, 15: 133-153.

Wanner, H., Brönnimann, S., Casty, C., Gyalistras, D., Luterbacher, J., Schmutz, C., Stephenson, D.B. i Xoplaki, E., 2001. North Atlantic Oscillation - concepts and studies; Surveys in Geophysics, 22: 321-382.

Watts, W.A., Allen, J.R.M. i Huntley, B., 2000. Palaeoecology of three interstadial events during oxygen-isotope Stages 3 and 4: a lacustrine record from Lago Grande di Monticchio, southern Italy; Palaeogeography, Palaeoclimatology, Palaeoecology, 155: 83-93.

Wehausen, R. i Brumsack, H.-J., 1998. The formation of Pliocene Mediterranean sapropels: constrains from high-resolution major and minor element studies, In: Robertson, A.H.F., Emeis, K.-C., Ritcher, C., Camerlenghi, A. (Eds.), Procedings of the Ocean Drilling Program, Scientific Results, College Station, Texas, EE.UU, p. 207-217.

Wehausen, R. i Brumsack, H.-J., 1999. Cyclic variations in the chemical composition of eastern Mediterranean Pliocene sediments: a key for understanding sapropel formation; Marine Geology, 153: 161-176.

Wehausen, R. i Brumsack, H.-J., 2000. Chemical cycles in Pliocene sapropel-bearing and sapropel-barren eastern Mediterranean sediments; Palaeogeography, Palaeoclimatology, Palaeoecology, 158: 325-352.

Weldeab, S., Siebel, W., Wehausen, R., Emeis, K.-C., Schmiedl, G. i Hemleben, C., 2003. Late Pleistocene sedimentation in the Western Mediterranean Sea: implications for

productivity changes and climatic conditions in the catchment areas; Palaeogeography, Palaeoclimatology, Palaeoecology, 190: 121-137.

Weltje, G.J. i Prins, M., 2003. Muddled or mixed? Inferring palaeoclimate from size distributions of deep-sea clastics; Sedimentary Geology, 162: 39-62.

Weltje, G.J. i Tjallingii, R., 2008. Calibration of XRF core scanners for quantitative geochemical logging of sediment cores: Theory and application; Earth and Planetary Science Letters, 274: 423-438.

Wüst, G., 1960. Die tiefenzirkulation des Mittelländischen Meeres in den Kernschichten des Zwischen-und des Tiefenwassers; Deutsche Hydrographische Zeitschrift, 13: 105-131.

Wüst, G., 1961. On the Vertical Circulation of the Mediterranean Sea; Journal of Geophysical Research, 66: 3261-3271.

Yokoyama, Y., Esat, T.M. i Lambeck, K., 2001. Coupled climate and sea-level changes deduced from Huon Peninsula coral terraces of the last ice age; Earth and Planetary Science Letters, 193: 579-587.

Zahn, R., Schönfeld, J., Kudrass, H.-R., Park, M.-H., Erlenkeuser, H. i Grootes, P., 1997. Thermohaline instability in the North Atlantic during melwater events: Stable isotope and ice-rafted detritus records from core S075-26KL, Portuguese margin; Paleoceanography, 12: 696-710.

Zuo, Z., Eisma, D. i Berger, G.W., 1991. Determination of sediment accumulation and mixing rates in the Gulf of Lions, Mediterranean Sea; Oceanologica Acta, 14: 253-262.

ANNEX I. ABREVIATURES

AHP: African Humid Period
AMIGE: Arctic Marine Engineering Geological Expeditions
AMOC: Atlantic Meridional Overturning Circulation
AW: Atlantic Water
CCD: Calcite Compensation Depth
CCiTUB: Centres Científico i Tecnològics de la Universitat de Barcelona
CLs: Condensed Layers
CLIVAR: Climate Variability and Predictability
COHMAP: Cooperative Holocene Mapping Project
DO: Dansgaard-Oeschger
DSWC: Dense Shelf Water Cascading
EMDW: Eastern Mediterranean Deep Water
EMT: Eastern Mediterranean Transient
ENSO: El Niño-Southern Oscillation
EPICA: European Project for Ice Coring in Antarctica
FRX: Fluorescència de raigs X
GIS: Greenland InterStadials
GISP: Greenland Ice Sheet Project
GS: Greenland Stadials
GoL: Golf of Lion
HE: Heinrich event
IMAGES: International Marine past Global Change Studies
IPCC: Intergovernmental Panel on Climate Change
IRD: Ice Rafted Debris/Detritus
ITCZ: Intertropical Convergence Zone
ka: kilo-anys (10^3 anys)
kyr: kilo-years (10^3 anys)
LGM: Last Glacial Maximum
LIW: Levantine Intermediate Water
LSR: Linear Sedimentation Rate
M0-M8: Minorca abrupt events
Ma: Milió d'anys (10^6 years)
MAW: Modified Atlantic Water
MD: Marion Dufresne
MEDOC: Mediterranean Ocean Convection experiment
MIS: Marine Isotope Stage
MMC: Mediterranean Meridional Circulation
MO: Mediterranean Oscillation
MOC: Meridional Overturning Circulation
MOW: Mediterranean Outflow Water

NADW: North Atlantic Deep Water
NAO: North Atlantic Oscillation
NC: Northern Current
NGRIP: North Greenland Ice core Project
NIOZ :Netherlands Institute for Sea Research
ORL: Organic Rich Layer
PRGL: Promess 1 Gulf of Lion
PROMESS1: Profiles across the Mediterranean Sedimentary Systems
psu: practical salinity units
RPU: Regressive Progradational Units
S1: Sapropel 1
SPECMAP: Spectral Mapping Project
SS: Sortable Silt
SST: Sea Surface Temperature
SR: Sedimentation Rate
TIb: Termination Ib
THC: Termohaline Circulation
UNEP: United Nations Environment Programme
UP10: Upper 10 microns fraction
V-PDB: Vienna pee Dee belemnite standard
WeMO: Western Mediterranean Oscillation
WMDW: Western Mediterranean Deep Water
XRD: X-ray diffraction
XRF: X-ray fluorescence
YD: Younger Dryas

ANNEX II. PUBLICACIONS

Clim. Past, 8, 1067–1077, 2012
www.clim-past.net/8/1067/2012/
doi:10.5194/cp-8-1067-2012

Climate of the Past

A 500 kyr record of global sea-level oscillations in the Gulf of Lion, Mediterranean Sea: new insights into MIS 3 sea-level variability

J. Frigola[1], M. Canals[1], I. Cacho[1], A. Moreno[2], F. J. Sierro[3], J. A. Flores[3], S. Berné[4,8], G. Jouet[4], B. Dennielou[4], G. Herrera[1], C. Pasqual[1], J. O. Grimalt[5], M. Galavazi[6], and R. Schneider[7]

[1]CRG Marine Geosciences, Department of Stratigraphy, Paleontology and Marine Geosciences, University of Barcelona, Spain
[2]Pyrenean Institute of Ecology, Spanish Research Council, Zaragoza, Spain
[3]Department of Geology, University of Salamanca, Spain
[4]IFREMER Laboratoire Environnements Sédimentaires, Plouzané, France
[5]Department of Environmental Chemistry, Spanish Research Council, Barcelona, Spain
[6]Fugro Engineers B.V., Leidschendam, The Netherlands
[7]Institut für Geowissenschaften, Christian-Albrechts-Universität zu Kiel, Germany
[8]Université de Perpignan Via Domitia, Perpignan, France

Correspondence to: M. Canals (miquelcanals@ub.edu)

Received: 22 November 2011 – Published in Clim. Past Discuss.: 20 December 2011
Revised: 16 April 2012 – Accepted: 18 May 2012 – Published: 22 June 2012

Abstract. Borehole PRGL1-4 drilled in the upper slope of the Gulf of Lion provides an exceptional record to investigate the impact of late Pleistocene orbitally-driven glacio-eustatic sea-level oscillations on the sedimentary outbuilding of a river fed continental margin. High-resolution grain-size and geochemical records supported by oxygen isotope chronostratigraphy allow reinterpreting the last 500 ka upper slope seismostratigraphy of the Gulf of Lion. Five main sequences, stacked during the sea-level lowering phases of the last five glacial-interglacial 100-kyr cycles, form the upper stratigraphic outbuilding of the continental margin. The high sensitivity of the grain-size record down the borehole to sea-level oscillations can be explained by the great width of the Gulf of Lion continental shelf. Sea level driven changes in accommodation space over the shelf cyclically modified the depositional mode of the entire margin. PRGL1-4 data also illustrate the imprint of sea-level oscillations at millennial time-scale, as shown for Marine Isotopic Stage 3, and provide unambiguous evidence of relative high sea-levels at the onset of each Dansgaard-Oeschger Greenland warm interstadial. The PRGL1-4 grain-size record represents the first evidence for a one-to-one coupling of millennial time-scale sea-level oscillations associated with each Dansgaard-Oeschger cycle.

1 Introduction

Sea level oscillations of about 120 m of amplitude paralleled the orbitally-driven 100-kyr climate cycles of the late Pleistocene in response to global ice volume changes (Imbrie et al., 1992; Siddall et al., 2006). Jointly with sediment input and subsidence, these sea-level oscillations controlled the stratal geometry of passive continental margins where migration of fluvial-influenced deposits generated regressive/transgressive depositional sequences. The seismostratigraphic study of those stacked sequences can help to develop the linkage between sea-level fluctuations and sedimentary unit deposition once the seismic interpretation is placed in a sequence stratigraphy framework (Posamentier and Vail, 1988; Vail et al., 1977). More refined sea-level curves based upon benthic and planktic oxygen isotopes in marine sediment cores, in some cases corrected for temperature variations, and dated uplifted coral terraces have been published during the last decade (Chappell, 2002; Miller et al., 2005; Rohling et al., 1998, 2009; Shackleton et al., 2000; Siddall et al., 2003; Thompson and Goldstein, 2005, 2006; Waelbroeck et al., 2002; Yokoyama et al., 2001). However, intrinsic limitations of sea-level reconstruction methods and limitations of obtaining better and more precise age control of marine

records make difficult the task to accurately constrain orbital and millennial time-scale sea-level fluctuations. Thus, continental margin sedimentary records consisting of depositional units characterised with very high sedimentation rates and precise chronology could provide a better time control and resolution high enough to improve the reconstruction of past sea level oscillations.

In the Gulf of Lion (GoL) margin, western Mediterranean Sea, deltaic forced Regressive Progradational Units (RPUs) stacked on the outer-shelf and upper slope during relative sea-level falls (Fig. 1), led some authors to describe this margin as a forced regressive system (Posamentier et al., 1992; Tesson et al., 1990, 2000). The significant subsidence rate of the margin, 250 m Myr^{-1} at the shelf edge (Rabineau, 2001), eased the preservation of RPUs in the upper slope, as it was continuously submerged even during pronounced lowstands. These significant subsidence rate allowed preserving the majority of the regressive/transgressive depositional sequences across the outer shelf (former coastal deposits from old lowstand coast lines) and the upper slope accumulation where dating is easier, thus, resulting in an ideal area for the study of the late Quaternary sedimentary succession. The huge amount of seismic reflection profiles obtained in the GoL margin facilitated the identification of major unconformities defining sequence boundaries in the outer-shelf that become correlative conformities in the upper slope. There five major RPUs were identified and interpreted to correspond to the last five 100-kyr cycle sea level falls (Fig. 1b) (Bassetti et al., 2008; Rabineau et al., 1998, 2005). However, precise dating of RPUs sequence boundaries was still needed to constrain better the imprint of sea-level oscillations on the GoL margin and to determine the leading cyclicity of the deposition of those units, i.e., if they originated during sea-level lowerings of 20 kyr or 100 kyr cycles (Lobo et al., 2004).

In addition, millennial-scale sea-level oscillations at times of rapid climate change during Marine Isotope Stage (MIS) 3 are of special interest, since determining their amplitude and phasing with ice core records is crucial to understand the behaviour and role of ice sheets on millennial climate variability (Siddall et al., 2008). In fact, MIS 3 relative sea-level rises have been tentatively associated with both contributions from the Antarctic and the Laurentide ice sheets (Arz et al., 2007; Rohling et al., 2008; Siddall et al., 2003, 2008; Sierro et al., 2009), thus, evidencing the lack of consensus on the sea-level response to rapid climate variability.

Here, we present grain-size and geochemical records from a borehole in the GoL upper slope, together with a robust oxygen isotope chronostratigraphy, which allow identifying and accurately dating the main RPUs of the last 500 ka, and obtaining the timing of millennial-scale sea-level changes in response to abrupt climate variability during MIS 3.

2 Setting and present day conditions

The GoL forms a crescent-shaped passive margin that is characterised by a 70 km wide continental shelf covering an area of about 11 000 km^2 (Fig. 1a). The GoL continental shelf was mainly built by late Quaternary glacio-eustatic oscillations and post late glacial sedimentation. The shelf can be subdivided in three distinct parts: (i) the inner shelf, extending from 0 to 90 m, is characterised by gradual and regular morphological gradients, as illustrated by parallel and regularly spaced isobaths; the inner shelf corresponds to the modern deltaic prism (Fig. 1); (ii) the middle shelf, ranging in depths from 90 to 110–120 m, is mostly flat with an irregular morphology, mainly capped by relict offshore sands shoals; and (iii) the outer shelf, a narrow band with depths ranging from 110–120 m that extends to the shelf break and is characterised by a general smooth morphology (Berné et al., 2004a) (Fig. 1a). The shelf break is located at 120–150 m and is indented by numerous submarine canyons and gullies which connect the continental shelf to the deep margin and basin. The overall GoL continental shelf physiography offered a huge accumulation space for water and sediment storage during periods of relative rising and high sea level during late Quaternary deglacial and interglacial intervals, while it remained totally or partly exposed subaerially during late Quaternary sea-level lowerings and lowstand glacial periods.

The Rhone River is the main source of sediment to the GoL shelf while other minor fluvial inputs also occur along the coastline (Pont et al., 2002). Modern fluvial sediments are mainly trapped on the inner shelf, although they can also be remobilised and subsequently transported to the middle and outer shelf and beyond to the upper slope by shelf erosional and re-suspension processes. These processes are mainly driven by dense shelf water formation and cascading events (DSWC) and easterly storms and, to a much lesser extent, by the southwestward general circulation pattern of the Northern Current (NC) (Fig. 1a) (Bassetti et al., 2006; Canals et al., 2006; Dufois et al., 2008; Ulses et al., 2005). In addition to northerly wind-induced DSWC, deep-water formation also occurs offshore during windy winters, where it may lead to deep convection (Millot, 1999). However, the sediment load involved in offshore convection is very low when compared to DSWC and major coastal storms, both constituting the most effective processes of sediment export from the shelf to the basin, mainly through submarine canyons (Canals et al., 2006; Palanques et al., 2006; Pasqual et al., 2010; Sanchez-Vidal et al., 2008, 2012).

3 Material and methods

This study is based on detailed analyses of the 300 m-long continuous sediment record recovered in borehole PRGL1-4 (42°41.39′ N and 03°50.26′ E), drilled at 298 m of water

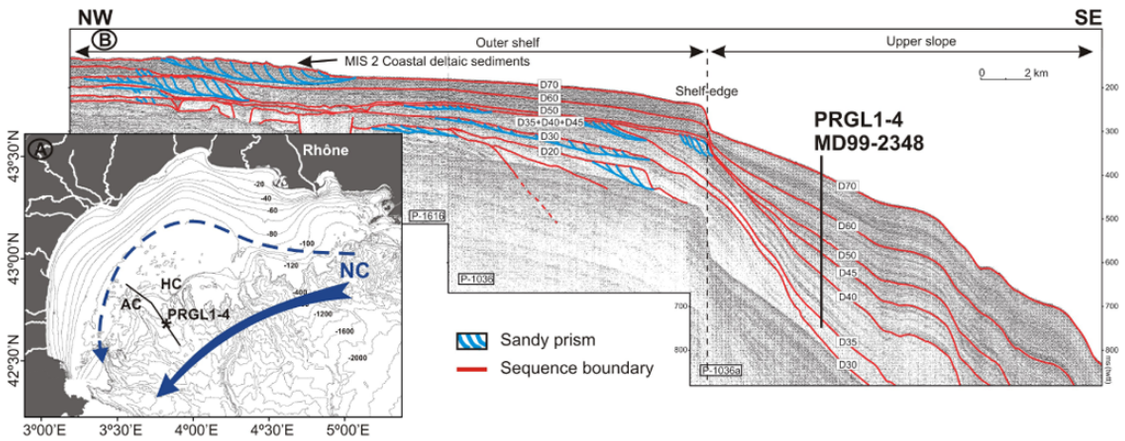

Fig. 1. (A) Bathymetric map of the Gulf of Lion with location of borehole PRGL1-4 in the interfluve separating Aude and Hérault submarine canyons, AC and HC, respectively. The dominant component of the general circulation is shown by the geostrophic Northern Current (NC), which flows southwestward along the slope and occasionally penetrates over the outer shelf, blue arrows. **(B)** Part of high-resolution seismic reflection profile P-1036a crossing the borehole location in a NW–SE direction across the outer shelf and upper slope (modified from Jouet, 2007). Stratigraphic sequences S1 to S5 delimited by main reflectors D35 to D70 marked as defined by Jouet (2007). Red reflectors show the main conformities separating RPUs while the blue ones correspond to sandy prisms.

depth in the interfluve separating Aude and Hérault submarine canyons during *MV Bavenit* PROMESS1 cruise, and on the overlapping 22.77 m long IMAGES core MD99-2348 retrieved at the same location (Fig. 1a).

Grain-size analyses on the bulk and the decarbonated sediment fractions were carried out at 20 cm sampling intervals with a Coulter LS 100 Laser Particle Size Analyser after removing organic matter by treatment with excess H_2O_2 and carbonates by treatment with HCl. Grain-size results are discussed here as the silt/clay ratio of the carbonate-free fraction, an established proxy for energy levels at the time of particle deposition (Frigola et al., 2007). Matching of silt/clay ratio records from both bulk and decarbonated sediments allows discarding the in situ paleoproductivity signal that could affect the grain-size record (Fig. 2b).

Semi-quantitative analysis of major elements (Ca, Fe, Ti and K) was carried out at 4 cm resolution using the first generation Avaatech non-destructive X-ray fluorescence (XRF) core scanner of the University of Bremen. The good correlation of the Ca record with sedimentation rates and with the clay content (not shown here), suggest that Ca delivery at the study site is mainly related to detrital carbonate inputs from fluvial sources. Calcite is at present one of the main mineralogical components in suspended matter delivered by the Rhône River (Pont et al., 2002), which is the most relevant sediment source to the GoL, as previously mentioned. These evidences support the use of the Ca record from borehole PRGL1-4 as a trustable proxy of changes in fluvial sediment delivery to the GoL upper slope (Fig. 2c).

The age model was obtained by synchronizing the records of planktic *Globigerina bulloides* δ^{18}O and abundance of temperate to warm planktic foraminifers to the North GRIP ice core isotope record for the last 100 ka (Andersen et al., 2006; NGRIP, 2004; Svensson et al., 2008). From 100 to 530 ka the age model was built by aligning the PRGL1-4 *G. bulloides* δ^{18}O record to the LR04 benthic isotope stack (Lisiecki and Raymo, 2005) (Fig. 3), with the support of the planktic oxygen isotope records from the Portuguese margin (Roucoux et al., 2006) and the North Atlantic region (Stein et al., 2009) for specific time intervals. For more details on the age model, tie points and ^{14}C-AMS dates see Sierro et al. (2009). Work is in progress to further improve time constrains during MIS 12 and 13 (F. J. Sierro, personal communication, 2012). Temporal variability of sedimentation rates (SR) resulted in a mean temporal resolution of 160 and 1550 yr during glacial and interglacial periods, respectively.

4 Results and discussion

4.1 The orbital 100-kyr sea-level imprint

The silt/clay ratio and Ca records from PRGL1-4 show a see-saw pattern defining five main units characterised by an upwards fining and Ca content increasing trend, which can be correlated with the main seismostratigraphic units in the seismic reflection profiles crossing the borehole location (Jouet, 2007) (Fig. 2). The sedimentary units end with an abrupt increase in the silt/clay ratio and a rapid decrease in the Ca content coinciding with the main reflectors corresponding to sequence boundaries in the seismic reflection profile. The excellent correlation of these analytical sequences with the seismostratigraphy, together with chronostratigraphic control from the *G. bulloides* δ^{18}O record (Sierro et al., 2009),

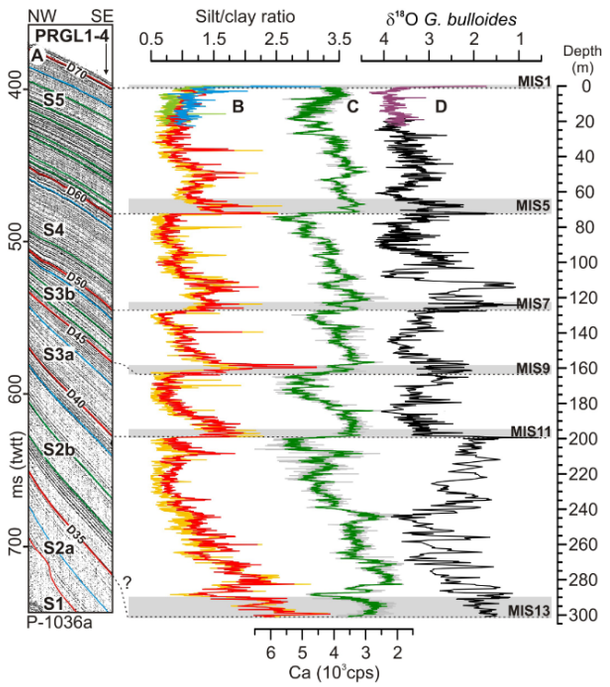

Fig. 2. (A) Close view of high-resolution seismic reflection profile P-1036a at the location of borehole PRGL1-4 (Jouet, 2007), visually correlated with **(B)** silt/clay ratio records from total (light orange and green) and Ca-free (red and blue) sediment fractions from PRGL1-4 and MD99-2348 sediment cores, respectively. **(C)** 5-point moving average (green) of Ca record (grey) from PRGL1-4. **(D)** Oxygen isotopic records from PRGL1-4 (black) and MD99-2348 (purple) obtained from *G. bulloides*. Grey bars correspond to condensed interglacials sequences 1, 5, 7, 9, 11 and 13. Dotted lines correlate the main seismic reflectors (sequence boundaries) and their expression on the different records.

confirm the 100-kyr-cycle origin of these units. The data derived from PRGL1-4 borehole allowed us to reinterpret the seismostratigraphy of the GoL upper slope, where seven units (S1, S2a, S2b, S3a, S3b, S4 and S5) are now documented (Jouet, 2007), instead of the five (S1 to S5) previously identified from seismic reflection profiles alone (Rabineau, 2001). These seven units result from subdividing the former sequences S2 and S3 into S2a and S2b, and S3a and S3b, respectively (Fig. 2a). The results obtained suggest that the lowermost seismostratigraphic units S1 and S2a were not penetrated at PRGL1-4, with the base of the drill most likely corresponding to MIS 13 taking into account extinction of coccolith *P. lacunosa* at about 275 m in the borehole (Figs. 2 and 3). Accordingly, the upper five main depositional sequences stacked on the upper slope of the GoL, corresponding to RPUs driven by global sea-level oscillations of the last five glacial cycles, are identified in the continuous sedimentary record of PRGL1-4 borehole. Consequently, abrupt increases in the silt/clay ratio and decreases in the Ca content respond to rapid sea level rise, continental shelf flooding and subsequent landward migration of deltaic systems during glacial-interglacial transitions, giving birth to sequence boundaries in the upper slope as defined by analytical results (Fig. 2).

RPU stacking in the upper slope resulted from seaward migration of deltaic systems and the subsequent enhancement of riverine supply because of the sea level lowering during each 100-kyr cycle. That is why maximum sedimentation rates (1.5–2.5 m kyr^{-1}) in the upper slope were recorded during periods when the distance to river mouths was minimal (i.e., during glacial lowstands) (Figs. 3g and 4a). The presence of relict offshore sands at 110–115 m depth along the outermost shelf further supports the location of lowstand glacial paleo-shorelines in the vicinity of the Aude Canyon head (Aloïsi, 1986; Bassetti et al., 2006; Berné et al., 2004a; Jouet et al., 2006). The increasing trend of SRs linked to sea level lowering across a glacial period is particularly well resolved for the last glacial period (MIS 2, 3 and 4), during which intervals the chronostratigraphic control is particularly robust (Fig. 3g). Sedimentation rates also peaked during previous 100-kyr cycles glacial sea level minima, although the weaker chronostratigraphic control with depth does not allow distinguishing SR trends during previous full forced regressions, but only low or high SR during interglacial and glacial stages, respectively. Co-occurrence of lowest silt/clay ratios and highest Ca contents during glacial sea level minima confirms the reinforced influence of nearby glacial river mouths on the sedimentation of fines over upper slope interfluves (Fig. 3d and f). Accordingly, while during glacial lowstands the coarsest fractions were mostly trapped and funnelled by glacial adjacent submarine canyons, as demonstrated by pronounced axial incisions within their upper courses (Baztan et al., 2005), large amounts of fine particles supplied by the nearby river mouths remained in suspension, probably transported by along shore current and un-trapped by the canyons, thus, leading to substantial accumulation in inter-canyon areas.

In contrast, SRs were lowest (0.10–0.25 m kyr^{-1}) during interglacial sea-level highstands associated with the landward migration of deltaic systems far away from the shelf-break and upper slope (Figs. 3g and 4b), as illustrated by the modern Holocene epicontinental prism extending down to 90 m water depth over the inner shelf (Aloïsi, 1986; Berné et al., 2007, 2004b). Obviously, these glacial/interglacial contrasting sedimentation rates resulted in expanded glacial intervals (therefore, resulting in higher temporal resolution) and condensed interglacial intervals down the 500 kyr-long record in PRGL1-4 borehole (Fig. 3). With each sea level rise, sedimentation rates reduce significantly in the upper slope and PRGL1-4 records experience a reduction of temporal resolution (e.g., just few points represent a full interglacial period). This same limitation in time resolution prevents us to establish the exact timing of SR reductions, which in turn are depending on selection of tie points in the age model. In

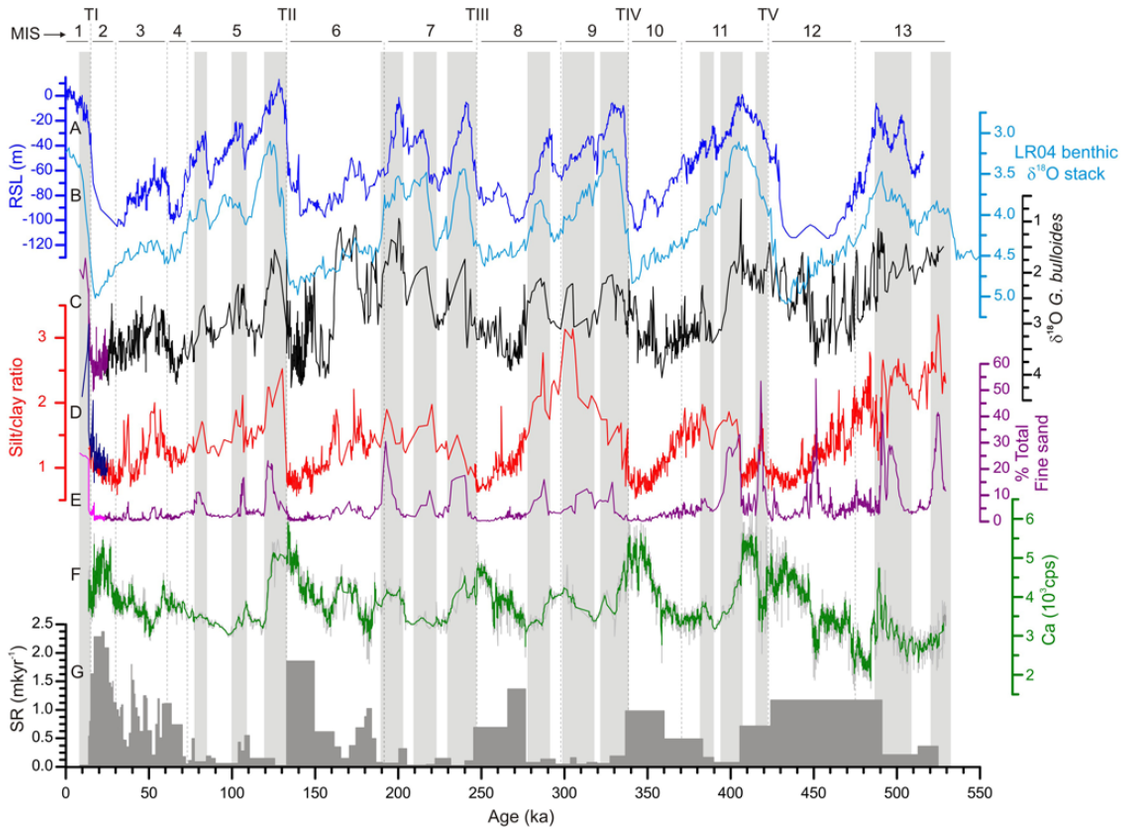

Fig. 3. Multiproxy continuous records of PRGL1-4 borehole with respect to relative sea-level oscillations for the last 500 ka. **(A)** Composite central Red Sea relative sea level reconstruction for the last 500 ka (Rohling et al., 2009). (**B)** LR04 benthic isotope stack record used as reference record (Lisiecki and Raymo, 2005). PRGL1-4 records of **(C)** *G. bulloides* δ^{18}O, **(D)** Ca-free silt/clay ratio, **(E)** total fine sand (%) (Sierro et al., 2009), **(F)** XRF-Ca, and **(G)** linear sedimentation rates. The top 22 ka of the *G. bulloides* δ^{18}O record (purple), the silt/clay ratio of the carbonate-free fraction (blue) and the total fine sand (pink) are from overlapping core MD99-2348, which include the abrupt change associated with the last deglaciation that is not covered by the XRF-Ca record of PRGL1-4. Vertical grey bars show how the main condensed layers (CLs), defined by abrupt increases in the total fine sand fraction record, fit with interglacial stages.

addition, the very low SRs during the main interglacial highstands led to the formation of condensed layers (CLs), i.e., sandy layers rich in pelagic skeletal material, along the GoL upper slope (Fig. 3e), as shown by the total (bulk fraction, non carbonate-free) fine sand record of Sierro et al. (2009) (Fig. 3e).

However, the landward excursion of deltaic systems linked to the updip migration of the coastline when sea level rise is rising and the associated reduction in sediment flux to the upper slope during glacial/interglacial transitions, cannot explain the continuous supply of coarse particles to the upper-slope during every interglacial stage, as evidenced by the high values of the carbonate-free silt/clay ratio (Fig. 3d), nor the observed increase in non-biogenic sand particles (mainly quartz grains) into the sediment. These results suggest that the interglacial flooding of the 70 km wide GoL shelf (Fig. 4b) likely reactivated oceanographic processes able to erode, re-suspend and transport coarse particles, like those contributing to the formation of CLs. While the southwards flowing Northern Current (NC) sweeping the shelf edge and upper slope (Fig. 1a) could contribute winnowing the finest particles during long lasting periods of reduced sediment input to the upper slope, it could not explain the arrival of new lithic coarse material found in deposits formed during interglacial periods, including CLs. The inundation of the shelf during interglacial periods generated a relatively thin layer of water that was highly sensitive to atmospheric forcing, which may trigger the remobilisation of sedimentary particles temporarily stored on the shelf, as it happens during the present day highstand (Bassetti et al., 2006; Canals et al., 2006; Dufois et al., 2008). Recent studies have demonstrated that nowadays northern cold, strong and persistent winds lead to DSWC down-slope at high speed (up to 1 m s^{-1} or more) during late winter and early spring months in the GoL (Canals et al., 2006). Cascading waters carry large amounts of organic matter and sedimentary particles whose

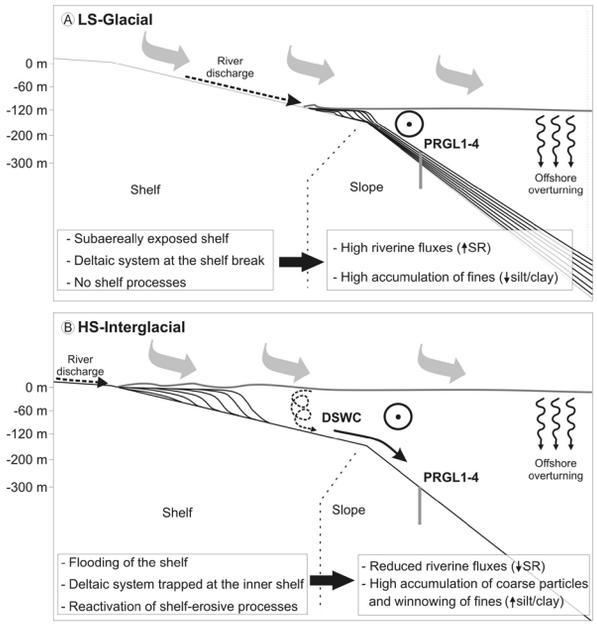

Fig. 4. Conceptual depositional model of the Gulf of Lion continental margin at orbital scale. **(A)** During the lowstand (LS) depositional mode (glacial periods) the continental shelf is subaerially exposed and the basinwards migration of deltaic system results in high amounts of fine particles supplied directly to the upper slope. **(B)** Flooding of the shelf during the high-stand (HS) depositional mode (interglacial periods) traps deltaic systems in the inner shelf, thus, disconnecting the upper slope from direct fluvial discharges. Moreover, the creation of a relatively thin layer of water over the continental shelf reactivates shelf erosive processes, such as Dense Shelf Water Cascading (DSWC), that are able to transport coarse particles down the slope. Both processes contribute to generate thin condensed layers (CLs) in the upper slope. Grey arrows represent the northern winds involved in cooling the superficial shelf water for dense shelf water formation and offshore overturning. Dot in a circle shows the dominant direction of the slope-parallel Northern Current. The discontinuous spiral arrow over the shelf represents shelf-erosive processes, as DSWC.

coarser fraction efficiently scours and erodes the shelf edge and canyon heads and upper courses (Gaudin et al., 2006; Lastras et al., 2007; Pasqual et al., 2010; Puig et al., 2008; Sanchez-Vidal et al., 2008). Activation in the past of continental shelf erosive processes like DSWC probably did not lead to significant sediment accumulation in upper slope interfluves, but favoured the winnowing of fines and the supply of coarse lithic particles that, in combination with low sedimentation rates, contributed to generate CLs. When the "cooling platform" disappeared, i.e., during subaerial exposure of the continental shelf (lowstand conditions, Fig. 4a), there was no room left for dense shelf waters to form and, therefore, these type of continental shelf erosive processes ceased. During transitional periods, when the shelf was partly flooded, the volume of water involved in cascading and other continental shelf erosive processes was smaller, subsequently lessening downslope transport by dense shelf waters. Therefore, changes in the silt/clay ratio also respond to the flooded shelf area and, consequently, to sea-level oscillations. This explains the relatively good match between the silt/clay ratio and sea level for the last 500 ka (Fig. 3a and d), which is especially evident for the last glacial cycle when the chronostratigraphic control is more precise. Obviously, the silt/clay ratio did not respond linearly to sea-level oscillations and reactivation of continental shelf erosive processes could be also related to some environmental threshold, e.g., the volume of water stored on the shelf. This, together with significant reductions of SRs during each sea level rise, and subsequent reductions in time resolution, prevent us using the silt/clay ratio as an exact indicator of the beginning of sea level rises. However, the persistent pattern observed in the silt/clay ratio through the last five glacial/interglacial cycles and also at millennial time scales, as described below, confirms this ratio is a good indicator of relative high sea-level conditions (highstands) in the GoL margin.

These results support a combined shelf and upper slope depositional model for inter-canyon RPU stacking over the last 500 ka that considers two main processes: (i) oscillations in sediment supply due to the migration of river mouths and deltaic systems, and (ii) activation-deactivation of continental shelf erosive processes like DSWC, both of them ultimately driven by the 100-kyr glacio-eustatic cyclicity (Fig. 4).

4.2 The millennial MIS 3 sea level imprint

Since this combined depositional model has been tested at glacial/interglacial scales, it is reasonable to expect that minor scale sea-level oscillations would also result in a similar sedimentary signature in the GoL margin outbuilding. Considering the passive character of the margin, the flatness and width of the GoL shelf, and the robust chronostratigraphic framework for the last glacial cycle (i.e., excellent synchronization between the PRGL1-4 *G. bulloides* δ^{18}O record and the NGRIP ice core record, Fig. 5a and b) due to elevated SRs (ranging from 0.2 to 2 m kry^{-1}), the PRGL1-4 record could be highly valuable for disentangling the millennial scale sea level variability during MIS 3. Independently of chronologies, the exhaustive compilation of MIS 3 sea-level reconstructions by Siddall et al. (2008) shows two common patterns of variability: (1) the mean sea level during the first half of MIS 3 was approximately 20 m higher than in the second half, and (2) four 20–30 m-amplitude millennial-scale sea-level fluctuations occurred during this period (Fig. 5e). These features are also observed in the PRGL1-4 silt/clay record (Fig. 5c), thereby demonstrating that the GoL system responded to both long and short-term sea-level fluctuations during MIS 3.

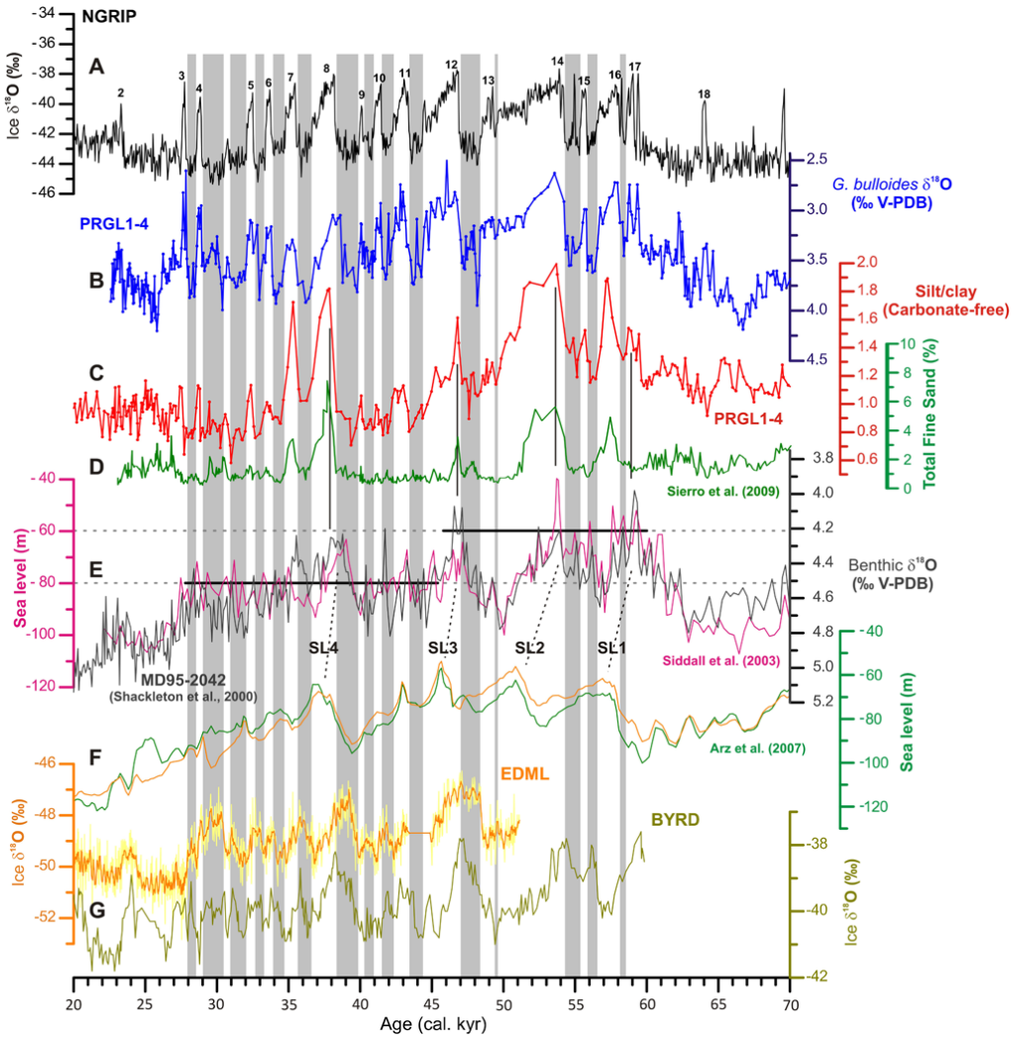

Fig. 5. Comparison of different records of climate variability and sea-level reconstructions for the MIS 3 period, all of them age-scaled to the Greenland ice core NGRIP (Svensson et al., 2008) **(A)**. **(B)** *G. bulloides* oxygen isotopic record (blue), **(C)** carbonate-free silt/clay ratio (red) and **(D)** total fine sand fraction (green) from PRGL1-4 borehole. **(E)** Benthic oxygen isotopic record from MD95-2042 (Shackleton et al., 2000) (dark grey) compared to Red Sea sea level reconstruction (Siddall et al., 2003) (pink), with horizontal lines showing that mean sea level was ∼20 m higher in early MIS 3 than in late MIS 3. Discontinuous lines point four millennial-scale peaks of relative high sea level (SL1, 2, 3 and 4). **(F)** Sea level reconstructions from the northern Red Sea based on two different temperature corrections for the deep basin (Arz et al., 2007). **(G)** Oxygen isotopic records from Antarctic ice cores EDML and BYRD (Blunier and Brook, 2001; EPICA Community Members, 2006) CH_4-synchronized to Greenland ice core NGRIP (Svensson et al., 2008). Numbers above the NGRIP record represent warm GIS, while vertical grey bars correspond to cold GS and HE.

The general decreasing trend observed in the PRGL1-4 silt/clay ratio during the progressive sea level lowering of the last glacial cycle (Fig. 3), is punctuated by a series of grain-size increases (Fig. 5c), which suggest that millennial-scale relative sea level rises occurred during MIS 3. By temporally extending the flooded area of the GoL shelf, MIS 3 relative sea level rises reduced the clay supply to the upper slope and contributed to expose a larger volume of water to atmospheric forcing, eventually leading to DSWC and, hence, indirectly reinforcing the transport of coarse particles to the upper slope. Both mechanisms contributed to increases in the silt/clay ratio (Fig. 5c). Those grain-size increases are unrelated to periods of intensification of deep-water formation in the GoL, since most of them occurred during relatively warm Greenland interstadials (GIS) (Fig. 5b and c), in contrast with observations of enhanced Western Mediterranean Deep Water (WMDW) formation during MIS 3 cold Greenland Stadials (GS) (Cacho et al., 2000, 2006; Frigola et al., 2008; Sierro et al., 2005).

Confirming or discarding the occurrence of sea-level oscillations at Dansgaard-Oeschger (D-O) scale has been prevented so far because none of the existing sea-level records was able to resolve variations lower than 12 m in amplitude during time intervals as short as 1 kyr (Siddall et al., 2008). Nevertheless, prominent increases in iceberg calving during cold Greenland stadials (GS) (non Heinrich Events, HE) suggest that sea level should have oscillated within each D-O cycle (Bond and Lotti, 1995; Chappell, 2002; Siddall et al., 2008; van Kreveld et al., 2000). Disentangling MIS 3 sea-level variability also faces the difficulty of establishing the absolute timing of the observed oscillations, which is necessary to understand the role of sea level in millennial-scale climate variability during MIS 3 and to determine the relative contribution of "northern" versus "southern" sources (Clark et al., 2007).

Early evidence of millennial-scale sea-level variability was obtained from the benthic δ^{18}O record of the Portuguese margin core MD95-2042 (Shackleton et al., 2000) and sea-level reconstruction from the Red Sea (Siddall et al., 2003) (Fig. 5e). Although the Portuguese record may be influenced by oscillations in deep ocean temperature and local hydrographic variability, an important part of the record is linked to global sea level change (Skinner et al., 2007). Since both records display a variability pattern that is remarkably similar to the one found in Antarctic ice cores (Fig. 5e and g), it has been suggested that MIS 3 sea-level oscillations followed Antarctic climate variability (Rohling et al., 2008; Siddall et al., 2003). Contrary to these interpretations, recent results from the Red Sea and the GoL have shown millennial-scale sea level rises to occur during major warm Greenland interstadials (GIS) (Fig. 5f and d) (Arz et al., 2007; Jouet et al., 2012; Sierro et al., 2009), further highlighting the still high uncertainty about the timing of MIS 3 sea-level variability.

The co-occurrence of silt/clay increases and planktic δ^{18}O depletions in the PRGL1-4 record (Fig. 5b and c) imply, independently of the age model applied, that relative high sea levels occurred during warm GIS events. Concurrently, Shackleton et al. (2000) and Siddall et al. (2003) records also show maximum sea levels to occur during the onset phase of major GIS interstadials (i.e., GIS14, 12 and 8) (Fig. 5a and e). However, discrepancies on the precise timing of the sea level rises exist with our PRGL1-4 record. The excellent time constrains provided by the *G. bulloides* δ^{18}O record of the PRGL1-4 borehole demonstrate a consistent peak to peak coupling between sea-level variability (as indicated by increases in the silt/clay ratio) and all D-O cycles, including the shortest ones. Nevertheless, not every relative high sea level resulted in the formation of CLs, since these were only observed during major GIS (16, 14, 12, 8 and 7) (Sierro et al., 2009), all of which coincide with higher values of the silt/clay ratio (Fig. 5c and d). The differences between the total fine sand record of Sierro et al. (2009) and our silt/clay ratio indicate that sea level increases during minor GIS (15, 13, 11, 10, 9, 6, 5, 4 and 3) were likely not high and/or long enough to generate CLs, therefore, demonstrating once more the strong sensitivity of the silt/clay ratio to sea-level oscillations. The great sensitivity of the silt/clay ratio during MIS 3 could be also related to the fact that sea level was oscillating between −60 m and −80 m, when the continental shelf was not fully exposed and prodeltaic deposits could be close to equilibrium with the accommodation space over the shelf.

A limitation of the PRGL1-4 silt/clay record is that the amplitude of sea level variations cannot be directly derived, as nowhere has it been shown that grain-size oscillations respond linearly to sea-level fluctuations. This very same limitation, and reduction of PRGL1-4 time resolution due to decreasing SRs with sea level increases, also prevents setting up the precise timing of sea level rises, whether they occurred at the beginning of each warm GIS or during the previous cold stadial. This relates to the exact timing of deltaic migration and their relative position following sea-level rise. In addition, the enhanced supply of coarse particles by reactivation of continental shelf erosive processes, such as DSWC, should normally occur some time after the start of each sea-level rise, i.e., when the volume of water over the shelf is again large enough.

Our results imply that sea-level was relatively high during all warm GIS within MIS 3 (Fig. 5a and c), although intrinsic limitations of the methodology applied in this study do not allow establishing the precise time nor the mechanisms involved in such millennial scale sea level rises, which could initiate by instabilities and melting of continental ice-sheets during cold GS, whether or not they correspond to HEs.

5 Conclusions

The last 500 ka continuous sediment record of the 300 m long PRGL1-4 borehole drilled in the upper slope of the river fed GoL holds the imprint of sea-level oscillations at orbital and millennial time scales during MIS 3. The sedimentary succession of PRGL1-4 consists of five regressive progradational units (more aggradational on the upper slope) that relate to the glacio-eustatic 100-kyr cyclicity. The consistent chronostratigraphy of the investigated section and the good matching between seismic reflection profiles and the grain-size record provide clues for understanding the nature of seismic reflections in mud-dominated slope sequences like the ones found at the investigated site, and also provides a tool to identify the boundaries of seismostratigraphic units while helping to tie them with global sea-level oscillations. These findings have resulted in the reinterpretation of the stratigraphy of the upper slope in the GoL, following an approach that can be extended to similar continental margin settings.

In addition of pushing the shoreline and associated sedimentary environments landwards, thus, disconnecting the upper slope from direct riverine sediment sources, we propose that sea level rise can reactivate transient energetic hydrosedimentary processes, such as DSWC, which are able of

eroding, resuspending and transporting significant volumes of sediment from the continental shelf and upper slope to the deep basin. The sedimentary starvation of the upper slope during highstands, jointly with both episodic and persistent hydrodynamic processes winnowing the fine fraction, determined the formation of CLs that mark the periods of continental shelf flooding during interglacial epochs, as evidenced by our grain-size records.

Finally, the excellent match of the PRGL1-4 silt/clay record with previous records of sea-level variability at millennial-scale during MIS 3, together with the good time constraint provided by the *G. bulloides* δ^{18}O record, strongly support the occurrence of relatively high sea levels during each single warm GIS, even the smallest ones. Unfortunately, the precise starting time of sea level rises cannot be established solely from the sediment record of the GoL upper slope, which points to the need of further devoted research to resolve the origin and magnitude of MIS 3 sea-level variability.

Acknowledgements. This study has been supported by the EC PROMESS1 (EVR1-CT-200240024) and HERMIONE (226354-HERMIONE) projects, and the Spanish GRACCIE CONSOLIDER (CSD2007-00067) and DOS MARES (CTM2010-21810-C03-01) projects and CGL2005-24147-E complementary action. The IMAGES programme contributed to the research by providing the MD99-2348 sediment core. French partners benefited from additional support by Agence Nationale de la Recherche (ANR, contract NT05-3-42040). We are also grateful for comments and suggestions of reviewers Jamie Austin and Andre Droxler, which helped to improve the manuscript. We thank Anders Sevensson and Thomas Blunier for providing NGRIP and EDML data, respectively. We are especially grateful to PROMESS1 participating scientists and to the staff of the various laboratories where sediment samples were analysed. We are grateful for the support provided by Fugro Engineers B. V. that made the challenging *MV Bavenit* cruise a success history. Generalitat de Catalunya recognises CRG Marine Geosciences within its excellence research groups program (ref. 2009 SGR 1305).

Edited by: L. Beaufort

References

Aloïsi, J. C.: Sur un modèle de sédimentation deltaïque: contribution à la connaissance des marges passives, University of Perpignan, Perpignan, 162 pp., 1986.

Andersen, K. K., Svensson, A., Johnsen, S. J., Rasmussen, S. O., Bigler, M., Rothlisberger, R., Ruth, U., Siggaard-Andersen, M.-L., Peder Steffensen, J., Dahl-Jensen, D., Vinther, B. M., and Clausen, H. B.: The Greenland Ice Core Chronology 2005, 15-42 ka. Part 1: constructing the time scale, Quaternary Sci. Rev., 25, 3246–3257, 2006.

Arz, H. W., Lamy, F., Ganopolski, A., Nowaczyk, N., and Patzold, J.: Dominant Northern Hemisphere climate control over millennial-scale glacial sea-level variability, Quaternary Sci. Rev., 26, 312–321, 2007.

Bassetti, M. A., Jouet, G., Dufois, F., Berne, S., Rabineau, M., and Taviani, M.: Sand bodies at the shelf edge in the Gulf of Lions (Western Mediterranean): Deglacial history and modern processes, Mar. Geol., 234, 93–109, 2006.

Bassetti, M. A., Berné, S., Jouet, G., Taviani, M., Dennielou, B., Flores, J. A., Gaillot, A., Gelfort, R., Lafuerza, S., and Sultan, N.: The 100-ka and rapid sea-level changes recorded by prograding shelf sand bodies in the Gulf of Lions (western Mediterranean Sea), Geochem. Geophy. Geosy., 9, Q11R05, doi:10.1029/2007GC001854, 2008.

Baztan, J., Berne, S., Olivet, J. L., Rabineau, M., Aslanian, D., Gaudin, M., Rehault, J. P., and Canals, M.: Axial incision: The key to understand submarine canyon evolution (in the western Gulf of Lion), Mar. Petrol. Geol., 22, 805–826, 2005.

Berné, S., Carré, B., Loubrieu, B., Mazé, J. P., Morvan, L., and Normand, A.: Notice de la carte morpho-bathymétrique du Golfe du Lion, IFREMER, Brest, 2004a.

Berné, S., Rabineau, M., Flores, J. A., and Sierro, F. J.: The impact of Quaternary Global Changes on strata formation. Exploration of the shelf edge in the Northwest Mediterranean Sea, Oceanography, 17, 92–103, 2004b.

Berné, S., Jouet, G., Bassetti, M. A., Dennielou, B., and Taviani, M.: Late Glacial to Preboreal sea-level rise recorded by the Rhone deltaic system (NW Mediterranean), Mar. Geol., 245, 65–88, 2007.

Blunier, T. and Brook, E. J.: Timing of Millennial-Scale Climate Change in Antarctica and Greenland During the Last Glacial Period, Science, 291, 109–112, 2001.

Bond, G. and Lotti, R.: Iceberg discharges into the North Atlantic on millennial time scales during the last deglaciation, Science, 267, 1005–1010, 1995.

Cacho, I., Grimalt, J. O., Sierro, F. J., Shackleton, N. J., and Canals, M.: Evidence for enhanced Mediterranean thermohaline circulation during rapid climatic coolings, Earth Planet. Sc. Lett., 183, 417–429, 2000.

Cacho, I., Shackleton, N., Elderfield, H., Sierro, F. J., and Grimalt, J. O.: Glacial rapid variability in deep-water temperature and δ^{18}O from the Western Mediterranean Sea, Quaternary Sci. Rev., 25, 3294–3311, 2006.

Canals, M., Puig, P., de Madron, X. D., Heussner, S., Palanques, A., and Fabres, J.: Flushing submarine canyons, Nature, 444, 354–357, 2006.

Clark, P. U., Hostetler, S. W., Pisias, N. G., Schmittner, A., and Meissner, K.: Mechanisms for an ∼7-kyr climate and sea-level oscillation during Marine Isotopic Stage 3, in: Ocean Circulation: Mechanisms and Impacts, edited by: Schmittner, A., Chiang, J. C. H., Hemming, S. R., AGU Geophysical Monograph Series, Washington DC, 209–246, 2007.

Chappell, J.: Sea level changes forced ice breakouts in the Last Glacial cycle: new results from coral terraces, Quaternary Sci. Rev., 21, 1229–1240, 2002.

Dufois, F., Garreau, P., Le Hir, P., and Forget, P.: Wave- and current-induced bottom shear stress distribution in the Gulf of Lions, Cont. Shelf Res., 28, 1920–1934, 2008.

EPICA Community Members: One-to-one coupling of glacial climate variability in Greenland and Antarctica, Nature, 444, 195–198, 2006.

Frigola, J., Moreno, A., Cacho, I., Canals, M., Sierro, F. J., Flores, J. A., Grimalt, J. O., Hodell, D. A., and Curtis, J. H.: Holocene climate variability in the western Mediterranean region from a deepwater sediment record, Paleoceanography, 22, PA2209, doi:10.1029/2006PA001307, 2007.

Frigola, J., Moreno, A., Cacho, I., Canals, M., Sierro, F. J., Flores, J. A., and Grimalt, J. O.: Evidence of abrupt changes in Western Mediterranean Deep Water circulation during the last 50 kyr: A high-resolution marine record from the Balearic Sea, Quaternary Int., 181, 88–104, doi:10.1016/j.quaint.2007.06.016, 2008.

Gaudin, M., Berne, S., Jouanneau, J. M., Palanques, A., Puig, P., Mulder, T., Cirac, P., Rabineau, M., and Imbert, P.: Massive sand beds attributed to deposition by dense water cascades in the Bourcart canyon head, Gulf of Lions (northwestern Mediterranean Sea), Mar. Geol., 234, 111–128, 2006.

Imbrie, J., Boyle, E., Clemens, C., Duffy, A., Howard, W., Kukla, G., Kutzbach, J. E., Martinson, D. G., McIntyre, A., Mix, A. C., Molfino, B., Morley, J. J., Peterson, L. C., Pisias, N. G., Prell, W., Raymo, M. E., Shackleton, N. J., and Toggweiler, J. R.: On the structure and origin of major glaciation cycles. 1. Linear responses to Milankovitch forcing, Paleoceanography, 7, 701–738, 1992.

Jouet, G.: Enregistrements stratigraphiques des cycles climatiques et glacio-eustatiques du Quaternaire terminal-Modélisations de la marge continentale du Golfe du Lion, PhD Thesis, Laboratoire Environnements Sédimentaires, Géosciences Marines. Ifremer, Brest, France, 443 pp., 2007.

Jouet, G., Berne, S., Rabineau, M., Bassetti, M. A., Bernier, P., Dennielou, B., Sierro, F. J., Flores, J. A., and Taviani, M.: Shoreface migrations at the shelf edge and sea-level changes around the Last Glacial Maximum (Gulf of Lions, NW Mediterranean), Mar. Geol., 234, 21–42, 2006.

Jouet, G., Berné, S., Sierro, F. J., Bassetti, M. A., Canals, M., Dennielou, B., Flores, J. A., Frigola, J., and Haq, B. U.: Geological imprints of millennial-scale sea-level changes, Terra Nova, accepted, 2012.

Lastras, G., Canals, M., Urgeles, R., Amblas, D., Ivanov, M., Droz, L., Dennielou, B., Fabrés, J., Schoolmeester, T., Akhmetzhanov, A., Orange, D., and García-García, A.: A walk down the Cap de Creus canyon, Northwestern Mediterranean Sea: Recent processes inferred from morphology and sediment bedforms, Mar. Geol., 246, 176–192, 2007.

Lisiecki, L. E. and Raymo, M. E.: A Pliocene-Pleistocene stack of 57 globally distributed benthic $d^{18}O$ records, Paleoceanography, 20, PA1003, doi:10.1029/2004PA001071, 2005.

Lobo, F. J., Tesson, M., and Gensous, B.: Stratral architectures of late Quaternary regressive-transgressive cycles in the Roussillon Shelf (SW Gulf of Lions, France), Mar. Petrol. Geol., 21, 1181–1203, 2004.

Miller, K. G., Kominz, M. A., Browning, J. V., Wright, J. D., Mountain, G. S., Katz, M. E., Sugarman, P. J., Cramer, B. S., Christie-Blick, N., and Pekar, S. F.: The Phanerozoic Record of Global Sea-Level Change, Science, 310, 1293–1298, 2005.

Millot, C.: Circulation in the Western Mediterranean Sea, J. Marine Syst., 20, 423–442, 1999.

NGRIP: High-resolution record of Northern Hemisphere climate extending into the last interglacial period, Nature, 431, 147–151, 2004.

Palanques, A., Durrieu de Madron, X., Puig, P., Fabres, J., Guillen, J., Calafat, A., Canals, M., Heussner, S., and Bonnin, J.: Suspended sediment fluxes and transport processes in the Gulf of Lions submarine canyons. The role of storms and dense water cascading, Mar. Geol., 234, 43–61, 2006.

Pasqual, C., Sanchez-Vidal, A., Zúñiga, D., Calafat, A., Canals, M., Durrieu de Madron, X., Puig, P., Heussner, S., Palanques, A., and Delsaut, N.: Flux and composition of settling particles across the continental margin of the Gulf of Lion: the role of dense shelf water cascading, Biogeosciences, 7, 217–231, doi:10.5194/bg-7-217-2010, 2010.

Pont, D., Simonnet, J. P., and Walter, A. V.: Medium-term Changes in Suspended Sediment Delivery to the Ocean: Consequences of Catchment Heterogeneity and River Management (Rhône River, France), Estuar. Coast. Shelf S., 54, 1–18, 2002.

Posamentier, H. W. and Vail, P. R.: Eustatic controls on clastic deposition II – sequence and systems tract models, in: Sea-level changes: an integrated approach, edited by: Wilgus, C. K., Hastings, B. S., Kendall, C. G. S. C., Posamentier, H., Ross, C. A., and Van Wagoner, J. C., Society of Economic Paleontologists and Mineralogists, Tulsa, Oklahoma, 125–154, 1988.

Posamentier, H. W., Allen, G. P., James, D. P., and Tesson, M.: Forced regressions in a sequence stratigraphic framework: concepts, examples, and exploration significance, AAPG Bull., 76, 1687–1709, 1992.

Puig, P., Palanques, A., Orange, D. L., Lastras, G., and Canals, M.: Dense shelf water cascades and sedimentary furrow formation in the Cap de Creus Canyon, northwestern Mediterranean Sea, Cont. Shelf Res., 28, 2017–2030, 2008.

Rabineau, M.: Un modèle géométrique et stratigraphique des séquences de dépôts quaternaires de la plate-forme du Golfe du Lion: enregistrement des cycles glacioeustatiques de 100 000 ans. Thèse de Doctorat, Université de Rennes 1 and IFREMER, Rennes, 392, p. 392 + p. 370, available at: http://archimer.ifremer.fr/doc/00000/331/, 2001.

Rabineau, M., Berné, S., Ledrezen, E., Lericolais, G., Marsset, T., and Rotunno, M.: 3D architecture of lowstand and transgressive Quaternary sand bodies on the outer shelf of the Gulf of Lion, France, Mar. Petrol. Geol., 15, 439–452, 1998.

Rabineau, M., Berne, S., Aslanian, D., Olivet, J.-L., Joseph, P., Guillocheau, F., Bourillet, J.-F., Ledrezen, E., and Granjeon, D.: Sedimentary sequences in the Gulf of Lion: A record of 100,000 years climatic cycles, Mar. Petrol. Geol., 22, 775–804, 2005.

Rohling, E. J., Fenton, M., Jorissen, F. J., Bertrand, P., Ganssen, G., and Caulet, J. P.: Magnitudes of sea-level lowstands of the past 500,000 years, Nature, 394, 162–165, 1998.

Rohling, E. J., Grant, K., Hemleben, C., Kucera, M., Roberts, A. P., Schmeltzer, I., Schulz, H., Siccha, M., Siddall, M., and Trommer, G.: New constrains on the timing of sea-level fluctuations during early to middle isotope stage 3, Paleoceanography, 23, PA3219, doi:10.1029/2008PA001617, 2008.

Rohling, E. J., Grant, K., Bolshaw, M., Roberts, A. P., Siddall, M., Hemleben, C., and Kucera, M.: Antarctic temperature and global sea-level closely coupled over the past five glacial cycles, Nat. Geosci., 2, 500–504, 2009.

Roucoux, K. H., Tzedakis, P. C., de Abreu, L., and Shackleton, N. J.: Climate and vegetation changes 180,000 to 345,000 years ago recorded in a deep-sea core off Portugal, Earth Planet. Sc. Lett., 249, 307–325, 2006.

Sanchez-Vidal, A., Pasqual, C., Kerhervé, P., Calafat, A., Heussner, S., Palanques, A., Durrieu de Madron, X., Canals, M., and Puig, P.: Impact of dense shelf water cascading on the transfer of organic matter to the deep western Mediterranean basin, Geophys. Res. Lett., 35, L05605, doi:10.1029/2007GL032825, 2008.

Sanchez-Vidal, A., Canals, M., Calafat, A., Lastras, G., Pedrosa-Pàmies, R., Menéndez, M., Medina, R., Company, J. B., Hereu, B., Romero, J., and Alcoverro, T.: Impacts on the deep-sea ecosystem by a severe coastal storm, PLoS ONE, 7, e30395, doi:10.1371/journal.pone.0030395, 2012.

Shackleton, N. J., Hall, M. A., and Vincent, E.: Phase relationships between millennial-scale events 64,000–24,000 years ago, Paleoceanography, 15, 565–569, 2000.

Siddall, M., Rohling, E. J., Almogi-Labin, A., Hemleben, C., Meischner, D., Schmelzer, I., and Smeed, D. A.: Sea-level fluctuations during the last glacial cycle, Nature, 423, 853–858, 2003.

Siddall, M., Chappell, J., and Potter, E.-K.: Eustatic sea-level during past interglacials, in: The climate of past interglacials, edited by: Sirocko, F., Litt, T., Claussen, M., and Sanchez Goñi, M.-F., Elsevier, Amsterdam, 2006.

Siddall, M., Rohling, E. J., Thompson, W. G., and Waelbroeck, C.: MIS 3 sea level fluctuations: data synthesis and new outlook, Rev. Geophys., 46, RG4003, doi:10.1029/2007RG000226, 2008.

Sierro, F. J., Hodell, D. A., Curtis, J. H., Flores, J. A., Reguera, I., Colmenero-Hidalgo, E., Bárcena, M. A., Grimalt, J. O., Cacho, I., Frigola, J., and Canals, M.: Impact of iceberg melting on Mediterranean thermohaline circulation during Heinrich events, Paleoceanography, 20, PA2019, doi:2010.1029/2004PA001051, 2005.

Sierro, F. J., Andersen, N., Bassetti, M. A., Berné, S., Canals, M., Curtis, J. H., Dennielou, B., Flores, J. A., Frigola, J., Gonzalez-Mora, B., Grimalt, J. O., Hodell, D. A., Jouet, G., Pérez-Folgado, M., and Schneider, R.: Phase relationship between sea-level and abrupt climate change, Quaternary Sci. Rev., 28, 2867–2881, 2009.

Skinner, L. C., Elderfield, H., and Hall, M.: Phasing of millennial climate events and Northeast Atlantic deep-water temperature change since 50 ka BP, in: Ocean Circulation: Mechanisms and Impacts, edited by: Schmittner, A., Chiang, J. C. H., and Hemming, S. R., AGU Geophysical Monograph Series, Washington DC, 197–208, 2007.

Stein, R., Hefter, J., Grützner, J., Voelker, A., and Naafs, B. D. A.: Variability of surface water characteristics and Heinrich-like events in the Pleistocene midlatitude North Atlantic Ocean: biomarker and XRD records from IODP Site U1313 (MIS 16-9), Paleoceanography, 24, PA2203, doi:10.1029/2008PA001639, 2009.

Svensson, A., Andersen, K. K., Bigler, M., Clausen, H. B., Dahl-Jensen, D., Davies, S. M., Johnsen, S. J., Muscheler, R., Parrenin, F., Rasmussen, S. O., Röthlisberger, R., Seierstad, I., Steffensen, J. P., and Vinther, B. M.: A 60 000 year Greenland stratigraphic ice core chronology, Clim. Past, 4, 47–57, doi:10.5194/cp-4-47-2008, 2008.

Tesson, M., Gensous, B., Allen, G. P., and Ravenne, C.: Late Quaternary deltaic lowstand wedges on the Rhône continental shelf, France, Mar. Geol., 91, 325–332, 1990.

Tesson, M., Posamentier, H. W., and Gensous, B.: Stratigraphic organization of late pleistocene deposits of the western part of the Golfe du Lion shelf (Languedoc shelf), Western Mediterranean Sea, using high-resolution seismic and core data, AAPG Bull., 84, 119–150, 2000.

Thompson, W. G. and Goldstein, S. L.: Open-System Coral Ages Reveal Persistent Suborbital Sea-Level Cycles, Science, 308, 401–404, 2005.

Thompson, W. G. and Goldstein, S. L.: A radiometric calibration of the SPECMAP timescale, Quaternary Sci. Rev., 25, 3207–3215, 2006.

Ulses, C., Grenz, C., Marsaleix, P., Schaaff, E., Estournel, C., Meulé, S., and Pinazo, C.: Circulation in a semi-enclosed bay under influence of strong freshwater input, J. Marine Syst., 56, 113–132, 2005.

Vail, P. R., Mitchum Jr., R. M., Todd, R. G., Widmier, J. M., Thompson III, S., Sangree, J. B., Bubb, J. N., and Hatleid, W. G.: Seismic stratigraphy and global changes of sea-level, in: Seismic stratigraphy – applications to hydrocarbon exploration, edited by: Payton, C. E., The American Association of Petroleum Geologists, Tulsa, Oklahoma, 49–212, 1977.

van Kreveld, S. A., Sarnthein, M., Erlenkeuser, H., Grootes, P., Jung, S. J. A., Nadeau, M.-J., Pflaumann, U., and Voelker, A.: Potential links between surging ice sheets, circulation changes, and the Dansgaard-Oeschger cycles in the Irminger Sea, 60–18 kyr, Paleoceanography, 15, 425–442, 2000.

Waelbroeck, C., Labeyrie, L., Michel, E., Duplessy, J. C., McManus, J. F., Lambeck, K., Balbon, E., and Labracherie, M.: Sea-level and deep water temperature changes derived from benthic foraminifera isotopic records, Quaternary Sci. Rev., 21, 295–305, 2002.

Yokoyama, Y., Esat, T. M., and Lambeck, K.: Coupled climate and sea-level changes deduced from Huon Peninsula coral terraces of the last ice age, Earth Planet. Sci. Lett., 193, 579–587, 2001.

Available online at www.sciencedirect.com
ScienceDirect
Quaternary International 181 (2008) 88–104

Evidence of abrupt changes in Western Mediterranean Deep Water circulation during the last 50 kyr: A high-resolution marine record from the Balearic Sea

J. Frigola[a], A. Moreno[b], I. Cacho[a], M. Canals[a,*], F.J. Sierro[c], J.A. Flores[c], J.O. Grimalt[d]

[a]*CRG Marine Geosciences, Department of Stratigraphy, Paleontology and Marine Geosciences, Faculty of Geology, University of Barcelona, Campus de Pedralbes, C/Martí i Franquès s/n, 08028 Barcelona, Spain*
[b]*Pyrenean Institute of Ecology, Consejo Superior de Investigaciones Científicas, Aptdo. 202, 50080 Zaragoza, Spain*
[c]*Department of Geology, University of Salamanca, Plaza de la Merced s/n, 37008 Salamanca, Spain*
[d]*Department of Environmental Chemistry, Institute of Chemical and Environmental Research, Consejo Superior de Investigaciones Científicas, C/Jordi Girona 18, 08034 Barcelona, Spain*

Available online 27 June 2007

Abstract

The IMAGES core MD99-2343, recovered from a sediment drift north of the island of Minorca, in the north-western Mediterranean Sea, holds a high-resolution sequence that is perfectly suited to study the oscillations of the overturning system of the Western Mediterranean Deep Water (WMDW). Detailed analysis of grain-size and bulk geochemical composition reveals the sensitivity of this region to climate changes at both orbital and centennial–millennial temporal scales during the last 50 kyr. The dominant orbital pattern in the K/Al record indicates that sediment supply to the basin was controlled by the insolation evolution at 40°N, which forced changes in the fluvial regime, with more efficient sediment transport during insolation maxima. This orbital control also modulated the long-term pattern of the WMDW intensity as illustrated by the silt/clay ratio.

However, deep convection was particularly sensitive to climatic changes at shorter time-scales, i.e. to centennial–millennial glacial and Holocene oscillations that are well documented by all the paleocurrent intensity proxies (Si/Al, Ti/Al and silt/clay ratios). Benthic isotopic records ($\delta^{13}C$ and $\delta^{18}O$) show a Dansgaard–Oeschger (D–O) pattern of variability of WMDW properties, which can be associated with changing intensities of the deep currents system. The most prominent reduction on the WMDW overturning was caused by the post-glacial sea level rise.

Three main scenarios of WMDW overturning are revealed: a strong mode during D–O Stadials, a weak mode during D–O Interstadials and an intermediate mode during cooling transitions. In addition, D–O Stadials associated with Heinrich events (HEs) have a very distinct signature as the strong mode of circulation, typical for the other D–O Stadials, was never reached during HE due to the surface freshening induced by the inflowing polar waters. Consequently, the WMDW overturning system oscillated around the intermediate mode of circulation during HE. Though surface conditions were more stable during the Holocene, the WMDW overturning cell still reacted synchronously to short-lived events, as shown by increments in the planktonic $\delta^{18}O$ record, triggering quick reinforcements of the deep water circulation. Overall, these results highlight the sensitivity of the WMDW to rapid climate change which in the recent past were likely induced by oceanographic and atmospheric reorganizations in the North Atlantic region.

1. Introduction

Abrupt climate changes of different intensity and scales characterize the climate history of the last 50 kyr in the North Atlantic region. During the last glacial period a series of coolings (Stadials) and warmings (Interstadials) known as the Dansgaard–Oeschger (D–O) events punctuated the Marine Isotopic Stage (MIS) 3 (Bond et al., 1993; Dansgaard et al., 1993). Additionally, abrupt coolings (known as Heinrich events, HEs) at the end of sequences of progressively weaker D–O oscillations resulted in massive iceberg discharges accompanied by deposition of ice rafted debris (IRD) (Heinrich, 1988; Bond et al., 1993). Climatic

*Corresponding author.
E-mail address: miquelcanals@ub.edu (M. Canals).

1040-6182/$ - see front matter © 2007 Elsevier Ltd and INQUA. All rights reserved.
doi:10.1016/j.quaint.2007.06.016

models suggest that reorganizations of the thermohaline circulation (THC) due to changes in the sea surface freshwater balance were the cause for the observed abrupt climate changes (Stocker, 2000). Similarly, the occurrence of abrupt climate changes during the Holocene at similar time-scales than those from the glacial period has been inferred from marine and terrestrial studies worldwide (Mayewski et al., 2004).

The rapid transmission of millennial-scale climate variability from the North Atlantic towards the Mediterranean region is supported by a number of studies (Rohling et al., 1998; Allen et al., 1999; Cacho et al., 1999, 2000, 2001; Combourieu Nebout et al., 2002; Moreno et al., 2002, 2004; Bartov et al., 2003; Martrat et al., 2004; Sierro et al., 2005). Both oceanic and atmospheric processes were proposed as forcing mechanisms for the climatic teleconnections between high and medium latitudes. However, an improved understanding on their effects over terrestrial and marine environments is still required. Recently, it has been demonstrated that the western Mediterranean overturning system was enhanced during collapse or reduction of the formation of North Atlantic Deep Water (NADW), likely favoured by the intensification of north-westerly winds as a consequence of the expansion of ice sheets in the North Atlantic region (Cacho et al., 2000; Moreno et al., 2002; Sierro et al., 2005). However, invasion of low-salinity waters from polar sources, including the melting of the icebergs released during the collapse of the NADW circulation at HEs, likely resulted in a temporary reduction of the formation of Western Mediterranean Deep Water (WMDW) (Sierro et al., 2005). In addition, changes in the properties and, possibly, in the volume of WMDW formed in the Gulf of Lion likely caused important modifications in the heat and salt volumes injected by the Mediterranean outflow water (MOW) into the North Atlantic, thus preconditioning the North Atlantic THC to switch from one mode to another (Bigg and Wadley, 2001; Voelker et al., 2006). The finding that a strong and dense MOW flowed at deeper levels during the Last Glacial Maximum than today (Rogerson et al., 2006) supports the view that the properties of the WMDW changed along the last deglaciation. Cacho et al. (2006) have reported changes in the deep-water temperature of WMDW related to the D–O cycles in core MD95-2043 from the Alboran Sea. Though on a very different time-scale, monitoring studies have revealed that WMDW density increased after the severe 2004/2005 winter in the north-western Mediterranean region (López-Jurado et al., 2005; Canals et al., 2006). From the above it becomes clear that both the influence of North Atlantic climate variability on WMDW formation and, inversely, the impact of Mediterranean Deep Waters on NADW production must be better understood as they are one of the key components of climate change during the last glacial period and the present interglacial in the concerned regions.

At present, the north/south displacements of the Azores high-Icelandic low-pressure system and their intensity variations control the transmission of heat and moisture between low and high latitudes (Barry and Chorley, 1998; Bolle, 2003). This pattern is known as the North Atlantic Oscillation (NAO), which oscillates at decadal scale modulating much of the present-day climate variability in the entire region (Hurrell, 1995; Rodó et al., 1997). During a positive phase of the NAO, an increased pressure gradient in the North Atlantic region results in more frequent and stronger winter storms following a more northerly track, resulting in warm and wet winters in northern Europe. During a negative phase of the NAO, a reduced pressure gradient results in a southward displacement of the winter storms bringing higher precipitation to the Mediterranean region.

In this work, the analysis and interpretation of combined sedimentological proxies, i.e. grain-size parameters, and bulk geochemical ratios, together with the isotopic signal from planktonic and benthic foraminifera from core MD99-2343, allow the identification of changes in deep water properties and behaviour in the western Mediterranean Basin during the last 50 kyr. The results achieved so far provide new clues for understanding the mechanisms behind and the feedbacks of abrupt climate changes in the western Mediterranean region and their transmission to the deepest part of the western Mediterranean Basin.

2. Core location and present conditions

The present work focuses on the study of the 32.44 m long IMAGES-V core MD99-2343 recovered north of the Minorca Island (40°29.84′N, 04°01.69′E) at 2391 m of water depth, onboard R/V *Marion Dufresne* (Fig. 1). The core was recovered in a sediment drift formed by deep contour currents belonging to the southward branch of the WMDW flow, which borders the Valencia Trough from north to south following a cyclonic pattern at depths of ~2000 m (Millot, 1999) (Fig. 1). At this place the abrupt slope of the Balearic Promontory opposes deep circulation that accelerates and turns eastward bordering the base-of-slope of Minorca in its way to the open basin. Although no current meter data have been collected at the core location, intense deep currents have been interpreted from seafloor bedforms (Mauffret et al., 1982; Maldonado et al., 1985a; Palanques et al., 1995). Additionally, the base-of-slope peripheral depression and the associated sediment drift, previously described by Velasco et al. (1996), demonstrate the existence of relatively intense deep currents sweeping the deep slope north of Minorca.

The formation of a sediment drift is also depending on sediment availability. Most sediment inputs to this region come from the Ebro and Rhône fluvial discharges. However, only 10% of this sediment discharge reaches the deep basin (Martin et al., 1989) and the core location is too far from the coast to directly receive material from riverine origin. In the specific setting of the Balearic margin local mass gravity flows and hemipelagic settling have been identified as significant contributors of sediment to the

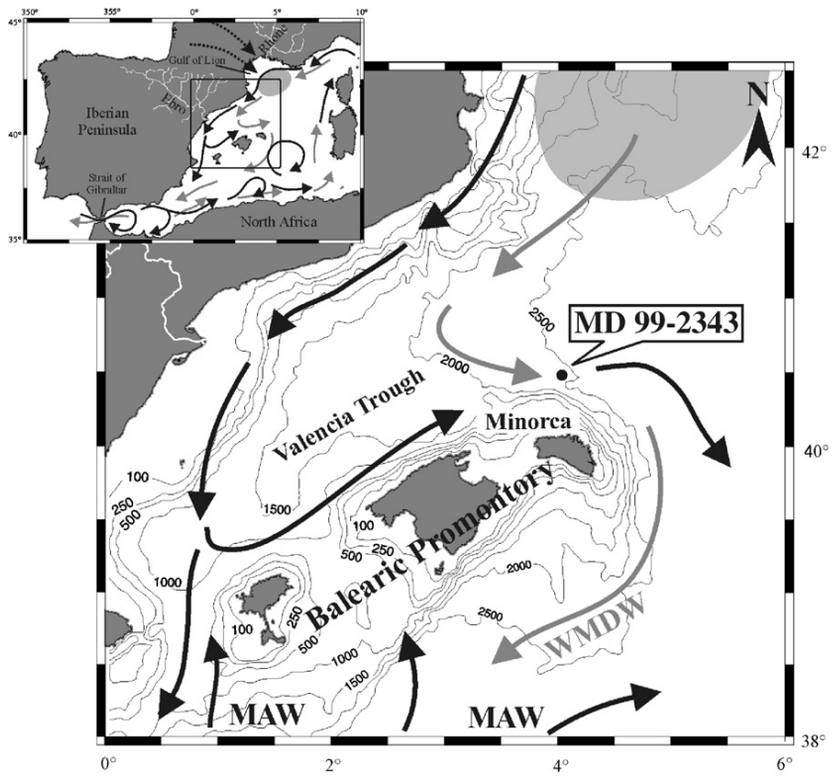

Fig. 1. Bathymetric map of the study area in the north-western Mediterranean Basin showing the location of core MD99-2343. Surface and deep main circulation patterns are represented by black and gray arrows, respectively. The shaded area shows the region of WMDW formation in the Gulf of Lion under the influence of north-westerly winds, illustrated as dotted arrows (inset). Rhône and Ebro Rivers supplying most freshwater inputs to this basin are also shown.

deep margin and basins surrounding the promontory (Maldonado et al., 1985a, b; Nelson and Maldonado, 1990; Alonso et al., 1995; Palanques et al., 1995; Calafat et al., 1996). Subsequently, deep water currents are assumed to rework, sort and transport these sediments and accumulate specific fractions on the sediment drift where core MD99-2343 was recovered (Fig. 1).

This Minorca sediment drift has been built under the action of deep contour currents related to the WMDW, which to a large extent forms in the Gulf of Lion by evaporation and cooling of the sea surface mostly during cold and windy winters, thus increasing the density of offshore surface waters until they sink (MEDOC, 1970; Lacombe et al., 1985; Millot, 1999). In addition to offshore convection, episodic dense shelf water cascading in the Gulf of Lion has been recently described to account for large volumes of sinking waters that add to WMDW (Canals et al., 2006). Deep water sources in the Gulf of Lion depend on wind stress variability and fluvial water discharge on the shelf preconditioning buoyancy. The formation of WMDW is also affected by the amount and depth of the warm and salty Levantine Intermediate Water (LIW) available in the basin before each event (Pinardi and Masetti, 2000; Millot and Taupier-Letage, 2005). LIW forms in the eastern Mediterranean basin as a consequence of evaporation and sinking of Modified Atlantic Water (MAW), which entered the Mediterranean Sea across the Strait of Gibraltar due to the negative hydrological balance caused by the excess of evaporation over freshwater inputs (Millot, 1999). At the end of a general cyclonic pattern, the dense LIW and WMDW leave the Mediterranean Basin through the Strait of Gibraltar as the deep MOW (Millot, 1999).

3. Material and methods

3.1. MD99-2343 core description

This study focuses on the top 17 m of the core that corresponds to the last 50 kyr (see Section 3.4 below). The upper 5 m (deglaciation and Holocene) consists of homogeneous gray nannofossil and foraminifer silty clay with moderate bioturbation. Below the top 5 m (last glacial period) the sediments are much more laminated and present mm to cm-thick grayish orange, yellowish brown, light olive brown and brownish black layers within a dominant homogeneous gray silty clay. Rare sandy layers were also described onboard. Moderate bioturbation, pyrite, organic matter, foram-rich and broken-shell layers were also observed throughout this section. Onboard

smear slides showed high contents of detrital minerals with abundant quartz and mica silt grains.

One centimeter thick samples were taken every 4–6 cm for grain-size and major element composition analyses of the bulk sediment. In addition, samples every 2 cm were taken for grain-size analyses along specific intervals.

3.2. Geochemical analyses

The content of major elements in sediment samples was determined by means of X-ray fluorescence using a PW 2400 sequential wavelength disperse X-ray spectrometer. Prior to the analysis, samples were ground and homogenized in an agate mortar and glass discs were prepared by fusing about 0.3 g of bulk sediment with lithium tetraborate in an induction oven Perle'X-2. Analytical accuracy was checked by measuring international standards (GSS-1–GSS-7) and was better than 1% of certified values. Precision of individual measurements was better than 0.9% as determined from replicate analyses of sediment samples (repeatability). Precision over the period of measurement was better than 3.4% (reproducibility) for all elements analyzed in this work. In order to avoid spurious correlations between elements due to closure effect to 100%, i.e. dilution effects caused by variations in biogenic carbonate content (Wehausen and Brumsack, 2000), element/Al ratios (Rollinson, 1993) are discussed.

3.3. Grain-size analyses

Grain-size analyses were performed on both the *total fraction* (organic matter removed with 10% H_2O_2) and the *non-carbonate fraction* (both organic matter and carbonate were removed with H_2O_2 and HCl, respectively). Grain-size distributions were measured with a Coulter LS 100 laser particle size analyzer (CLS), which determines particle grain-sizes between 0.4 and 900 μm as volume percentages based on diffraction laws (McCave et al., 1986; Agrawal et al., 1991). Diffraction is assumed to be given by spherical particles and the particle size is given as an "equivalent spherical diameter". Consequently, laser diffraction methods are claimed to underestimate plate-shaped clay mineral percentages. This underestimation has been corrected following Konert and Vandenberghe (1997). CLS precision and accuracy were tested by several control runs using latex micro-spheres with pre-defined diameters and the LS size control G15, which gave a coefficient of variation of 1.5%. Grain-size results are presented as the median of each sample since it represents the distribution midpoint and it usually constitutes a representative value of grain-size distribution better than the mean. In addition, the UP10 size (i.e. particles coarser than 10 μm) is considered, which adds the fine sand subpopulation to the sortable silt size fraction (10–63 μm) (McCave et al., 1995) and the silt/clay ratio as both parameters provide information about changes in paleocurrent intensity (Hall and McCave, 2000).

3.4. Chronostratigraphy

The age model for the upper 17 m of core MD99-2343 is based on 10 ^{14}C-AMS datings covering the last 17 ka (Sierro et al., 2005; Frigola et al., 2007), the correlation of the *Globigerina bulloides* $\delta^{18}O$ signal with the GISP2 oxygen isotopic record (Grootes et al., 1993; Meese et al., 1997) for MIS3 following (Sierro et al., 2005) and four additional tie points with the *G. bulloides* oxygen isotopic record from the Alboran Sea core MD95-2043 for the deglaciation and MIS2 (Cacho et al., 1999; Sierro et al., 2005) (Fig. 2 and Table 1). The ages were calibrated with the standard marine correction of 408 yr and the regional average marine reservoir correction (ΔR) for the western Mediterranean Sea by means of the Calib 5.0.1 program (Stuiver and Reimer, 1993) and the MARINE04 calibration curve (Hughen et al., 2004). Following this age model, which covers the last 50 kyr, the mean sedimentation rate for the top 17 m of core MD99-2343 is 36 cm kyr^{-1} (Fig. 2), therefore allowing a centennial resolution in the study of the sediment record.

4. Results

4.1. Geochemical record

Several authors have used Si/Al, Ti/Al and K/Al ratios as proxies for terrigenous inputs in the Mediterranean region (Wehausen and Brumsack, 1999; Moreno et al., 2002; Weldeab et al., 2003; Frigola et al., 2007). Si mostly comes from alumino-silicates and quartz since biogenic opal is of minor importance in this sea due to its oligotrophic conditions and the dissolution of silica (Weldeab et al., 2003). Ti resides within heavy minerals such as ilmenite and rutile. K is associated with clay minerals, mainly illite (Wehausen and Brumsack, 1998, 2000).

Si/Al, Ti/Al and K/Al records from core MD99-2343 are shown in Fig. 3. The highly similar records of Si/Al and Ti/Al display a minimum from 13 to 10.5 ka that coincides with high summer insolation values (Fig. 3e). The decrease in the geochemical signal occurred during a pronounced decreasing trend of the oxygen isotopic signal from *G. bulloides* marking the last deglaciation (Frigola et al., 2007). The observed minima divides the Si/Al and Ti/Al records in to two parts: (i) from 50 to 13 ka, with high though variable values that characterize the glacial period, and (ii) from 10 ka to present time, with lower values and a smoother pattern. The last 10 kyr record, as described in detail in Frigola et al. (2007), can be divided into three successive phases: (i) an increasing phase in both ratios coincident with the end of the second phase of Termination (TIb) and the early Holocene (10.5–7 ka), (ii) a central plateau with relatively high values during the mid-Holocene (7–4 ka) and (iii) a gradually decreasing phase during the late Holocene (4–0 ka) (Fig. 3). The general long-term trend in the Si/Al and Ti/Al ratios is punctuated

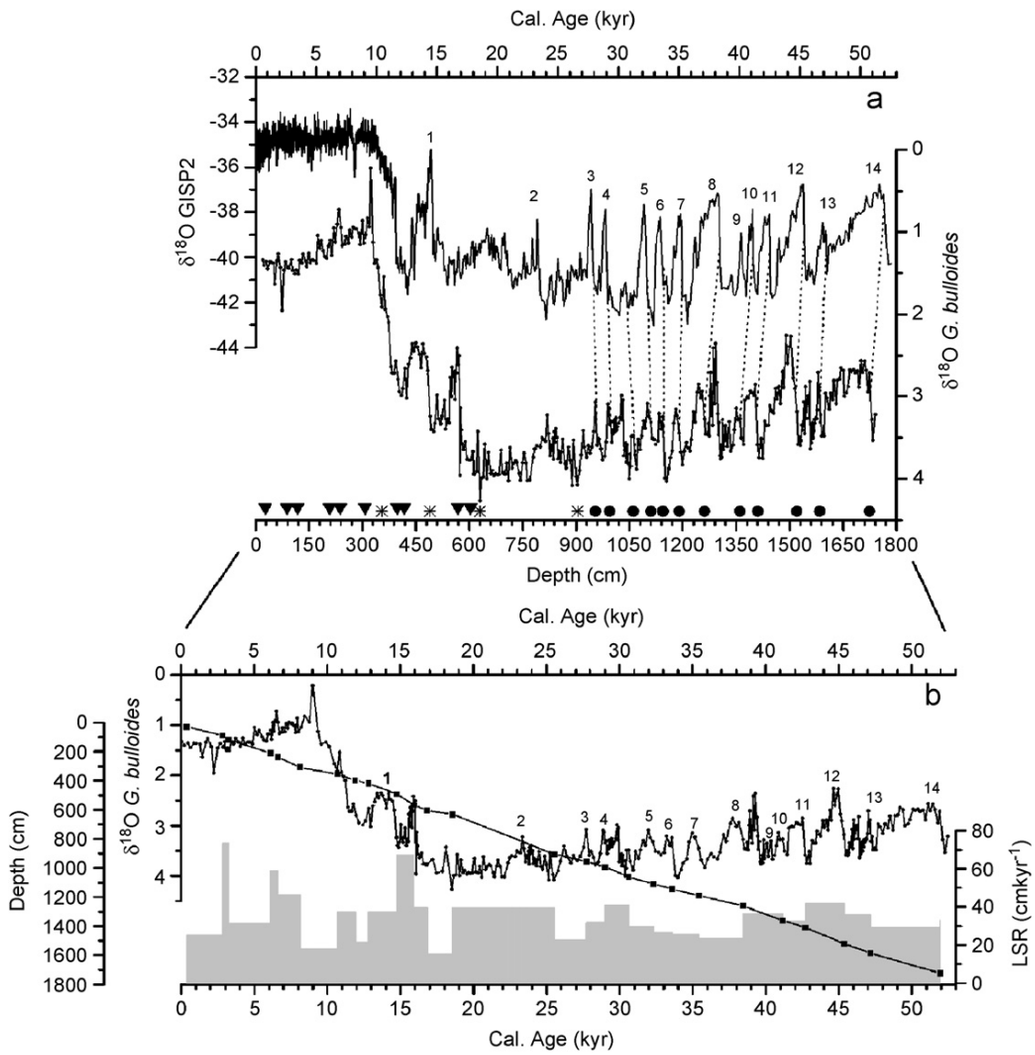

Fig. 2. (a) Age model of core MD99-2343 developed by means of 10 ^{14}C-AMS dates (triangles), the tuning of the *G. bulloides* δ^{18}O record with the ice δ^{18}O record from the GISP2 core (circles) and the tuning with the δ^{18}O record of the core MD95-2043 from the Alboran Sea (asterisks). See Table 1 for details. (b) Linear sedimentation rates (LSR) of core MD99-2343 for the last 50 kyr oscillating between 15 and 73 cm kyr^{-1}.

by eight abrupt relative increasing events coincident with increments in the planktonic δ^{18}O record. The general pattern of the K/Al record is completely different with its most remarkable feature being its high parallelism with the summer insolation curve at 40°N, which is particularly apparent for the last 40 kyr (Fig. 3d and e).

In addition to the observed general trends, geochemical ratios from core MD99-2343 exhibit pronounced millennial-scale changes during MIS3 that roughly correspond to the D–O oscillations described in the planktonic δ^{18}O record (Sierro et al., 2005), which parallel the Greenland Stadials (GSs) and Interstadials (GISs) from δ^{18}O ice records (Dansgaard et al., 1993; Grootes et al., 1993). That the geochemical and the isotopic records from core MD99-2343 are not completely in phase can be observed by comparing the plots in Fig. 3a–d. Abrupt increases of the geochemical ratios generally occur just after the lightest values of the δ^{18}O record have been reached coinciding with the GIS/GS transitions. In contrast, the lowest Si/Al and Ti/Al values most often coincide with low values in the δ^{18}O record corresponding to GIS.

Five abrupt increases in Si/Al and Ti/Al ratios have been identified at 46, 39, 30, 24 and 16 ka that, with one exception, parallel the incursions of the polar water species *Neogloboquadrina pachyderma* (s) (Fig. 3f). These increases in the geochemical proxies also fit with peaks of abundance of the coccolithophore *Emiliania huxleyi* (>4 μm) (Fig. 3(g) (Sierro et al., 2005), which is identified as a cold water species indicator in NE Atlantic and Mediterranean regions (Colmenero-Hidalgo et al., 2002, 2004). These intervals correlate with HE1–HE5 described in the North Atlantic region (Heinrich, 1988; Bond et al., 1992; Broecker et al., 1992). Opposite to Si/Al and Ti/Al ratios, the K/Al record generally shows abrupt decreases during the HEs, which are especially pronounced during the latest part of HE5, HE4 and HE1 (Fig. 3d). The lowest values in

Table 1
Tie points used for the age model of core MD99-2343

Radiocarbon sample or isotope event/foram type	Core depth (cm)	^{14}C age (yr BP)/tie points tuned with	Calendar years
AMS 14C/multispecific	28	790 (±40)	386±55
AMS 14C/*G. inflata*	88	3110 (±30)	2816±50
AMS 14C/multispecific	118	3390 (±50)	3225±80
AMS 14C/*G. inflata*	208	5720 (±40)	6091±70
AMS 14C/multispecific	238	6210 (±50)	6601±70
AMS 14C/*G. inflata*	308	7700 (±40)	8110±60
TIb—Onset of the Holocene	354	MD95-2043	10,696
AMS 14C/*G. bulloides*	398	10,650 (±50)	11,883±230
AMS 14C/*G. inflata*	418	11,200 (±50)	12,811±30
Base Bolling–Allerod	490	MD95-2043	14,750
AMS 14C/*G. bulloides*	568	13,850 (±40)	15,912 ±190
AMS 14C/multispecific	604	14,550 (±110)	16,820 ±240
LGM	630	MD95-2043	18,539
Enrichment after Interstadial 3	904	MD95-2043	25,525
Base Interstadial 3	954	GISP2	27,736
Base Interstadial 4	994	GISP2	29,000
Base warming event	1060	GISP2	30,619
Base Interstadial 5	1110	GISP2	32,300
Base Interstadial 6	1144	GISP2	33,587
Base Interstadial 7	1190	GISP2	35,400
Base Interstadial 8	1260	GISP2	38,432
Base Interstadial 10	1360	GISP2	41,172
Base Interstadial 11	1410	GISP2	42,713
Base Interstadial 12	1520	GISP2	45,360
Base Interstadial 13	1584	GISP2	47,146
Base Interstadial 14	1724	GISP2	51,933

Ten ^{14}C-AMS dates were calibrated with the Calib 5.0.1. program (Stuiver and Reimer, 1993) and the MARINE04 calibration curve (Hughen et al., 2004). Prior to 27 ka the age model is based on the correlation with the GISP2 ice core (Grootes et al., 1993; Meese et al., 1997). Four additional tie points were added through the comparison of the *G. bulloides* δ^{18}O from both cores MD99-2343 and MD95-2043 (Cacho et al., 1999; Sierro et al., 2005). The age model was performed with the AnalySeries Version 1.1 (Paillard et al., 1996).

the K/Al record are the most recent ones that correspond to the current summer insolation minimum (Fig. 3d and e).

4.2. Grain-size record

Median grain-size values (between 4 and 9 μm) of both bulk and non-carbonate sediment fractions show fairly similar features (Fig. 4b) thus pointing to the same processes controlling the deposition of the two fractions. However, due to the mixed origin of the carbonate fraction (e.g. sea surface production of carbonate particles and inputs from the carbonate Balearic shelf), the non-carbonate fraction better represents the intensity of bottom currents (McCave et al., 1995).

The sortable silt size (10–63 μm) has been used as a proxy to infer the intensity of deep water currents (McCave et al., 1995). However, since strong contour currents are also able to rework particles coarser than 63 μm, the UP10 fraction has been considered here for the study of paleocurrent intensity (Frigola et al., 2007). The general trend from UP10 and silt/clay ratio profiles through the last 50 kyr shows affinities with the summer insolation record at 40°N (Fig. 4c–e). As for the geochemical proxies, grain-size records present different patterns during the glacial and interglacial periods, with a marked decreasing trend from 15 ka until 10.5 ka, which corresponds to the highest part of the rising limb of the summer insolation curve at 40°N. This reduction in the grain-size records is two-step and seems to show some relation with the two phases of the deglaciation interval marked by almost synchronous decreases in the *G. bulloides* δ^{18}O profile (thus embracing the Younger Dryas). After the minimum grain-size values at 10.5 ka, relatively coarse grain-size values quickly resume at the onset of the Holocene. A general decreasing trend characterizes the last 9 kyr of the UP10 and silt/clay records that roughly parallel the *G. bulloides* δ^{18}O increasing trend (Fig. 4a, c and d). This overall Holocene tendency towards grain-size reduction coincides with a diminution of the seasonal insolation differences at 40°N (Fig. 4e). Superimposed on the general long-term trend, the grain-size record is punctuated by eight abrupt increases known as Minorca abrupt events (Frigola et al., 2007).

The glacial period is characterized by mean higher and more variable grain-size values than the Holocene. From 50 to 29 ka background levels are punctuated by a series of millennial-scale oscillations at D–O cyclicities (Fig. 4c and d). It is worth to note that these records are not totally synchronous with the *G. bulloides* δ^{18}O: low values of the grain-size proxies are coincident with low values in the δ^{18}O record (GIS), while abrupt increases in the grain-size

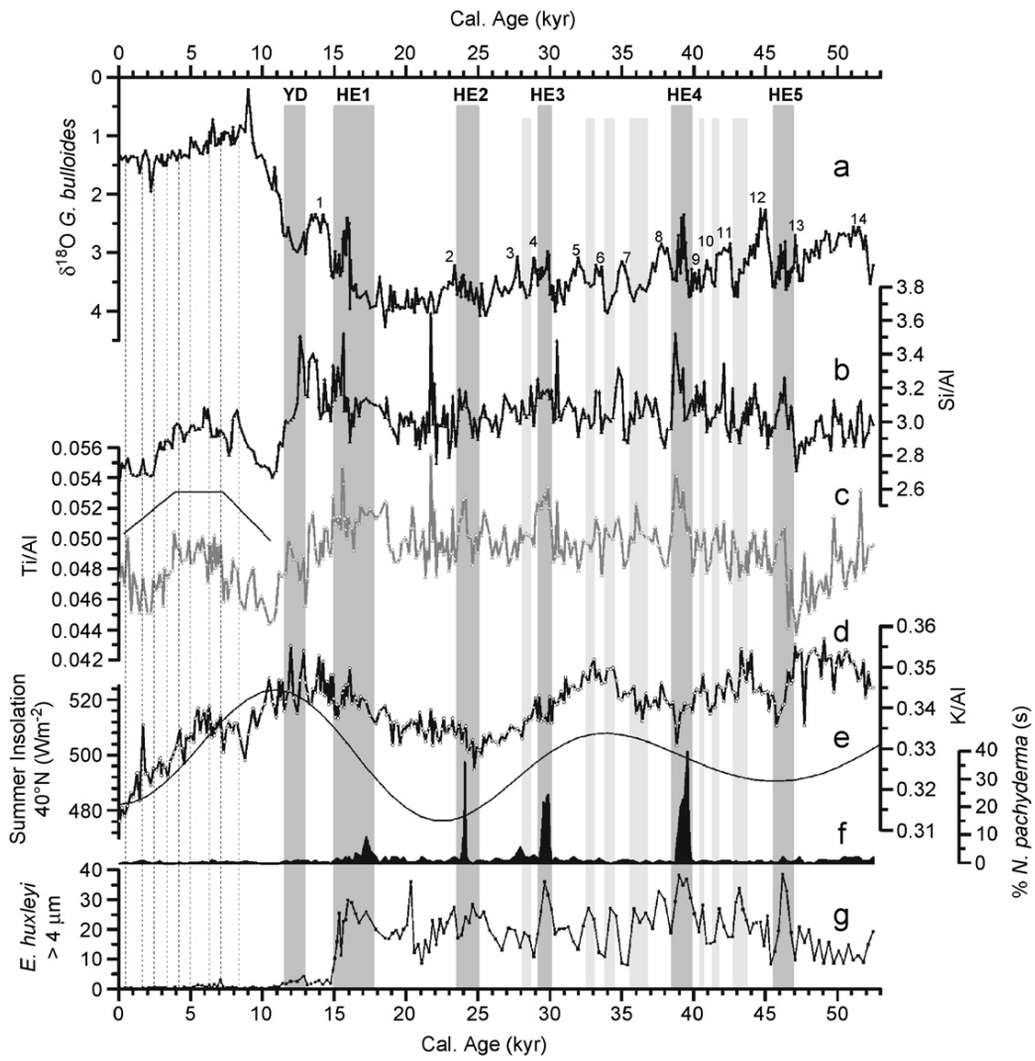

Fig. 3. (a) *G. bulloides* $\delta^{18}O$ record from core MD99-2343 for the last 50 kyr. Numbers above the curve represent warm GIS while gray bars correspond to cold GS, HEs and YD cold events. Vertical dashed lines to the left correspond to the Minorca abrupt events defined by Frigola et al. (2007) during the Holocene. (b, c and d) Si, Ti and K geochemical records normalized to Al, respectively. A continuous line between the Si/Al and the Ti/Al ratios embracing the 10.5–0 ka period represents three main phases within the general trend (see main text). (e) Summer insolation curve at 40°N for the last 50 kyr. (f) Percentages of polar water species *Neogloboquadrina pachyderma* (s). (g) Percentages of *E. huxleyi* larger than 4 μm.

proxies occur coincident with the GIS/GS transitions (Fig. 4a, c and d). In spite of the lack of synchrony among grain-size proxies and the planktonic $\delta^{18}O$ record, the pattern that characterizes a D–O cycle is very systematic. Increases in the silt/clay and in the UP10 fraction are abrupt while decreases are somewhat smoother, e.g. during GIS12 or GIS8, and almost parallel to the increasing trend observed in the $\delta^{18}O$ record from GIS to GS transitions (Fig. 4a, c and d). In addition, sudden increases in the silt/clay ratio also occur at the end of a series of abrupt progressively shorter oscillations, which are coincident with HE5, HE4 and HE3, identified from the *G. bulloides* $\delta^{18}O$ record (Sierro et al., 2005). The D–O variability in the grain-size proxies is interrupted by an abrupt decrease at 29–28 ka where very low values occur. This reduction in the grain-size proxies was contemporary with an important decrease in the orbitally induced seasonal differences at times when winter insolation values were higher than at present (Fig. 4e). After that reduction a general increasing trend in both proxies from 26 to 15 ka is almost coincident with the increase in the summer insolation at 40°N or, in other words, with an increase in the orbitally induced seasonal differences (Fig. 4e).

5. Discussion

5.1. Orbitally-driven trends in the terrigenous signal

The K/Al record from core MD99-2343 shows a rather smooth pattern during the last 50 kyr that roughly parallels the summer insolation at 40°N with minimum values occurring during times of low summer insolation (Fig. 3).

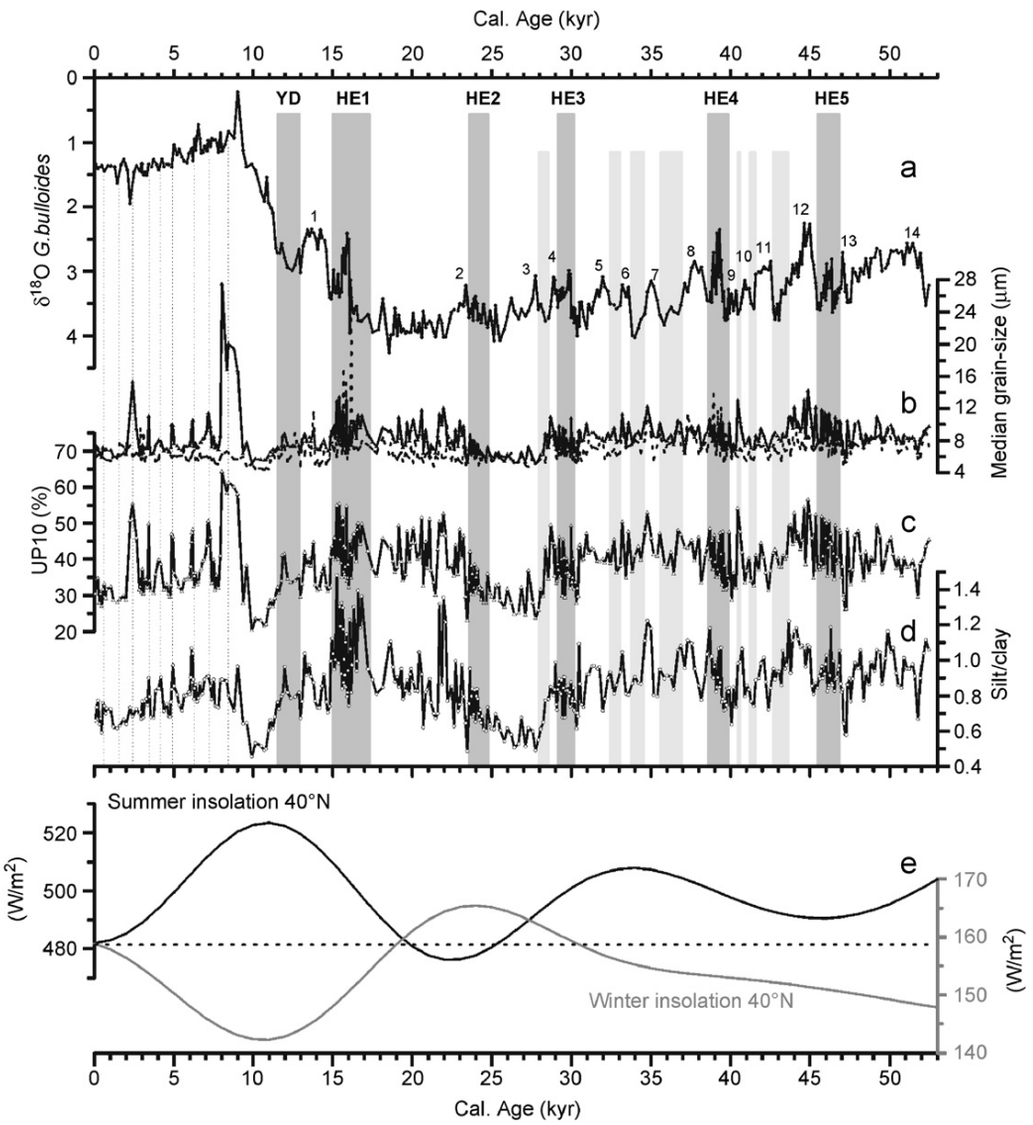

Fig. 4. (a) *G. bulloides* $\delta^{18}O$ record from MD99-2343 for the last 50 kyr. Numbers above the curve represent warm GIS while gray bars correspond to cold GS, HEs and YD cold events. Vertical dashed lines to the left correspond to the Holocene Minorca abrupt events defined by Frigola et al. (2007). (b) Median grain-size records of the total (dashed line) and non-carbonate sediment fractions (solid line). (c and d) UP10 fraction (> 10 μm) and silt/clay ratio of the non-carbonate fraction, respectively. (e) Summer and winter insolation curves at 40°N for the last 50 kyr. Current values of both summer and winter insolation are plotted at the same level so that distances between both records through time can be interpreted as orbitally induced seasonal differences.

Superimposed on this long-term trend, millennial-scale oscillations appear as relatively minor features of the record. Sea level changes associated with the last deglaciation did not seem to produce any clear modulation in the K/Al record. These results suggest that K/Al oscillations have been mainly controlled by processes driven by orbitally induced insolation changes. Potassium (K) used to be mainly associated with clays, i.e. illite from continental runoff, and hence the K/Al ratio is interpreted in terms of river discharge (Wehausen and Brumsack, 1998, 2000). In the north-western Mediterranean region the Rhône and the Ebro rivers are the main sources of fluvial sediment inputs, with water supply mostly reflecting precipitation in the Alps and the Pyrenees, respectively. Of these two main rivers, the Ebro clearly has a stronger Mediterranean character (i.e. a more pronounced seasonality). According to the MD99-2343 record, enhanced supply of clays (high K/Al values) occurred during periods of high summer insolation pointing to elevated precipitation or to a more efficient sediment transport regime, such as that produced due to increased torrential rains in general in the watersheds supplying the basin. In addition, enhanced aridification of the watersheds facilitates erosion resulting in higher lithogenic fluxes when seasonal rains occur (Fabres et al., 2002). These results indicate the strong control that orbitally induced insolation changes exerted on the fluvial runoff of detrital material in the western Mediterranean Basin at least during the last 50 kyr. In the

Eastern Mediterranean a precession control on Pliocene–Pleistocene sapropel formation and, therefore, on climatic and hydrographic conditions has been proposed by several authors (Hilgen, 1991; Rohling and Hilgen, 1991; Wehausen and Brumsack, 2000). The K/Al record from core MD99-2343 supports the precessional control on the climatic conditions of the western Mediterranean region as well.

Grain-size records, i.e. the silt/clay ratio, display a more complex pattern of variability. Although millennial-scale oscillations are very pronounced, a precessional frequency is also present, especially after 30 ka, when seasonal insolation differences are well marked (Fig. 4). Low silt/clay values occur during periods of relatively high winter insolation like the late Holocene and around 28 ka (Fig. 4d). Increments in the silt versus the clay fraction are attributed to enhanced deep currents able to transport coarse material to the Minorca sediment drift and winnow the finest sediment fraction. Deep water currents at the drift location belong to the WMDW mass whose overturning occurs in the Gulf of Lion. Formation of WMDW is a wintertime process and is strongly dependent on the intensity of north-westerly winds (MEDOC, 1970; Lacombe et al., 1985; Bethoux et al., 1990). The dominance of weaker deep currents at times of maximum winter insolation, as interpreted from the silt/clay ratio, is consistent with reduced intensities of the north-westerly winds during milder winters due to lower atmospheric pressure gradient and, consequently, with a less intense overturning in the Gulf of Lion.

This precessional-induced long-term pattern in the silt/clay ratio is sharply interrupted at 12–10 ka when winter insolation was at its minimum. Therefore, the silt/clay reduction occurred synchronously with the second phase of the Termination (TIb) suggesting that sea level oscillations also influenced deep water overturning in the basin. The low grain-size values recorded during this specific time interval are consistent with reduced deep water ventilation, which allowed the preservation of an organic rich layer (Cacho et al., 2002) and the dominance of low-oxygen benthic fauna (Caralp, 1988) in the Alboran Sea. Such a reduction in the western Mediterranean overturning further supports the effect of the post-glacial sea level rise on the stratification of Mediterranean waters during TIb, as suggested by former models (Rohling, 1994; Matthiesen and Haines, 2003). In addition, high K/Al values point to increased fluvial discharge because of more humid conditions at that time (Fig. 3d), which would also confirm persistent water column stratification. More humid conditions during the 12–10 ka interval have been also inferred from pollen and lacustrine sequences from the borderlands (Harrison and Digerfeldt, 1993; González-Sampériz et al., 2006). Overall, these results demonstrate that the combined effect of the post-glacial sea level rise (and the subsequent global reduction of the salinities of surface waters) and an astronomically induced precipitation increase enhanced water column stratification and, therefore, were responsible for the reduction of the deep water overturning in the western Mediterranean. These mechanisms likely extended to the whole Mediterranean Basin and anticipated the formation of Sapropel 1 in the eastern Mediterranean Basin (Rohling, 1994).

Contrarily to the K/Al ratio, the Si/Al and Ti/Al records do not show consistent patterns of variability related to precessional insolation changes. Both Si/Al and Ti/Al ratios are associated with terrigenous inputs and should reflect changes in the processes controlling the amount and/or distribution of such inputs to the basin (Matthewson et al., 1995; Reichart et al., 1997; Wehausen and Brumsack, 2000; Moreno et al., 2002; Weldeab et al., 2003; Frigola et al., 2007). The observed differences between Si/Al, Ti/Al and K/Al ratios should be related to grain-size geochemical segregation since Si and Ti are related to coarse minerals and K to clay minerals. Consequently, Si/Al and Ti/Al ratios should be linked to processes controlling the grain-size distribution in the Minorca rise at higher frequencies than precessional. This interpretation is supported by the good correlation of these two geochemical ratios and the silt/clay ratio where most variability occurs at millennial time-scales.

5.2. Millennial-scale variability during the Holocene

The general pattern of the Si/Al and Ti/Al records during the Holocene, following their marked reduction during the last deglaciation (see Section 5.1 and Fig. 3b and c), can be subdivided into three phases. The first phase (10.5–7 ka) shows increasing values in both geochemical ratios but also embraces a sharp increase in the grain-size proxies (Figs. 3 and 4) indicating the recovery of the WMDW formation at the onset and early Holocene after the highest sea level rise rate was achieved (Fleming et al., 1998).

During the second phase (7–4 ka), which is synchronous with the end of the post-glacial sea level rise (Fleming et al., 1998), a sort of plateau is observed in the Si/Al and Ti/Al ratios (Fig. 3b and c). This mid-Holocene phase illustrates the high control that the sea level rise exerted on the overturning system in the Gulf of Lion. This was a period when the rather small range of variation of the geochemical proxies (Fig. 3) suggests no significant changes occurred in the fluvial supply to the basin neither in the overturning cell in the Gulf of Lion. By contrast, during the same interval, strong changes were reported worldwide (Steig, 1999) and, in particular, from the Mediterranean borderlands (COHMAP, 1988; Cheddadi et al., 1997; Prentice et al., 1998; Magny et al., 2002) and the North African region (Vernet and Faure, 2000) as associated with the end of the African Humid Period (deMenocal et al., 2000). Such a mid-Holocene climate variability is attributed to the reduction of seasonal insolation differences after 5.5 ka (Fig. 4e), which lead to an abrupt transition from humid to arid conditions in North Africa and in the western Mediterranean region. However, the Si/Al and Ti/Al records do not

seem to respond to those changes and only K/Al shows a clear reduction after that moment. The observed discrepancies between the various geochemical proxies suggest again different forcings: while Si/Al and Ti/Al mainly reflect changes in deep water currents, with a fluvial input modulation, K/Al mainly shows changes of humidity conditions on the borderlands. Therefore, the K/Al descending general trend after 5.5 ka is in phase with the end of the African Humid Period (deMenocal et al., 2000) and marks the establishment of drier conditions.

During the third phase (4–0 ka) the trends of the Si/Al and Ti/Al ratios point to an overall reduction of fluvial inputs likely due to the establishment of drier conditions and reduced precipitation. The overall continued rapid descent of the K/Al recorded also during the late Holocene confirms the reduction of fluvial inputs that parallel diminishing seasonal insolation differences (Figs. 3d and 4e). In addition, the rather subtle decreasing trend observed in the silt/clay ratio during the late Holocene (Fig. 4d) also points to a reduction of the overturning cell in the Gulf of Lion. Less intense deep water currents and reduced fluvial inputs would translate into an overall decreasing trend of the sedimentation rates as observed in Fig. 2b. A lower atmospheric pressure gradient due to the diminished seasonal insolation differences likely favored the establishment of drier conditions during the late Holocene (McDermott et al., 1999; Jalut et al., 2000; Magny et al., 2002). In addition, reduced north-westerly winds from a lowered pressure gradient system would be responsible for the lessening of deep water overturning and, consequently, for lower values in the silt/clay ratio (Fig. 4d).

Superimposed on the general Holocene trends, nine $\delta^{18}O$ incremental events with a periodicity close to 1000 yr relate to short cooling events, known as Minorca abrupt events (Fig. 3) (Frigola et al., 2007). Most of these events are characterized by parallel increases in the UP10 and in the Si/Al records (Figs. 3b and 4c) suggesting an intensification of the deep water currents intensity related to an enhancement in the Gulf of Lion's overturning system likely promoted by strengthened north-westerly winds. The timing of the Minorca abrupt events fits well with temperature oscillations from the Holocene $\delta^{18}O$ record in Greenland (Frigola et al., 2007) and suggests a coupled ocean–atmosphere teleconnection mechanism for climate variability transfer between high latitudes and the Mediterranean region. A similar pattern was proposed by Rohling et al. (2002) for the Aegean Sea in the eastern Mediterranean Sea. The occurrence of rapid climate cooling events during the Holocene has been reported worldwide (Mayewski et al., 2004) although disagreements about their precise timing, character and impact require more devoted research to understand the ultimate causes of these millennial-scale climate variability. Although insolation changes (Bond et al., 2001) and instabilities inherent to the North Atlantic THC (Schulz and Paul, 2002) have been proposed as the main causes of the Holocene climate variability, the climatic oscillations recorded in the terrigenous signal of core MD99-2343 are better linked to the temperature signal from the North Atlantic region as highlighted by the correlation with the GISP2 $\delta^{18}O$ profile (Frigola et al., 2007). These results suggest that the atmospheric teleconnection between high latitudes and the Mediterranean region through the westerly winds system was the main control over the western Mediterranean deep circulation during the Holocene.

5.3. D–O variability in WMDW formation

Oxygen and carbon isotopic records from benthic foraminifera in cores MD99-2343 (Fig. 5) and MD95-2043, the later from the Alboran Sea, follow a pattern that is coherent with the D–O events (Cacho et al., 2000; Sierro et al., 2005). These oscillations have been interpreted in terms of changes in the ventilation rates and properties of the deep water masses indicating the dominance of well-ventilated, colder/saltier, WMDW during the GS in contrast to the GIS (Cacho et al., 2006). The increase of WMDW ventilation was suggested to be associated with the strengthening of the north-westerly winds in the Gulf of Lion during GS (Cacho et al., 2000; Sierro et al., 2005). Prevailing dry and cold conditions on land were observed along the same intervals (Allen et al., 1999; Combourieu Nebout et al., 2002; Sánchez Goñi et al., 2002). Thus, the increased WMDW formation during GS likely favored stronger deep-water currents, and hence deposition of coarser material in the Minorca sediment drift. However, maximum values in the paleocurrent intensity proxies are not recorded during the intervals of maximum ventilation according to benthic isotopes (maximum $\delta^{13}C$ values). In contrast, grain-size and geochemical increments occur slightly after the warmest phases of GIS (minimum planktonic $\delta^{18}O$ values), that is, during the recovering of deep water ventilation in parallel to the starting of the SST cooling phase (B. Martrat, personal communication) (see dotted lines in Fig. 5). This pattern is very consistent for all the GIS/GS cooling transitions and also in all three proxies for paleocurrents intensity (silt/clay, Si/Al and Ti/Al). All three records show synchronous peaks during GIS/GS transitions, which lead by several centuries the maximum ventilation conditions (Fig. 5b and c). These consistent but unexpected results reflect a dichotomy between proxies indicating water chemical properties (benthic and planktonic isotopes) and proxies of water physical properties (grain-size and sediment geochemical proxies). Such a pattern as found in the Minorca sediment drift indicates the high sensitivity of deep water conditions to changes in the properties of surface waters associated with GIS/GS transitions. Overall, these results suggest that the deep-water Minorca sediment drift is particularly sensitive to changes in the vertical position of the WMDW core. Considering that the drift extends from 2100 m to more than 2700 m of water depth, the WMDW core may only occasionally flow at the depth of core MD99-2343, that is,

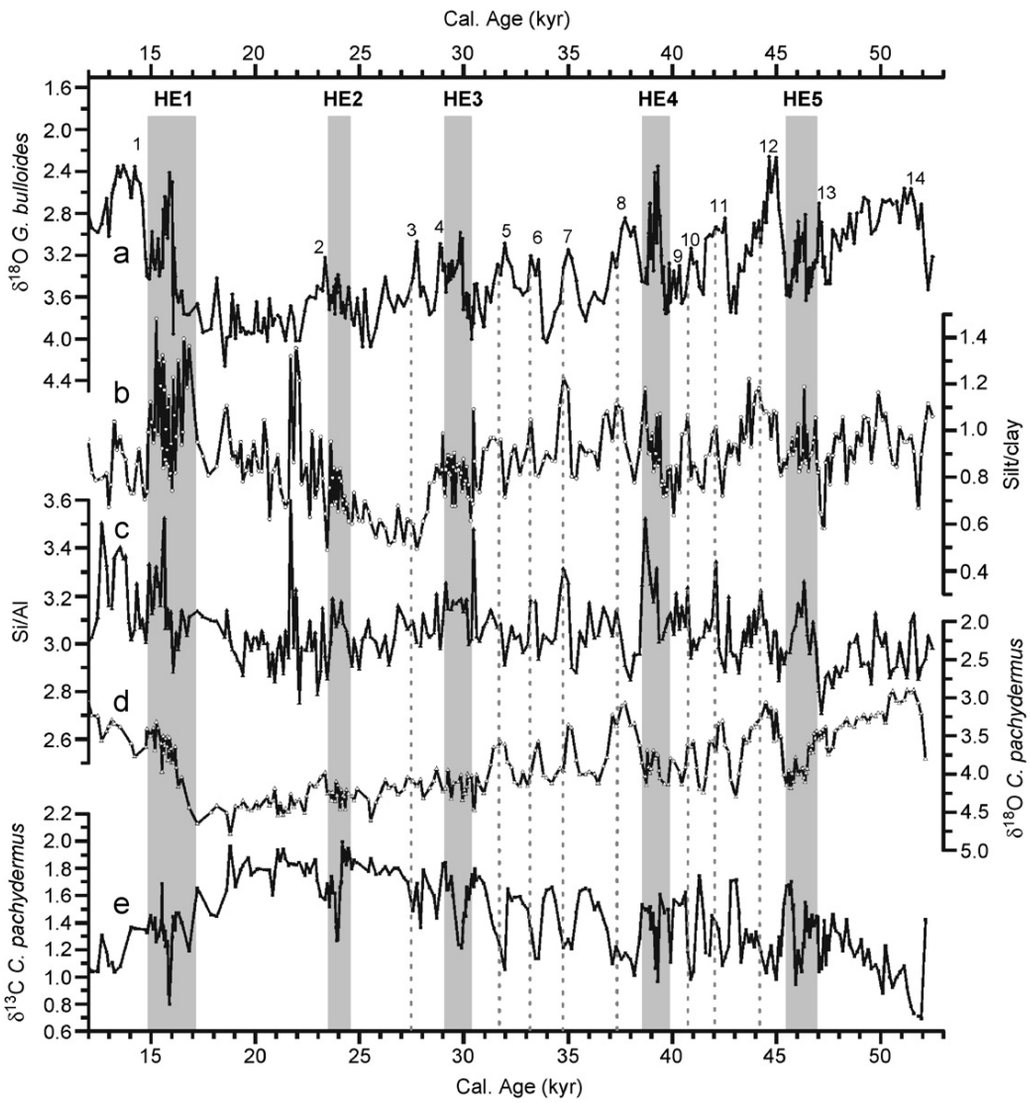

Fig. 5. Records from core MD99-2343 for the 12–50 ka time interval. (a) Planktonic $\delta^{18}O$. (b) Silt/clay ratio. (c) Si/Al. (d) Benthic $\delta^{18}O$. (e) Benthic $\delta^{13}C$. Numbers represent warm GIS while gray bars correspond to HEs. Dashed lines mark maximum values in the silt/clay ratio during MIS3.

2400 m. Therefore, paleointensity proxies indicate that GIS/GS transitions were the time when the WMDW core reached maximum strength at 2400 m. On the other hand, $\delta^{18}O$ and $\delta^{13}C$ records reflect chemical properties of the whole WMDW mass independently of the intensity and depth location of the flow core.

According to the patterns in the chemical and physical proxies along D–O cycles three main stages related to changes in WMDW properties can be defined (Fig. 6a). Stage 1 is a pure GIS stage with the lightest benthic and planktonic $\delta^{18}O$, light benthic $\delta^{13}C$ and low silt/clay values. Stage 2 corresponds to GIS/GS transitions, when SST cooled progressively, and benthic isotopes indicate improving ventilation (increasing $\delta^{13}C$) and incrementing density (increasing $\delta^{18}O$) of the WMDW. It is during Stage 2 when deep current speed proxies (i.e. silt/clay) indicate maximum velocities at the studied site. Stage 3 implies truly GS conditions characterized by maximum $\delta^{18}O$ values in both planktonic and benthic foraminifera, maximum benthic $\delta^{13}C$ and intermediate values of the silt/clay ratio. Stages 1, 2 and 3 can be associated with a weak mode, an intermediate mode and a strong mode of deep-water overturning in the western Mediterranean Sea, respectively. These modes relate to GIS, GIS/GS transitions and GS situations.

Stage 1 corresponds then to intervals of minimum ventilation and lightest WMDW, which is consistent with the relatively warm and humid conditions on land during GISs (Combourieu Nebout et al., 2002; Sánchez Goñi et al., 2002) and minimum deep currents velocities at the MD99-2343 site. Stage 2 started after climate became gradually colder and drier, when the surface water cooling during GIS/GSs transitions likely resulted in an abrupt reduction of the water column density gradient thus

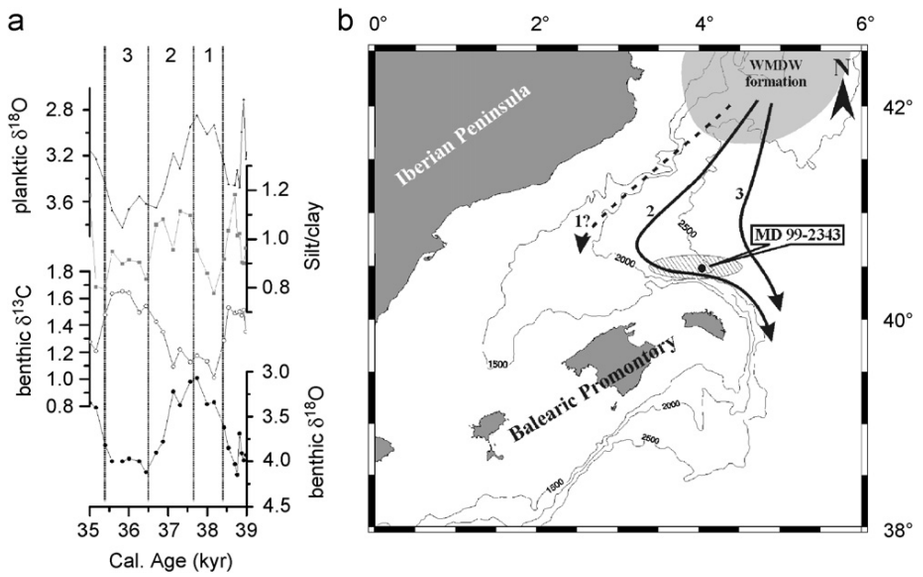

Fig. 6. (a) Detail of the planktonic $\delta^{18}O$, silt/clay, benthic $\delta^{13}C$ and benthic $\delta^{18}O$ records for the 35–39 ka time interval that corresponds to D–O cycle 8 (see Fig. 5). Numbers and vertical dotted lines limit the three stages described for each D–O cycle: Stage 1 during GIS, Stage 2 during GIS/GS transition and Stage 3 during GS. (b) Schematic bathymetric map showing the three modes of circulation within a D–O cycle. (1) weak mode, (2), intermediate mode and (3) strong mode. Depending on the properties of the WMDW formed in the Gulf of Lion (shaded area) the core of the deep currents circulates at different depths, thus having different effects on the Minorca sediment drift (striped area) where core MD99-2343 was recovered.

favoring reinforcement of deep water convection. Increased convection improved deep ventilation and resulted in maximum deep current velocities at the coring site as suggested by the highest silt/clay ratio (Figs. 5 and 6). During Stage 3, as surface conditions were becoming colder, the newly formed WMDW became progressively more ventilated and denser (increasing trends in $\delta^{13}C$ and $\delta^{18}O$) leading to a deepening of the bottom current core and, consequently, to a gradual speed reduction at the coring site as decreasing silt/clay ratio values suggest (Figs. 5 and 6). These results indicate that during times of maximum deep water formation (GS) the influence of the newly formed WMDW over the MD99-2343 site was reduced, likely due to a deeper circulation of those waters. Nevertheless, the silt/clay values recorded during Stage 3 suggest that currents were still active though to a lesser degree than at Stage 2 situations. The comparison among the benthic $\delta^{18}O$ and the grain-size records supports this hypothesis since current intensity systematically decreases when the heaviest $\delta^{18}O$ are reached (Fig. 5b and d). This observation is consistent with a new reconstruction of the properties of WMDW based on Mg/Ca paleothermometry in the Alboran Sea, which documents that the densest WMDW was formed during GS (Cacho et al., 2006). The recurrence of this pattern of variability with D–O cyclicities, with an offset between the physical proxies (e.g. silt/clay ratio) and the planktonic $\delta^{18}O$ record, demonstrates the extremely high sensitivity of the whole water column in the north-western Mediterranean Sea to climate-forced changes of surface water properties that modified the entire density gradient. Denser WMDW formed during GS changed the MOW density in a way that, during intervals of denser MOW, the speed of its lower core increases as shown by coarsening mean grain-sizes from core MD99-2339 in the Gulf of Cadiz (Voelker et al., 2006).

The above described three modes of WMDW overturning appear as triggered by a rapid millennial-scale variability teleconnection between high and medium latitudes. Climate on land and intensity of westerly winds are the main forcing factors of present inter-annual variability in the intensity of WMDW formation together with the salt supply at intermediate levels from the eastern basin through the LIW (Lacombe et al., 1985; Schott and Leaman, 1991; Millot and Taupier-Letage, 2005). The westerlies intensity depends on the atmospheric pressure gradient over the North Atlantic region, in which decadal-scale variability presently is controlled by the NAO (Hurrell, 1995; Rodó et al., 1997). Assuming that a similar variability pattern acted during glacial times, it is likely that the observed changes in the WMDW circulation were controlled by NAO shifts. It has been already proposed that NAO oscillations dominated the glacial variability of the vegetation cover in the Iberian Peninsula and dust inputs from the Sahara region to the western Mediterranean Basin (Moreno et al., 2002; Sánchez Goñi et al., 2002). In addition, changes in the precipitation–evaporation budget at basin scale with D–O cyclicity have been inferred from pollen records in Italy, Greece and Iberia (Watts et al., 1996; Tzedakis, 1999; Sánchez Goñi et al., 2002). It is likely that these shifts in the precipitation–evaporation balance affected WMDW formation due to changes in surface salinity and, therefore, water density. These results also suggest that changes in the heat and salt

volumes exported through the MOW across the Strait of Gibraltar were associated with WMDW fluctuations and could have played an important feedback role in driving millennial-scale climate changes in the North Atlantic region (Bigg and Wadley, 2001).

5.4. Shifts in WMDW formation during HEs

The isotopic record during the GS associated with HEs shows a more complex pattern than the regular GS. Light benthic $\delta^{13}C$ events occur at the middle of these intervals in parallel with planktonic $\delta^{18}O$ depletions (Fig. 7). These surface anomalies would correspond to 2–4‰ salinity lowering caused by the entrance of fresher polar surface waters through the Strait of Gibraltar during each of the HEs (Cacho et al., 1999; Sierro et al., 2005). Such a surface freshening should have reinforced the water column stratification and opposed deep water convection in the Gulf of Lion (Sierro et al., 2005). Weak overturning during HE was not expected since extremely dry and cold conditions on land were reconstructed from pollen sequences (Combourieu Nebout et al., 2002; Sánchez Goñi et al., 2002) and confirmed by the relatively low K/Al values recorded in MD99-2343 (Fig. 3d). Nevertheless, the benthic record indicates that, despite the climatic regime, the freshening of surface water was sufficient to reduce deep water formation (Sierro et al., 2005). Consequently, the GS associated with the HEs in the western Mediterranean had a complex deep ventilation evolution with high ventilation during the early and late phases (gray bars in Fig. 7) and a weakening in the middle of each HE due to surface water freshening (white bars in Fig. 7). All the proxies of deep water current speed (silt/clay, Si/Al and Ti/Al) show high values during the GS associated with the HEs which are consistent with the dominance of stronger deep currents by an active WMDW overturning (Figs. 3 and 4). These results are in contrast with the relatively low values recorded during the non-Heinrich GS and can only compare to the values recorded during GIS/GS transitions (stage 2 in Fig. 6).

The silt/clay record from the GS associated with the HEs does not show a clear systematic pattern of variability

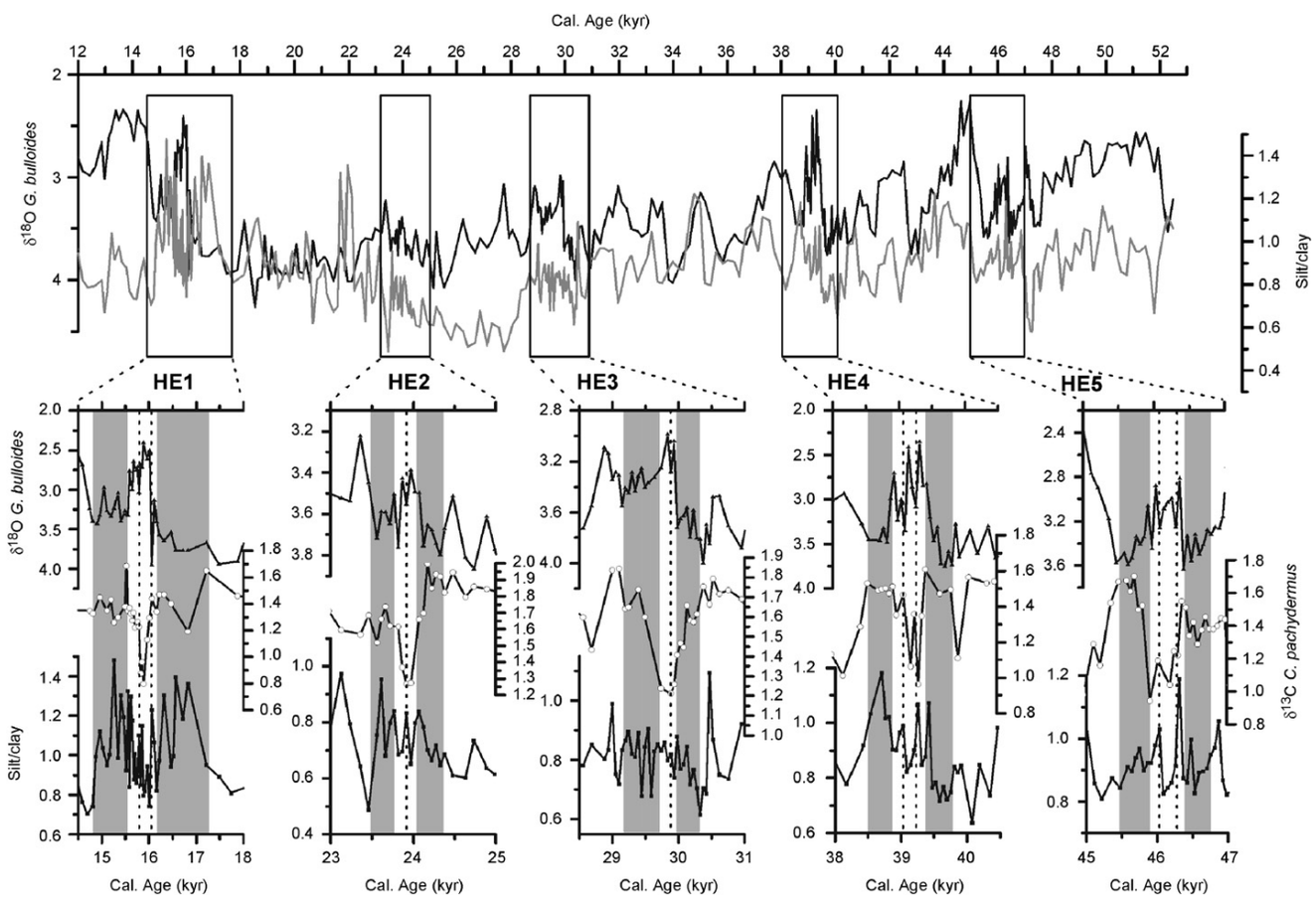

Fig. 7. Comparison of the planktonic $\delta^{18}O$ and the silt/clay ratio for the 12–50 ka time interval. A centuries long offset is observed among the silt/clay ratio and the planktonic $\delta^{18}O$ record during MIS3. Below, a close-up of HE1–HE5 through the planktonic $\delta^{18}O$, benthic $\delta^{13}C$ and silt/clay records from core MD99-2343 is shown. Gray bars represent the early and late phases of each HE while the white central bar corresponds to the isotopic anomaly described in the text. The high resolution reached on these records allows identification of several events in the central phase of each HE related to punctual returns to pure HE conditions (vertical dashed lines).

during the three phases described above. During HE1 and, to a lesser extent, during HE2 and HE4 lower silt/clay ratios are observed during the central phase (white bars in Fig. 7) compared to the early and late phases (gray bars). This pattern is clearly consistent with a weakening of the deep water current during the entrance of low-salinity polar waters. However, silt/clay values are comparable for all three phases during HE3 and HE5. These discrepancies in the pattern of each HE could be attributed to orbitally induced insolation changes, e.g. HE1 occurs in a period of increasing seasonal differences while HE3 occurs in a period of lessening seasonal differences (Fig. 4d and e).

The very high resolution of the silt/clay and isotopic records allows identifying additional minor structures within HEs (Fig. 7). In particular, during the surface freshwater anomaly (white bars in Fig. 7) one to two minor *G. bulloides* $\delta^{18}O$ increments are observed (dotted lines within white bars in Fig. 7). Most of them, i.e. those from HE5, HE4 and HE1, coincide with small *C. pachydermus* $\delta^{13}C$ increases. These minor recovering pulses are concurrent with marked increases in the silt/clay ratio, which supports the occurrence of deep currents short-lived strengthening events in the Minorca drift. These results suggest that the invasion of sub-polar less salty water from the North Atlantic was not steady but pulsating within each HE, which in turn triggered a response of the overturning cell in the Gulf of Lion. The combined interpretation of the isotopic and sedimentological records from core MD99-2343 suggests that, during GS associated with HEs, WMDW overturning was always strong enough to release fast currents to the Minorca drift, though not enough to reach the strongest mode 3 (Fig. 6) of non-Heinrich related GS. In consequence, sub-polar water pulses entering the western Mediterranean Basin induced changes in the intensity of WMDW ventilation but always allowed an intermediate mode of overturning.

6. Conclusions

The high-resolution sedimentological and geochemical analyses of the sediment core MD99-2343, recovered in the deep water Minorca sediment drift, resulted in new contributions to disentangle the variability of WMDW formation during the last 50 kyr. The strong parallelism between the K/Al record and the insolation curve at 40°N points to orbitally induced insolation changes as the main direct control over fluvial runoff in the western Mediterranean Basin, itself related to changes in the long-term precipitation pattern. This astronomical forcing also had an important effect on deep water formation in the western Mediterranean Basin as reflected by changes in the grain-size records from core MD99-2343, thus highlighting the strong climate sensitivity of the Mediterranean region to orbitally induced changes.

Millennial-scale oscillations from silt/clay, Si/Al and Ti/Al proxies paralleling oscillations in the isotopic records during MIS3 illustrate a pattern of high variability in the deep water formation system in the western Mediterranean Basin that operates at three different intensity modes: strong, intermediate and weak. A centennial offset between the sedimentological and the isotopic proxies suggests that changes of intensity in deep water currents at MD99-2343 site resulted from density and paleodepth variations of the WMDW core flow thus affecting differently the Minorca sediment drift record. Since the formation of deep water during GIS was likely reduced, the cooling conditions prevailing after these warm events promoted the reduction of the column water density gradient thus favoring rapid reinforcement of deep water overturning and formation of denser WMDW that flowed into the deep basin. Accordingly, both silt/clay and Si/Al records from core MD99-2343 suggest maximum deep water currents intensity during the GIS/GS transitions, when WMDW core flowed shallower than the MD99-2343 site water depth. The continuous decreasing trend of silt/clay and Si/Al records until GS suggests a reduction of the effect of deep water currents at the core site location, thus pointing to the deepening of the WMDW core due to its increased density. On the other hand, silt/clay ratio centennial-scale oscillations recorded during HEs confirm the strong influence that the entrance of sub-polar low-salinity waters had on the overturning system in the Gulf of Lion and suggest the occurrence of fresh water pulses within each HE. The study of additional sequences from shallower and/or deeper water depths from the Minorca sediment drift is the only way to confirm or adjust the hypothesis of WMDW vertical shifts hypothesis during MIS3.

Furthermore, the grain-size and geochemical proxies from core MD99-2343 have shown to be very useful for the study of the deep water conditions in the western Mediterranean Basin providing the first Holocene reconstruction of WMDW variability in the absence of benthic foraminifera. The reduction observed in both grain-size and geochemical records during the 12–10 ka time interval corresponds to the slowing down or collapse of the deep water overturning system due to enlarged freshwater input during the last deglaciation. The general pattern followed by both grain-size and geochemical proxies during the Holocene suggests a transition from relatively high-energetic and humid conditions to drier conditions and less intense deep water currents. This transition was modulated by a reduction of the orbitally induced seasonal differences around 4 ka. Superimposed on this general trend, several rapid grain-size and geochemical excursions have been related to abrupt climate events. Thus, parallel increases in both the grain-size and geochemical records suggest a reinforcement of the deep water formation system coinciding with relative increases in the planktonic $\delta^{18}O$. The occurrence of such abrupt events during the Holocene at a periodicity close to 1000 yr and the good agreement with temperature oscillations in Greenland suggest a direct climatic teleconnection between the North Atlantic and the Mediterranean regions. The results from this work highlight the rapid response of the western Mediterranean

overturning system to changes in the properties of surface waters, indicating the rapid transmission of climate variability to the deep basin.

Acknowledgments

We are especially grateful to R/V *Marion Dufresne* crew and the IMAGES program that allowed collecting the core MD99-2343. We also thank Montse Guart and Elisenda Seguí for their help in the laboratory. This work has been supported by the European projects PROMESS 1 (EVR1-CT-2001-00041), EURODOM (RTN2-2001-00281), ADIOS (EVK3-2000-00604), EUROSTRATAFORM (EVK3-2001-00200) and HERMES (GOCE-CT-2005-511234-1). The Spanish funded CGL200500642/BTE, SA008C05 and REN2003-08642-C02-02 projects are equally acknowledged. COMER Foundation and I3P postdoctoral program (CSIC) are also acknowledged for their support to I. Cacho and A. Moreno, respectively. CRG Marine Geosciences is recognized within the *Generalitat de Catalunya* excellence research groups program (ref. 2005SGR 00152).

References

Agrawal, Y.C., McCave, I.N., Riley, J.B., 1991. Laser diffraction size analysis. In: Syvitski, J.P.M. (Ed.), Principles, Methods, and Application of Particle Size Analysis. Cambridge University Press, Cambridge, pp. 119–129.

Allen, J.R.M., Brandt, U., Brauer, A., Hubberten, H.W., Huntley, B., Keller, J., Michael, K., Mackensen, A., Mingram, J., Negendank, J.F.W., Nowaczyk, N.R., Oberhänsli, H., Watts, W.A., Wulf, S., Zolitschka, B., 1999. Rapid environmental changes in southern Europe during the last glacial period. Nature 400, 740–743.

Alonso, B., Canals, M., Palanques, A., Rehault, J.P., 1995. A deep-sea channel in the Northwestern Mediterranean Sea: morphology and seismic structure of the Valencia channel and its surroundings. Marine Geophysical Researches 17, 469–484.

Barry, R.G., Chorley, R.J., 1998. Atmosphere, Weather and Climate. Routledge, London, New York.

Bartov, Y., Goldstein, S.L., Stein, M., Enzel, Y., 2003. Catastrophic arid episodes in the Eastern Mediterranean linked with the North Atlantic Heinrich events. Geology 31, 439–442.

Bethoux, J.P., Gentili, B., Raunet, J., Tailliez, D., 1990. Warming trend in the western Mediterranean deep water. Nature 347, 660–662.

Bigg, G., Wadley, M.R., 2001. Millennial-scale variability in the oceans: an ocean modelling view. Journal of Quaternary Science 16, 309–319.

Bolle, H.-J., 2003. Mediterranean Climate. Variability and trends. Springer, Heidelberg.

Bond, G., Heinrich, H., Broecker, W.S., Labeyrie, L., McManus, J., Andrews, J.T., Huon, S., Jantschik, R., Clasen, S., Simet, C., Tedesco, K., Klas, M., Bonani, G., Ivy, S., 1992. Evidence for massive discharges of icebergs into the North Atlantic ocean during the last glacial period. Nature 360, 245–249.

Bond, G., Broecker, W.S., Johnsen, S.J., McManus, J., Labeyrie, L., Jouzel, J., Bonani, G., 1993. Correlations between climate records from North Atlantic sediments and Greenland ice. Nature 365, 143–147.

Bond, G., Kromer, B., Beer, J., Muscheler, R., Evans, M., Showers, W., Hoffmann, S., Lotti-Bond, R., Hajdas, I., Bonani, G., 2001. Persistent solar influence on North Atlantic climate during the Holocene. Science 294, 2130–2136.

Broecker, W.S., Bond, G., Klas, M., Clark, E., McManus, J., 1992. Origin of the North Atlantic's Heinrich events. Climate Dynamics 6, 265–273.

Cacho, I., Grimalt, J.O., Pelejero, C., Canals, M., Sierro, F.J., Flores, J.A., Shackleton, N.J., 1999. Dansgaard–Oeschger and Heinrich event imprints in Alboran Sea temperatures. Paleoceanography 14, 698–705.

Cacho, I., Grimalt, J.O., Sierro, F.J., Shackleton, N.J., Canals, M., 2000. Evidence for enhanced Mediterranean thermohaline circulation during rapid climatic coolings. Earth and Planetary Science Letters 183, 417–429.

Cacho, I., Grimalt, J.O., Canals, M., Sbaffi, L., Shackleton, N., Schönfeld, J., Zahn, R., 2001. Variability of the western Mediterranean Sea surface temperature during the last 25,000 years and its connection with the northern hemisphere climatic changes. Paleoceanography 16, 40–52.

Cacho, I., Grimalt, J.O., Canals, M., 2002. Response of the Western Mediterranean Sea to rapid climate variability during the last 50,000 years: a molecular biomarker approach. Journal of Marine Systems 33-34, 253–272.

Cacho, I., Shackleton, N., Elderfield, H., Sierro, F.J., Grimalt, J.O., 2006. Glacial rapid variability in deep-water temperature and $\delta^{18}O$ from the Western Mediterranean Sea. Quaternary Science Reviews 25, 3294–3311.

Calafat, A.M., Casamor, J.L., Canals, M., Nyffeler, F., 1996. Distribución y composición elemental de la materia particulada en suspensión en el Mar Catalano-Balear. Geogaceta 20, 370–373.

Canals, M., Puig, P., de Madron, X.D., Heussner, S., Palanques, A., Fabres, J., 2006. Flushing submarine canyons. Nature 444, 354–357.

Caralp, M.H., 1988. Late Glacial to recent deep-sea benthic foraminifera from the Northeastern Atlantic (Cadiz Gulf) and Western Mediterranean (Alboran Sea): paleoceanographic results. Marine Micropaleontology 13, 265–289.

Cheddadi, R., Yu, G., Guiot, J., Harrison, S.P., Prentice, I.C., 1997. The climate of Europe 6000 years ago. Climate Dynamics 13, 1–9.

COHMAP, M., 1988. Climatic changes of the last 18,000 years: observations and model simulations. Science 241, 1043–1052.

Colmenero-Hidalgo, E., Flores, J.-A., Sierro, F.J., 2002. Biometry of *Emiliania huxleyi* and its biostratigraphic significance in the Eastern North Atlantic Ocean and Western Mediterranean Sea in the last 20000 years. Marine Micropaleontology 46, 247–263.

Colmenero-Hidalgo, E., Flores, J.-A., Sierro, F.J., Bárcena, M.A., Löwemark, L., Schönfeld, J., Grimalt, J.O., 2004. Ocean surface water response to short-term climate changes revealed by coccolithophores from the Gulf of Cadiz (NE Atlantic) and Alboran Sea (W Mediterranean). Palaeogeography, Palaeoclimatology, Palaeoecology 205, 317–336.

Combourieu Nebout, N., Turon, J.L., Zahn, R., Capotondi, L., Londeix, L., Pahnke, K., 2002. Enhanced aridity and atmospheric high-pressure stability over the western Mediterranean during the North Atlantic cold events of the past 50 k.y. Geology 30, 863–866.

Dansgaard, W., Johnsen, S.J., Clausen, H.B., Dahl-Jensen, D., Gundestrup, N.S., Hammer, C.U., Hvidberg, C.S., Steffensen, J.P., Sveinbjörnsdóttir, A.E., Jouzel, J., Bond, G., 1993. Evidence for general instability of past climate from a 250-kyr ice-core record. Nature 364, 218–220.

deMenocal, P., Ortiz, J., Guilderson, T., Adkins, J., Sarnthein, M., Baker, L., Yarusinsky, M., 2000. Abrupt onset and termination of the African Humid Period: rapid climate responses to gradual insolation forcing. Quaternary Science Reviews 19, 347–361.

Fabres, J., Calafat, A., Sanchez-Vidal, A., Canals, M., Heussner, S., 2002. Composition and spatio-temporal variability of particle fluxes in the Western Alboran Gyre, Mediterranean Sea. Journal of Marine Systems 33,34, 431–456.

Fleming, K., Johnston, P., Zwartz, D., Yokoyama, Y., Lambeck, K., Chappell, J., 1998. Refining the eustatic sea-level curve since the Last Glacial Maximum using far- and intermediate-field sites. Earth and Planetary Science Letters 163, 327–342.

Frigola, J., Moreno, A., Cacho, I., Canals, M., Sierro, F.J., Flores, J.A., Grimalt, J.O., Hodell, D.A., Curtis, J.H. 2007. Holocene climate

variability in the western Mediterranean region from a deep water sediment record. Paleoceanography, 22, PA2209, doi:10.1029/2006PA001307.

González-Sampériz, P., Valero-Garcés, B.L., Moreno, A., Jalut, G., García-Ruíz, J.M., Martí-Bono, C., Delgado-Huertas, A., Navas, A., Otto, T., Dedoubat, J.J., 2006. Climate variability in the Spanish Pyrenees during the last 30,000 yr revealed by the El Portalet sequence. Quaternary Research 66, 38–52.

Grootes, P., Stuiver, M., White, J.W.C., Johnsen, S.J., Jouzel, J., 1993. Comparison of oxygen isotope records from the GISP2 and GRIP Greenland ice cores. Nature 366, 552–554.

Hall, I.R., McCave, I.N., 2000. Palaeocurrent reconstruction, sediment and thorium focussing on the Iberian margin over the last 140 ka. Earth and Planetary Science Letters 178, 151–164.

Harrison, S.P., Digerfeldt, G., 1993. European lakes as palaeohydrological and palaeoclimatic indicators. Quaternary Science Reviews 12, 233–248.

Heinrich, H., 1988. Origin and consequences of cyclic ice rafting in the Northeast Atlantic Ocean during the past 130,000 years. Quaternary Research 29, 142–152.

Hilgen, F.J., 1991. Astronomical calibration of Gauss to Matuyama sapropels in the Mediterranean and implication for the geomagnetic polarity time scale. Earth and Planetary Science Letters 104, 226–244.

Hughen, K., Baillie, M., Bard, E., Bayliss, A., Beck, J., Bertrand, C., Blackwell, P., Buck, C., Burr, G., Cutler, K., Damon, P., Edwards, R., Fairbanks, R., Friedrich, M., Guilderson, T., Kromer, B., McCormac, F., Manning, S., Bronk Ramsey, C., Reimer, P., Reimer, R., Remmele, S., Southon, J., Stuiver, M., Talamo, S., Taylor, F., van der Plicht, J., Weyhenmeyer, C., 2004. Marine04 Marine radiocarbon age calibration, 26–0 ka BP. Radiocarbon 46, 1059–1086.

Hurrell, J.W., 1995. Decadal trends in the North Atlantic Oscillation: regional temperatures and precipitation. Science 269, 676–679.

Jalut, G., Esteban Amat, A., Bonnet, L., Gauquelin, T., Fontugne, M., 2000. Holocene climatic changes in the Western Mediterranean, from south-east France to south-east Spain. Palaeogeography, Palaeoclimatology, Palaeoecology 160, 255–290.

Konert, M., Vandenberghe, J., 1997. Comparison of laser grain size analysis with pipette and sieve analysis: a solution for the underestimation of the clay fraction. Sedimentology 44, 523–535.

Lacombe, H., Tchernia, P., Gamberoni, L., 1985. Variable bottom water in the Western Mediterranean Basin. Progress in Oceanography 14, 319–338.

López-Jurado, J.L., González-Pola, C., Vélez-Belchí, P., 2005. Observation of an abrupt disruption of the long-term warming trend at the Balearic Sea, western Mediterranean Sea, in summer 2005. Geophysical Research Letters 32, doi:10.1029/2005GL024430.

Magny, M., Miramont, C., Sivan, O., 2002. Assessment of the impact of climate and anthropogenic factors on Holocene Mediterranean vegetation in Europe on the basis of palaeohydrological records. Palaeogeography, Palaeoclimatology, Palaeoecology 186, 47–59.

Maldonado, A., Got, H., Monaco, A., O'Connell, S., Mirabile, L., 1985a. Valencia Fan (Northwestern Mediterranean): distal deposition fan variant. Marine Geology 62, 295–319.

Maldonado, A., Palanques, A., Alonso, B., Kastens, K.A., Nelson, C.H., O'Connell, S., Ryan, W.B.F., 1985b. Physiography and deposition on a distal deep-sea system: the Valencia Fan (Northwestern Mediterranean). Geo-Marine Letters 5, 157–164.

Martin, J.-M., Elbaz-Poulichet, F., Guieu, C., Loyë-Pilot, M.-D., Han, G., 1989. River versus atmospheric input of material to the Mediterranean Sea: an overview. Marine Chemistry 28, 159–182.

Martrat, B., Grimalt, J.O., Lopez-Martinez, C., Cacho, I., Sierro, F.J., Flores, J.A., Zahn, R., Canals, M., Curtis, J.H., Hodell, D.A., 2004. Abrupt temperature changes in the Western Mediterranean over the past 250,000 years. Science 306, 1762–1765.

Matthewson, A.P., Shimmield, G.B., Kroon, D., Fallick, A.E., 1995. A 300 kyr high-resolution aridity record of the North African continent. Paleoceanography 10, 677–692.

Matthiesen, S., Haines, K., 2003. A hydraulic box model study of the Mediterranean response to post-glacial sea-level rise. Paleoceanography 18(4), 1084, doi:10.1029/2003PA000880.

Mauffret, A., Labarbarie, M., Montadert, L., 1982. Les affleurements de series sedimentaires pre-pliocenes dans le bassin Mediterraneen nord-occidental. Marine Geology 45, 159–175.

Mayewski, P.A., Rohling, E.E., Stager, J.C., Karlen, W., Maasch, K.A., Meeker, L.D., Meyerson, E.A., Gasse, F., van Kreveld, S., Holmgren, K., 2004. Holocene climate variability. Quaternary Research 62, 243–255.

McCave, I.N., Bryant, R.J., Cook, H.F., Coughanowr, C.A., 1986. Evaluation of a laser-diffraction-size analyzer for use with natural sediments. Journal of Sedimentary Research 56, 561–564.

McCave, I.N., Manighetti, B., Robinson, S.G., 1995. Sortable silt and fine sediment size/composition slicing: parameters for palaeocurrent speed and palaeoceanography. Paleoceanography 10, 593–610.

McDermott, F., Frisia, S., Huang, Y., Longinelli, A., Spiro, B., Heaton, T.H.E., Hawkesworth, C.J., Borsato, A., Keppens, E., Fairchild, I.J., 1999. Holocene climate variability in Europe: evidence from $\delta^{18}O$, textural and extension-rate variations in three speleothems. Quaternary Science Reviews 18, 1021–1038.

MEDOC, G., 1970. Observation of formation of deep water in the Mediterranean Sea, 1969. Nature 227, 1037–1040.

Meese, D.A., Gow, A.J., Alley, R.B., Zielinski, P.M., Grootes, G.A., Ram, M., Taylor, K.C., Mayewski, P.A., Bolzan, J.F., 1997. The Greenland ice sheet project 2 depth–age scale: methods and results. Journal of Geophysical Research 102, 26411–26423.

Millot, C., 1999. Circulation in the Western Mediterranean Sea. Journal of Marine Systems 20, 423–442.

Millot, C., Taupier-Letage, I., 2005. Circulation in the Mediterranean Sea. In: The Handbook of Environmental Chemistry. Springer, Berlin, Heidelberg, pp. 29–66.

Moreno, A., Cacho, I., Canals, M., Prins, M.A., Sanchez-Goni, M.-F., Grimalt, J.O., Weltje, G.J., 2002. Saharan dust transport and high-latitude glacial climatic variability: the Alboran Sea record. Quaternary Research 58, 318–328.

Moreno, A., Cacho, I., Canals, M., Grimalt, J.O., Sanchez-Vidal, A., 2004. Millennial-scale variability in the productivity signal from the Alboran Sea record, Western Mediterranean Sea. Palaeogeography, Palaeoclimatology, Palaeoecology 211, 205–219.

Nelson, C.H., Maldonado, A., 1990. Factors controlling late Cenozoic continental margin growth from the Ebro Delta to the western Mediterranean deep sea. Marine Geology 95, 419–440.

Paillard, D., Labeyrie, L., Yiou, P., 1996. Macintosh program performs time-series analysis. Eos Transactions, American Geographical Union 77, 379.

Palanques, A., Kenyon, N.H., Alonso, B., Limonov, A., 1995. Erosional and depositional patterns in the Valencia channel mouth: an example of a modern channel–lobe transition zone. Marine Geophysical Researches 17, 503–517.

Pinardi, N., Masetti, E., 2000. Variability of the large scale general circulation of the Mediterranean Sea from observations and modelling: a review. Palaeogeography, Palaeoclimatology, Palaeoecology 158, 153–173.

Prentice, I.C., Harrison, S.P., Jolly, D., Guiot, J., 1998. The climate and biomes of Europe at 6000 yr BP: comparison of model simulations and pollen-based reconstructions. Quaternary Science Reviews 17, 659–668.

Reichart, G.J., den Dulk, M., Visser, H.J., van der Weijden, C.H., Zachariasse, W.J., 1997. A 225 kyr record of dust supply, paleoproductivity and the oxygen minimum zone from the Murray Ridge (northern Arabian Sea). Palaeogeography, Palaeoclimatology, Palaeoecology 134, 149–169.

Rodó, X., Baert, E., Comin, F.A., 1997. Variations in seasonal rainfall in Southern Europe during the present century: relationships with the North Atlantic oscillation and the El Niño-southern oscillation. Climate Dynamics 13, 275–284.

Rogerson, M., Rohling, E.J., Weaver, P.P.E., 2006. Promotion of meridional overturning by Mediterranean-derived salt during the last deglaciation. Paleoceanography 21, PA4101, doi:10.1029/2006PA001306.

Rohling, E.J., 1994. Review and new aspects concerning the formation of eastern Mediterranean sapropels. Marine Geology 122, 1–28.

Rohling, E.J., Hilgen, F.J., 1991. The eastern Mediterranean climate at times of sapropel formation: a review. Geologie en Mijnbouw 70, 253–264.

Rohling, E.J., Hayes, A., Rijk, D., Kroon, D., Zachariasse, W.J., Eisma, D., 1998. Abrupt cold spells in the northwest Mediterranean. Paleoceanography 13, 316–322.

Rohling, E.J., Mayewski, P.A., Abu-Zied, R.H., Casford, J.S.L., Hayes, A., 2002. Holocene atmosphere–ocean interactions: records from Greenland and the Aegean Sea. Climate Dynamics 18, 587–593.

Rollinson, H., 1993. Using Geochemical Data. Evaluation, Presentation, Interpretation. Longman Scientific and Technical, New York.

Sánchez Goñi, M.F., Cacho, I., Turon, J.-L., Guiot, J., Sierro, F.J., Peypouquet, J.-P., Grimalt, J.O., Shackleton, N.J., 2002. Synchroneity between marine and terrestrial responses to millennial scale climatic variability during the last glacial period in the Mediterranean region. Climate Dynamics 19, 95–105.

Schott, F., Leaman, K.D., 1991. Observations with moored acoustic doppler current profiles in the convection regime in the Gulfe de Lion. Journal of Physical Oceanography 13, 316–322.

Schulz, M., Paul, A., 2002. Holocene climate variability on centennial-to-millennial time scales: 1. Climate records from the North-Atlantic realm. In: Wefer, G., Berger, W., Behre, K.-E., Jansen, E. (Eds.), Climate Development and History of the North Atlantic Realm. Springer, Berlin, Heidelberg, pp. 41–54.

Sierro, F.J., Hodell, D.A., Curtis, J.H., Flores, J.A., Reguera, I., Colmenero-Hidalgo, E., Bárcena, M.A., Grimalt, J.O., Cacho, I., Frigola, J., Canals, M., 2005. Impact of iceberg melting on Mediterranean thermohaline circulation during Heinrich events. Paleoceanography 20, PA2019, doi:10.1029/2004PA001051.

Steig, E.J., 1999. Mid-Holocene climate change. Science 286, 1485–1487.

Stocker, T.F., 2000. Past and future reorganizations in the climate system. Quaternary Science Reviews 19, 301–319.

Stuiver, M., Reimer, P.J., 1993. Extended ^{14}C database and revised CALIB radiocarbon calibration program. Radiocarbon 35, 215–230.

Tzedakis, P.C., 1999. The last climatic cycle at Kopais, central Greece. Journal of the Geological Society, London 156, 425–434.

Velasco, J.P.B., Baraza, J., Canals, M., 1996. La depresión periférica y el lomo contourítico de Menorca: evidencias de la actividad de corrientes de fondo al N del Talud Balear. Geogaceta 20, 359–362.

Vernet, R., Faure, H., 2000. Isotopic chronology of the Sahara and the Sahel during the late Pleistocene and the early and Mid-Holocene (15,000–6,000 BP). Quaternary International 68–71, 385–387.

Voelker, A.H.L., Lebreiro, S.M., Schonfeld, J., Cacho, I., Erlenkeuser, H., Abrantes, F., 2006. Mediterranean outflow strengthening during northern hemisphere coolings: a salt source for the glacial Atlantic? Earth and Planetary Science Letters 245, 39–55.

Watts, W.A., Allen, J.R.M., Huntley, B., 1996. Vegetation history and palaeoclimate of the last glacial period of Lago Grande di Monticchio, southern Italy. Quaternary Science Reviews 15, 133–153.

Wehausen, R., Brumsack, H.-J., 1998. The formation of Pliocene Mediterranean sapropels: constrains from high-resolution major and minor element studies. In: Robertson, A.H.F., Emeis, K.-C., Ritcher, C., Camerlenghi, A. (Eds.), Proceedings of the Ocean Drilling Program, Scientific Results, pp. 207–217.

Wehausen, R., Brumsack, H.-J., 1999. Cyclic variations in the chemical composition of eastern Mediterranean Pliocene sediments: a key for understanding sapropel formation. Marine Geology 153, 161–176.

Wehausen, R., Brumsack, H.-J., 2000. Chemical cycles in Pliocene sapropel-bearing and sapropel-barren eastern Mediterranean sediments. Palaeogeography, Palaeoclimatology, Palaeoecology 158, 325–352.

Weldeab, S., Siebel, W., Wehausen, R., Emeis, K.-C., Schmiedl, G., Hemleben, C., 2003. Late Pleistocene sedimentation in the Western Mediterranean Sea: implications for productivity changes and climatic conditions in the catchment areas. Palaeogeography, Palaeoclimatology, Palaeoecology 190, 121–137.

PALEOCEANOGRAPHY, VOL. 22, PA2209, doi:10.1029/2006PA001307, 2007

Holocene climate variability in the western Mediterranean region from a deepwater sediment record

J. Frigola,[1] A. Moreno,[2] I. Cacho,[1] M. Canals,[1] F. J. Sierro,[3] J. A. Flores,[3] J. O. Grimalt,[4] D. A. Hodell,[5] and J. H. Curtis[5]

Received 21 April 2006; revised 3 December 2006; accepted 3 December 2006; published 4 May 2007.

[1] The detailed analysis of the International Marine Past Global Changes Study core MD99-2343 recovered from a sediment drift at 2391 m water depth north of the island of Minorca illustrates the effects of climate variability on thermohaline circulation in the western Mediterranean during the last 12 kyr. Geochemical ratios associated with terrigenous input resulted in the identification of four phases representing different climatic and deepwater overturning conditions in the Western Mediterranean Basin during the Holocene. Superimposed on the general trend, eight centennial- to millennial-scale abrupt events appear consistently in both grain size and geochemical records, which supports the occurrence of episodes of deepwater overturning reinforcement in the Western Mediterranean Basin. The observed periodicity for these abrupt events is in agreement with the previously defined Holocene cooling events of the North Atlantic region, thus supporting a strong Atlantic-Mediterranean climatic link at high-frequency time intervals during the last 12 kyr. The rapid response of the Mediterranean thermohaline circulation to climate change in the North Atlantic stresses the importance of atmospheric teleconnections in transferring climate variability from high latitudes to midlatitudes.

Citation: Frigola, J., A. Moreno, I. Cacho, M. Canals, F. J. Sierro, J. A. Flores, J. O. Grimalt, D. A. Hodell, and J. H. Curtis (2007), Holocene climate variability in the western Mediterranean region from a deepwater sediment record, *Paleoceanography*, *22*, PA2209, doi:10.1029/2006PA001307.

1. Introduction

[2] The Holocene (last ~10 kyr) has been classically considered a climatically stable episode, especially when compared with climate changes of the last glacial period. However, there is increasing evidence of significant climate variability at orbital and suborbital scales during the present interglacial [*Bianchi and McCave*, 1999; *Bond et al.*, 2001; *Magny et al.*, 2002; *Kuhlmann et al.*, 2004; *Mayewski et al.*, 2004; *Alley and Agustsdottir*, 2005].

[3] Orbitally induced differences in seasonal insolation have determined the long-term climatic evolution of the Holocene with a warm Climate Optimum during the early-to-mid Holocene and a transition to colder conditions around 5 ka [*COHMAP Members*, 1988; *Cheddadi et al.*, 1997, 1998; *Prentice et al.*, 1998; *Claussen et al.*, 1999; *Magny et al.*, 2002; *Davis et al.*, 2003; *Sbaffi et al.*, 2004]. Superimposed on this pattern are events of rapid climate change with periods of 2800–2000, 1500 and 900 years [*Mayewski et al.*, 2004]. While solar flux variability has been proposed to be the main forcing of these Holocene events [*O'Brien et al.*, 1995; *Bond et al.*, 2001; *Rohling et al.*, 2002; *Mayewski et al.*, 2004], oscillations in the production rates of the North Atlantic Deep Water (NADW) and in the poleward heat transport could also have triggered or amplified such instabilities [*Bond et al.*, 1997; *Bianchi and McCave*, 1999; *Schulz and Paul*, 2002; *Oppo et al.*, 2003]. In any case, the direct causative mechanism remains unknown.

[4] Paleoclimatic records have demonstrated the high sensitivity of the western Mediterranean region to rapid climate changes during the last glacial interval, including Dansgaard/Oeschger and Heinrich events, thereby supporting the view of a strong link between the Mediterranean and the North Atlantic climate [*Rohling et al.*, 1998, 2002; *Cacho et al.*, 1999, 2000, 2001; *Moreno et al.*, 2002, 2004; *Martrat et al.*, 2004; *Sierro et al.*, 2005]. This rapid connection between both regions has been interpreted to result from the entrance of cold surface waters into the Mediterranean Sea through the Strait of Gibraltar, but also from the intensification of the atmospheric circulation. A strengthened westerly system enhanced the marine overturning cell in the Gulf of Lion leading to a more efficient formation of Western Mediterranean Deep Water (WMDW) and to the enhancement of deep circulation [*Cacho et al.*, 2001; *Sierro et al.*, 2005].

[5] In contrast to the glacial period, information about Holocene rapid variability in the western Mediterranean region and its links to North Atlantic climate is comparatively scarce. One of the most useful proxies for the study of

[1] Consolidated Research Group Marine Geosciences, Department of Stratigraphy, Paleontology and Marine Geosciences, Faculty of Geology, University of Barcelona, Barcelona, Spain.
[2] Pyrenean Institute of Ecology, Spanish Research Scientific Council, Zaragoza, Spain.
[3] Department of Geology, University of Salamanca, Salamanca, Spain.
[4] Department of Environmental Chemistry, Institute of Chemical and Environmental Research-Spanish Research Scientific Council, Barcelona, Spain.
[5] Department of Geological Sciences, University of Florida, Gainesville, Florida, USA.

0883-8305/07/2006PA001307$12.00

WMDW formation and circulation during glacial periods, carbon and oxygen isotopic records from *Cibicidoides spp* foraminifera, is lacking during the Holocene because of poor ventilation and oxygenation conditions of deep waters that caused the disappearance of this species [*Caralp*, 1988; *Reguera*, 2004]. Core MD99-2343 was recovered from the deepwater Minorca sediment drift in the path of the southward branch of the WMDW. In this study, we use grain size distributions and bulk geochemical ratios of terrigenous material down this core to reconstruct Holocene changes in WMDW.

2. Study Area

2.1. Climate and Physical Oceanography Setting

[6] The climate regime of the Mediterranean region is transitional between the temperate maritime type and the arid subtropical desert climate [*Barry and Chorley*, 1998]. The Icelandic low–Azores high system controls present-day meteorology and climate in western Europe including the western Mediterranean region. Summers in the western Mediterranean are usually hot and dry because of the influence of the expanded Azores anticyclone. The southward displacement of the anticyclone during winter allows Atlantic depressions to enter the western Mediterranean region bringing high atmospheric instability and wetter conditions. At decadal scale, this pattern is known as the North Atlantic Oscillation (NAO), which modulates much of the present-day climate variability in this region [*Rodó et al.*, 1997]. The NAO system and the strong influence of the Mediterranean Sea expose the region to large-scale climate changes [*Bolle*, 2003]. The western Mediterranean region is also influenced by Saharan air masses that transport considerable amounts of dust toward the Mediterranean Sea and farther north [*Prospero*, 1996]. This short overview highlights the complexity of the climatic behavior of the western Mediterranean region and evidences its high sensitivity to heat and moisture flux variations.

[7] Because of winter southward displacement of the Azores high, Atlantic depressions follow southern trajectories coming into the Mediterranean region more frequently [*Barry and Chorley*, 1998]. This process leads to the formation of strong and cold northerly and northwesterly winds in the Rhône and Ebro valleys funneling the airflow into the western Mediterranean (i.e., Mistral and Cierzo winds, respectively). These winds cause strong evaporation and cooling offshore in the Gulf of Lion thus increasing surface water density until it sinks to greater depths [*MEDOC*, 1970; *Lacombe et al.*, 1985; *Millot*, 1999]. This process gives birth to the formation of the Western Mediterranean Deep Water (WMDW), which fills the deepest part of the Western Mediterranean Basin (Figure 1). Deep water formation in the Gulf of Lion depends on wind stress variability but is also affected by the amount and depth of the Levantine Intermediate Water (LIW) before WMDW formation events [*Pinardi and Masetti*, 2000]. As consequence of the negative balance of water created by the excess of evaporation over fresh water input in the Mediterranean Sea a compensating surface Atlantic water layer enters through the Strait of Gibraltar as Modified Atlantic Water (MAW) (Figure 1) [*Millot*, 1999]. The dense LIW and WMDW leave the Mediterranean Basin through the Strait of Gibraltar forming the deep Mediterranean Outflow Water (MOW) [*Millot*, 1999].

[8] In the northwestern Mediterranean Sea the Balearic Promontory influences the circulation acting as a topographic barrier. The dense WMDW that forms and sinks in the Gulf of Lion flows south and southwestward into the Valencia Trough at depths closer to 2000 m [*Millot*, 1999] (Figure 1). When the deep current encounters the Balearic Promontory it shifts direction eastward and southeastward bordering the Minorca base of slope. The abruptness of the Balearic slope and the topographically induced change in the current direction likely result in an intensification of the current, as this process has been described for the North Atlantic deep sediment drifts [*McCave and Tucholke*, 1986]. Off Minorca this has led to the formation of the Minorca peripheral depression and associated sediment drift [*Velasco et al.*, 1996] (Figure 2a) where our core MD99-2343 was recovered.

2.2. Particle Sources and Sedimentary Setting

[9] Sediment is supplied to the northwestern Mediterranean Sea mainly by fluvial discharge from the north, by aeolian inputs form the south, and by primary production from surface waters. The two main rivers are the Rhône and the Ebro (Figure 1) with estimated historical pre-damming sediment fluxes of 30×10^6 t yr^{-1} and $17–25 \times 10^6$ t yr^{-1}, respectively [*United Nations Environment Programme*, 2003]. However, only 10% of the fluvial discharge reaches the deep basin while the remaining 90% is deposited in deltaic and inner continental shelf areas [*Martin et al.*, 1989]. Saharan dust fluxes account for 10–20% of present-day deep-sea sedimentation in the western Mediterranean [*Loyë-Pilot et al.*, 1986; *Zuo et al.*, 1991; *Guerzoni et al.*, 1997] although this contribution may have changed substantially through time [*Moreno et al.*, 2002; *Weldeab et al.*, 2003]. The contribution of local pelagic, mostly carbonate particles is limited by the oligotrophic character of most of the western Mediterranean Sea [*Bethoux et al.*, 1998]. In any case, at the location of the studied sediment core, carbonate may also have been contributed by shelf edge spillover processes from the nearby Balearic Promontory [*Maldonado and Stanley*, 1979; *Maldonado and Canals*, 1982].

[10] High-resolution seismic reflection profiles across the Minorca drift show a reflector configuration that is typical of contourite drifts (Figure 2b) [*Vanney and Mougenot*, 1981; *Stow*, 1982; *Stow et al.*, 2002]. While the peripheral depression is filled with coarse sediment [*Canals*, 1980] it is assumed that the fine fraction escaped out of the depression and contributed to the development of the sediment drift in its way toward the basin centre. The MD99-2343 site on the Minorca drift, and the drift itself, occupy a relatively shallower position [*Alonso et al.*, 1995] that is beyond the direct influence of turbidite sedimentation (Figure 2a). However, it is likely that suspended particles escaping from the turbidite systems to the west (Ebro margin) and north (Gulf of Lion margin) may have been caught by the near-bottom circulation and added to the background sedimen-

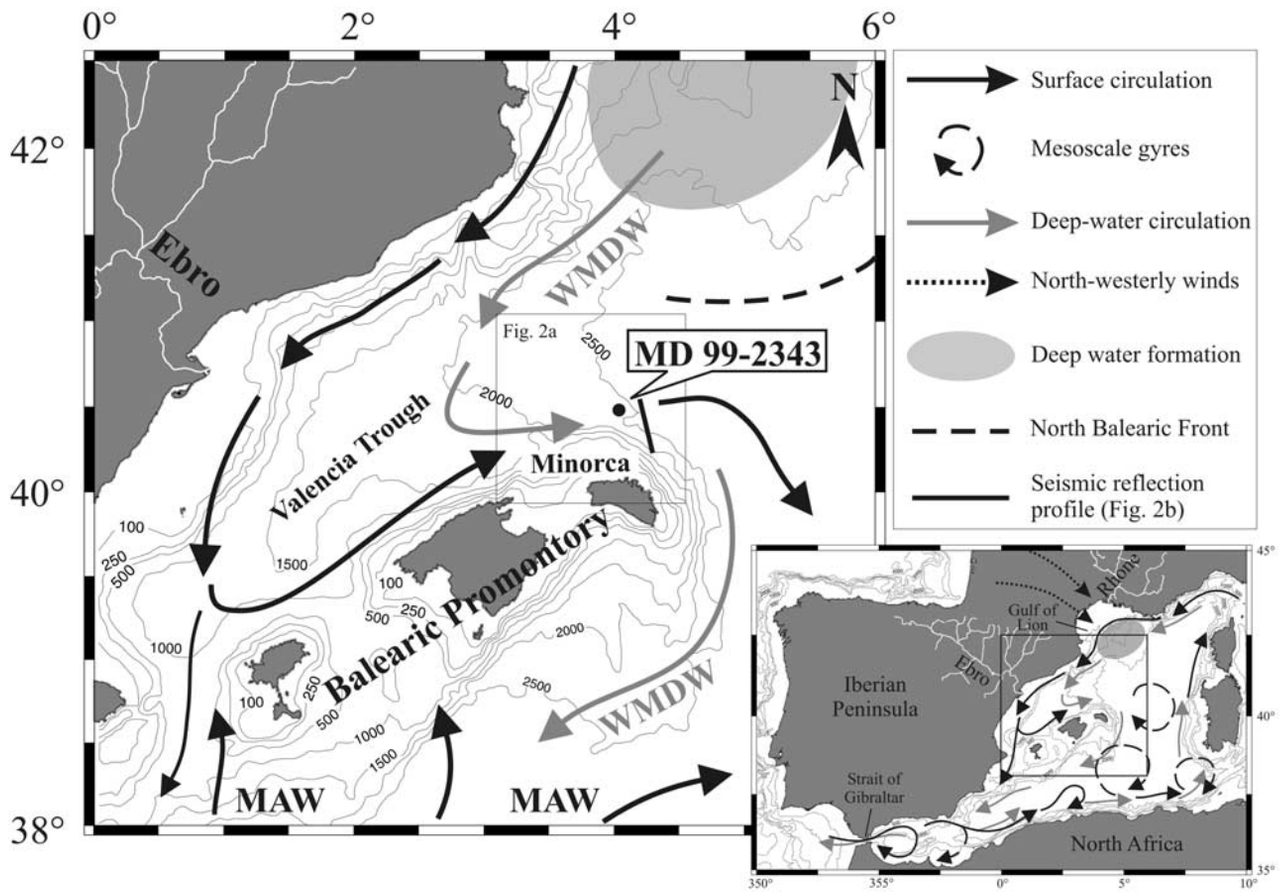

Figure 1. Bathymetric map of the study area showing the general surface and deepwater circulation patterns and the position of core MD99-2343. The box in the main map shows the location of Figure 2a, while the solid line illustrates the location of the seismic reflection profile in Figure 2b. WMDW is Western Mediterranean Deep Water; MAW is Modified Atlantic Water.

tation of the Minorca drift (Figure 2a). Large-scale bed forms found in the deep northwestern Mediterranean Basin further indicate that bottom currents likely played a significant role in the shaping of the seafloor, and thus in sediment particle transport, winnowing and sorting in the recent past [*Mauffret et al.*, 1982; *Maldonado et al.*, 1985; *Palanques et al.*, 1995; *Acosta*, 2005]. Although no current meter data exist for the vicinity of the core site, near-bottom current measurements during a 3-month period at 1800 m water depth in the Gulf of Lion deep margin, where WMDW formation takes place, gave maximum values of 50 cm s^{-1} and mean values of 20 cm s^{-1} [*Millot and Monaco*, 1984].

3. Material and Methods

[11] Sediment core MD99-2343 was recovered with a Calypso piston corer north of Minorca at 40°29.84′N, 04°01.69′E and 2391 m of water depth in the northwestern Mediterranean Sea (Figure 1), during Leg 5 of the R/V Marion Dufresne expedition within the International Marine Past Global Changes Study (IMAGES) programme. From the total 32.44 m of core length, only the top 4 m corresponding to the last 12 kyr are discussed in this paper. The top 4 m consists of grey nannofossil and foraminifer silty clay. Layers with high content of pteropod and gastropod shell fragments have been also observed all along the upper core section. As a general rule, one centimeter thick sediment samples were taken every 4 to 6 cm for oxygen and carbon isotope analyses of foraminifer shells, and grain size and major element composition analyses of the bulk sediment. Additional samples for grain size analyses were collected at 2 cm resolution over selected intervals.

[12] Samples for isotope analyses were washed over a 63-μm sieve and the retained fraction was dried and dry-sieved again using a 150-μm sieve. About 10 mg of *Globorotalia inflata* and *Globigerina bulloides* were hand-picked for radiocarbon isotope analyses. The AMS ^{14}C analyses were performed in the U.S. National Ocean Sciences Accelerator Mass Spectrometry Facility (NOSAMS). The ages were calibrated with the standard marine correction of 408 years and the regional average marine reservoir correction (ΔR) for the western Mediterranean Sea by means of the Calib 5.0.1 programme [*Stuiver and Reimer*, 1993] and the MARINE04 calibration curve [*Hughen et al.*, 2004].

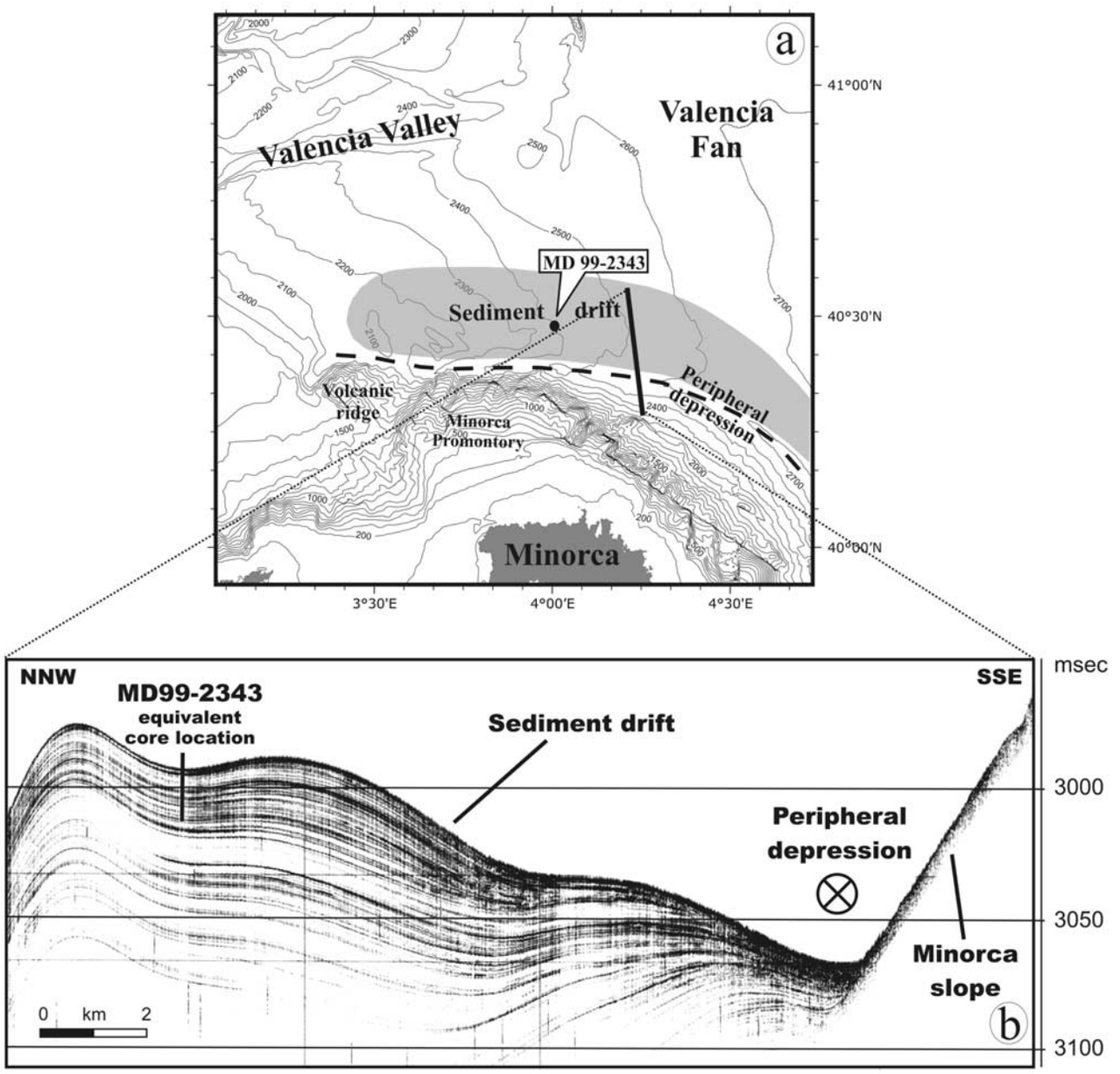

Figure 2. (a) Detailed bathymetric map showing the main seafloor features nearby core MD99-2343. Shaded area roughly delimits the Minorca sediment drift. The abrupt step on the NE Minorca slope is the result from the merging of the high-resolution swath bathymetry data set with the General Bathymetric Chart of the Oceans (GEBCO) digital database [*Intergovernmental Oceanographic Commission et al.*, 2003]. (b) Very high resolution seismic reflection profile across the Minorca sediment drift and peripheral depression (modified from *Velasco et al.* [1996]). The cross within a circle represents the direction of the contour current that is normal to the image. Equivalent position of core MD99-2343 is also shown.

[13] Approximately 5 to 10 specimens of *Globigerina bulloides* from the 300–350 μm size fraction were picked to measure stable isotope ratios. Foraminifer tests were soaked in 15% H_2O_2 to remove organic matter and sonically cleaned in methanol to remove fine-grained particles. The foraminifer calcite was loaded into individual reaction vessels and each sample was reacted with 3 drops of H_3PO_4 (specific gravity = 1.92) using a Finnigan MAT Kiel III carbonate preparation device. Isotope ratios were measured online using a Finnigan MAT 252 mass spectrometer. Analytical precision was estimated to be ±0.08‰ for $\delta^{18}O$ and ±0.03‰ for $\delta^{13}C$ (1σ) by measuring 8 standards (NBS-19) with each carousel containing 38 samples. All isotope results are reported in standard delta notation relative to V-PDB [*Coplen*, 1996].

Table 1. Age Model for Core MD99-2343[a]

Isotope Event or Radiocarbon Sample/Foram Type	Depth, cm	^{14}C Age, years	Calendar Years
AMS ^{14}C/multispecific	28	790 (±40)	386 ± 55
AMS ^{14}C/*G. inflata*[b]	88	3,110 (±30)	2,816 ± 50
AMS ^{14}C/multispecific	118	3,390 (±50)	3,225 ± 80
AMS ^{14}C/*G. inflata*[b]	208	5,720 (±40)	6,091 ± 70
AMS ^{14}C/multispecific	238	6,210 (±50)	6,601 ± 70
AMS ^{14}C/*G. inflata*[b]	308	7,700 (±40)	8,110 ± 60
T1b, onset of the Holocene	354		10,696[c]
AMS ^{14}C/*G. bulloides*[b]	398	10,650 (±50)	11,883 ± 230
AMS ^{14}C/*G. inflata*[b]	418	11,200 (±50)	12,811 ± 30
AMS ^{14}C/*G. bulloides*[b]	568	13,850 (±40)	15,912 ± 190
AMS ^{14}C/multispecific	604	14,550 (±110)	16,822 ± 240

[a]New and previous ^{14}C AMS dates after *Sierro et al.* [2005] calibrated with the Calib 5.0.1 programme [*Stuiver and Reimer*, 1993]. Linear interpolation between dated points was performed with the AnalySeries Version 1.1 [*Paillard et al.*, 1996].

[b]New ^{14}C AMS dates.

[c]Tie point used for the age model of core MD99-2343 by correlation with the oxygen isotopic record from core MD95-2043 in the near Alboran Sea.

[14] Grain size was measured on the total fraction and the noncarbonate fraction after removing organic matter and carbonates by treatment with excess H_2O_2 and HCl, respectively. A Coulter LS 100 Laser Particle Size Analyser (CLS), which determines particle grain sizes between 0.4 and 900 μm, was used to determine grain size distributions as volume percentages. The laser diffraction size analyzer principle is based on the measurement of the diffraction angle produced by the particles when a laser beam goes through the sample in an aqueous solution. The correlation between diffraction angle and particle size is opposite [*McCave et al.*, 1986]. Since diffraction is assumed to be given by spherical particles, the resulting particle size is that diameter (known as equivalent spherical diameter). Subsequently, laser diffraction methods are claimed to underestimate plate-shaped clay mineral percentages. To correct such effect we have followed the method proposed by *Konert and Vandenberghe* [1997]. CLS precision and accuracy is tested by systematic control runs using latex microspheres with predefined diameters. The high precision (reproducibility) of the measurements was demonstrated by small variations in the mean diameter (0.97% of variation) and in the standard deviation (1.37% of variation). The accuracy of the measurements, as indicated by the relative departure from the nominal mean diameter is 0.30%, corresponding to absolute deviations between 0.09 and 0.34 μm. Additional test runs were performed using microsphere assemblages with mixed grain sizes to ensure that CLS accurately determined polymodal grain size distributions.

[15] We discuss grain size results as the median of each sample since it represents the distribution midpoint and it usually constitutes a more representative value of the grain size distribution than the mean. In order to extract palaeoclimate information from a mixture of sediments with different sources numerical-statistical modeling of large grain size data sets provides the best results [*Weltje and Prins*, 2003]. However, core MD99-2343 was recovered on a contouritic drift built by the influence of near bottom currents where minor or no changes in sediment sources are expected (see below). Subsequently, instead of statistical modeling of end-members, we have considered the UP10 fraction, which composes the volume percentage of the fraction coarser than 10 μm, a good indicator of deep currents variability at this site. The UP10 integrates the sortable silt fraction (SS, 10–63 μm), defined as the coarser fraction of the silt with noncohesive behavior during transport and deposition [*McCave et al.*, 1995], while taking also into account the influence of the fine sand subpopulation (>63 μm) that could be reworked by strong contour currents. Finally, the silt/clay ratio has also proven to be useful for the study of deepwater currents intensity [*Hall and McCave*, 2000].

[16] The percentages of major elements in sediment samples were determined by means of X-ray fluorescence using a Philips PW 2400 sequential wavelength X-ray spectrometer. Prior to the analyses, samples were dried at 100°C, and then ground and homogenized in an agate mortar. 0.3 g of homogenized bulk sediment with lithium tetraborate at a 1:20 dilution factor were fused at 1150°C in an induction oven Perle'X-2 to 30-mm-diameter glass discs. The content of major elements Si, Ti, Al, K, Ca, Fe, Mn, Mg, P and Na was calculated as oxide percentages. Analytical accuracy was checked by measuring international standards (GSS-1 to GSS-7) being better than 1% of certified values. Precision of individual measurements was better than 0.9% as determined from replicate analyses of sediment samples (repeatability). Precision over the period of measurement was better than 3.4% (reproducibility) for all elements analyzed in this work. Spurious correlations between elements due to closure effect to 100% are avoided by discussion of element/Al ratios [*Rollinson*, 1993].

[17] X-ray diffraction (XRD) analyses were carried out in selected samples using a Siemens D-500 X-ray diffractometer on untreated, glycolated and heated (550°C) samples. Prior to the analysis, samples were mounted on smear slides after clay separation by decantation.

4. Chronostratigraphy

[18] *Sierro et al.* [2005] provided an age model for core MD99-2343 based on four ^{14}C AMS dates and several tie points with the Greenland ice core GISP2. This age model has been modified to account for six additional monospecific foraminifer ^{14}C AMS dates of which four lie within the 0–12 ka interval (Table 1). A mid Termination Ib (TIb) additional tie point has been added by correlating the Minorca *G. bulloides* oxygen isotopic record to the one from the Alboran Sea core MD95-2043 [*Cacho et al.*, 1999] (Table 1). Both oxygen isotopic profiles for the last 12 kyr are plotted in Figure 3.

[19] Sedimentation rates for the upper 4 m of core MD99-2343 range between 18 and 73 cm kyr^{-1} with an average value of 37 cm kyr^{-1} (Figure 3). These rates are much higher than those determined for nearby sites (e.g., 4 cm kyr^{-1} in core SL87 south of Minorca [*Weldeab et al.*, 2003]), even accounting for potential core stretching [*Skinner and McCave*, 2003]. The high rates likely reflect local enhancement of particle deposition associated with the building of the Minorca sediment drift, as illustrated by seismic

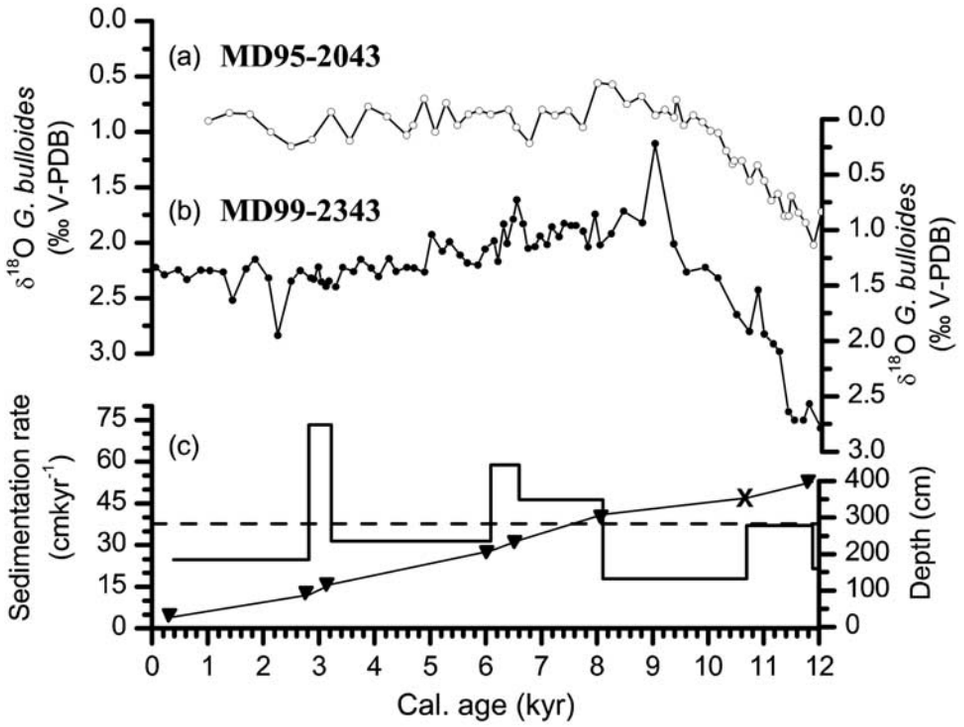

Figure 3. Comparison of the *G. bulloides* oxygen isotopic records from (a) MD95-2043 (Alboran Sea) and (b) MD99-2343 (this study) cores for the last 12 kyr. (c) Sedimentation rates along MD99-2343 sediment core calculated linearly among calendar years from ^{14}C accelerator mass spectrometry (AMS) dates (triangles) and tie points (cross) utilized in the age model (see text for details and Table 1). The mean sedimentation rate of 37 cm kyr^{-1} is represented by a dashed line.

reflection profiles (Figure 2b). Because of the variation in sedimentation rates as a consequence of the sedimentary environment and because of the number of available dates, the final age model was constructed by linear interpolation between calibrated ages instead of using other age-depth extrapolation models [*Telford et al.*, 2004]. The age model accuracy and the sampling interval result in a mean time resolution of 135 years for the top 4 m section of core MD99-2343.

5. Results

5.1. Oxygen Isotopic Record

[20] The heaviest values in the *G. bulloides* δ^{18}O record from core MD99-2343 during the last 12 kyr correspond to the late Younger Dryas (12–11.5 ka) (Figure 4). During the deglaciation (11.5–9 ka), the δ^{18}O record shows a continuously decreasing trend that ends at 9 ka when the lightest δ^{18}O values were reached. The Holocene is characterized by a long-term rising trend punctuated by nine centennial to millennial-scale oscillations (Figure 4a). Some of the δ^{18}O increases are significant, e.g., >0.5‰ from 6.5 to 5.8 ka, or >0.9‰ from 9 to 7.8 ka. Moreover, as discussed below, these oxygen isotopic anomalies (arrows in Figures 4, 5, and 6 and Table 2) correlated with changes in other proxies (see below). We name these events as "Minorca abrupt events" with M8 being the oldest and M0 the youngest. M0 is not very well expressed in the δ^{18}O record but we have also labeled this event considering the other studied proxies. The duration and intensity of these δ^{18}O shifts are similar to those recorded during some of the glacial period Dansgaard/Oeschger cycles [*Sierro et al.*, 2005] and only M0 may fit within the δ^{18}O analytical error. Following previous results [*Cacho et al.*, 1999; *Shackleton et al.*, 2000; *Skinner and Shackleton*, 2003; *Sierro et al.*, 2005] these δ^{18}O fluctuations would be driven by SST coolings of about 2° to 3°C. However, the influence of other properties (i.e., salinity) on the isotopic signal cannot be discarded with the available information.

5.2. Grain Size Distribution

[21] Down-core trends in median grain size are similar for bulk sediment and the noncarbonate fraction (Figures 4b and 4c). The median grain size ranges between 5 and 8 μm, thus pointing to the same processes controlling the deposition of the two fractions. Only a small number of samples from the noncarbonate fraction have median grain sizes coarser than 10 μm. Since the carbonate fraction integrates biological production plus detrital carbonate particles, it is considered that the fraction better representing the intensity of bottom currents is the noncarbonate one [*McCave et al.*, 1995]. This noncarbonate fraction displays seven median grain size peaks at 8.4, 7.2, 6.2, 5, 4.1, 3.2 and 2.5 ka, which are coincident with isotopic enrichment events, i.e., M8 to M2 (Figures 4a and 4c).

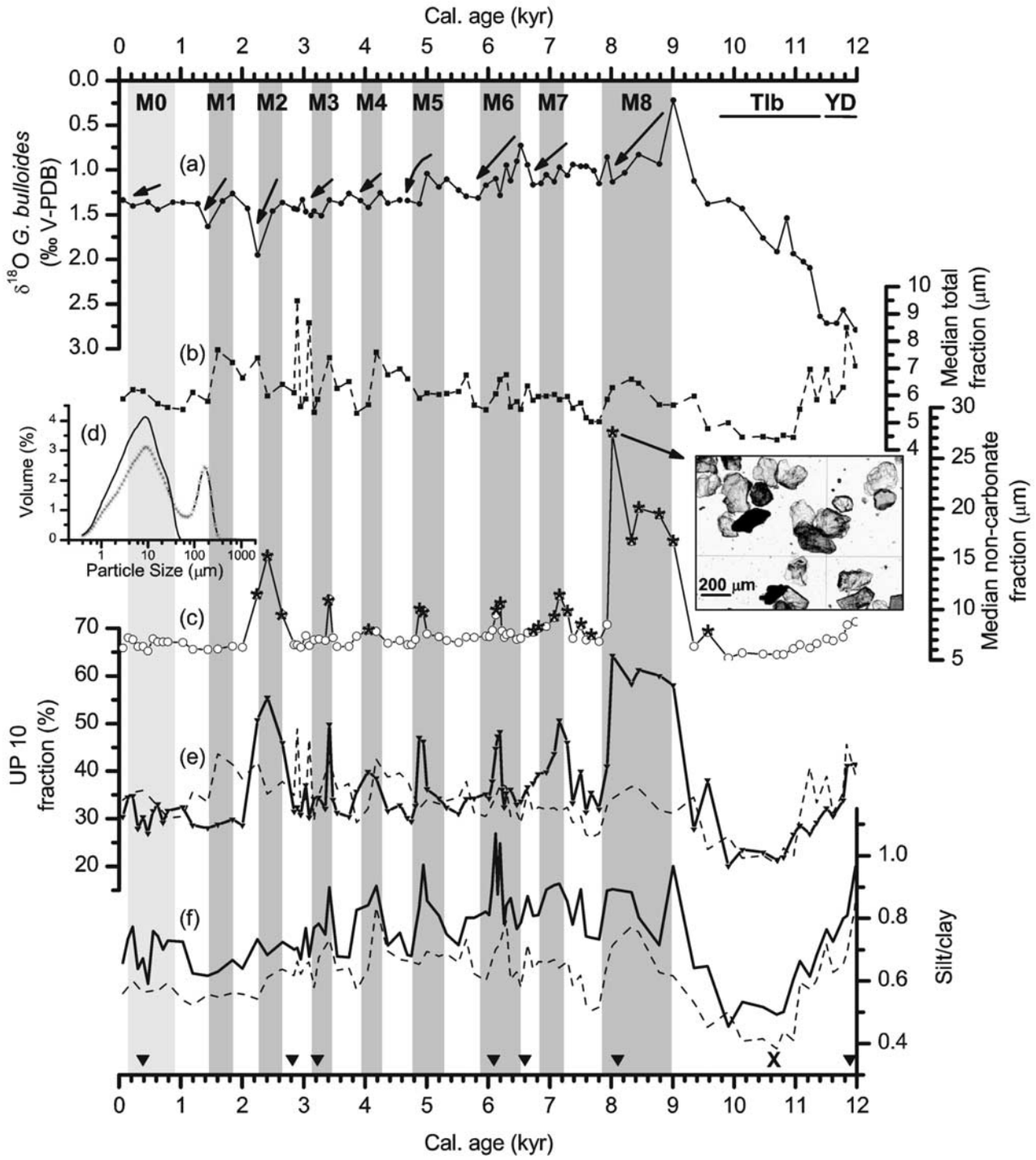

Figure 4. (a) *G. bulloides* oxygen isotopic record from core MD99-2343 for the last 12 kyr. Grain size records of the (b) total and (c) noncarbonate fraction of the sediment, expressed as the median (μm) of each sample. The image is a plane light photograph of the noncarbonate fraction coarser than 63 μm from 304-cm core depth. Asterisks indicate bimodal samples. (d) Examples of unimodal (solid line, sample between M5 and M6) and bimodal (dotted line, from one M7 sample) grain size distributions. (e) UP10 fraction (>10 μm) and (f) silt/clay ratio for the noncarbonate fraction (solid line) and the total fraction (dashed line). Arrows and bars indicate the position of the Minorca abrupt events M8 to M0 as defined in the text. The ^{14}C AMS dates (triangles) and tie point (cross) are also shown.

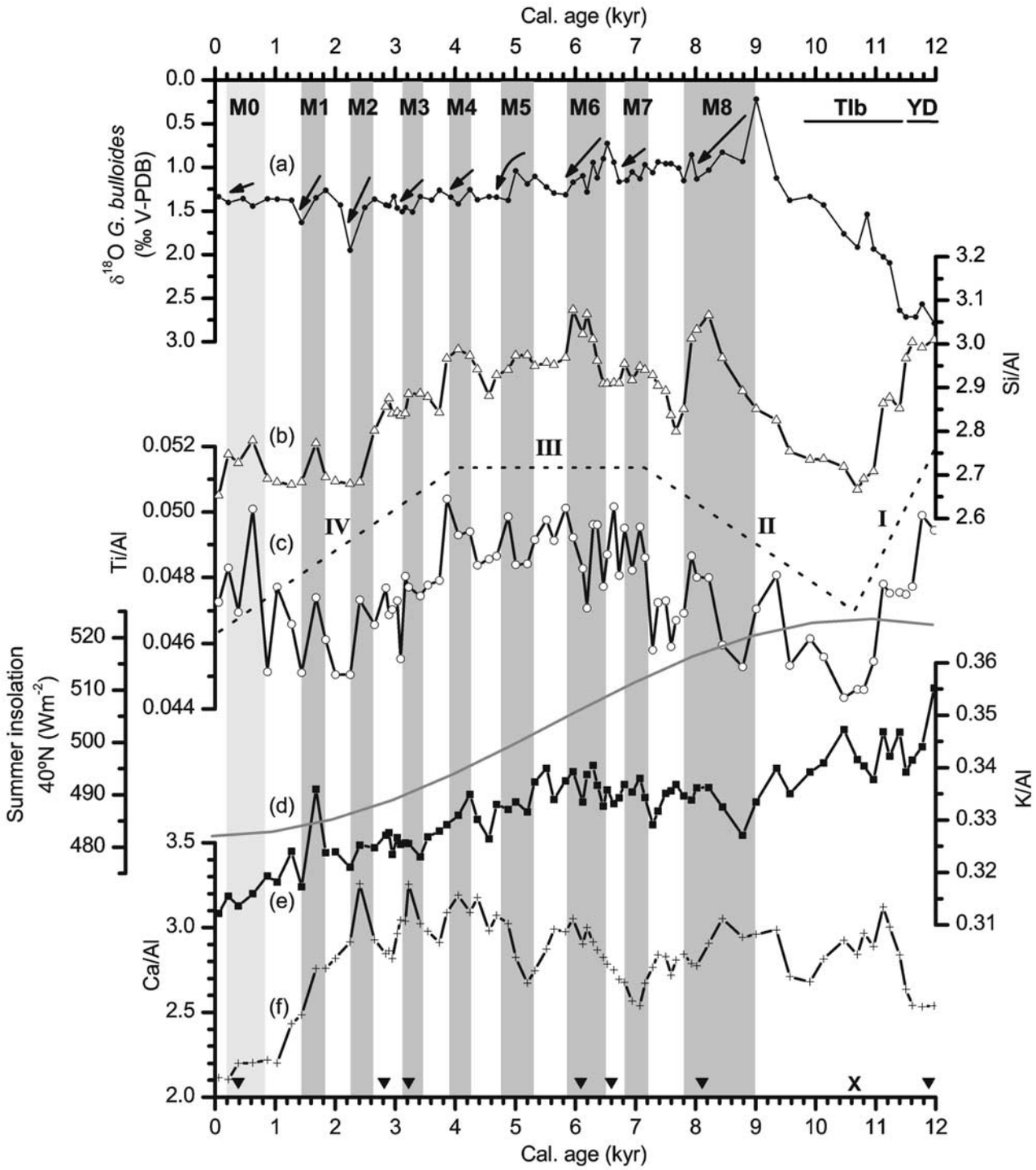

Figure 5. (a) *G. bulloides* oxygen isotopic record from core MD99-2343 for the last 12 kyr. (b) Si, (c) Ti, (e) K, and (f) Ca geochemical records from core MD99-2343 normalized to Al. (d) Summer insolation curve at 40°N for the last 12 kyr. A dashed line between Si/Al and Ti/Al ratios represents the four distinct phases described in the general trend (see text). Arrows and grey bars indicate the Minorca abrupt events M8 to M0 as defined in the text. The ^{14}C AMS dates (inverted triangles) and tie point (cross) are also shown.

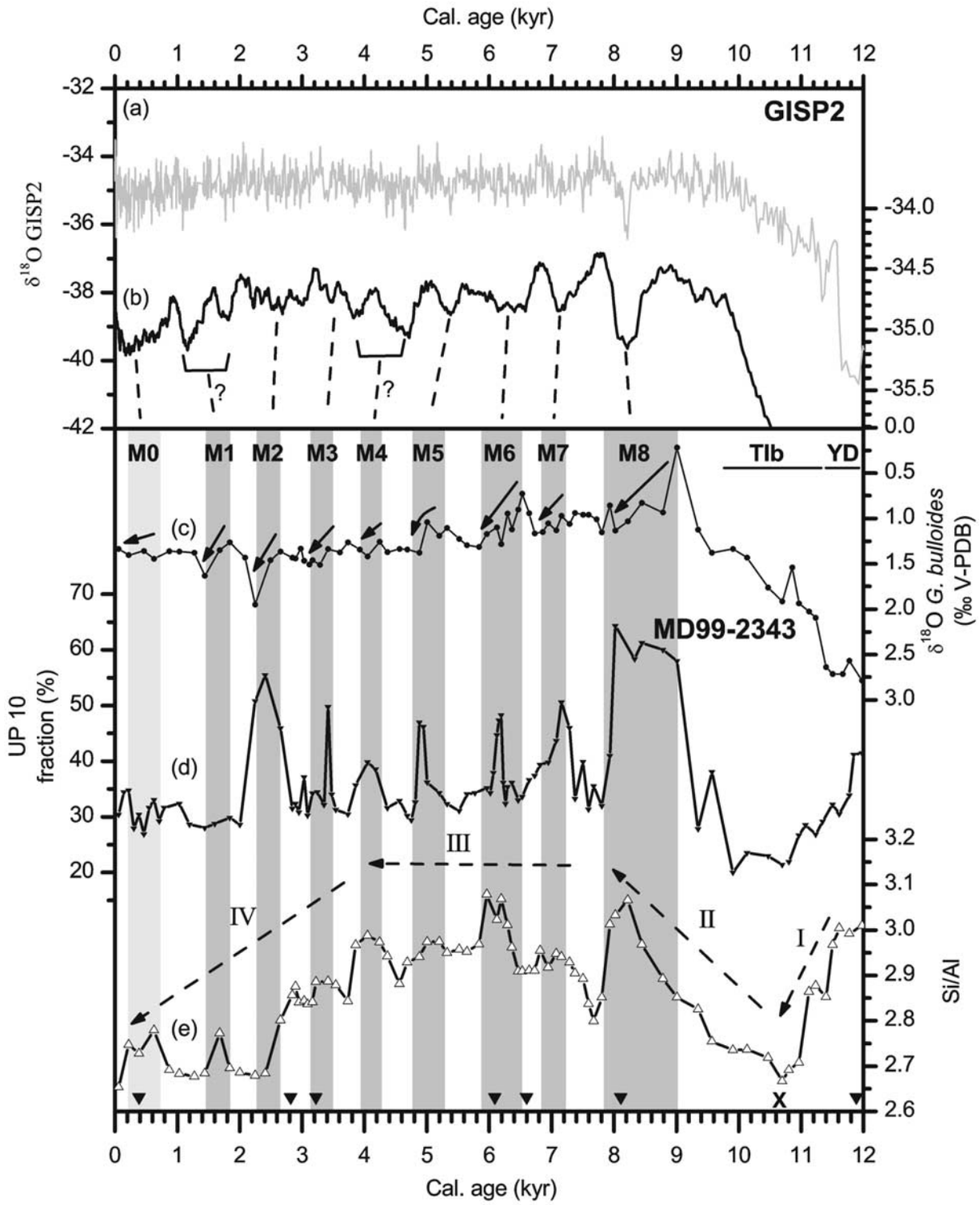

Figure 6. (a) Continuous and (b) 300-year running mean records of the oxygen isotopic profile from the GISP2 ice core [*Grootes et al.*, 1993; *Meese et al.*, 1997]. (c) *G. bulloides* oxygen isotopic record from core MD99-2343 for the last 12 kyr. (d) UP10 fraction (>10 μm) record for the noncarbonate fraction. (e) Si/Al profile with an indication of the four phases identified (I–IV). The arrows and the grey bars represent the nine Minorca abrupt events M8 to M0. Dashed lines represent an attempt to correlate the Minorca events with the oxygen isotopic record from the GISP2 ice core. The ^{14}C AMS dates (inverted triangles) and tie point (cross) are also shown.

Table 2. Timing of Holocene Abrupt Climate Events[a]

Event	Central Age, ka	Time Since Previous Event, ka	Age Interval, ka	Duration, ka	Cold Events in the North Atlantic and Mediterranean Regions				Global Compilation of Events
					SST Alboran	Lakes and Rivers Mediterranean	IRD North Atlantic	Salt and Dust Greenland	
M0	0.5	1.1	0.8–0.2	0.6	-	0.8	-	0.6–0	0.6–0.15
M1	1.6	0.9	1.8–1.4	0.4	1.4	2	1.4	-	1.2–1
M2	2.5	0.7	2.6–2.3	0.3	-	-	-	3.1–2.4	–
M3	3.2	0.9	3.4–3.1	0.3	-	3	2.8		3.5–2.5
M4	4.1	0.9	4.2–4	0.2	-	4	4.2	-	4.2–3.8
M5	5	1.2	5.3–4.7	0.6	5.4	-	-	6.1–5	6–5
M6	6.2	0.9	6.5–5.8	0.7	-	-	5.9	-	-
M7	7.2	1.5	7.4–6.9	0.5	-	7	-	-	-
M8	8.4	-	9–7.8	1.2	8.24	9	8.1	8.8–7.8	9–8

[a]Timings of the Holocene Minorca abrupt events found in core MD99-2343 and tentative correlation with abrupt events recorded from SST in the Alboran Sea [*Cacho et al.*, 2001], in lakes and rivers from the Mediterranean region [*Magny et al.*, 2002], in ice-rafted detritus (IRD) from the North Atlantic region [*Bond et al.*, 1997], in salt and dust from Greenland ice [*O'Brien et al.*, 1995], and the compilation of Holocene rapid climate change events from *Mayewski et al.* [2004].

[22] A detailed study of grain size distributions from the noncarbonate fraction reveals that most of the samples within the Holocene are unimodal, with mode values around 8–10 μm (Figure 4d). Few samples show bimodal distributions with a second mode around 150–200 μm (Figure 4d), which is given by the presence of coarser grains, mainly quartz and mica packets, as observed by microscope (see photograph in Figure 4c). Such bimodal samples (marked with an asterisk in Figure 4c) correspond, with rare exceptions, to the samples with high median grain size values in the noncarbonate fraction and hence to the Minorca abrupt events M8 to M2.

[23] The UP10 general trend mimics the median grain size records and highlights additional features (Figures 4b, 4c, and 4e), for example a marked decrease from 11.5 to 10 ka, and a better expression of M4 (Figure 4a). From 9 ka to present, the UP10 fraction oscillates between 30 and 35%, except for M8 to M2 events. In the M8 to M2 peaks the UP10 fraction may represent as much as 50% of the sample (Figure 4e). The UP10 peaks are consistent with the above mentioned median grain size increases (Figure 4c), and correlative with the oxygen isotopic enrichments of the Minorca abrupt events (Figure 4a). A slight increase in the UP10 fraction is recognized in the last millennium.

[24] Silt/clay ratio (Figure 4f) complements the information gathered from grain size parameters. Like UP10, this ratio also illustrates a marked fall of silt accumulation during the deglaciation, displays relatively high values during the early Holocene and shows a decreasing trend during the last 9 kyr ending with relatively low values during the late Holocene (Figure 4f). The overall record is again punctuated by a number of peaks linked to the Minorca abrupt events identified from previous proxies. These long-term trends and short-lived events are visible in both the bulk (dashed lines in Figure 4) and the noncarbonate fraction (solid lines in Figure 4), where they are more obvious.

5.3. Geochemical Record

[25] The Si/Al, Ti/Al, K/Al and Ca/Al geochemical profiles of core MD99-2343 are plotted in Figures 5b, 5c, 5e, and 5f. Four main phases or trends are identified through the last 12 kyr: I, a decreasing trend in Si/Al and Ti/Al ratios (Figures 5b and 5c) during the deglaciation that leads to a minimum at 10.5 ka that coincides with minimum values in grain size proxies (Figure 4) and maximum values of summer solar insolation at 40°N (Figure 5d); II, an increasing trend in both Si/Al and Ti/Al ratios coincides with the end of the second phase of Termination (TIb) and the early Holocene (10.5–7 ka); III, high Si/Al and Ti/Al ratios with moderate oscillations during the mid-Holocene (7–4 ka); and IV, a gradual decreasing trend in Si/Al and Ti/Al during the late Holocene (4–0 ka), which parallels the decrease in the insolation curve (Figure 5d). Interestingly, the K/Al record (Figure 5e) presents a distinctive pattern during TIb and the early Holocene (phases I and II), therefore suggesting the operation of differentiated controlling factors on K/Al. The Ca/Al ratio (Figure 5f) shows a rather distinct pattern with an almost continuous increasing trend across the Younger Dryas, TIb and early and mid-Holocene, with maximum values between 4 and 2.4 ka that drop abruptly after 2.4 ka (Figure 5f).

[26] The above described general trends are punctuated by oscillations lasting from centuries to millennia. The Si/Al record shows eight abrupt events during the Holocene that are centered at 8.4, 7.2, 6.2, 5, 4.1, 3.2, 1.6 and 0.5 ka (Figure 5b). Most of these events can be identified in the Ti/Al and Ca/Al records as well (Figures 5c and 5f). However, they are not noticeable in the K/Al record (Figure 5e). The abrupt events in the geochemical records coincide with the Minorca abrupt events identified in the *G. bulloides* oxygen isotopic record and the grain size proxies. The only exception to the described overall pattern is M2, which is represented by one of the largest isotopic excursions (Figure 5a), and a Ca/Al peak but lacks of expression in the Si/Al record (Figures 5f and 5b).

[27] The main mineralogical components obtained from the clay size XRD analysis confirm the high percentage of calcite and illite within all the analyzed samples, with chlorite, kaolinite, quartz and very low percentages of feldspars. The lack of major changes in the mineralogical composition of the clay fraction shows that geochemical variability is dominated by the composition of the coarser fraction. This enhances the value of the geochemical

records for the interpretation of processes controlling coarse particle release, transport and accumulation.

6. Discussion

6.1. Particle Sources

[28] Sediment particles resulting from riverine influx, aeolian transport and sea surface biogenic production (see section 2.2) form a mixed population that is expected to settle in the water column where it is advected by water mass movements before final deposition on the seabed. The proxies used in our study allow identifying the ultimate factors controlling sediment deposition in the MD99-2343 core site.

[29] The location of the core MD99-2343 on a sediment drift off the carbonate shelf of the Balearic Islands points to a mixed signal in our Ca/Al ratio resulting from carbonate productivity [*Rühlemann et al.*, 1999] and resedimented carbonate particles [*Van Os et al.*, 1994]. Surface productivity and subsequent particle settling in such an oligotrophic area [*Bethoux et al.*, 1998] can contribute only partly to the carbonate flux and to the relatively high sedimentation rates of core MD99-2343.

[30] Most of the samples within the Minorca abrupt event layers display a characteristic bimodal distribution (Figures 4c and 4d) that could be tentatively attributed to pulses of enhanced aeolian transport. The relatively low rates of Saharan dust deposition and the high sedimentation rates measured in our core lead us to consider the aeolian contribution as largely diluted within particle populations from other sources. In addition, the coarser grains from these layers yield a 150–200 μm mode that is much coarser than the one found in modern and glacial Saharan dust samples in the western Mediterranean [*Guerzoni et al.*, 1997; *Moreno et al.*, 2002]. Furthermore, microscope inspection of the coarse grains observed within the Minorca event layers shows quartz grains with moderate angularity and undisturbed mica packets (sea photograph in Figure 4c), an uncommon feature in aeolian dust particles [*Guerzoni et al.*, 1997]. Those observations point to a rather proximal source for these coarse grains whose release and transport did not involve particularly aggressive physical or chemical weathering processes as would be the case for the aeolian transported particles.

[31] Core MD99-2343 was recovered from a contourite drift and the occurrence of this coarse grain population may be related to the formation of the drift itself. The building of the contourite drift demonstrates the efficiency of deepwater circulation in the area to rework, winnow, transport and accumulate originally fluvial terrigenous particles from the Valencia Valley and therefore explains the relatively high sedimentation rates observed in core MD99-2343. We interpret changes in the grain size distribution as mostly governed by the strength of such deep currents as previously observed in other contourite systems [*McCave and Tucholke*, 1986; *Llave et al.*, 2006; *Voelker et al.*, 2006]. Intervals of enhanced currents resulted in a more efficient transport of coarse particles from both far fluvial sources and local sources as pointed out by the presence of coarse quartz and mica grains with minimal alteration. A prominent volcanic ridge [*Maillard and Mauffret*, 1999] at the very head of the Minorca peripheral depression (Figure 2a), to the west of the Minorca drift, is a firm candidate as source area for such unaltered particles. Therefore the coarse particles deposited during the Minorca abrupt events accumulated during intervals of near-bottom current strengthening able to vigorously erode seafloor relieves and transport to the sediment drift location the coarse particles thus released.

[32] K/Al, Si/Al and Ti/Al ratios are associated with terrigenous inputs [*Krom et al.*, 1999; *Wehausen and Brumsack*, 1999, 2000; *Moreno et al.*, 2001, 2002; *Martínez-Ruiz et al.*, 2003; *Weldeab et al.*, 2003; *Moreno et al.*, 2005], probably from the Ebro and Rhône rivers north of the study site. Si mostly comes from aluminosilicates and quartz as biogenic opal is a minor sediment component in the region [*Weldeab et al.*, 2003], as further confirmed by our microscopic examinations. Ti resides within heavy minerals such as ilmenite and rutile, and Al and K are associated with clay minerals. In particular, the K/Al ratio is considered a good indicator for clay inputs (mainly illite) from river runoff. The presence of noticeable amounts of illite at the study site has been confirmed by peaks in XRD diffractograms. Consequently, the K/Al ratio can be interpreted as an indicator of illite entrance by river discharge and hence may provide a diagnosis of humidity conditions in the northwestern Mediterranean region. The parallelism between the K/Al record and the insolation curve at 40°N not only for the Holocene (Figures 5d and 5e) but also for the last glacial period (J. Frigola et al., Evidences of abrupt changes in Western Mediterranean Deep Water circulation during the last 50 kyr: A high-resolution marine record from the Balearic Sea, submitted to *Quaternary International*, 2006) reinforce the view that precipitation controls long-term K/Al ratio oscillations. The differences observed between Si/Al and Ti/Al, and the K/Al record (Figures 5b, 5c, and 5e) are attributed to grain size geochemical segregation processes since K is mostly associated with clay particles while Si and Ti relate to coarser grains. Parallel increases of the median grain size and the Si/Al and Ti/Al ratios support the view that grain size distribution controls the variability of these geochemical ratios rather than changes in source area.

6.2. Holocene Onset and General Trends

[33] The decrease in the oxygen isotopic record from 12 to 9 ka (Figure 4a) embraces the end of the Younger Dryas, the second phase of Termination (TIb), and the onset of the Holocene. The variations observed in both grain size and geochemical records during this time interval (Figures 4 and 5) reflect the strong changes in the sedimentary dynamics driven by the shifting climatic conditions. Diminutions in grain size parameters and Si/Al and Ti/Al ratios (phase I), which reached minimum values between 10 and 11 ka (Figures 4 and 5), are consistent with a slowdown of deepwater circulation in the western Mediterranean. Accordingly, the glacial benthic isotopic record from our core ends at 12 ka when *C. pachydermus* disappears from the benthic assemblage [*Reguera*, 2004; *Sierro et al.*, 2005], likely replaced by species inhabiting poorly oxygenated environments [*Caralp*, 1988; *Reguera*,

2004]. Reduced deepwater ventilation conditions for this time interval (12–9 ka) are also suggested by the preservation of an Organic Rich Layer in the Alboran Sea [*Cacho et al.*, 2002]. In parallel, TIb sedimentation rates were minimal (Figure 3c) because of the combined effect of the reduction in the input of terrigenous particles forced by the inshore migration of the coastline caused by the postglacial sea level rise, and to a lowered transport of particles into weakened deepwater currents.

[34] The weakening of the deep overturning cell could also result (or be amplified) from more humid conditions in the western Mediterranean region during the time of maximum summer insolation (Figure 5d) as suggested from maximum values of the K/Al record (Figure 5e) and supported by other studies [*Harrison and Digerfeldt*, 1993; *González-Sampériz et al.*, 2006]. A more pronounced stratification in the upper water column favored by an enhanced freshwater input due to increased precipitation during summer insolation maxima, and higher atmospheric stability associated with the retreat of the Northern Hemisphere ice sheet, would have lead to the slowdown of the deepwater overturning cell in the Gulf of Lion and to a reduction of contour current activity in the Minorca sediment drift. After 10.5 ka both grain size and geochemical records show a steady increasing trend (phase II in Figures 5 and 6), which points to the recovery of the deepwater overturning cell in the Gulf of Lion coincident with the decreasing trend in the summer insolation at 40°N (Figure 4d).

[35] The relative stabilization of grain size parameters (Figures 4e and 4f) and the Si/Al ratio around 7 ka (phase III in Figure 6e) is synchronous with the end of the postglacial sea level rise [*Fleming et al.*, 1998] and suggests the reestablishment of deepwater circulation and a stable supply of fluvial material. Such a synchronicity illustrates how significant was the sea level rise control on the western Mediterranean thermohaline circulation and, consequently, on the outbuilding of the Minorca sediment drift. The essentially stable conditions found for the mid-Holocene (7–4 ka) in the Minorca deep sea site contrast with marked changes reported in many locations worldwide [*Steig*, 1999] and, in particular, in the Mediterranean borderlands [*COHMAP Members*, 1988; *Cheddadi et al.*, 1997; *Prentice et al.*, 1998; *Magny et al.*, 2002] and the North African region [*Vernet and Faure*, 2000] associated with the end of the African Humid Period [*deMenocal et al.*, 2000]. This mid-Holocene climate variability is attributed to the reduction of seasonal insolation differences after 5.5 ka, which lead to an abrupt transition from humid to arid conditions in North Africa and in the western Mediterranean region.

[36] This well-known mid-Holocene variability does not seem to influence our proxies until 4 ka when an evident decrease in the silt/clay ratio and the Si/Al points to a slowdown of the deepwater overturning cell and to a reduction of fluvial inputs due to drier conditions (Figure 4f and phase IV in Figure 6e). These drier conditions would be also consistent with the δ^{18}O stabilization at high values during the late Holocene. A southward displacement of the ITCZ and the subsequent decrease in the atmospheric pressure gradient due to reduced seasonal insolation differences likely favored the establishment of drier conditions [*McDermott et al.*, 1999; *Jalut et al.*, 2000]. Accordingly, the lessening in the activity of the northwesterlies would account for the reduction of deepwater circulation during the late Holocene. Our results stress the high sensitivity of the western Mediterranean thermohaline circulation to both the atmospheric (i.e., northwesterlies variability that induced changes in the deepwater overturning in the Gulf of Lion) and the hydrologic systems (i.e., orbitally induced precipitation variability and meltwater pulses).

6.3. Holocene Abrupt Events

[37] The nine Holocene δ^{18}O enrichment events had an average duration of 500 years and an observed periodicity close to 1000 years (Table 2 and Figure 6). Most of the Holocene increases in the oxygen isotopic record parallel increases in the UP10 fraction and the Si/Al ratio (Figure 6), therefore suggesting that relatively cold surface conditions coexisted with more energetic deepwater conditions. An intensification of the northwesterly winds in the western Mediterranean would account for the conditions described during the Holocene Minorca events, similarly to the mechanism proposed for the glacial Dansgaard-Oeschger variability [*Cacho et al.*, 2000; *Sierro et al.*, 2005]. These cold and dry winds enhanced the deepwater overturning in the Gulf of Lion by cooling of the surface waters and, consequently, they steered the activity of bottom currents on the Minorca rise. Such vigorous currents were able to transport coarser particles to the Minorca rise as shown by the accumulation of quartz grains and mica packets coarser than 63 μm. This resulted in the increase of the UP10 fraction (Figure 6d) and the apparition of bimodal samples (Figure 4c). In parallel, higher values in the silt/clay ratio are interpreted as resulting from the winnowing effect of the finest particles (Figure 4f).

[38] While events M8 to M3 are consistently represented in both grain size and geochemical proxies, M0, M1 and M2 are not always well represented. For instance, M2 is not recorded by the Si/Al ratio while it forms one of the larger peaks in the UP10 fraction and, in contrast, M1 and M0 do not show a clear expression in the UP10 ratio but they present significant increases in the Si/Al record (Figure 6). Interestingly, this distinctive sensitivity between the different proxies occurs during the phase IV, late Holocene, related to the establishment of drier conditions due to reduced seasonal insolation differences (section 6.2). Overall, reduced deep overturning is interpreted to occur because of the weakening of northwesterlies and more stable conditions. Furthermore, the expression of the Minorca events in the studied proxies seems to become weaker through the Holocene in parallel to the relative stabilization of the oxygen isotopic signal. These different climatic boundary conditions may have determined a lower sensitivity of the system to millennial-centennial-scale climatic variability toward late Holocene and, consequently, provided an ambiguous signature in the studied records.

[39] The fact that Holocene cooling events have been reported elsewhere all around the globe [*Mayewski et al.*, 2004] demonstrates their global extent and the lack of stability of the Holocene climate. There are, however, disagreements about the precise timing, the character and

the impact of these Holocene abrupt events. Some of the cooling events recorded in the Atlantic and Mediterranean regions are summarized and tentatively correlated to our Minorca cold events M0 to M8 for the last 9 kyr (Table 2). Furthermore, a correlation attempt between the Minorca events and the 300-year running mean of the GISP2 isotopic curve (Figure 6b) results in fairly good agreement, even considering the uncertainties of our age model. This supports the hypothesis of a highly efficient climatic coupling between the North Atlantic and the western Mediterranean region during the last 10 kyr.

[40] The UP10 fraction of our core MD99-2343 displays a periodic oscillation close to 900 years in between 9 and 2 ka (Figure 6e and Table 2), which is in agreement with those obtained from the GISP2 ice core oxygen isotopic record [*Schulz and Paul*, 2002], from a Saharan dust record [*Kuhlmann et al.*, 2004], and from varved sediments in California [*Nederbragt and Thurow*, 2005]. Several hypotheses aim at explaining the periodicity of about 900 years. Though it may be triggered by insolation changes or result from internal feed back mechanisms [*Schulz and Paul*, 2002], the recorded climatic oscillations are better linked to the temperature signal from the North Atlantic climate system, in agreement with other records from the Northern Hemisphere [*Cacho et al.*, 2001; *Kuhlmann et al.*, 2004].

[41] The most pronounced Holocene abrupt event, M8, occurred at 9–7.8 ka, therefore embracing the well-known 8.2 ka cold North Atlantic event [*Mayewski et al.*, 2004; *Alley and Agustsdottir*, 2005; *Rohling and Pälike*, 2005]. The intensification of the atmospheric circulation during M8 led to good ventilation conditions in the Western Mediterranean Basin thus stopping the formation of the ORL in the Alboran Sea [*Cacho et al.*, 2002], synchronously with the middle interruption of sapropel S1 in the Eastern Mediterranean Basin [*Rohling et al.*, 1997; *Mercone et al.*, 2000]. We propose that the atmospheric teleconnection between high latitudes and the Mediterranean region through the westerly winds system was the main control over the western Mediterranean thermohaline circulation through the Holocene. This atmospheric forcing of the climate variability for the last 10 kyr is quite similar to the present pattern of the North Atlantic Oscillation (NAO) that exerts a first-order control at decadal scales [*Rodó et al.*, 1997]. Positive NAO years are associated with Iberian dryness and cold temperatures in Greenland, and more persistent and stronger winter storms crossing the Atlantic Ocean [*Hurrell*, 1995]. Consequently, the Minorca abrupt events could be associated with periods of persistent positive NAO index, which would strengthen the northwesterlies over the northwestern Mediterranean Basin and hence reinforce deepwater overturning. Although we do not exclude a pervasive solar influence or instabilities inherent to the North Atlantic thermohaline circulation [*Bond et al.*, 2001; *Schulz and Paul*, 2002] as main precursors of the Holocene climate oscillations recorded in the core MD99-2343, we suggest that the rapid transmission of these changes from high latitudes to the Mediterranean region was mainly driven by the northwesterly wind system variability modulated by a NAO-like mechanism. A similar atmospheric linkage mechanism, though acting at a millennial scale, was proposed to explain the Dansgaard/Oeschger variability in the deepwater ventilation and Saharan dust input during the last glacial period in the Alboran Sea [*Cacho et al.*, 2000; *Moreno et al.*, 2002; *Sánchez-Goñi et al.*, 2002].

7. Conclusions

[42] The sedimentary record from core MD99-2343 recovered from a deepwater contourite drift reveals the effects of Holocene climate variability over the thermohaline circulation in the Western Mediterranean Basin during the last 12 kyr. Geochemical proxies associated with terrigenous inputs like Si/Al, Ti/Al and K/Al display a decreasing trend through the Holocene that parallels the summer insolation curve at 40°N showing the marked influence of the precipitation pattern over the region. Four different phases have been identified in the Si/Al and Ti/Al ratios from the last 12 kyr. The first from 12 to 10.5 ka shows a slowdown of deepwater circulation due to the combined effect of the increasing sea level and the relatively humid conditions installed on land which both favored the stratification of water masses. The second phase (10.5–7 ka) is associated with the recovery of deepwater circulation until the end of the postglacial sea level rise at 7 ka. The third phase (7–4 ka) corresponds to a plateau with high values of the terrigenous proxies translating the good functioning of deepwater circulation during a progressive orbitally driven change toward dryer conditions in the western Mediterranean borderlands. Finally, the fourth phase (4–0 ka) indicates a progressive decrease of the terrigenous contributions because of reduced fluvial inputs during drier conditions induced by lower seasonal insolation differences, also modulated by the thermohaline circulation weakening because of more stable atmospheric conditions.

[43] Superimposed on this general Holocene pattern, marked oscillations have been noticed and related to abrupt climate changes. The new grain size parameter presented in this work that represents the fraction coarser than 10 μm (UP10) has been tested as a convenient proxy for paleocurrent intensity in the study area for Holocene sediments. The UP10 record presents a 900-year cycle oscillation, which is consistent with the geochemical record of terrigenous input between 9 and 2 ka and the surface cooling events uncovered by the oxygen isotopic record. Such periodicity fits with temperature oscillations from the Holocene δ^{18}O record in Greenland and points to the pressure gradient system as a direct teleconnection mechanism for climate variability transfer from the North Atlantic to the Mediterranean region. The centennial to millennial-scale Holocene oscillations observed in our records reveal a coupled atmospheric/oceanographic forcing equivalent to the present-day NAO and sustains the hypothesis of a rapid fitting with Mediterranean climate conditions. Furthermore, our results demonstrate the high sensitivity of deepwater overturning in the Gulf of Lion to the transfer of climate oscillations from high latitudes to midlatitudes.

[44] **Acknowledgments.** Funding by the European Commission Fifth and Sixth Framework Programmes to projects ADIOS (EVK3-2000-00035), PROMESS 1 (EVR1-CT-2002-40024), EUROSTRATAFORM

(EVK3-2002-00079), and HERMES (GOCE-CT-2005-511234-1) supported the research effort behind this paper. The Spanish-funded BTE2002-04670 and REN2003-08642-C02-02 projects are equally acknowledged. We are especially grateful to the *Marion Dufresne* and the IMAGES programme that enabled the collection of cores MD99-2343 and MD95-2043. GRC Geociències Marines is recognized within the Generalitat de Catalunya excellence research groups program (reference 2005SGR 00152). We thank M. Guart (Departament d'Estratigrafia, Paleontologia i Geociències Marines, University of Barcelona) and E. Seguí (Serveis Cientifico-Tècnics, University of Barcelona) for their help with the laboratory work and G. Lastras and D. Amblas for their help with the artwork. The Editor G. Dickens, J. B. Stuut, and two anonymous reviewers are greatly acknowledged for their positive comments on an earlier version of the manuscript. COMER Foundation and I3P postdoctoral programme (CSIC) are also acknowledged for their support to I. Cacho and A. Moreno, respectively. J. Frigola benefited from a fellowship of the University of Barcelona.

References

Acosta, J. (2005), El Promontorio Balear: Morfología submarina y recubrimiento sedimentario, Ph.D. thesis, 154 pp., Univ. de Barcelona e Inst. Español de Oceanogr., Barcelona.

Alley, R. B., and A. M. Agustsdottir (2005), The 8k event: Cause and consequences of a major Holocene abrupt climate change, *Quat. Sci. Rev.*, *24*, 1123–1149.

Alonso, B., M. Canals, A. Palanques, and J. P. Rehault (1995), A deep-sea channel in the northwestern Mediterranean Sea: Morphology and seismic structure of the Valencia channel and its surroundings, *Mar. Geophys. Res.*, *17*, 469–484.

Barry, R. G., and R. J. Chorley (1998), *Atmosphere, Weather and Climate*, 7th ed., 409 pp., Routledge, London.

Bethoux, J. P., P. Morin, C. Chaumery, O. Connan, B. Gentili, and D. Ruiz-Pino (1998), Nutrients in the Mediterranean Sea, mass balance and statistical analysis of concentrations with respect to environmental change, *Mar. Chem.*, *63*, 155–169.

Bianchi, G. G., and I. N. McCave (1999), Holocene periodicity in North Atlantic climate and deep-ocean flow south of Iceland, *Nature*, *397*, 515–517.

Bolle, H.-J. (2003), *Mediterranean Climate: Variability and Trends*, 372 pp., Springer, New York.

Bond, G., W. Showers, M. Cheseby, R. Lotti, P. Almasi, P. de Menocal, P. Priore, H. Cullen, I. Hajdas, and G. Bonani (1997), A pervasive millennial-scale cycle in North Atlantic Holocene and glacial climates, *Science*, *278*, 1257–1266.

Bond, G., B. Kromer, J. Beer, R. Muscheler, M. Evans, W. Showers, S. Hoffmann, R. Lotti-Bond, I. Hajdas, and G. Bonani (2001), Persistent solar influence on North Atlantic climate during the Holocene, *Science*, *294*, 2130–2136.

Cacho, I., J. O. Grimalt, C. Pelejero, M. Canals, F. J. Sierro, J. A. Flores, and N. J. Shackleton (1999), Dansgaard-Oeschger and Heinrich event imprints in Alboran Sea temperatures, *Paleoceanography*, *14*, 698–705.

Cacho, I., J. O. Grimalt, F. J. Sierro, N. J. Shackleton, and M. Canals (2000), Evidence for enhanced Mediterranean thermohaline circulation during rapid climatic coolings, *Earth Planet. Sci. Lett.*, *183*, 417–429.

Cacho, I., J. O. Grimalt, M. Canals, L. Sbaffi, N. Shackleton, J. Schönfeld, and R. Zahn (2001), Variability of the western Mediterranean Sea surface temperature during the last 25,000 years and its connection with the Northern Hemisphere climatic changes, *Paleoceanography*, *16*, 40–52.

Cacho, I., J. O. Grimalt, and M. Canals (2002), Response of the western Mediterranean Sea to rapid climate variability during the last 50,000 years: A molecular biomarker approach, *J. Mar. Syst.*, *33-34*, 253–272.

Canals, M. (1980), Sedimentos y procesos en el margen continental sur-Balear: Control climático y oceanográfico sobre su distribución y evolución durante el Cuaternario superior, M. S. thesis, 210 pp., Inst. "Jaume Almera" (CSIC) y Univ. de Barcelona, Barcelona.

Caralp, M. H. (1988), Late glacial to recent deep-sea benthic foraminifera from the northeastern Atlantic (Cadiz Gulf) and western Mediterranean (Alboran Sea): Paleoceanographic results, *Mar. Micropaleontol.*, *13*, 265–289.

Cheddadi, R., G. Yu, J. Guiot, S. P. Harrison, and I. C. Prentice (1997), The climate of Europe 6000 years ago, *Clim. Dyn.*, *13*, 1–9.

Cheddadi, R., H. F. Lamb, J. Guiot, and S. van der Kaars (1998), Holocene climatic change in Morocco: A quantitative reconstruction from pollen data, *Clim. Dyn.*, *14*, 883–890.

Claussen, M., C. Kubatzki, V. Browkin, and A. Ganopolski (1999), Simulation of an abrupt change in Saharan vegetation in the mid-Holocene, *Geophys. Res. Lett.*, *26*, 2037–2040.

COHMAP Members, (1988), Climatic changes of the last 18,000 years: Observations and model simulations, *Science*, *241*, 1043–1052.

Coplen, T. B. (1996), New guidelines for the reporting of stable hydrogen, carbon, and oxygen isotope ratio data, *Geochim. Cosmochim. Acta*, *60*, 3359–3360.

Davis, B. A. S., S. Brewer, A. C. Stevenson, and J. Guiot (2003), The temperature of Europe during the Holocene reconstructed from pollen data, *Quat. Sci. Rev.*, *22*, 1701–1716.

deMenocal, P., J. Ortiz, T. Guilderson, J. Adkins, M. Sarnthein, L. Baker, and M. Yarusinsky (2000), Abrupt onset and termination of the African Humid Period: Rapid climate responses to gradual insolation forcing, *Quat. Sci. Rev.*, *19*, 347–361.

Fleming, K., P. Johnston, D. Zwartz, Y. Yokoyama, K. Lambeck, and J. Chappell (1998), Refining the eustatic sea-level curve since the Last Glacial Maximum using far- and intermediate-field sites, *Earth Planet. Sci. Lett.*, *163*, 327–342.

González-Sampériz, P., B. L. Valero-Garcés, A. Moreno, G. Jalut, J. M. García-Ruíz, C. Martí-Bono, A. Delgado-Huertas, A. Navas, T. Otto, and J. J. Dedoubat (2006), Climate variability in the Spanish Pyrenees during the last 30,000 yr revealed by the El Portalet sequence, *Quat. Res.*, *66*, 38–52.

Grootes, P., M. Stuiver, J. W. C. White, S. J. Johnsen, and J. Jouzel (1993), Comparison of oxygen isotope records from the GISP2 and GRIP Greenland ice cores, *Nature*, *366*, 552–554.

Guerzoni, S., E. Molinaroli, and R. Chester (1997), Saharan dust inputs to the western Mediterranean Sea: Depositional patterns, geochemistry and sedimentological implications, *Deep Sea Res., Part II*, *44*, 631–654.

Hall, I. R., and I. N. McCave (2000), Palaeocurrent reconstruction, sediment and thorium focussing on the Iberian margin over the last 140 ka, *Earth Planet. Sci. Lett.*, *178*, 151–164.

Harrison, S. P., and G. Digerfeldt (1993), European lakes as palaeohydrological and palaeoclimatic indicators, *Quat. Sci. Rev.*, *12*, 233–248.

Hughen, K., et al. (2004), Marine04 marine radiocarbon age calibration, 26–0 ka BP, *Radiocarbon*, *46*, 1059–1086.

Hurrell, J. W. (1995), Decadal trends in the North Atlantic Oscillation: Regional temperatures and precipitation, *Science*, *269*, 676–679.

Intergovernmental Oceanographic Commission, International Hydrographic Organization, and British Oceanographic Data Centre (2003) *Centenary Edition of the GEBCO Digital Atlas* [CD-ROM], Br. Oceanogr. Data Cent., Liverpool, U.K.

Jalut, G., A. Esteban Amat, L. Bonnet, T. Gauquelin, and M. Fontugne (2000), Holocene climatic changes in the western Mediterranean, from south-east France to south-east Spain, *Palaeogeogr. Palaeoclimatol., Palaeoecol.*, *160*, 255–290.

Konert, M., and J. Vandenberghe (1997), Comparison of laser grain size analysis with pipette and sieve analysis: A solution for the underestimation of the clay fraction, *Sedimentology*, *44*, 523–535.

Krom, M. D., A. Michard, R. A. Cliff, and K. Strohle (1999), Sources of sediment to the Ionian Sea and western Levantine basin of the eastern Mediterranean during S-1 sapropel times, *Mar. Geol.*, *160*, 45–61.

Kuhlmann, H., H. Meggers, T. Freudenthal, and G. Wefer (2004), The transition of the monsoonal and the N Atlantic climate system off NW Africa during the Holocene, *Geophys. Res. Lett.*, *31*, L22204, doi:10.1029/2004GL021267.

Lacombe, H., P. Tchernia, and L. Gamberoni (1985), Variable bottom water in the Western Mediterranean Basin, *Prog. Oceanogr.*, *14*, 319–338.

Llave, E., J. Schonfeld, F. J. Hernandez-Molina, T. Mulder, L. Somoza, V. Diaz del Rio, and I. Sanchez-Almazo (2006), High-resolution stratigraphy of the Mediterranean outflow contourite system in the Gulf of Cadiz during the late Pleistocene: The impact of Heinrich events, *Mar. Geol.*, *227*, 241–262.

Loyë-Pilot, M. D., J. D. Martin, and J. Moreli (1986), Influence of Saharan dust on the rain acidity and atmospheric input to the Mediterranean, *Nature*, *321*, 427–428.

Magny, M., C. Miramont, and O. Sivan (2002), Assessment of the impact of climate and anthropogenic factors on Holocene Mediterranean vegetation in Europe on the basis of palaeohydrological records, *Palaeogeogr. Palaeoclimatol. Palaeoecol.*, *186*, 47–59.

Maillard, A., and A. Mauffret (1999), Crustal structure and riftogenesis of the Valencia

Trough (north-western Mediterranean Sea), *Basin Res.*, *11*, 357–379.

Maldonado, A., and M. Canals (1982), El margen continental sur-balear: Un modelo deposicional reciente sobre un margen de tipo pasivo, *Acta Geol. Hisp.*, *17*, 241–254.

Maldonado, A., and D. J. Stanley (1979), Depositional patterns and late Quaternary evolution of two Mediterranean submarine fans: A comparison, *Mar. Geol.*, *31*, 215–250.

Maldonado, A., H. Got, A. Monaco, S. O'Connell, and L. Mirabile (1985), Valencia Fan (northwestern Mediterranean): Distal deposition fan variant, *Mar. Geol.*, *62*, 295–319.

Martin, J.-M., F. Elbaz-Poulichet, C. Guieu, M.-D. Loyë-Pilot, and G. Han (1989), River versus atmospheric input of material to the Mediterranean Sea: An overview, *Mar. Chem.*, *28*, 159–182.

Martínez-Ruiz, F., A. Paytan, M. Kastner, J. M. Gonzalez-Donoso, D. Linares, S. M. Bernasconi, and F. J. Jimenez-Espejo (2003), A comparative study of the geochemical and mineralogical characteristics of the S1 sapropel in the western and eastern Mediterranean, *Palaeogeogr. Palaeoclimatol. Palaeoecol.*, *190*, 23–37.

Martrat, B., J. O. Grimalt, C. Lopez-Martinez, I. Cacho, F. J. Sierro, J. A. Flores, R. Zahn, M. Canals, J. H. Curtis, and D. A. Hodell (2004), Abrupt temperature changes in the western Mediterranean over the past 250,000 years, *Science*, *306*, 1762–1765.

Mauffret, A., M. Labarbarie, and L. Montadert (1982), Les affleurements de series sedimentaires pre-pliocenes dans le bassin Mediterraneen nord-occidental., *Mar. Geol.*, *45*, 159–175.

Mayewski, P. A., E. E. Rohling, J. C. Stager, W. Karlen, K. A. Maasch, L. D. Meeker, E. A. Meyerson, F. Gasse, S. van Kreveld, and K. Holmgren (2004), Holocene climate variability, *Quat. Res.*, *62*, 243–255.

McCave, I. N., and B. E. Tucholke (1986), Deep current-controlled sedimentation in the western North Atlantic, in *The Geology of North America, Volume M, The Western North Atlantic Region*, edited by P. R. Vogt and B. E. Tucholke, pp. 451–468, Geol. Soc. of Am., Boulder, Colo.

McCave, I. N., R. J. Bryant, H. F. Cook, and C. A. Coughanowr (1986), Evaluation of a laser-diffraction-size analyzer for use with natural sediments, *J. Sediment. Res.*, *56*, 561–564.

McCave, I. N., B. Manighetti, and S. G. Robinson (1995), Sortable silt and fine sediment size/composition slicing: Parameters for paleocurrent speed and paleoceanography, *Paleoceanography*, *10*, 593–610.

McDermott, F., S. Frisia, Y. Huang, A. Longinelli, B. Spiro, T. H. E. Heaton, C. J. Hawkesworth, A. Borsato, E. Keppens, and I. J. Fairchild (1999), Holocene climate variability in Europe: Evidence from $\delta^{18}O$, textural and extension-rate variations in three speleothems, *Quat. Sci. Rev.*, *18*, 1021–1038.

Medoc, G. (1970), Observation of formation of Deep Water in the Mediterranean Sea, 1969, *Nature*, *227*, 1037–1040.

Meese, D. A., A. J. Gow, R. B. Alley, P. M. Zielinski, G. A. Grootes, M. Ram, K. C. Taylor, P. A. Mayewski, and J. F. Bolzan (1997), The Greenland Ice Sheet Project 2 depth-age scale: Methods and results, *J. Geophys. Res.*, *102*, 26,411–26,423.

Mercone, D., J. Thomson, and I. W. Croudace (2000), Duration of S1, the most recent sapropel in the eastern Mediterranean Sea, as indicated by accelerator mass spectrometry radiocarbon and geochemical evidence, *Paleoceanography*, *15*, 336–347.

Millot, C. (1999), Circulation in the western Mediterranean Sea, *J. Mar. Syst.*, *20*, 423–442.

Millot, C., and A. Monaco (1984), Deep strong currents and sediment transport in the northwestern Mediterranean Sea, *Geo Mar. Lett.*, *4*, 13–17.

Moreno, A., J. Targarona, J. Henderiks, M. Canals, T. Freudenthal, and H. Meggers (2001), Orbital forcing of dust supply to the North Canary Basin over the last 250 kyrs, *Quat. Sci. Rev.*, *20*, 1327–1339.

Moreno, A., I. Cacho, M. Canals, M. A. Prins, M.-F. Sanchez-Goni, J. O. Grimalt, and G. J. Weltje (2002), Saharan dust transport and high-latitude glacial climatic variability: The Alboran Sea record, *Quat. Res.*, *58*, 318–328.

Moreno, A., I. Cacho, M. Canals, J. O. Grimalt, and A. Sanchez-Vidal (2004), Millennial-scale variability in the productivity signal from the Alboran Sea record, western Mediterranean Sea, *Palaeogeogr. Palaeoclimatol. Palaeoecol.*, *211*, 205–219.

Moreno, A., I. Cacho, M. Canals, J. O. Grimalt, M. F. Sanchez-Goni, N. Shackleton, and F. J. Sierro (2005), Links between marine and atmospheric processes oscillating on a millennial time-scale: A multi-proxy study of the last 50000 yr from the Alboran Sea (western Mediterranean Sea), *Quat. Sci. Rev.*, *24*, 1623–1636.

Nederbragt, A. J., and J. Thurow (2005), Geographic coherence of millennial-scale climate cycles during the Holocene, *Palaeogeogr. Palaeoclimatol. Palaeoecol.*, *221*, 313–324.

O'Brien, S. R., P. A. Mayewski, L. D. Meeker, D. A. Meese, M. S. Twickler, and S. I. Whitlow (1995), Complexity of Holocene climate as reconstructed from a Greenland ice core, *Science*, *270*, 1962–1964.

Oppo, D. W., J. F. McManus, and J. L. Cullen (2003), Deepwater variability in the Holocene epoch, *Nature*, *422*, 277–278.

Paillard, D., L. Labeyrie, and P. Yiou (1996), Macintosh program performs time-series analysis, *Eos Trans. AGU*, *77*(39), 379.

Palanques, A., N. H. Kenyon, B. Alonso, and A. Limonov (1995), Erosional and depositional patterns in the Valencia channel mouth: An example of a modern channel-lobe transition zone, *Mar. Geophys. Res.*, *17*, 503–517.

Pinardi, N., and E. Masetti (2000), Variability of the large scale general circulation of the Mediterranean Sea from observations and modelling: A review, *Palaeogeogr. Palaeoclimatol. Palaeoecol.*, *158*, 153–173.

Prentice, I. C., S. P. Harrison, D. Jolly, and J. Guiot (1998), The climate and biomes of Europe at 6000 yr BP: Comparison of model simulations and pollen-based reconstructions, *Quat. Sci. Rev.*, *17*, 659–668.

Prospero, J. M. (1996), Saharan dust transport over the North Atlantic Ocean and Mediterranean: An overview, in *The Impact of Desert Dust Across the Mediterranean*, edited by S. Guerzoni, and R. Chester pp. 133–151, Kluwer Acad., Dordrecht, Netherlands.

Reguera, I. (2004), Respuesta del Mediterráneo Occidental a los cambios climáticos bruscos ocurridos durante el último ciclo glacial: Estudio de las asociaciones de foraminíferos, Ph.D. thesis, 231 pp., Univ. de Salamanca, Salamanca, Spain.

Rodó, X., E. Baert, and F. A. Comin (1997), Variations in seasonal rainfall in southern Europe during the present century: Relationships with the North Atlantic Oscillation and the El Niño-Southern Oscillation, *Clim. Dyn.*, *13*, 275–284.

Rohling, E. J., and H. Pälike (2005), Centennial-scale climate cooling with a sudden cold event around 8,200 years ago, *Nature*, *434*, 975–979.

Rohling, E. J., F. J. Jorissen, and H. C. de Stigter (1997), 200 year interruption of Holocene sapropel formation in the Adriatic Sea, *J. Micropaleontol.*, *16*, 97–108.

Rohling, E. J., A. Hayes, D. Rijk, D. Kroon, W. J. Zachariasse, and D. Eisma (1998), Abrupt cold spells in the northwest Mediterranean, *Paleoceanography*, *13*, 316–322.

Rohling, E. J., P. A. Mayewski, R. H. Abu-Zied, J. S. L. Casford, and A. Hayes (2002), Holocene atmosphere-ocean interactions: Records from Greenland and the Aegean Sea, *Clim. Dyn.*, *18*, 587–593.

Rollinson, H. (1993), *Using Geochemical Data: Evaluation, Presentation, Interpretation*, 352 pp., Longman Sci. and Technical, New York.

Rühlemann, C., P. J. Müller, and R. Schneider (1999), Organic carbon and carbonate as paleoproductivity proxies: Examples from high and low productivity areas of the tropical Atlantic, in *Use of Proxies in Paleoceanography: Examples From the South Atlantic*, edited by G. Fischer and G. Wefer pp. 1–31, Springer, New York.

Sánchez-Goñi, M. F., I. Cacho, J. L. Turon, J. Guiot, F. J. Sierro, J.-P. Peypouquet, J. O. Grimalt, and N. J. Shackleton (2002), Synchroneity between marine and terrestrial responses to millennial scale climatic variability during the last glacial period in the Mediterranean region, *Clim. Dyn.*, *19*, 95–105.

Sbaffi, L., F. C. Wezel, G. Curzi, and U. Zoppi (2004), Millennial- to centennial-scale palaeoclimate variations during Termination I and the Holocene in the central Mediterranean Sea, *Global Planet. Change*, *40*, 201–217.

Schulz, M., and A. Paul (2002), Holocene climate variability on centennial-to-millennial time scales: 1. Climate records from the North-Atlantic realm, in *Climate Development and History of the North Atlantic Realm*, edited by G. Wefer et al., pp. 41–54, Springer, New York.

Shackleton, N. J., M. A. Hall, and E. Vincent (2000), Phase relationships between millennial-scale events 64,000–24,000 years ago, *Paleoceanography*, *15*, 565–569.

Sierro, F. J., et al. (2005), Impact of iceberg melting on Mediterranean thermohaline circulation during Heinrich events, *Paleoceanography*, *20*, PA2019, doi:10.1029/2004PA001051.

Skinner, L. C., and I. N. McCave (2003), Analysis and modelling of gravity- and piston coring based on soil mechanics, *Mar. Geol.*, *199*, 181–204.

Skinner, L. C., and N. Shackleton (2003), Millennial-scale variability of deep-water temperature and $\delta^{18}O_{dw}$ indicating deep-water source variations in the northeast Atlantic, 0–34 cal. ka BP, *Geochem. Geophys. Geosyst.*, *4*(12), 1098, doi:10.1029/2003GC000585.

Steig, E. J. (1999), Mid-Holocene climate change, *Science*, *286*, 1485–1487.

Stow, D. A. V. (1982), Bottom currents and contourites in the North Atlantic, *Bull. Inst. Geol. Bassin Aquitaine*, *31*, 151–166.

Stow, D. A. V., J. C. Faugères, J. A. Howe, C. J. Pudsey, and A. R. Viana (2002), Bottom cur-

rents, contourites and deep-sea sediment drifts: Current state-of-the-art, in *Deep-Water Contourite Systems: Modern Drifts and Ancient Series, Seismic and Sedimentary Characteristics*, *Geol. Soc. Mem.*, vol. 22, edited by D. A. V. Stow et al., pp. 7–20, Geol. Soc., London.

Stuiver, M., and P. J. Reimer (1993), Extended ^{14}C database and revised CALIB radiocarbon calibration program, *Radiocarbon*, *35*, 215–230.

Telford, R. J., E. Heegaard, and H. J. B. Birks (2004), All age-depth models are wrong: But how badly?, *Quat. Sci. Rev.*, *23*, 1–5.

United Nations Environment Programme (2003) Riverine transport of water, sediments and pollutants to the Mediterranean Sea, *MAP Tech. Rep. Ser. 141*, Athens.

Vanney, R., and D. Mougenot (1981), La plate-forme continentale du Portugal et des provinces adjancetes: Analyse géomorphologique, *Mem. Serv. Geol. Port.*, *28*, 1–86.

Van Os, B. J. H., L. J. Lourens, F. J. Hilgen, G. J. de Lange, and L. Beaufort (1994), The formation of Pliocene and carbonate cycles in the Mediterranean: Diagenesis, dilution and productivity, *Paleoceanography*, *9*, 601–617.

Velasco, J. P. B., J. Baraza, and M. Canals (1996), La depresión periférica y el lomo contourítico de Menorca: Evidencias de la actividad de corrientes de fondo al N del Talud Balear, *Geogaceta*, *20*, 359–362.

Vernet, R., and H. Faure (2000), Isotopic chronology of the Sahara and the Sahel during the late Pleistocene and the early and mid-Holocene (15,000–6,000 BP), *Quat. Int.*, *68–71*, 385–387.

Voelker, A. H. L., S. M. Lebreiro, J. Schonfeld, I. Cacho, H. Erlenkeuser, and F. Abrantes (2006), Mediterranean outflow strengthening during Northern Hemisphere coolings: A salt source for the glacial Atlantic?, *Earth Planet. Sci. Lett.*, *245*, 39–55.

Wehausen, R., and H.-J. Brumsack (1999), Cyclic variations in the chemical composition of eastern Mediterranean Pliocene sediments: A key for understanding sapropel formation, *Mar. Geol.*, *153*, 161–176.

Wehausen, R., and H.-J. Brumsack (2000), Chemical cycles in Pliocene sapropel-bearing and sapropel-barren eastern Mediterranean sediments, *Palaeogeogr. Palaeoclimatol. Palaeoecol.*, *158*, 325–352.

Weldeab, S., W. Siebel, R. Wehausen, K.-C. Emeis, G. Schmiedl, and C. Hemleben (2003), Late Pleistocene sedimentation in the western Mediterranean Sea: Implications for productivity changes and climatic conditions in the catchment areas, *Palaeogeogr. Palaeoclimatol. Palaeoecol.*, *190*, 121–137.

Weltje, G. J., and M. Prins (2003), Muddled or mixed? Inferring palaeoclimate from size distributions of deep-sea clastics, *Sediment. Geol.*, *162*, 39–62.

Zuo, Z., D. Eisma, and G. W. Berger (1991), Determination of sediment accumulation and mixing rates in the Gulf of Lions, Mediterranean Sea, *Oceanol. Acta*, *14*, 253–262.

I. Cacho, M. Canals, and J. Frigola, Consolidated Research Group Marine Geosciences, Department of Stratigraphy, Paleontology and Marine Geosciences, Faculty of Geology, University of Barcelona, Campus de Pedralbes, C/Martí i Franquès s/n, E-08028 Barcelona, Spain. (miquelcanals@ub.edu)

J. H. Curtis and D. A. Hodell, Department of Geological Sciences, University of Florida, Gainesville, FL 32611-2120, USA.

J. A. Flores and F. J. Sierro, Department of Geology, University of Salamanca, Plaza de la Merced s/n, E-37008 Salamanca, Spain.

J. O. Grimalt, Department of Environmental Chemistry, ICER-CSIC, Jordi Girona 18, E-08034 Barcelona, Spain.

A. Moreno, Pyrenean Institute of Ecology, Spanish Research Scientific Council, Aptdo. 202, E-50080 Zaragoza, Spain.

Artifacts provide the first sign that
a tangent universe has occured

"The philosophy of travel time"
Roberta A. Sparrow